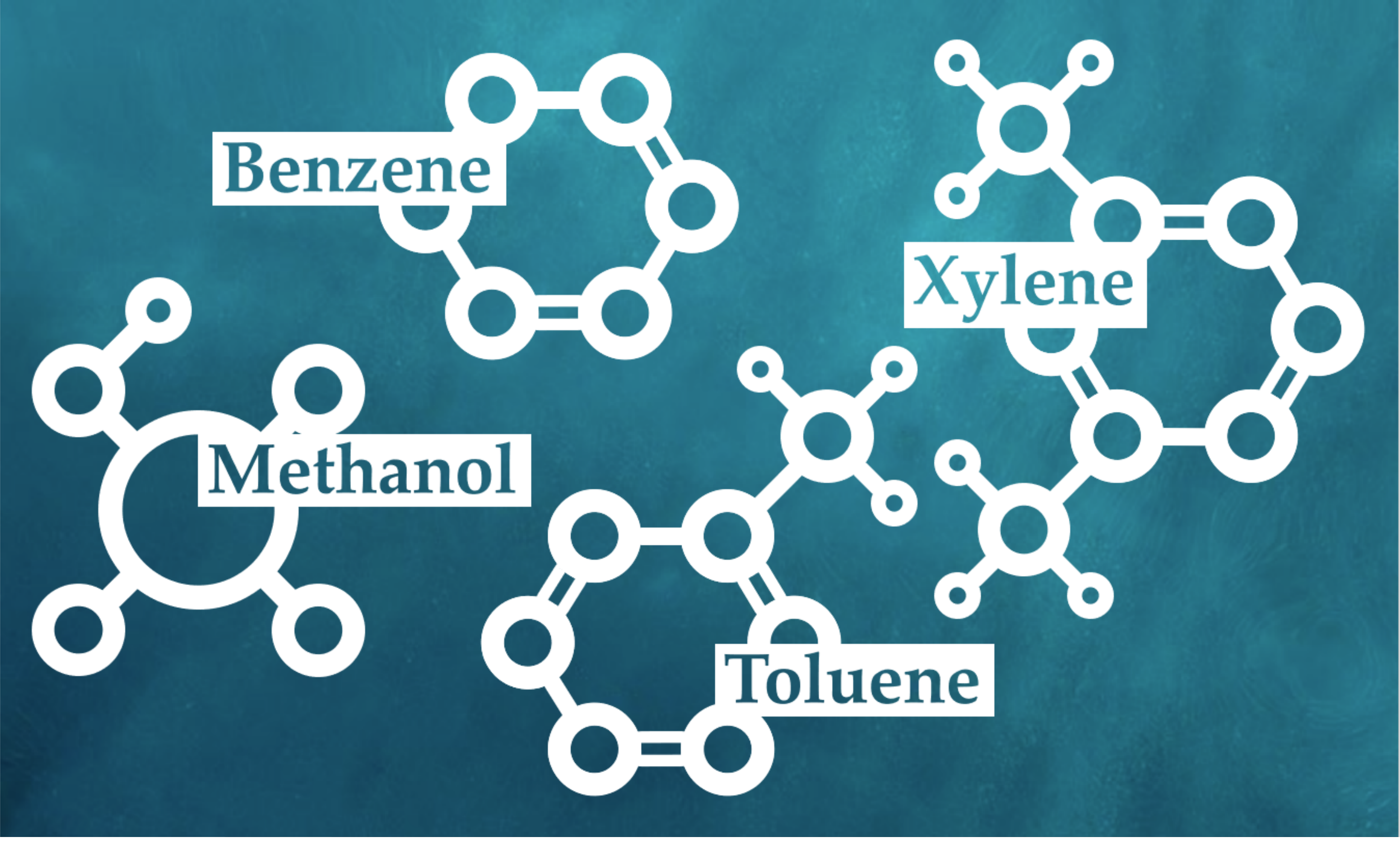

Techno-Economic Analysis of Green Methanol and Green BTX Production from Syngases

Frederik Meyer Elimar
Nicolai Hermann Rasmussen
Nikolaj Hornshøj Petersen

Energy Technology, TEPE4-1014, 2021

Master's Thesis

STUDENT REPORT
AALBORG UNIVERSITY

Summary

The use of carbon neutral fuels and chemicals is receiving an increased interest from both industry and private consumers, as the need to reduce one's carbon footprint is increasingly encouraged. This carbon reduction requires modification to numerous aspects in industries and private consumer habits. One of these aspects is to produce carbon neutral fuels and chemicals.

This is the aim of the presented study, which seeks to investigate the feasibility of producing Green methanol that may serve as a fuel or it may be converted into other Green chemicals. This production of Green methanol is achieved through a process that consumes CO_2 and H_2, which are obtained from carbon capture and water electrolysis. The CO_2 is captured from the flue gas of RenoNord, whose CO_2 emission serves as the size to which the remainder of the system is scaled. The CO_2 is removed from the flue gas using an absorber/stripper system, where a solvent is utilised to transport the CO_2 from the flue gas into a pure CO_2 stream for the methanol synthesis. The H_2 is produced using an alkaline electrolyser cell, where water is split into its two constituents, being hydrogen and oxygen. The H_2 is used in the methanol synthesis, while the O_2 can be sold as a separate product. The electricity required for all processes is partly supplied by on-site wind turbines and photovoltaic panels, while the remainder is assumed to be supplied by external renewable sources.

The methanol synthesis is done using an adiabatic reactor equipped with a packed catalyst consisting of $Cu/ZnO/Al_3O_3$, in which hydrogenation of CO_2- and a reverse water-gas shift reaction occur. The ensuing product stream consists of water, methanol and dissolved gases, which is sent through two distillations to yield fuel grade methanol. The methanol may also be further treated to produce larger organic molecules, i.e. chemicals, such as benzene, toluene and xylene (BTX). This is achieved in an adiabatic reactor packed with a ZSM-5 catalyst where 13 different reactions occur, yielding 17 species. Similar to the methanol synthesis, the product stream from the BTX synthesis also contains a significant amount of water along with a multitude of Light Gases, Alkanes and Aromatic molecules, which may be separated.

The feasibility of producing either methanol or BTX, also designated as System 1 and System 2, respectively, is determined based on a capital expenses (CAPEX) and operational expenses (OPEX) analysis of both systems. All components modelled in the Aspen Plus software have their CAPEX and OPEX determined by the add-on 'Aspen Process Economic Analyzer', while any additional components are investigated through the literature. With the asking price of the products from both systems defined, the profit, when accounting for the CAPEX and OPEX, can be determined. In order to investigate the sensitivity of the potential profits, a sensitivity analysis is conducted for both systems, where the most influential components and parameters are varied to analyse their impact. The results of these sensitivity analyses are shown in Figure 1 on page iv.

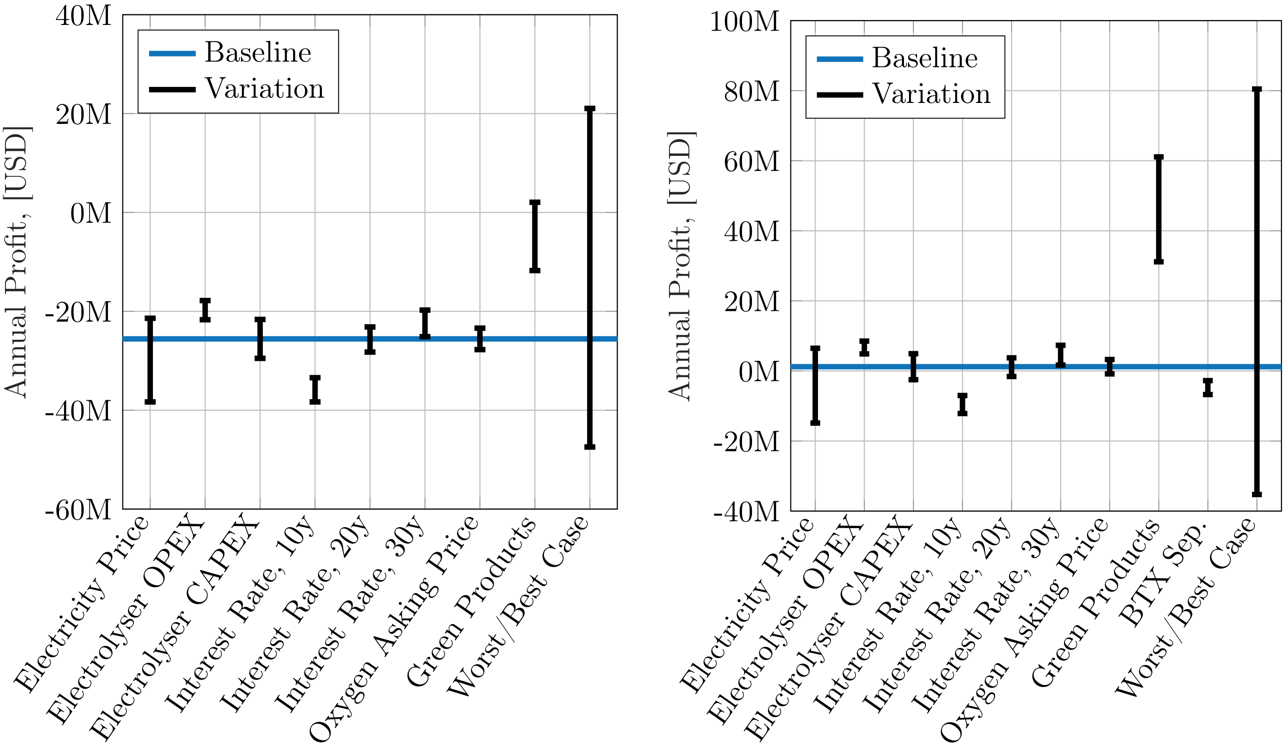

(a) System 1 - Green methanol as end product.

(b) System 2 - Green BTX as end product.

Figure 1: Sensitivity analysis of CAPEX and OPEX by variation in component pricing and various variables.

With respect to the Green methanol, its sensitivity analysis indicates the baseline value will result in a deficit. To achieve a profitable system, the asking price must be at a premium level for the Green methanol, otherwise the system will produce a deficit. A more profitable tendency is observed if BTX is the end product, where the baseline value produces a minor profit. Only if the electricity price, electrolyser CAPEX and BTX separation costs are increased, or a bad capital loan is taken, will System 2 become unprofitable. Lastly, similar to System 1, the elevated asking price of Green products will result in an increased profit.

The presented study has hence shown that in order for methanol or BTX production from renewable sources to be considered profitable, the asking price for such chemicals must be at a premium level compared to their traditionally produced Black counterparts.

AALBORG UNIVERSITY
STUDENT REPORT

Department of Energy Technology
Aalborg University
http://www.aau.dk

Title:
Techno-Economic Analysis of Green Methanol and Green BTX Production from Syngases

Theme:
Master's Thesis

Project Period:
Spring Semester 2021

Project Group:
TEPE4-1014

Participant(s):
Frederik Meyer Elimar
Nicolai Hermann Rasmussen
Nikolaj Hornshøj Petersen

Supervisor(s):
Vincenzo Liso
Samuel Simon Araya
Xiaoti Cui

Copies: 1

Page Numbers: 146

Date of Completion:
May 28, 2021

Abstract:

Carbon neutral fuels and chemicals are receiving an increased interest from both industry and consumers, as the need to reduce one's carbon footprint is increasingly encouraged.
The presented study seeks to investigate the feasibility of producing carbon neutral methanol sold as a fuel, or convert into other chemicals, such as benzene, toluene and xylene (BTX). The methanol is synthesised in a catalyst filled adiabatic reactor using CO_2 obtained from carbon capture and H_2 produced through electrolysis, whose power is supplied by renewable energy sources.
Fuel grade methanol is achieved through distillation where water is separated, while the synthesis of BTX is commenced without distilling the methanol stream. The product stream of the BTX synthesis consists of numerous species, which are separated into lumps using compression and distillation.
The feasibility of a system producing methanol or BTX showed that unless premium Green asking prices are applied to methanol it is unprofitable, while a system producing BTX is more likely to yield a profit.

[This page is intentionally left blank]

Contents

[This page is intentionally left blank]

Preface

This Master's Thesis has been written by the project group TEPE4-1014 at the Department of Energy Technology at Aalborg University, with specialisation in Thermal Energy and Process Engineering during the spring semester of 2021. The objective of this project, prescribed as 'the presented study' from here on out, is to assess the feasibility of producing Green methanol and determine if it would be lucrative to further convert the produced Green methanol into other Green chemicals. The Green methanol is produced by a process which consumes CO_2 and H_2. The CO_2 is captured from the flue gas exiting the incineration plant of RenoNord, where biomass is combusted. Furthermore, the H_2 is acquired through an electrolysis of water which is powered by renewable energy. Two systems are designed where the end product of the first system is methanol and chemicals (BTX) for the second, named System 1 and System 2, respectively. In order to estimate the potential feasibility of each system, both must be modelled in order to determine the capital- and operational expenses of both systems.

During this Master's Thesis the following software have been utilised:

- **Aspen Plus V9** - Performing process modelling.
- **Aspen Process Economic Analyzer V9** - Estimate component- and utility costs.
- **Engineering Equation Solver** - Look up physical properties of species, and model the electrolysis process and storage of gases.
- **Excel** - Processing data.
- **Graph** - Extrapolate or interpolate data from literature.
- **Inkscape** - Produce illustrative figures.
- **Maple** - Perform calculations.
- **MatLAB** - Create McCabe-Thiele diagrams.
- **Overleaf** - Writing and formatting the presented study.
- **PGFPlots** - Create plots and other illustrative figures.
- **WebPlotDigitizer** - Extract data from plots and images listed in literature.

Readers' Guide

On page vii, the Table of Contents can be found. Viewing this document as a PDF the Table of Contents will function with hyper-links allowing fast navigation to the desired chapters and sections.

The nomenclature on page xv lists the different subscripts, superscripts, abbreviations, chemical formulas, notations and symbols along with their respective units. They will be presented in alphabetical order.

The bibliography on page 125 presents the sources and literature used in the presented study. The bibliography is structured according to the Harvard format, and is hence ordered alphabetically with respect to the authors. The reference will be placed prior to the subsequent period if refer to the current sentence. Whereas if it placed after the period it refers to the presented segment.

The units used in the presented study will be following the metric system. Decimal numbers will be indicated with a dot, while a comma will function as a thousands separator.

The graphs used in the presented study can either be single y-axis graphs or dual y-axis graphs. In order to distinct between what function is associated to which axis in a dual y-axis graph, a solid lined function will be associated to the left axis, while a dotted line is associated to the right axis.

All chapters, sections and subsections are labelled with a unique number according to the order of which they are presented. The figures and tables are numbered similarly, for instance "Figure 5.3" refers to the third figure in Chapter 5. Viewing in a PDF format these references work as hyperlinks.

When equations are presented they will have a number assigned in the right margin. This number will be used for referencing to the equation. Viewing in a PDF format the references work as hyperlinks. The variables used in the equations will only be explained the first time they are used.

The final pages of this Master's thesis consist of the Appendices. The appendices contain additional results or calculations. The appendices will, in contrary to the other chapters, be assigned a letter which is ordered alphabetically.

Finally, it is recommended to read the presented study in a colourised format to get the optimum visual- and reading experience, mainly in regards to the graphs and figures.

Chapter Structure

Chapter 1 on page 1 will shortly present the required species when producing Green methanol, being CO_2 and H_2, and further also the state of the art of such plants. Additionally, the challenges of utilising renewable energy sources will be presented which results in a general process design. Finally, the objective of this Master's Thesis will be presented.

As it is desired to either produce Green methanol or further convert this into other Green chemicals, it is necessary to understand each of the subsystems presented in the process design. This will be presented in Chapter 2.

Chapter 2 on page 11 describes all the theories, concepts and reactions necessary to model each of these subsystems. Some subsystems are modelled as dynamic whereas the remainder are modelled as steady state. The dynamic- and steady state subsystems will be modelled in Chapter 3 and 4, respectively.

Chapter 3 on page 39 seeks to implement the general theories and concepts for the dynamic subsystems into a dynamic model. This includes the carbon capture and the electrolyser due to their fluctuating production. As it is desired to model the consecutive subsystems as steady state, storage of CO_2 and H_2 is implemented in order to couple the dynamic- and steady state models.

Chapter 4 on page 59 seeks to implement the general theories and concepts for the steady state subsystems into two steady state systems, differentiated by their desired end products. The first system produces Green methanol, while the second further converts the Green methanol into other Green chemicals. With the two complete systems defined, heat- and mass integration between the subsystems can be performed in order to reduce the utility costs of the two systems. This will be done in Chapter 5.

Chapter 5 on page 89 performs heat- and mass integration of the two systems. With the systems being optimised with respect to the excess heat and mass within each system, the costs of both systems can be estimated in order to determine the feasibility of the two systems. This will be done in Chapter 6.

Chapter 6 on page 103 performs the feasibility assessment of the two systems. A sensitivity analysis for each system is conducted in order to determine the uncertainty of the feasibility for both systems, depending on specific parameters. A multitude of assumptions are made throughout this Master's thesis, where the most influential require a discussion.

Chapter 7 on page 121 discusses these assumptions in order to justify if they are acceptable.

Chapter 8 on page 123 concludes the presented Master's Thesis and summarises the acquired results.

This Master's Thesis has been written by the following authors:

Signatures of project participants

Frederik Elimar
Frederik Meyer Elimar
<felima16@student.aau.dk>

Nicolai Hermann Rasmussen
<nhra16@student.aau.dk>

Nikolaj H. Petersen
Nikolaj Hornshøj Petersen
<nhpe16@student.aau.dk>

Aalborg University, May 28, 2021

[This page is intentionally left blank]

Nomenclature

Symbols	Explanation	Unit
A	Area	m^2
A_{C}	Pre-exponential factor	$\mathrm{m}^3/(\mathrm{kmol}\cdot\mathrm{s})$, $1/\mathrm{s}$, $\mathrm{kmol}/(\mathrm{kg}\cdot\mathrm{h})$, $\mathrm{kmol}/(\mathrm{kg}\cdot\mathrm{s}\cdot\mathrm{bar})$, $\mathrm{kmol}/(\mathrm{kg}\cdot\mathrm{s}\cdot\mathrm{bar}^2)$
a_{p}	Surface area per volume of packing	$\mathrm{m}^2/\mathrm{m}^3$
B	Correlation constant	-
b	Correlation constant	-
C	Capacity factor	m/s
C_{f}	Fair's capacity	m/s
C_{p}	Heat capacity	kJ/K
c_{p}	Mass specific heat capacity	$\mathrm{kJ}/(\mathrm{kg}\cdot\mathrm{K})$
D	Diameter	m
E	Energy	kJ
E_{A}	Activation energy	kJ/mol, kJ/kmol
F	Factor	-
F_{LV}	Liquid-vapour flow factor	-
f	Flooding factor	-
G	Gibbs' free energy	kJ
H	Enthalpy	kJ
h	Molar specific enthalpy	kJ/kmol
H_{C}	Henry's constant	kPa
$HETP$	Height equivalent theoretic plate	m
I	Current	A
I_{solar}	Solar irradiance	$\mathrm{kWh}/\mathrm{m}^2$
i	Current density	A/cm^2
k	Kinetic factor	$\mathrm{kmol}/(\mathrm{kg}\cdot\mathrm{s}\cdot\mathrm{bar})$, $\mathrm{kmol}/(\mathrm{kg}\cdot\mathrm{s}\cdot\mathrm{bar}^2)$
k_{ads}	Adsorption constant	-, $\sqrt{1/\mathrm{bar}}$, 1/bar
L	Length	m
m	Mass	kg
$m^{\star}_{\mathrm{V}}$	Vapour mass per unit column cross-sectional area	kg/m^2
MW	Molecular weight	kg/kmol
N	Arbitrary number	-
n	Moles	kmol
P	Pressure	kPa, bar

P_{sat}	Saturation pressure	kPa, bar
p	Partial pressure	kPa, bar
PR	Pressure ratio	-
Q	Heat	kJ, MJ
R	Reflux ratio	-
r	Rate of reaction	$\mathrm{mol/(kg \cdot s)}$
R_{gas}	Gas constant	$\mathrm{kJ/(K \cdot kmol)}$
S	Entropy	kJ/K
s	Molar specific entropy	$\mathrm{kJ/(K \cdot kmol)}$
T	Temperature	K, °C
t	Time	s
V	Voltage	V
$\not{V}$	Volume	$\mathrm{m^3}$
v	Velocity	m/s
W	Work	kJ, MJ
wt	Weight fraction	-
x	Liquid molar fraction	-
y	Vapour molar fraction	-
z	Electrons transferred per ion	-

Greek letter	**Explanation**	**Unit**
α	Relative volatility	-
β	Initial loan	USD
γ	Interest rate	-
Δ	Change in value	-
ζ	Activity coefficient	-
η	Efficiency	-
η_{F}	Faraday's efficiency	-
κ	Balance after number of periods	USD
λ	Number of periods	-
μ	Dynamic viscosity	$\mathrm{Pa \cdot s}$
ν	Stoichiometric coefficient	-
ν_{s}	Molar specific volume	$\mathrm{m^3/kmol}$
ξ	Activity coefficient	-
ρ	Density	$\mathrm{kg/m^3}$
σ	Surface tension	N/m
τ	Yearly payment	USD/year
ϕ	Chemical potential	kJ/kmol
ψ	Base size solvent flow rate	kg/s

Subscripts	
a	Active
air	Air
an	Anode
B	Bottom
cat	Cathode
cell	Cell

CO	Carbon monoxide
CO_2	Carbon dioxide
conc	Concentration
cool	Cooling
D	Distillate
d	Downcomer
elec	Electrolyser
eq	Equilibrium
F	Foaming
f	feed
g	Gas
gen	Generated
h	Hole
H_2	Hydrogen
H_2O	Water
HA	Hole-to-active area
i	Integer
in	Input
ini	Initial
L	Liquid stream
l	Liquid
max	Maximum
MeOH	Methanol
O_2	Oxygen
ohm	Ohm
out	Outlet
p	Power
pack	Packed distillation column
phy	Physical
PV	Photovoltaic
q-line	Characteristic line used in distillation
reboil	Reboiler
rev	Reversible
RWGS	Reverse water-gas shift
ST	Surface tension
stage	Stage
swept	Swept
tank	Tank
th	Theoretic
tot	Total
V	Vapour stream
w	Wind

Superscript	
eq	Equilibrium
i	Integer
N	Arbitrary number

Abbreviations	
AEC	Alkaline electrolysis cell
APEA	Aspen Process Economic Analyzer
BTX	Benzene, toluene and xylene
CAPEX	Capital expenses
CCS	Carbon capture and storage
CCU	Carbon capture and utilisation
CHP	Combine heat-power
DKK	Danish krone
elec-NRTL	Redlich-Kwong coupled with electrolyte Non-Random Two Liquid
FUG	Fenske, Underwood and Gilliland
HEN	Heat exchanger network
HETP	Height equivalent to a theoretical plate
M	Million
MEA	Monoethanolamine
MSA	Mass-separating agent
MTBE	Methyl tertiary-butyl ether
MTO	Methanol-to-Olefins
MTP	Methanok-to-propylene
NRTL	Non-random two liquid
OPEX	Operational expenses
O&M	Operation and maintenance
PEMEC	Polymer electrolyte membrane electrolysis cell
PFR	Plug flow reactor
PV	Photovoltaic
RKSMHV	Redlich-Kwong-Soave equation of state with a modified Huron-Vidal mixing rule
RWGS	Reverse water-gas shift
SOEC	Solid oxide electrolysis cell
SQP	Sequential quadratic programming
UNUQUAC	Universal quasichemical
USD	United States dollar
VLE	Vapour-liquid equilibrium

Chemical form	
Al_2O_3	Aluminium oxide
CH_4	Methane
C_2H_4	Ethane
C_3H_6	Propene
C_3H_8	Propane
C_4H_{10}	Butane
C_5H_{12}	Pentane
C_6H_{14}	Hexane
C_6H_6	Benzene
C_7H_8	Toluene
C_8H_{10}	Xylene
C_9H_{12}	1,2,4-Trimethylbenzene

$C_{10}H_{14}$	1,2,4,5-Tetramethylbenzene
CO	Carbon monoxide
CO_2	Carbon dioxide
Cu	Copper
H_2	Hydrogen
MeOH, CH_3OH	Methanol
N_2	Nitrogen
O_2	Oxygen
ZnO	Zinc oxide

Notation	
$\dot{x}$	Time derivative
$[x]$	Concentration
∇x	Gradient
$\overline{x}$	Time average
$\widetilde{x}$	Time fluctuating

[This page is intentionally left blank]

Chapter 1

Motivation and Objective

Before the reader embarks on reading through the following chapters of the presented study, it is highly encouraged that the reader reviews the Readers' Guide presented on page xi in order to get a thorough understanding of the structure in which the following chapters are presented and their intercorrelation.

The motivation of the presented study originates in the vision of a future where renewable energy is the main source of energy. The renewable energy is not only of great importance with respect to the electricity demand, but also for instance in the transport- and chemical sector. The incorporation of renewable energy into the transport sector is slowly increasing from 1.4 % in 2004 to 8 % in 2018 for the members of the European Union [eurostat, 2020]. Furthermore, as the technological development continues, indispensable products are desired to be manufactured from renewable energy sources as well.

A product which has a multitude of uses in both the transport- and chemical sector is methanol, which will be denoted MeOH for the remainder of the presented study, as may be seen in Figure 1.1.

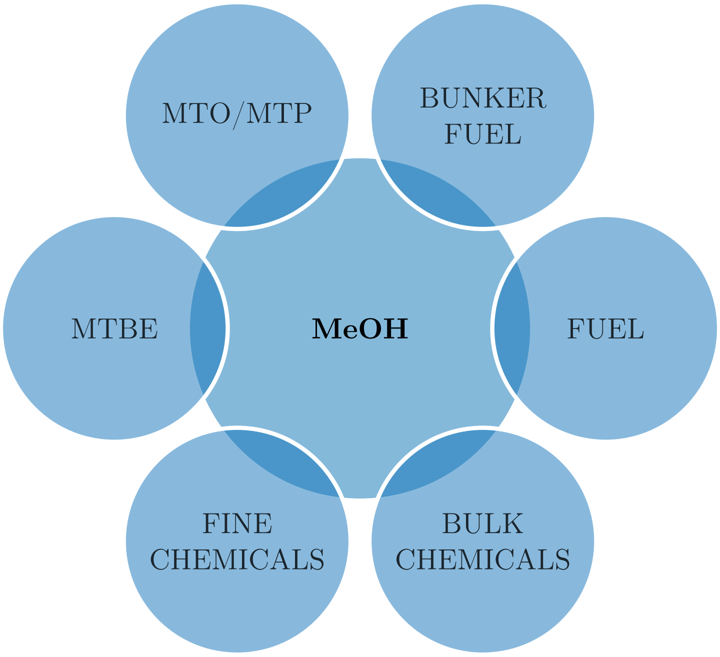

Figure 1.1: Overview of products manufactured from MeOH. Adapted from RoyalGlobalEnergy [2020].

MeOH can be used both in its pure form as a fuel in a combustion engine, or it may be diluted with other fuels extracted from fossil sources, such as bunker fuel. Furthermore, it can be processed into methyl tertiary-butyl ether (MTBE) which can replace otherwise toxic, yet necessary, additives in the petrol fuel [ICIS, 2010]. Among other chemicals, conversion of MeOH-to-Olefins (MTO) and MeOH-to-propylene (MTP) can be performed, which are used in the plastic production industry [Americanchemistry, 2020][LindeGas, 2020]. Due to this variety, it is of interest to further investigate the business potential of MeOH both as a product but also as an intermediate.

However, in order to ensure the vision of a future where the use of fossil fuels are reduced, the MeOH must be produced from renewable energy sources.

1.1 Renewable Methanol

The classification of renewable MeOH is defined by how the syngases, which are used to make the MeOH, are produced. In order for the MeOH to be considered Green, the synthetic gases must be produced from renewable sources with net zero CO_2 emission. The traditional MeOH is produced from fossil resources, such as natural gas, coal and crude oil, which is classified as Black MeOH.[Hobson and Márquez, 2018] Similarly, the MeOH can also be identified as Grey of which the synthetic gases are produced from waste or by-products, which are only partially renewable.

1.1.1 Renewable Carbon Dioxide

The reactants used to produce Green MeOH are CO_2 and H_2. As already claimed these must be acquired from renewable sources. The source of CO_2 could be provided by either extracting it from the air directly or from the flue gas of a plant run on biomass. The technologies for capturing CO_2 from the atmosphere is however still at a research state of which this method is not viable [Bui et al., 2018].

For instance, the flue gas from biogas plants contains 30 % to 45 % CO_2 and in bioethanol plants up to 85 %, both on a volume basis.[Benato et al., 2017][Laude et al., 2011]. As such it would be advantageous to use this produced CO_2 to supply the MeOH production plant, which will also be economically lucrative for the biomass plant, due to the ensuing avoidance of carbon emission fees.

1.1.2 Renewable Hydrogen

To achieve a Green MeOH production the second reactant, H_2, must as mentioned also be obtained through renewable methods. Currently, the vast majority of H_2 production is achieved through reforming of natural gases and other fossil fuels, i.e. Black H_2 is produced, which accounts for about 90 % of the total production.[Liu et al., 2021][Hosseini and Wahid, 2016]

However, other methods for H_2 production exist, such as water electrolysis, where the potential of utilising renewable energy sources is possible. Several electrolysis technologies are available, namely the polymer electrolyte membrane electrolysis cell (PEMEC), alkaline electrolysis cell (AEC), and solid oxide electrolysis cell (SOEC). All three technologies do however suffer from various disadvantages such as expensive materials, low durability, and crossover of gases leading to poor purity.[Rashied et al., 2015]

As a result, H_2 production from electrolysis remains the more expensive production method, compared to reforming from fossil sources [Acar and Dincer, 2014]. With a continued interest in using H_2 for different processes and technologies like MeOH production, the need for H_2 will continue to rise.[Dalena et al., 2018][Okolie et al., 2021]

In comparison to CO_2, H_2 is the bottleneck in the production of Green MeOH due to its limited availability and price. If the Green H_2 was to be produced by electrolysis, it would be lucrative to utilise the fluctuating production of electricity, where the surplus can reduce the Green H_2 production cost.[Brynolf et al., 2018] Hence, in order for Green MeOH production to become a reality, it is necessary for the production price of Green H_2 to be reduced to a level similar to that of Black H_2. If the production price of Green H_2 cannot decline to the level of Black H_2, the need for governmental subsidies may be required to incentivise the use of Green H_2.[Klenert et al., 2018] Even if governmental subsidies are not available, Green branding could make the renewable MeOH attractive.

1.2 State of the Art Plants

A pilot plant is already established at Aalborg University, where the production capacity is 300,000 litres of Green MeOH per year. This is a combined H_2 and MeOH plant, since the H_2 is produced by an electrolyser located on site. The CO_2 is however supplied by an externally located biogas plant and as such the pilot plant is not directly coupled to a CO_2 supply.[Green Hydrogen Systems, 2020] The next step for the Green MeOH technology is to scale from pilot plant to commercial plant.

A Green industrial business park is currently under construction in Skive, where one of the world's first commercially scale combined Green H_2 and MeOH plants will be located [GreenLab, 2021]. There will be established a 10 MW MeOH plant and a 12 MW electrolysis plant [GreenLab, 2019]. The expected production capacity of this MeOH plant is 10 million litres per year, which is equivalent to eliminating the CO_2 emission of 7,000 cars [GreenLab, 2020]. Additionally, a biogas plant with a production capacity of 19 million m^3 bio-methane per year will also be located in the park. The produced CO_2 of the biogas plant will then be used for the MeOH plant [GreenLab Skive Biogas Aps, 2021]. The Green MeOH production is set to start in 2022 [GreenLab, 2020]. The industrial business park is coupled to an energy grid powered locally by a 80 MW hybrid wind- and solar power plant, making the entire park operate on renewable energy [GreenLab, 2019].

1.3 Plant Sizing

The production of Green MeOH is approaching commercialisation and as such it is of interest to identify potential business partners to whom a business case can be established. There are however two requirements they must fulfil. The first being that the industry in question must emit an appropriate amount of CO_2. The second is that the CO_2 must be produced by processes in which biomass is the feedstock, in order for the produced MeOH to be classified as being Green. To determine a suitable industrial partner, an investigation regarding the largest private Danish CO_2 emitting companies has been conducted, as shown in Figure 1.2 on the next page.

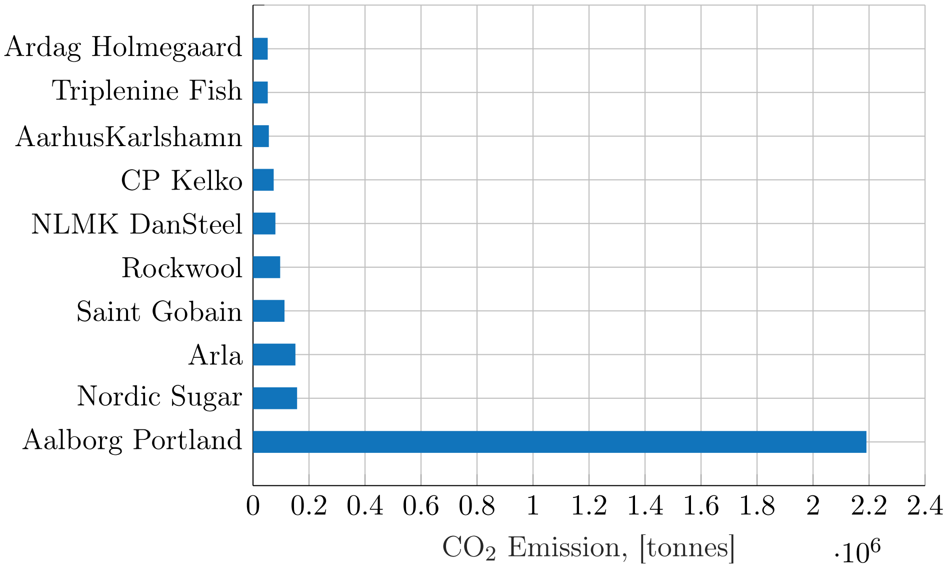

Figure 1.2: Top 10 most CO_2 emitting private industrial companies in 2018.[DR.DK, 2020]

Due to the governmental restriction, that the Danish greenhouse gas emissions must be reduced by 70 % by 2030 [State of Green, 2019], the industrial companies are looking for solutions to this restriction. For instance, Aalborg Portland A/S states that they require the implementation of CO_2 capture in order to comply with the greenhouse gas restriction [Nikolajsen, 2019]. From Figure 1.2 it is evident that Aalborg Portland was the largest industrial emitter in 2018, the company emitted in that year approximately 14 times more than the second largest. As such Aalborg Portland could be an interesting business partner, since it might be possible to receive governmental subsidies, due to the potential significant decrease in the Danish net CO_2 emission. Yet, the resulting MeOH would not be identified as being Green which is a constraint in the presented study. Biomass must be the feedstock of the process and an appropriate biomass could be sorted municipal waste.

According to senior advisor Søren Dyck-Madsen from CONCITO: "The waste incineration plants are obvious for further development in CO_2 capture, since the flue gas that exits the chimney has a stable and high concentration of CO_2, which originates from both fossil sources and biomass based sources. The captured CO_2 could either be directly stored underground by the CCS-process (Carbon Capture and Storage), or used together with H_2 to make fuels by the CCU-process (Carbon Capture and Utilisation)".[S. Dyck-Madsen, 2020]

As such it is expected that there would be a mutual interest from both industries, of which RenoNord has been chosen. RenoNord is a waste management company which has one of the most modern incineration plants in Europe [Linkedin, 2021]. This incineration plant emitted approximately 224,000 tonnes of CO_2 in 2019, where 59 wt% was generated from biomass. However, the CO_2 must at first be captured from the flue gas, where different technologies are available. The efficiencies of these technologies are in the range of 80 wt% to 90 wt% [Leung et al., 2014]. As a result, by assuming that 90 wt% of the CO_2 is captured, a total of approximately 119,000 tonnes of Green CO_2 is available to supply the MeOH plant. Throughout the presented study, the dimensioning of the MeOH plant will be based on this CO_2 supply.

1.4 Fluctuating Feedstock Supply and Energy

To obtain Green CO_2 it must be supplied by the combustion of biomass, such is the case at RenoNord. Similarly, to obtain Green H_2 the electricity needed for the electrolysis could be supplied by wind turbines and photovoltaics (PV) panels.

These two technologies were chosen since they are currently the most presented Green energy sources in the Danish renewable electricity production. Wind- and solar power are responsible for 33.0 % and 3.5 %, respectively, of the total primary energy production in Denmark.[EnergiStyrelsen, 2020]

However, due to the desire of producing MeOH at a continuous rate, it may become necessary to store both the CO_2 and H_2. This is a result of the possibility that the CO_2 and energy supply from the renewable sources may fluctuate.

1.4.1 Carbon Dioxide

The production of energy from power plants, such as the combined heat-power plant (CHP) of RenoNord, varies according to monthly demand. The fuel burned at RenoNord is converted to both electricity and heat, as shown in Figure 1.3.

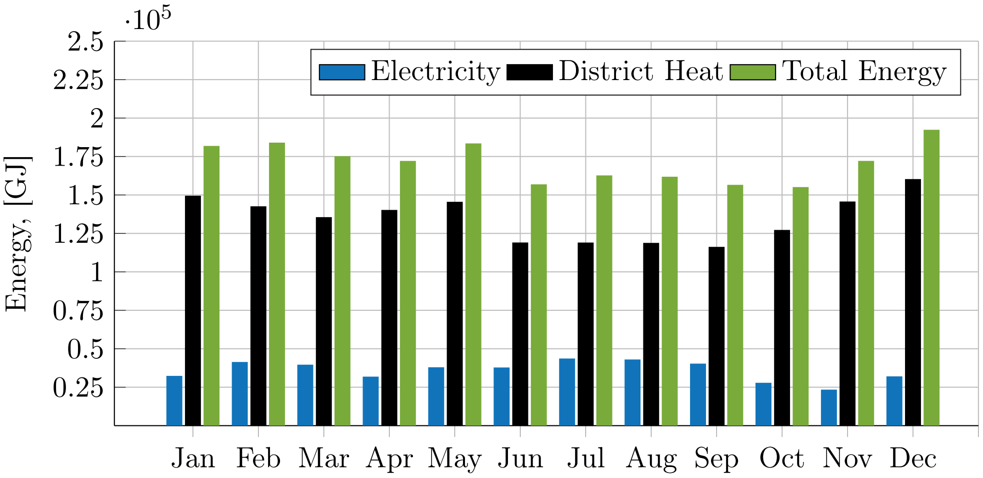

Figure 1.3: Monthly variation in electricity- and heat production from RenoNord, averaged over the years of 2018, 2019 and 2020.[Sørensen, 2020]

As is evident, the energy production is generally slightly lower during the summer months compared to the higher values seen during the winter months. This is likely due to the decreased heat requirement during the warm summer months, and as a result the CHP plant produces more electricity. The slight difference in energy production throughout the year is also reflected in the emitted CO_2 as indicated in Figure 1.4 on the following page.

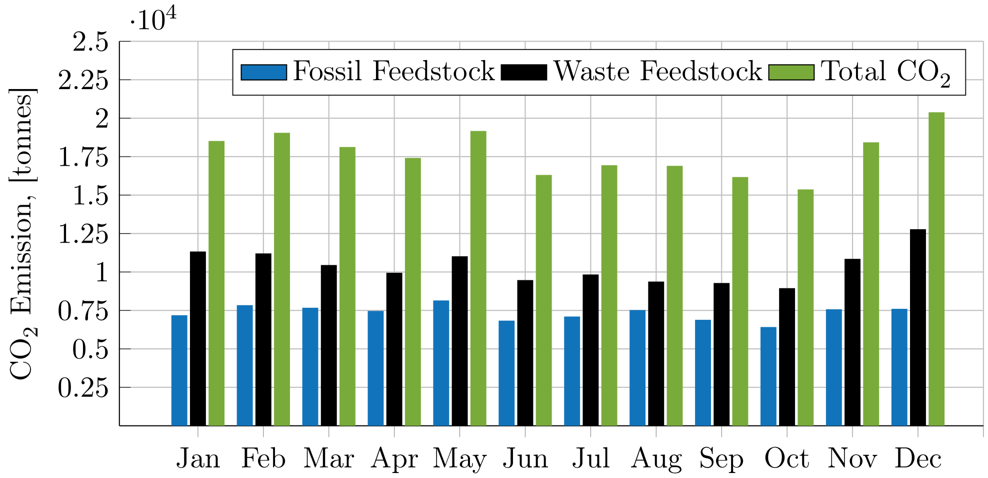

Figure 1.4: Monthly variation in CO_2 emission from RenoNord, averaged over the years of 2018, 2019 and 2020.[Sørensen, 2020]

Here the same trend is obvious as the CO_2 emission is greater in the late autumn until early summer. This fluctuating CO_2 production must be taken into consideration when attempting to model a carbon capture plant.

1.4.2 Wind Power

Wind energy is, like the CO_2 emissions from RenoNord, also relatively constant on a monthly basis as shown in Figure 1.5. However, daily variations are significant, and it should also be noted that the wind speeds are measured 10 m above terrain, hence the actual wind speed experienced by the wind turbine may be greater.

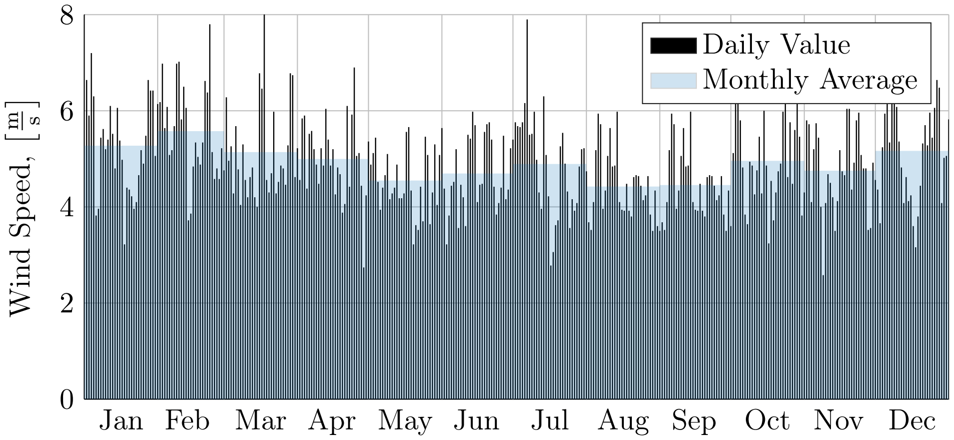

Figure 1.5: Monthly- and daily variation in wind speed at Aalborg Airport measured 10 m above terrain and as a daily mean value, averaged over the years of 2016 to 2020.[Danish Meteorological Institute, 2020]

Due to the power curve of wind turbines being highly dependent on the wind speed, days with high wind speeds will produce more power, as shown in Eq. 1.1

$$\dot{W}_w = 0.5 \cdot F_p \cdot \rho_{air} \cdot \pi \cdot A_{swept} \cdot v_{air}^3 \tag{1.1}$$

where F_p is the power factor, ρ_{air} is air density, A_{swept} is the swept area and v_{air} is the air speed. However, multiple factors, such as the power factor, are proportional to the generated power. The power factor is not equal to unity, as may be seen in Figure 1.6 on the next page.

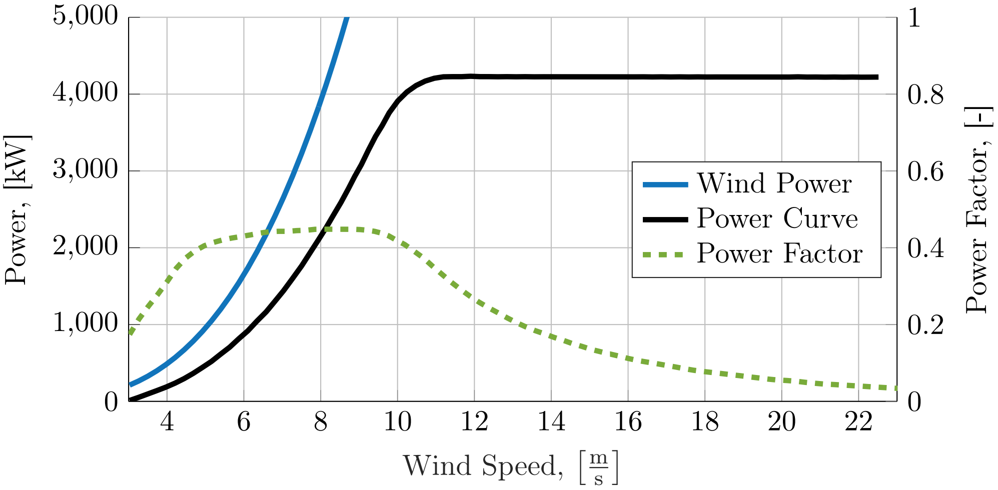

Figure 1.6: Wind power is the maximum theoretical power content in wind. The power curve and power factor for Vestas V126-3.45MW are also displayed, which are linearly scaled to match the 4.2 MW turbines used in Skive. Adapted from Wind Turbine Models [2020].
As presented in the Preface, the solid lines belong to the left y-axis, while the dotted line belongs to the right y-axis.

Due to the power factor, the power production that can be achieved is much lower than the theoretical power, which is obtained when not including the power factor in Eq. 1.1 on the facing page. This is also indicated by the wind power and power curve in Figure 1.6. Nonetheless, there is still a strong influence of wind speed until the rated wind speed of about 12 m/s is reached. Hence, when taking into account the daily mean wind speed shown in Figure 1.5 on the facing page, the power produced by wind turbines will remain to vary significantly, since the wind speed generally varies between 3 m/s to 8 m/s for the given altitude of 10 m.

1.4.3 Solar Power

Unlike the power produced from wind, the power from PV is not exponential to the solar irradiation. Instead it is directly proportional to the solar irradiance, as is shown in Eq. 1.2

$$\dot{W}_{\mathrm{PV}} = \mathrm{F}_{\mathrm{PV}} \cdot I_{\mathrm{solar}} \cdot A_{\mathrm{PV}} \tag{1.2}$$

where F_{PV} accounts for the cell efficiency, packing factor, transitivity of glass and others, I_{solar} is the solar irradiance and A_{PV} is the area covered by the PV panels.[Kaldellis et al., 2014][Ratlamwala et al., 2011].

Contrary to the wind speed, the solar irradiance varies more noticeably, which is mainly due to the annual change in position of the earth in relation to the sun. This may also be seen in Figure 1.7 on the following page.

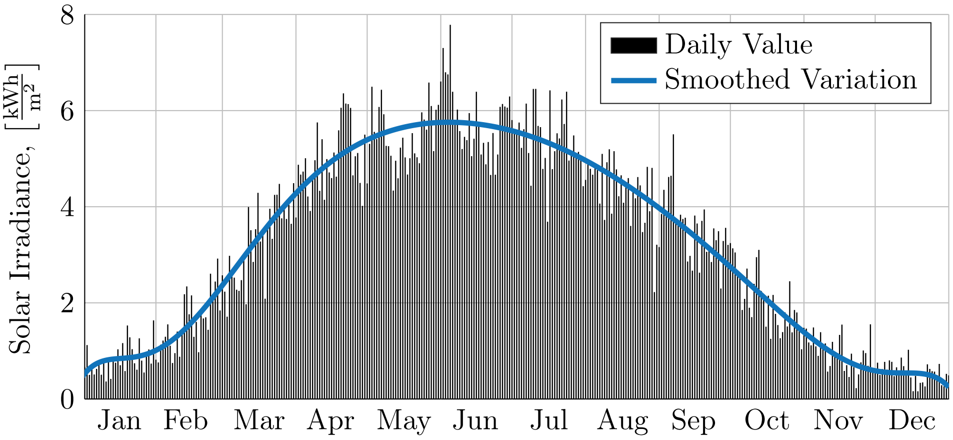

Figure 1.7: Average daily solar irradiance throughout the last decade at Ulsted district heating facility.[Dansk Fjernvarme, 2020]

As is clear from Figure 1.7 a larger production of H_2 can be made from solar energy during the late spring, summer and early autumn, as this period accounts for the majority of the solar irradiance.

1.5 Overall Process

In order to estimate the business potential for a Green MeOH synthesis at RenoNord, the processes from initial reactants to the end products need to be defined. As previously discussed, this system needs to account for the fluctuating inputs of CO_2 and H_2. If a constant output is desired throughout the year, the system must hence include storage of both CO_2 and H_2 due to their fluctuating and seasonally opposite production tendencies. However, another approach is to have a varying output depending on the CO_2. Since the trends of the CO_2 emission, wind speed and solar irradiance are relatively predictable the system could utilise this. It would require an excess production of H_2 in the months where the yields are relatively high from wind turbines and PV panels. Therefore, in the months where the H_2 production is lower than what is required to convert all the emitted CO_2, the excess H_2 could be used as a buffer to supply the remaining months. However, if the latter process is utilised the workload for the system will vary as a function of the CO_2 emissions. This will affect the efficiency of the system, if it is designed to operate on the maximum CO_2 supply, due to partial load operation. Instead, it is expected to be more feasible to design the system to operate from a mean value of the CO_2 emission, which in return would make it necessary to also store excess CO_2 supply.

MeOH has a multitude of uses, where it can either be used as a final product or used to produce other products. An economical assessment will be made in order to determine if the plant would be more feasible if the MeOH is used as an intermediate to produce a different product in contrast to having the Green MeOH as the end product. This will require an analysis of the possible products and the determination of which are the most feasible in relation to the MeOH plant. In order to conduct the economical assessment, two systems are considered. One in which Green MeOH is the final product and a second where it is used as an intermediate to produce Green chemicals, denoted System 1 and System 2, respectively. An overview of such systems may be seen in Figure 1.8 on the facing page.

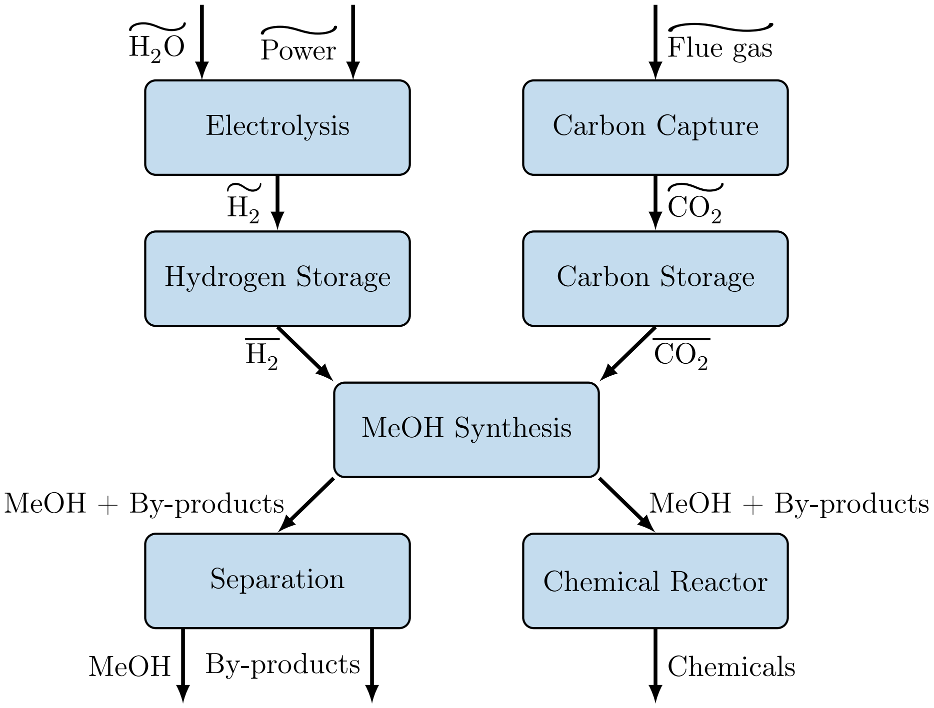

Figure 1.8: Block diagram of the overall processes where either Green MeOH or Green Chemicals are the end products.

Figure 1.8 can be divided into six different subsystems, namely electrolysis, carbon capture, storage, MeOH synthesis, separation of the produced Green MeOH and the possible production of other Green chemicals. In the electrolysis subsystem, H_2 is produced from H_2O and electricity. The CO_2 emission of RenoNord is included in the carbon capture, where it is separated from the flue gas which consists of numerous gases. The storage processes concern the necessary storage of H_2 and CO_2, in order for the plant to operate at full load at all times. The MeOH synthesis process concerns the production of MeOH from H_2 and CO_2. This MeOH may then either be separated so that the MeOH can be sold in its pure state or it can be converted to other chemicals or fuels as presented in Figure 1.1 on page 1.

From this overview of all the subsystems of the plant, the objective of the presented study may be defined as shown on page 10.

1.6 Objective

The presented study seeks to investigate the business potential of producing Green chemicals from the carbon neutral CO_2 emitted by the waste incineration plant of RenoNord and renewable H_2 produced from electrolysis. The objective is to determine the feasibility of a system producing Green MeOH and to explore if further conversion of the Green MeOH into other Green chemicals will be more lucrative. In order to make such a study, a techno-economic analysis must be conducted, wherein the design and modelling of the entire system is required. This leads to the following problem statement and further research questions.

How can a system, in which syngases are converted into Green methanol, be designed, whereupon it may be purified to fuel grade methanol or converted to other chemicals, from which the economics of these products may be investigated to determine their feasibility?

To answer the problem statement, the following research questions will be investigated, which will indirectly be answered in the following chapters.

- How can the system be designed in order to account for the fluctuating CO_2 and H_2 supply?
- How can a numerical model of the methanol synthesis and the conversion to other chemicals be made?
- How can an optimisation of the system be done in order to increase its feasibility?
- Which are the most influential parameters in regards to the feasibility and how sensitive is the system to these?

Chapter 2

System Analysis

In order to perform the techno-economic analysis and thereby determine the most profitable product, the two systems need to be modelled. However, before the systems are modelled, an analysis of the subsystems previously shown in Figure 1.8 on page 9, is required in order to obtain knowledge of the individual processes and how the subsystems operate. These will be outlined in the following sections regarding their belonging theories, concepts and reactions necessary to model each of these subsystems. Hence, the specific input parameters and component specifications will not be presented until the following chapters, where the knowledge presented in this chapter will be used to incorporate the individual subsystems into the two complete systems.

2.1 Carbon Capture

The CO_2 required for the MeOH synthesis may be obtained from combustion of carbon rich sources, where different technologies are available for extracting the CO_2. Additionally, the individual combustion technologies affect the gas composition, hence the CO_2 concentration. In order to determine the best suited capture technology, the combustion technologies will be presented firstly.

2.1.1 Combustion Technologies

In *pre-combustion* technology the fuel undergoes gasification, i.e. heated under low oxygen conditions, which releases several gases to form a syngas consisting mainly of CO and H_2. This syngas may then be used in a water-gas shift reaction to form CO_2. In pre-combustion, a CO_2 concentration above 20 wt% is obtainable, which can then be separated. However, this technology involves adding additional process steps, mainly in the form of the gasifier.[Leung et al., 2014] Additionally, the feedstock for the gasification process will, in the case of RenoNord, not be simply coal or natural gas but will instead consist of multiple constituents. Only about 9 wt% of the material received for combustion at RenoNord is primary residue biomass, while the remainder is a mixture of residual waste at 40 wt%, industrial waste at 28 wt%, and several types of environmentally dangerous waste.[RenoNord, 2019] This discrepancy may lead to the syngas, if produced by the pre-combustion process, being less pure and containing more undesirable gases compared to the commonly used coal or natural gas.

In *post-combustion* technology the feedstock is not pretreated as in pre-combustion. Instead it is simply fed to the combuster and as a result it is easy to retrofit into power plants which are already in operation. Although easy to implement, the CO_2 concentration is usually relatively low at about 7 wt% to 14 wt% for coal fired power plants, which is a result of air mainly consisting of N_2 and the combustion also producing water and other minor species. As a result the CO_2 concentration is lower compared to pre-combustion.[Leung et al., 2014]

In *oxyfuel-combustion* the principle is similar to post-combustion, with the difference being that pure O_2 is used instead of air. This results in the flue gas containing no N_2 and other minor species associated with Nitrogen, hence making higher CO_2 concentrations possible. However, the need for pure O_2 increases the price significantly, making this method less feasible.[Leung et al., 2014]

Even though different combustion technologies are available, complications occur if an existing plant was to be modified. Hence, RenoNord would likely continue to utilise the post-combustion technology, however, oxyfuel-combustion could become a possibility. Besides H_2, O_2 is also produced from the electrolysis which could be utilised for the combustion, since the electrolysis would be placed on site, and it should be relatively easy to incorporate. Not only would this affect the concentration of CO_2 in the flue gas, but it would also increase the adiabatic flame temperature within the combustor and thereby increase the power output of RenoNord.

2.1.2 Carbon Capture Technologies

Regardless of the chosen combustion technology, the CO_2 still has to be separated from the syngas or flue gas. Many technologies are available, however, only a few are developed to a degree that can be considered viable.

Absorption utilises a solvent, such as monoethanolamine (MEA) or diethanolamine, which act as a sorbent of the CO_2. Many solvents are available, but the MEA solvent is the most mature and studied solvent [Madeddu et al., 2019]. In this process the CO_2 is absorbed by the solvent, which may then later be stripped to release the absorbed CO_2 through heating or depressurisation of the solvent [Wilberforce et al., 2021]. The main advantages of this technology include high absorption efficiency of more than 90 wt%, as well as being well established, mature and having easy regeneration of the solvent [Veawab et al., 2002] [Aaron and Tsouris, 2005]. The disadvantages consist of substantial energy requirements for heating of the solvent and the potential degradation of the solvent.

Contrary to absorption, the *Adsorption* technology uses a solid sorbent instead of a liquid sorbent, where the CO_2 is bound to the surface of the solid. As such the main criteria for an effective solid sorbent is a large surface area, but also high selectivity towards binding CO_2 specifically and how easily the sorbent may be regenerated. The adsorbed CO_2 can be stripped by lowering the pressure or by heating the sorbent, both resulting in recovery efficiencies of about 80 wt% [Leung et al., 2014].

As mentioned several other carbon capture technologies are available, such as *Chemical looping combustion*, *Hydrate-based separation*, *Membrane separation*, and *Cryogenic distillation*. However, these suffer from being immature in their development or having low output rates, while the latter mentioned Cryogenic distillation technology requires high concentrations of CO_2 to be feasible [Leung et al., 2014].

Following the comparison presented above, the technology with the best potential for the presented study is the absorption process with MEA as the solvent. The overall details for how such a subsystem operates is described in the following.

2.1.3 Absorption Carbon Capture

As previously mentioned the purpose of a solvent, in this case MEA, is to absorb the CO_2 from the flue gas. The conceptual principle of this process is outlined in the following.

In order to utilise MEA it is dissolved in H_2O at a mixture of 30 wt%, into which CO_2 may then be absorbed [Madeddu et al., 2019]. However, in order to utilise the CO_2 it must be separated from the H_2O-MEA mixture, which is achieved through a stripper. After the separation of CO_2 the lean solvent is recirculated back into the subsystem. An overview of such a subsystem may be seen in Figure 2.1.

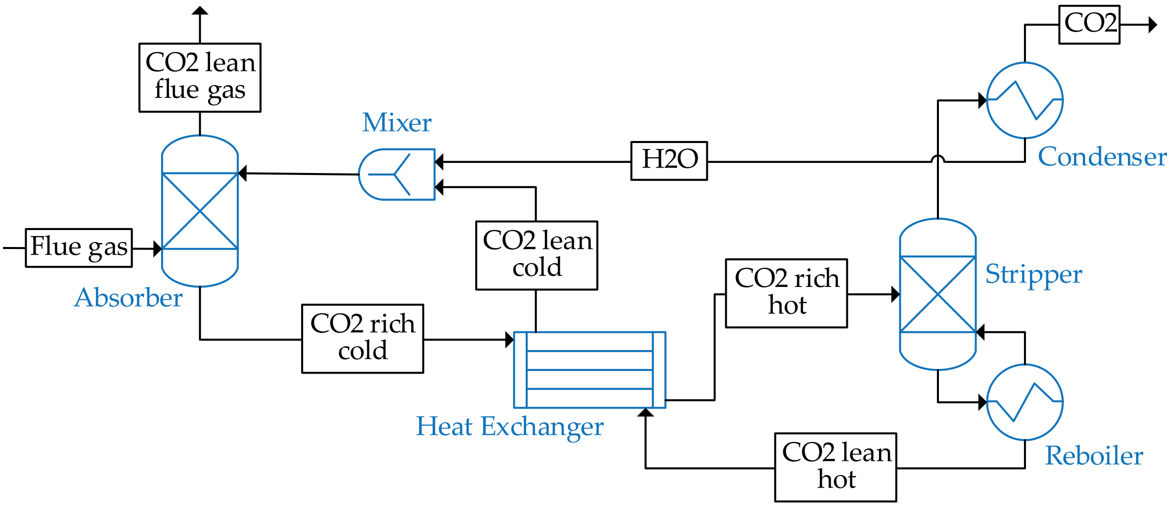

Figure 2.1: Overview of carbon capture subsystem, utilising the absorption method with MEA as the solvent.

The overall concept of this subsystem is to have a certain amount of CO_2 from the flue gas being captured by a solvent within the Absorber, which for the presented study is defined as 90 wt% capture rate in accordance to former studies such as Madeddu et al. [2019]. The CO_2 rich solvent exiting the Absorber, is heated in a heat exchanger by the regenerated CO_2 lean solvent exiting the Stripper, before it enters the Stripper. In the stripper the CO_2 is distilled from the solvent after which the gas stream enters the Condenser. The pure CO_2 exits the condenser from which it can be used in the consecutive subsystem. H_2O is condensed in the Condenser, from which it is recycled and mixed with the CO_2 lean solvent, before it enters the absorber once again through. The pressure in the stripper is slightly elevated at around 1.5 bar to 2.0 bar, thus implying relatively high temperatures at 95 °C to 120 °C. Due to the Clausius-Clapeyron correlation between the heat of absorption of CO_2 in MEA and the heat of vaporisation of H_2O, the vapour pressure of CO_2 increases more rapidly than for H_2O when increasing the temperature, leading to the CO_2 being separated from the liquid [Freguia, 2002]. The absorption process of CO_2 into the MEA can be described from the reaction scheme shown in Figure 2.2 on the next page, which are based on the study done by Errico et al. [2016].

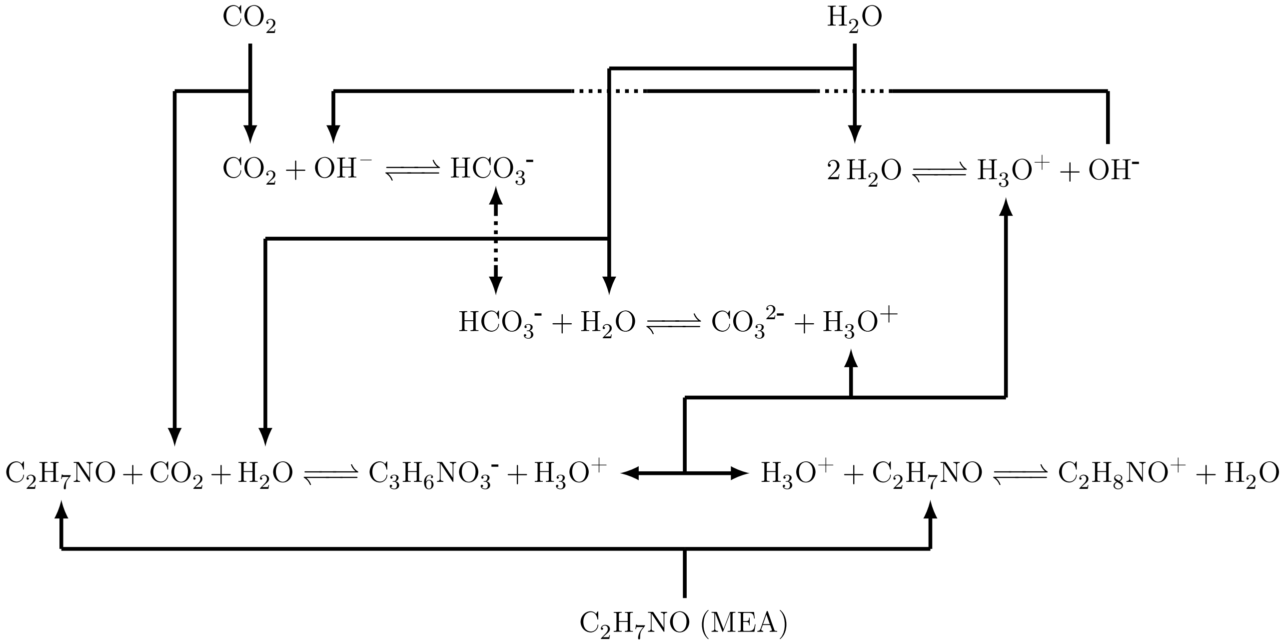

Figure 2.2: Reaction scheme of the absorption process based on the study done by Errico et al. [2016].

The conversion rates for the reactions illustrated in the reaction scheme above are either defined from the standard Gibbs′ free energy change or a first/second order rate law expression. The following reactions are determined from the standard Gibbs′ free energy change, where the equilibrium constants can be determined according to Eq. 2.1

$$\begin{aligned} \text{MEA} + H_3O^+ &\rightleftharpoons \text{MEAH}^+ + H_2O \\ 2\,H_2O &\rightleftharpoons H_3O^+ + OH^- \\ HCO_3^- + H_2O &\rightleftharpoons CO_3^{2-} + H_3O^+ \end{aligned}$$

$$K^{eq} = \prod (x_i \cdot \xi_i)^{\nu_i} \tag{2.1}$$

where x_i is the mole fraction of the species, ξ_i is the activity coefficient and ν_i is the stoichiometric coefficient. Lastly, the following reactions are determined from first or second order rate law expressions, where the reaction order is marked by the exponents.

Table 2.1: Carbon capture rate law expressions, with corresponding pre-exponential factors, A_C, and activation energies, E_A. Furthermore, the exponents represent the order of reaction for the corresponding species.

			A_C	Unit	$E_A\left[\frac{kJ}{kmol}\right]$
$[CO_2]^1 + [OH^-]^1$	$\longrightarrow$	HCO_3^-	4.32e+13	$\left[\frac{m^3}{kmol\cdot s}\right]$	55,433
$[MEA]^1 + [CO_2]^1 + [H_2O]^0$	$\longrightarrow$	$MEACOO^- + H_3O^+$	9.77e+10	$\left[\frac{m^3}{kmol\cdot s}\right]$	41,236
$[MEACOO^-]^1 + [H_3O^+]^1$	$\longrightarrow$	$MEA + CO_2 + H_2O$	3.23e+19	$\left[\frac{m^3}{kmol\cdot s}\right]$	65,500
$[HCO_3^-]^1$	$\longrightarrow$	$CO_2 + OH^-$	2.38e+17	$\left[\frac{1}{s}\right]$	123,222

Given the above analysis the fundamental knowledge of carbon capture has been presented. More details on this process and the design specifications of the individual species will be outlined in the following Chapter 3 on page 39.

2.2 Electrolyser

The H_2 required for the MeOH synthesis will be supplied by an electrolyser. Different electrolysis technologies exist, as described in Chapter 1, but due to the maturity and scale-ability of the Alkaline Electrolyser Cell (AEC), it is chosen as the technology to be used in the presented study.[Rashied et al., 2015] The concept of this technology is to use electrical current to split liquid H_2O into its two constituents, namely H and O, which occurs through a non-spontaneous chemical reaction. The electrolyser used for this reaction consists of three main components: an anode, a cathode, and an electrolyte. In combination they make up a subsystem of two electronic conductors and an ionic conductor. As current is passed through the subsystem, the anode facilitates oxidation while the cathode allows for a reduction to occur, and lastly the electrolyte serves as a conductor of the free ions.[Zhang et al., 2011] This subsystem can be described visually as shown in Figure 2.3.

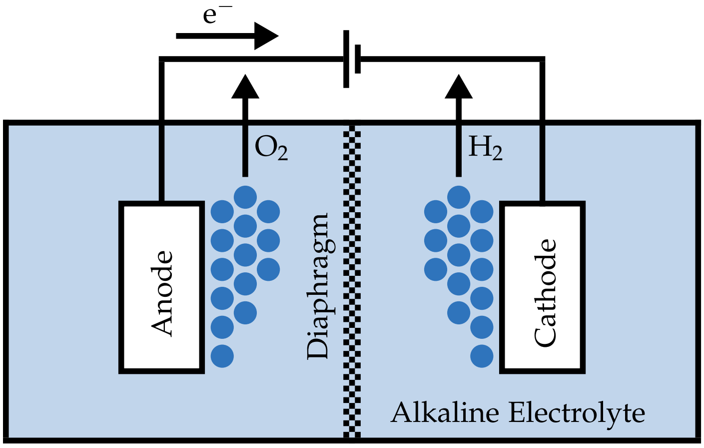

Figure 2.3: Schematic of AEC subsystem.

The reactions occurring at the two electrodes lead to the following reactions.[Zhang et al., 2011]

$$\begin{array}{llcl} \text{Cathode:} & 2\,H_2O(l) + 2\,e^- & \longrightarrow & H_2(g) + 2\,OH^-(g) \\ \text{Anode:} & 2\,OH^-(g) & \longrightarrow & H_2O(l) + 0.5\,O_2(g) + 2\,e^- \\ \text{Overall reaction:} & H_2O(l) & \longrightarrow & H_2(g) + 0.5\,O_2(g) \end{array}$$

Since the electrolysis is an electrochemical process the rate of reaction is not determined by kinetics but instead by the electric potential. The molar flow of H_2 given in the overall reaction can be expressed as seen in Eq. 2.2, which is derived from Faraday's law of electrolysis stating that the amount of substance produced is proportional to the current passed through the electrolyte

$$\dot{n}_{H_2} = \eta_F \cdot \frac{I}{z \cdot F_C} \cdot N \tag{2.2}$$

where η_F is Faraday's efficiency, I is the current, z is the electrons transferred per ion, F_C is Faraday's constant and N is the number of cells in the stack. Due to the correlation between the current and voltage defined by Ohm's law, the voltage is also of interest. The electrolysis cell voltage denoted V_{cell} can be expressed as seen in Eq. 2.3

$$V_{cell} = V_{rev} + V_{cat} + V_{an} + V_{ohm} + V_{conc} \tag{2.3}$$

where V is voltage and the subscripts rev, cat, an, omh and conc denote reversible, cathode, anode, ohmic and concentration, respectively. It can be seen that multiple voltages contribute to the total cell voltage. The first term V_{rev} is the minimum voltage needed to make the reaction seen in the overall reaction occur. This corresponds to the voltage required to reach the electrochemical equilibrium which can be described from the change in Gibbs' free energy as seen in Eq. 2.4.

$$\Delta G = \text{z} \cdot F_{\text{C}} \cdot V_{\text{rev}} \tag{2.4}$$

Since the change in Gibbs' free energy can be determined from look-up the value of V_{rev} can be defined, from which four terms remain undefined in Eq. 2.3 on the preceding page. However, these terms are dependent on the physical properties of the electrolyser, from which empirical data is required. A study conducted by Sánchez et al. [2018] made an empirical correlation for an AEC to determine these four terms, based on the current density, temperature and pressure. With all terms determined, V_{cell} can be defined as in Eq. 2.5

$$\begin{aligned} V_{\text{cell}} = V_{\text{rev}} &+ (4.139\text{e-}5 + 6.889\text{e-}9 \cdot T + 4.471\text{e+}7 \cdot P) \cdot i \\ &+ 0.338 \cdot \log_{10}\left[\left(-0.015 + \frac{2.002}{T} + \frac{15.243}{T^2}\right) \cdot i + 1\right] \end{aligned} \tag{2.5}$$

where i is the current density, T is the temperature and P is the pressure. Given Eq. 2.5 the polarisation curve for the cell voltage at different temperatures may be seen in Figure 2.4.

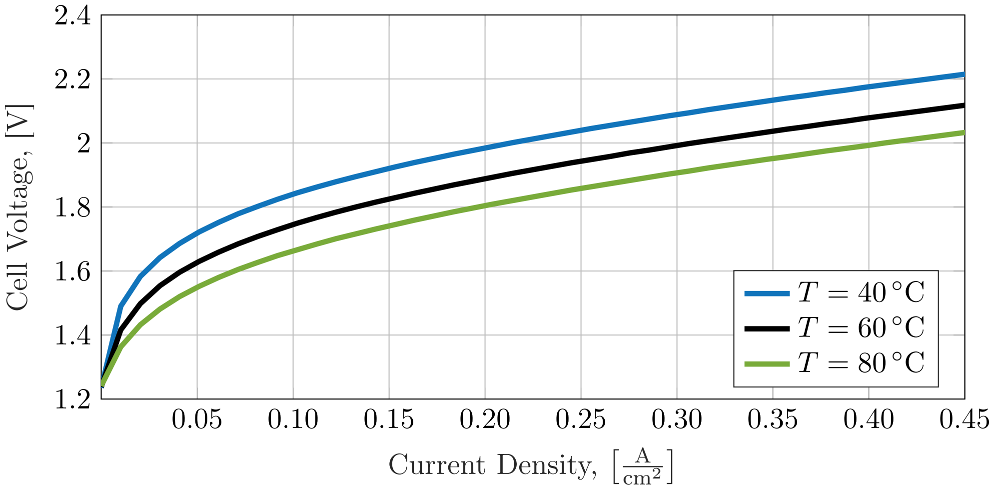

Figure 2.4: Polarisation curve for the cell voltage at different temperatures.

From the figure it may be seen that an increased temperature reduces the cell voltage. This corresponds to an increased cell performance as a result of the reduction in the Gibbs' free energy of the electrochemical reaction, due to the temperature increment.

In Eq. 2.2 on the preceding page Faraday's efficiency was also introduced which is the ratio between the actual- and theoretical production of H_2. The study by Sánchez et al. [2018] also made an empirical correlation based on the current density and temperature as seen in Eq. 2.6.

$$\eta_{\text{F}} = \left(\frac{i^2}{478{,}645.74 - 2{,}953.15 \cdot T + i^2}\right) \cdot (1.040 - 0.001 \cdot T) \tag{2.6}$$

With the Faraday's efficiency defined, the molar flow of H_2 can be determined as outlined in Eq. 2.2 on page 15. The remaining molar flows can be determined from the stoichiometric balance, resulting in the molar flow rates shown in Eq. 2.7 and 2.8.

$$\dot{n}_{H_2O} = \dot{n}_{H_2} \tag{2.7}$$

$$\dot{n}_{O_2} = \dot{n}_{H_2} \cdot 0.5 \tag{2.8}$$

Eq. 2.7 and 2.8 defines the mole balance for the electrolysis, however, the required power to run the process is also of interest which can be described by Eq. 2.9.

$$\dot{W} = \mathrm{N} \cdot V_{\mathrm{cell}} \cdot I \tag{2.9}$$

Furthermore, the energy balance is also of interest where the generated heat can be expressed as described by Eq. 2.10

$$\dot{Q}_{\mathrm{gen}} = \mathrm{N} \cdot I \cdot (V_{\mathrm{cell}} - V_{\mathrm{th}}) \tag{2.10}$$

where V_{th} denotes the thermoneutral voltage. Depending on V_{cell} the reaction can either be endothermic or exothermic which is defined by V_{th}. V_{th} defines the voltage at which the added thermal energy equals the required electrical energy. This can be described by the change in enthalpy which is determined as seen in Eq. 2.11

$$\Delta H = \Delta G - T \cdot \Delta S \tag{2.11}$$

where S is entropy. Therefore V_{th} can be defined from the change in enthalpy as may be seen in Eq. 2.12.

$$V_{\mathrm{th}} = \frac{\Delta H}{\mathrm{z} \cdot F_{\mathrm{C}}} \tag{2.12}$$

Since the reaction can both be endothermic or exothermic it will be desirable for V_{cell} to approach V_{th}, to reduce the cooling utility usage. It is however known that all the voltage contributions are temperature dependent as shown in Figure 2.5.

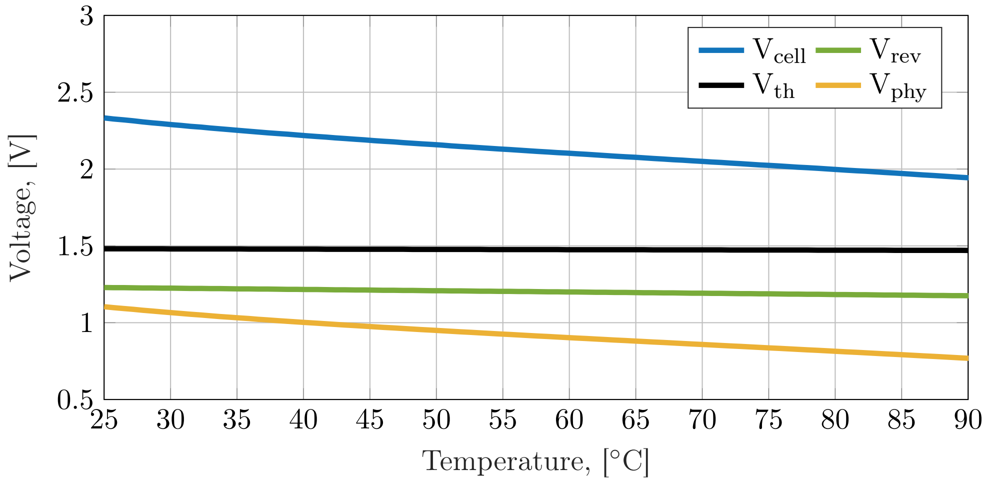

Figure 2.5: V_{cell}, V_{th}, V_{rev}, along with V_{phy} which corresponds to the sum of V_{cat}, V_{an}, V_{ohm} and V_{conc}. All at constant pressure and current of 7 bar and 0.45 A/cm^2, respectively.

From Figure 2.5 it can be concluded that V_{cell} is greater than V_{th} resulting in the reaction being exothermic, hence making cooling a necessity. V_{th} can be assumed constant whereas

V_{cell} decreases as the temperature increases. In order to minimise the required cooling the electrolysis should be operated at a relatively high temperature. However, the influence of the temperature with respect to the produced molar flow should also be considered. Figure 2.6 shows the molar flow as function of the current density at different temperatures. Since the absolute molar flow is not of interest in this analysis the molar flows have been normalised with respect to the flow obtained at 20 °C. Furthermore, Figure 2.6 also illustrates the generated heat as function of the current density at different temperatures. Similar to the molar flows, the absolute value of the generated heat is not of interest from which they have been normalised with respect to the heat generated at 20 °C.

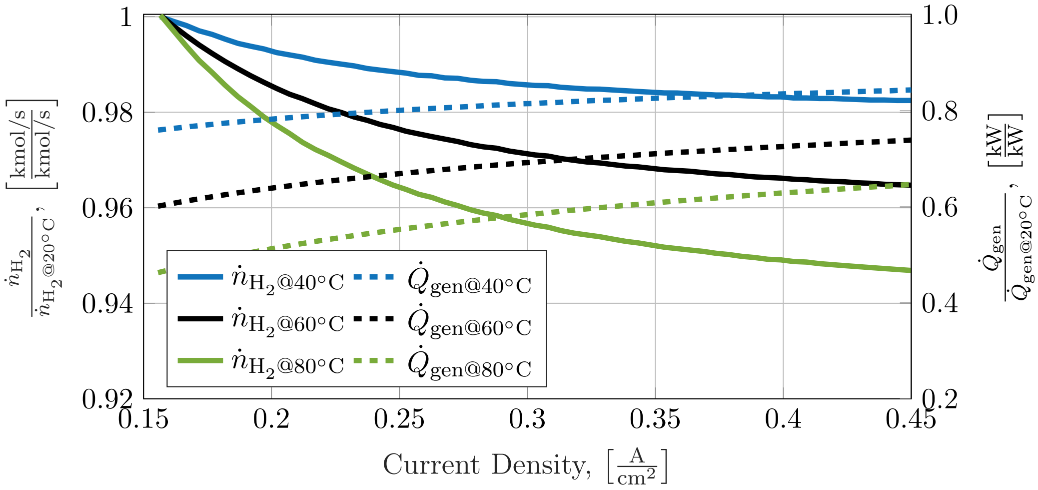

Figure 2.6: Molar flows and heat generation as function of the current density at different temperatures normalised with respect to the molar flow and heat generation, respectively, at 20 °C. The pressure and number of cells in the stack are constant at 7 bar and 12, respectively.

From Figure 2.6 it can be concluded that the trend, of which the molar flows decrease as function of the temperature, is linear. However, the molar flows decay exponentially as function of the current density. This occurs due to the influence of Faraday's efficiency. The optimum operating temperature for the molar flow is relatively low, opposite to the generated heat. When the temperature increases the generated heat is reduced due to V_{cell} approaching V_{th}. The relative change in generated heat as function of the temperature, is however, greater than the change in molar flow. From this analysis it can be concluded that the optimum operation of the electrolysis is at the higher temperatures of the 20 °C to 80 °C range. Throughout this section the pressure has been assumed to be constant at a value of 7 bar. The influence of varying the pressure has been discussed by multiple authors, however due to practical aspects, which is not of interest, the pressure is fixed at 7 bar for the remainder of the presented study.[Sánchez et al., 2018]

Given the above analysis the fundamental knowledge of electrolysis has been presented. More details on this process and the design specifications of the individual components will be outlined in the following Chapter 3 on page 39.

2.3 Storage of Gases

In order to obtain a constant MeOH production, storage of CO_2 and H_2 is needed. As presented in Chapter 1, the production of H_2 is influenced by the fluctuating supply of energy from renewable energy sources, from which it becomes necessary to store the H_2. Similarly, the production of CO_2 is also fluctuating, due to the change in heat- and electricity demand throughout the year. At standard conditions the density of CO_2 and H_2 is $1.82\,\mathrm{kg/m^3}$ and $0.083\,\mathrm{kg/m^3}$, respectively, where they are in gaseous state. If the gases are to be stored at these densities it will require disproportionately large containers.

Numerous technologies exists for H_2 storage, including *adsorption*, *chemical hydrides* and *mechanical storage*, each with multiple sub-technologies [Durbin and Malardier-Jugroot, 2013]. Oppositely, technologies regarding storage of CO_2 generally involve suppressing it into geological storage, such as underground reservoirs [Leung et al., 2014]. This suggests that the focus of most studies have been on removing the CO_2 completely from the ecosystem, rather than storing it for further use [Jackson and Brodal, 2018]. Since the technologies regarding storage of H_2 is described in more detail compared to CO_2, these will be analysed to gain an understanding of the possibilities.

2.3.1 Hydrogen Storage Technologies

Although it is not desired to store H_2 at standard conditions, it is not always required to increase the density too much, as would be the case when using some of the technologies mentioned above. Relatively high densities are primarily required in the transport sector, due to spatial restrictions, whereas in stationary systems this requirement is loosened. The most common methods for storage are as liquid or as compressed gas, which are subcategories to the mechanical storage method.

In *compressed storage* the H_2 is compressed to increase the density, while retaining its gaseous state. The pressure ranges from 200 bar to 800 bar at ambient temperature, resulting in densities of $20\,\mathrm{kg/m^3}$ to $40\,\mathrm{kg/m^3}$, where the reachable pressure is linked to the costs of the storage unit.[Makridis, 2016]

In *liquid storage*, also known as cryogenic storage, the H_2 is cooled instead of pressurised. The saturation temperature of H_2 is 20 K at standard pressure where the corresponding density at liquid state is $71\,\mathrm{kg/m^3}$, hereby increasing the volumetric energy density. This concludes that a higher density is achievable for liquid storage compared to compressed storage, however, the liquid storage of H_2 is more energy expensive. The required power to compress H_2 from 20 bar to 700 bar is 1.36 kWh/kg where the minimum theoretical energy to liquefy the H_2 at standard conditions is 3.3 kWh/kg [Gardiner, 2009]. Additionally, the liquid H_2 requires continuous cooling to retain its liquid state [Makridis, 2016].

Since the two above mentioned storage technologies are simply based on applying power to the H_2 in order to change its physical properties, they are also applicable for storage of CO_2. From the analysis of the MeOH synthesis it is known that CO_2 and H_2 enter the reactor as gases. Therefore, it is not desirable to make a phase change of the gases in order to store them since they would have to be converted back into gases, which would add unnecessary entropy to the system. Furthermore, the power required to convert H_2 into liquid is as stated earlier higher than compressing it. The compression storage is therefore chosen as the technology used for storing both CO_2 and H_2.

2.3.2 Compressed Storage

In order to store CO_2 and H_2 as compressed gases, the saturation point must be considered. The saturation point is known to be affected both by the temperature and pressure. The density of CO_2 and H_2 as function of the temperature at different pressures may be seen in Figure 2.7.

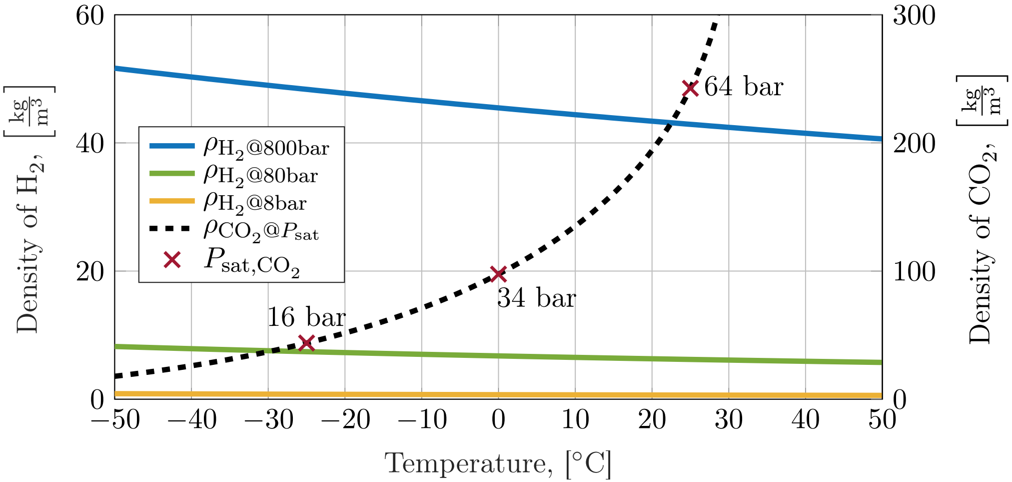

Figure 2.7: Density for CO_2 and H_2 as function of the temperature at different pressures.

From Figure 2.7 it can be concluded that a pressure of 800 bar, within the corresponding temperature range of −50 °C to 50 °C, is not enough to reach the saturation pressure for H_2. Oppositely, CO_2 becomes saturated at much lower pressures, as shown by the dotted line. There are, however, also a relatively large difference in the obtainable densities depending on the pressure. For example, at a temperature of 0 °C the saturation pressure of CO_2 is approximately 34 bar where the corresponding density is approximately twice as large than for H_2 at a pressure of 800 bar. It can therefore be concluded that H_2 requires higher pressure levels to increase its density, compared to CO_2, at a fixed temperature within −50 °C to 50 °C. Contrary, the influence of the temperature for H_2 within the range of −50 °C to 50 °C can be assumed insignificant compared to CO_2, due to the saturation pressure.

The storage is desired to convert the fluctuating production of CO_2 and H_2 into mean flows such that the MeOH synthesis does not operate at partial loading. The three above mentioned processes, being carbon capture, electrolysis and storage, will therefore be analysed as dynamic subsystems in the following Chapter 3 on page 39. The remaining processes, presented in the following sections of this chapter, will be analysed as steady state subsystems in Chapter 4 on page 59.

2.4 Methanol Synthesis

The synthesis of syngases into MeOH can be performed from a various of methods, however, some key components and processes do not vary. A simplified version of the MeOH synthesis subsystem may be seen in Figure 2.8 on the next page. It should be noted that the components used to control the operational conditions are not included since they are dependent on the operation of the key components.

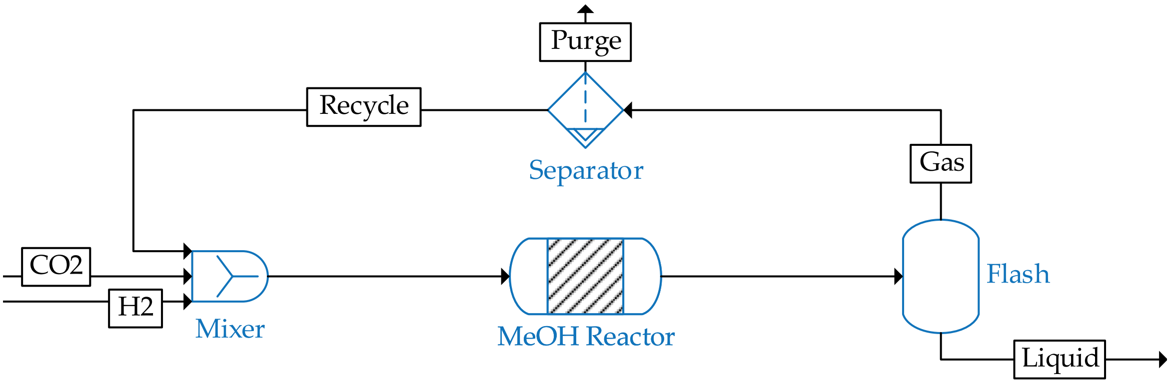

Figure 2.8: Key components in the MeOH synthesis subsystem.

The conceptual idea of MeOH synthesis is to convert CO_2 and H_2 into MeOH in a chemical reactor. The reactor type of choice is a plug flow reactor (PFR) to ensure a continuous flow. Since a complete conversion is unattainable, due to reversibility of the reactions, a separation of the products and excess reactants is required. A suitable separator may be an *equilibrium flash vaporisation separator*, due to its simplicity and low energy requirement, which will be discussed later. From the flash separator, a liquid product can be extracted. The unconverted reactants, which are separated in the flash separator, are recirculated and used once again, by utilising a feedback loop. This is done to optimise the absolute yield of MeOH. Since the overall process utilises a feedback loop it can become a concern that undesired products will accumulate in the subsystem. To avoid this problem a separator is implemented at the feedback loop.

The operation of the flash separator is determined by the vapour-liquid phase equilibrium which is defined by the chemical potential. The chemical potential differences are the driving force for mass transfer from one phase to another phase. When equilibrium is reached the chemical potential of a substance must be the same in all co-existing phases, as described by Eq. 2.13

$$dG = \sum_{i=1}^{N} \left(\phi_{l,i} - \phi_{g,i}\right) \cdot dn_{g,i} = 0 \tag{2.13}$$

where ϕ is the chemical potential, dn is the change in moles, N defines the number of species and the subscripts l and g denotes, liquid- and gaseous states, respectively.

The equilibrium is a function of temperature and pressure. Therefore, the performance of the flash separator is determined by the operational conditions and the composition of the fluid.[Klein and Nellis, 2017] To increase the liquid yield in the flash separator, the temperature should be reduced or the pressure should be increased, however, it must be taken into account that the flash separator is integrated in a closed loop subsystem. Therefore, the optimum operational conditions for the flash separator is not necessarily the optimum for the entire subsystem. A concern regarding the modelling of the MeOH synthesis process, is the PFR. The produced molar flow of MeOH is determined by kinetics, which is empirically determined. The study done by Bussche and Froment [1996] investigated the kinetics in an adiabatic PFR with a catalysed bed consisting of $Cu/ZnO/Al_2O_3$. The data is based on a cylindrical bench scale reactor with an internal diameter of 15.8 mm and a length of 150 mm. It is however known that the kinetics are highly dependent on the system [Fogler, 2016]. Therefore, when up-scaling this reactor, the assumptions suited for the bench scale reactor may no longer be representative, which includes uniform velocity, temperature and pressure in the radial direction. Nonetheless, this data is accepted with the knowledge that it will differ in a commercial plant.

Among others, the MeOH synthesis could be based on the global reactions of the hydrogenation of CO and CO_2 and the reverse water-gas shift (RWGS). However, the study done by Bussche and Froment [1996] assumes CO_2 to be the main supply of carbon in the MeOH synthesis. Therefore, the reaction scheme is defined from the RWGS reaction and the hydrogenation of CO_2 as may be seen in Figure 2.9. It should be noticed the chemical form of MeOH is CH_3OH.

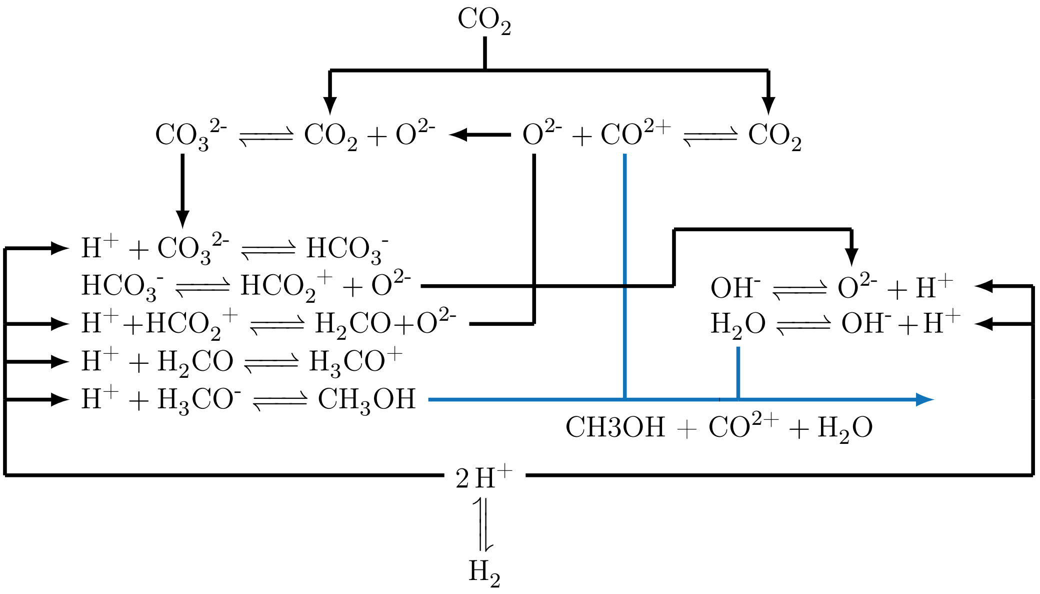

Figure 2.9: MeOH reaction scheme based on hydrogenation of CO_2 and RWGS. Adapted from [Bussche and Froment, 1996].

It may be seen that the right hand side of the reaction scheme defines the RWGS, whereas the left hand side defines the hydrogenation of CO_2. The two global reactions with their belonging heat of formation ire shown below.

$$
\begin{array}{lcllr}
CO_2 + H_2 & \rightleftharpoons & CO + H_2O & \Delta H_{298K} = & 41{,}157\,\frac{kJ}{kmol} \\
CO_2 + 3\,H_2 & \rightleftharpoons & CH_3OH + H_2O & \Delta H_{298K} = & -49{,}316\,\frac{kJ}{kmol}
\end{array}
$$

The study done by Bussche and Froment [1996] defines the rate of reaction for the two global reactions based on the reaction scheme defined in Figure 2.9, as may be seen in Eq. 2.15 and 2.14, respectively

$$
r_{RWGS} = k_1 \cdot \frac{p_{CO_2} \cdot \left(1 - K^{eq}_{RWGS} \cdot \frac{p_{CO} \cdot p_{H_2O}}{p_{CO_2} \cdot p_{H_2}}\right)}{1 + k_{ads,1} \cdot \frac{p_{H_2O}}{p_{H_2}} + k_{ads,2} \cdot \sqrt{p_{H_2}} + k_{ads,3} \cdot p_{H_2O}} \left[\frac{mol}{kg_{cat} \cdot s}\right] \tag{2.14}
$$

$$
r_{MeOH} = k_2 \cdot \frac{p_{CO_2} \cdot p_{H_2} \cdot \left(1 - \frac{1}{K^{eq}_{MeOH}} \cdot \frac{p_{CH_3OH} \cdot p_{H_2O}}{p_{CO_2} \cdot p^3_{H_2}}\right)}{\left(1 + k_{ads,1} \cdot \frac{p_{H_2O}}{p_{H_2}} + k_{ads,2} \cdot \sqrt{p_{H_2}} + k_{ads,3} \cdot p_{H_2O}\right)^3} \left[\frac{mol}{kg_{cat} \cdot s}\right] \tag{2.15}
$$

where p is the partial pressure and K^{eq}_n is the equilibrium constant for the reactions of hydrogenation of CO_2 and RWGS. The correlations of the equilibrium constants may be seen in Eq. 2.17 and 2.16.

$$K^{eq}_{RWGS} = \exp\left(\frac{4,773.26}{T} - 4.67\right) \tag{2.16}$$

$$K^{eq}_{MeOH} = \exp\left(\frac{7,059.73}{T} - 24.39\right) \tag{2.17}$$

Lastly, k_1 and k_2 are the kinetic factors whereas $k_{ads,1}$, $k_{ads,2}$ and $k_{ads,3}$ are the adsorption constants, based on the reaction scheme. They are defined by Arrhenius equation and their corresponding coefficients may be seen in Table 2.2 and 2.3.

Table 2.2: Reaction constants used in the RWGS and hydrogenation of CO_2. R_{gas} is the gas constant.

$k_n = A_{C,n} \cdot \exp(E_{A,n}/(R_{gas} \cdot T))$	A_C	Unit	$E_A \left[\frac{kJ}{kmol}\right]$
k_1	1.22e+7	$\left[\frac{kmol}{kg \cdot s \cdot bar}\right]$	-94,765
k_2	0.001	$\left[\frac{kmol}{kg \cdot s \cdot bar^2}\right]$	36,696

Table 2.3: Adsorption constants used in the RWGS and hydrogenation of CO_2. b_n and B_n are correlation constants.

$k_{ads,n} = \exp(b_n + B_n/T)$	Unit	b	B
$k_{ads,1}$	$[-]$	8.147	-
$k_{ads,2}$	$\left[\left(\frac{1}{bar}\right)^{0.5}\right]$	-0.695	2.068
$k_{ads,3}$	$\left[\frac{1}{bar}\right]$	-23.438	14.929

The kinetics defined by Bussche and Froment [1996] have been validated in the temperature range of 180 °C to 280 °C. Since the hydrogenation of CO_2 is assumed to be the dominating reaction, the MeOH synthesis becomes an exothermic process. As a result it favours a cold environment, of which it is expected that the MeOH reactor should operate at the lower end of the temperature range, to enhance the MeOH yield.[Fogler, 2016] Additionally, the MeOH yield is influenced by the amount of reactants in the subsystem. CO_2 is the limited reactant whereas the concentration of H_2 can be increased, which could influence the reactions due to the increased collision frequency.

From the MeOH synthesis subsystem, the end product could either be purified Green MeOH or other Green chemicals. Therefore, depending on which end product is desired, the processes downstream to the MeOH synthesis will be different, which will further be analysed.

Given the above analysis, the fundamental knowledge of the MeOH synthesis subsystem has been presented. More details on this subsystem and the design specifications of its individual components will be described in the Chapter 4 on page 59.

2.5 Liquid-Liquid Separation of Methanol

From the MeOH synthesis process, a liquid mixture of MeOH and H_2O is produced. Additionally, the remaining unconverted- and intermediate gases are also present in this stream. As presented in Section 2.4, a flash separator could be implemented to separate the gases from the liquid mixture to ensure that the liquid mole fraction of the mixture entering the liquid-liquid separation approaches unity. However, depending on the operating conditions for the MeOH synthesis, it could occur that some gases are not separated and exits along with the MeOH and H_2O. This will be analysed when the modelling of the MeOH synthesis has been conducted, from which it can be concluded if further separation of gases is required before the liquid-liquid separation. Currently, it is assumed that all gases are separated from which the liquid-liquid separation can be analysed.

The purity level of MeOH has a direct influence on the asking price, hence it requires purification if it is the desired end product. As such a liquid-liquid separation is required for the MeOH-H_2O mixture. The following section discusses the best suited separation technique in order to obtain MeOH at high purity and the designing of this technique.

MeOH is an alcohol which contains a hydroxyl group. This enables the MeOH to easily form hydrogen bonds with the hydroxyl groups in H_2O, resulting in the MeOH-H_2O mixture being homogeneous, which is commonly know as a solution.[Dalena et al., 2017]

Numerous separation techniques exists for separating a solution. Due to the mixture being a single-phase solution it excludes techniques using *barriers*, *solid agents* and *separation by external fields* such as centrifugal, thermal or electric forces. This identifies the requirement of phase creation or phase addition in order to separate the two liquids. Phase creation is defined as the conversion of a liquid to vapour which is accomplished by an energy-separation agent, typically in the form of heat transfer. Phase addition is defined as the addition of another phase which is done by a mass-separating agent (MSA), in which the MSA may be partly immiscible with one of the species. However, the MSA option is not applicable in commercial plants since it leads to issues, such as product contamination and the need of additional separators to remove the MSA.[Sorsamäki and Nappa, 2015] This results in phase creation being the most suitable separation technique for the presented application. Phase creation is accomplished by distillation, which will be presented in the following.

2.5.1 Distillation

The concept of distillation is to separate the species of a solution based on the volatility of the individual species, hence the relative volatility is the driving factor. The distillation technique is generally not recommended for a relative volatility below 1.2, as the difficulty in separating the species results in the technique being infeasible [Sorsamäki and Nappa, 2015]. Distillation is carried out by either *flash distillation* or *fractional distillation*. *Flash distillation* is the simplest technique and it is based on producing vapour by boiling the liquid solution and then condensing the vapour without letting any condensed vapour recirculate. This technique is well suited for a solution with a high relative volatility, resulting in the species boiling at widely different temperatures. If the volatility of the species are similar, the resulting liquid- and vapour streams would become less pure.[McCabe et al., 1993]

The relative volatility is determined in order to justify if the flash distillation, and distillation technique in general, is suited for this separation process. The solution for the presented study, is a binary MeOH-H_2O solution, where the relative volatility is defined as shown in Eq. 2.18

$$\alpha_{\mathrm{MeOH,H_2O}} = \frac{(y_{\mathrm{MeOH}}/x_{\mathrm{MeOH}})}{(y_{\mathrm{H_2O}}/x_{\mathrm{H_2O}})} = \frac{K^{eq}_{\mathrm{MeOH}}}{K^{eq}_{\mathrm{H_2O}}} \tag{2.18}$$

where y_n is the molar fraction in the vapour. By assuming the solution to be an ideal mixture, Raoult's law can be applied as shown in Eq. 2.19

$$\alpha_{\mathrm{MeOH,H_2O}} = \frac{K^{\mathrm{eq}}_{\mathrm{MeOH}}}{K^{\mathrm{eq}}_{\mathrm{H_2O}}} = \frac{P_{\mathrm{sat,MeOH}}}{P_{\mathrm{sat,H_2O}}} \tag{2.19}$$

where P_{sat} is the temperature dependent saturation pressure.[Halvorsen, 2001] The resulting relative volatility of this solution is shown in Figure 2.10.

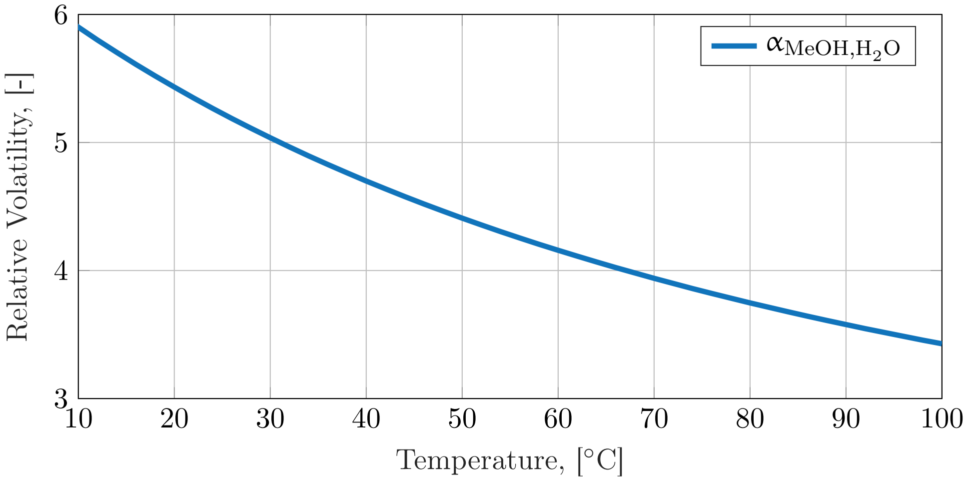

Figure 2.10: Relative volatility of the binary MeOH-H_2O solution as function of temperature.

From Figure 2.10 it becomes evident that the relative volatility is above the advised minimum value of 1.2, hence the distillation technique is deemed suitable. The relative volatility of the binary MeOH-H_2O solution drops as function of temperature, as shown in Figure 2.10, indicating that this separation is theoretically easier at lower temperatures. The pressure also varies depending on the temperature, hence if the distillation column operates at 20 °C the corresponding pressure must be somewhere in between the saturation pressure range of MeOH and H_2O to separate this solution. This is due to that the boiling point of a binary solution depending on the boiling point of the two species as well as the composition of the solution [Klein and Nellis, 2017]. The saturation pressure of MeOH and H_2O at 20 °C is 12.7 kPa and 2.3 kPa, respectively. However, by performing vacuum distillation, i.e. distillation under reduced pressure, the capital expenses (CAPEX) increases due to the need of more robust materials and an additional pump, among others, compared to if it operated at atmospheric pressure. This results in the necessity of performing a preliminary optimum study, due to the trade-off between operational expenses (OPEX) and CAPEX [Luyben, 2016][Cui et al., 2018]. Usually, the operating pressure of a distillation column for a MeOH-H_2O binary solution, is 110 kPa [Cui et al., 2017b][Cui et al., 2017a]. At this pressure the corresponding boiling point for MeOH and H_2O is 67.1 °C and 102.3 °C, respectively. The boiling point of the solution is somewhere within this range, corresponding to the relative volatility being within approximately 3.4 to 4, according to Figure 2.10. Given the constraint of a relative volatility of 1.2 being satisfied, the distillation technique is suitable. However, as mentioned two different techniques are available where flash distillation is the simplest. It is therefore analysed if separation by flash distillation can achieve a sufficient purity of MeOH, otherwise fractional distillation is required.

2.5.2 Flash Distillation

A sensitivity analysis for the flash distillation is conducted to determine if this technique is suitable. Ideally the produced distillate stream will consist solely of MeOH and the bottom will consists solely of H_2O, due to the MeOH being the most volatile species. The crude MeOH produced from a MeOH synthesis typically contains about 30 wt% to 40 wt% H_2O [Bertau et al., 2014]. The sensitivity analysis has been conducted for this feed composition range, with a 5 wt% increment. The temperature has been varied from 71 °C to 82 °C, since this is the approximate boiling point of the mixture at a pressure of 110 kPa. The results corresponding to a feed composition of 70 wt % MeOH and 30 wt% H_2O, is illustrated in Table 2.4. The two other feed compositions may be seen in Appendix A.

T	$MeOH_D$	$MeOH_B$	H_2O_D	H_2O_B	$MeOH_D$	$MeOH_B$	Recovery
[°C]	$\left[\frac{kg}{s}\right]$				[wt%]		
71	0.00	0.70	0.00	0.30	0.00	70.00	0.00
72	0.10	0.60	0.01	0.29	88.22	67.59	14.75
73	0.25	0.45	0.04	0.26	86.64	63.17	36.01
74	0.36	0.34	0.06	0.24	85.04	58.81	51.83
75	0.45	0.25	0.09	0.21	83.39	54.54	63.83
76	0.51	0.19	0.12	0.19	81.71	50.41	73.07
77	0.56	0.14	0.14	0.16	79.97	46.43	80.28
78	0.60	0.10	0.17	0.13	78.17	42.64	85.99
79	0.63	0.07	0.20	0.10	76.31	39.06	90.55
80	0.66	0.04	0.23	0.07	74.36	35.68	94.25
81	0.68	0.02	0.26	0.04	72.34	32.50	97.28
82	0.70	0.00	0.30	0.00	70.00	0.00	100.00

Table 2.4: Mass flow outputs from the flash distillation at different temperatures. The distillate is denoted D, whereas the bottom is denoted B. The mass fractions of the input is 70 wt% MeOH and 30 wt% H_2O.

From the sensitivity analysis it can be concluded that the feed composition with the highest MeOH content, yields the highest MeOH purity in the distillate stream. From Table 2.4 it can also be concluded that the maximum achievable purity of MeOH is 88.22 wt% with a feed composition of 70 wt % and 30 wt% of MeOH and H_2O, respectively. It should however be noted that only 14.75 wt% of the MeOH is recovered in the distillate stream. If instead 90 wt% of the MeOH was to be recovered, the corresponding purity would be approximately 76 wt%. However, the composition of the underflow would then consist of approximately 39 wt% MeOH and 61 wt% H_2O, resulting in the necessity to clean this stream prior to disposing it. From the sensitivity analysis it may be concluded that the feed composition affects the achievable purity in the distillate stream. As such the purity could be further increased by numerous successive flash distillers. However this method is inefficient and infeasible when nearly pure species are desired [McCabe et al., 1993].

The minimum purity requirement for commercial MeOH is 99.85 wt% to fulfil the ASTM purity grades: A, AA, and IMPCA. The difference in the grades depend on content restrictions regarding specific impurities, such as ethanol, acetone etc. [Ullmann et al., 2011]. Furthermore, the IMPCA purity grade requirement for MeOH is also used in studies relating to the use of MeOH in biodiesel [Winther, 2019]. This clearly indicates that the flash distillation is not suitable for the separation of the MeOH-H_2O solution, due to the nearly pure requirement for commercial MeOH. Instead, fractional distillation will be utilised.

2.5.3 Fractional Distillation

Contrary to flash distillation, the fractional distillation returns a fraction of the condensed liquid which comes into contact with the rising vapour. The phases come into contact on either plates or packing beds inside the distillation column, where the choice depends on the diameter of the distillation column. For plate columns, the vapour partly condenses as it hits the plate, due to the lower temperature of the plate. This releases energy of which a fraction of the liquid vaporises, resulting in an enrichment of MeOH in the vapour phase and likewise for H_2O in the liquid phase. This leads to the purity being enhanced as the number of plates increases. A schematic of a fractional plate distillation column is shown in Figure 2.11.

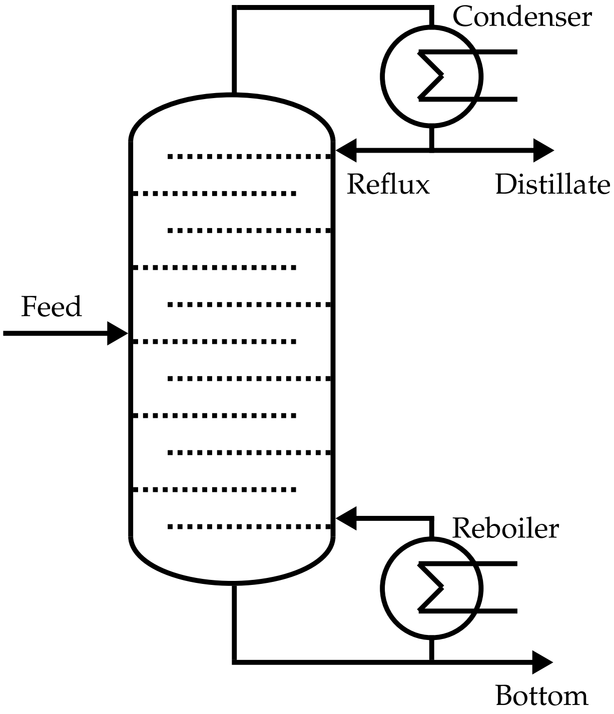

Figure 2.11: Fractional distillation where the internals consist of plates.

In contrary to plate columns, the packed column provides a continuous contact between the liquid and vapour between the top and bottom of the packed bed. The liquid wets the surface of the packing while the vapour passes across the wetted packing, leading to mass transfer. This results in the necessity of well distributed liquid throughout the column to achieve efficient performance. There are two general types of column packings, being random and structured. Random packing consists of numerous small pieces in sizes ranging from 0.015 m to 0.1 m which are loaded into the column, such that they are randomly arranged. Structured packing is often constructed as blocks with numerous layers of sheets or meshes within. The structured packing enables a uniform spreading of the vapour and liquid in the cross-section of the column. The structured packing outperforms the random packing on both reducing the pressure drop throughout the column and achieving better separation efficiencies at lower packed bed heights. However, the structured packing is also more expensive than the random packing of which the random packing is preferred if the packed column operates in an environment that rapidly degrades the packing, such as in corrosive applications.[Pilling and Holden, 2009] This is however not the case in the presented study of which the structured packing is used if packed columns are utilised. A schematic of a structured packed column is shown in Figure 2.12.

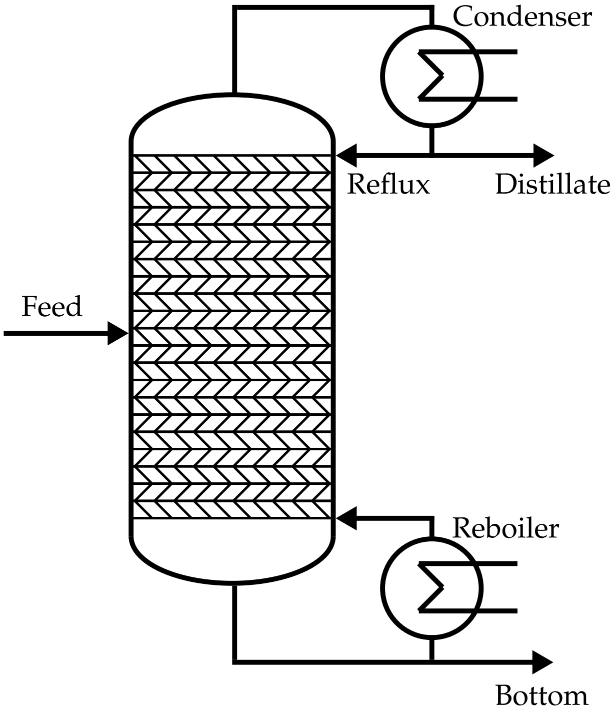

Figure 2.12: Fractional distillation where the internals consist of structured packing.

The designing of the distillation column is done through a process design followed by a mechanical design. The objective of the process design is to determine the number of theoretical plates and the reflux ratio. The mechanical design covers the choice of either plates or packed beds and the determination of column height and diameter. The process design is based on theoretical models, while the choice of the mechanical design is based on practical aspects. Both design processes will be presented in the following.

Process Design

The process design is used to acquire an initial estimation of the number of plates and the corresponding reflux ratio. The difficulty in performing a process design depends mainly on the number of species in the feed- and output streams. An example of a distillation process where numerous species are present in the feed- and output streams is in petroleum refining processes. For such a distillation process, the designing is performed by the analytic Fenske, Underwood and Gilliland (FUG) method [Mamudu et al., 2019]. However, the FUG method is quite comprehensive, where numerous calculations are required [García et al., 2017]. However, if the mixture is binary the graphical McCabe-Thiele method is suitable, which is easier to perform compared to the FUG method. The McCabe-Thiele method is a commonly used tool, which is based on the following assumptions: The mixture is binary, the heat of vaporisation of the two species are equal and 100 % stage efficiency is imposed [Neutrium.net, 2017]. However, it is known that the second assumption is violated since the relative difference in heat of vaporisation is approximately 15 %. Nonetheless, the McCabe-Thiele method is further used as an initial prediction of the process design, from which further adjustments can be done. This method uses the vapour-liquid equilibrium (VLE) curve to determine the number of theoretical plates to achieve the desired degree of separation. The VLE curve is based on data at operational conditions. The liquid equilibrium is a 45 ° line drawn from molar fraction 0 to 1, as shown in Figure 2.13. At this line the relative volatility is 1, as separation by use of distillation is only possible if the difference in volatility is non-zero. The vapour equilibrium curve of an ideal mixture is formulated in Eq. 2.20 [Ullmann et al., 2011].

$$y = \frac{\alpha \cdot x}{1 + (\alpha - 1)} \tag{2.20}$$

Figure 2.13 shows a schematic of the McCabe-Thiele diagram, where a relative volatility of 3.5 is used. The VLE curve is based on the most volatile species in the solution, MeOH, where the molar fraction of the vapour is plotted as function of the molar fraction of the liquid.

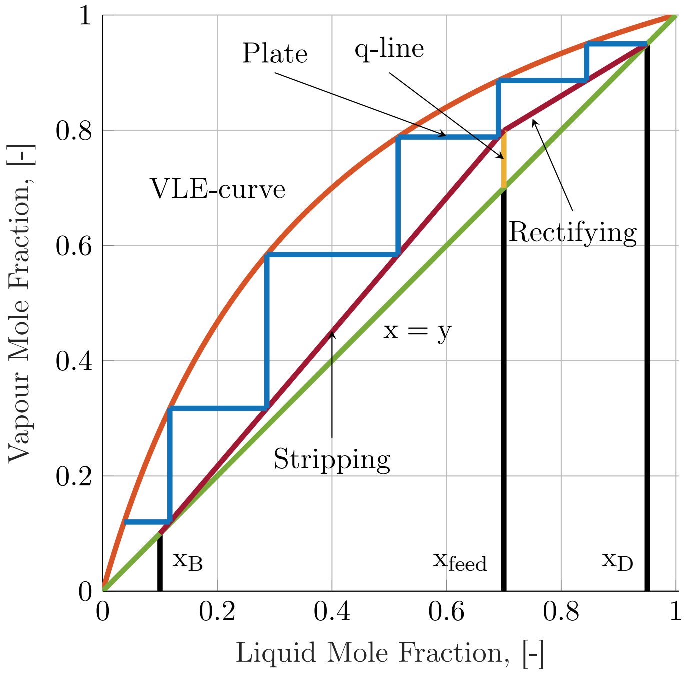

Figure 2.13: Conceptual representation of McCabe-Thiele diagram with a relative volatility of 3.5.

In Figure 2.13, the desired composition of the distillate and the bottom product is marked as x_D and x_B, respectively. The feed composition is marked as x_{feed}. This composition is controlled by the overall system, since the distillation column is the last subsystem in System 1. The slope of the q-line depends on if the feed is a liquid, a vapour or a two-phase mixture. The slope is determined by Eq. 2.21.

$$\text{slope}_{\text{q-line}} = \frac{x}{x - 1} \tag{2.21}$$

According to Eq. 2.21, if the feed is a liquid the q-line will become vertical, whereas it becomes horizontal if the feed is a vapour. The operational line in the rectifying section, denoted Rectifying in Figure 2.13, is drawn from the point x_D to the intersection with the q-line. This operational line is formulated by Eq. 2.22

$$y = \frac{R}{R + 1} \cdot x + \frac{x_D}{R + 1} \tag{2.22}$$

where R is the external reflux ratio defined by Eq. 2.23

$$\mathrm{R} = \frac{\dot{n}_{\mathrm{L}}}{\dot{n}_{\mathrm{D}}} \tag{2.23}$$

where the subscripts L and D denote the liquid stream returning to the column and the distillate stream, respectively. The higher the reflux ratio the fewer equilibrium plates are required, but this also increases the energy demand. A reflux ratio can be chosen freely, where two extreme cases exist, referred to as total reflux and minimum reflux. The total reflux is when the operational line, denoted Rectifying in Figure 2.13 on the previous page, intersects with the q-line at point x_{feed}. This yields the lowest number of theoretical plates, however, no distillate is produced as it is all returned to the column. The minimum reflux is when the intersection of the operation line on the q-line is at the equilibrium curve. This results in the necessity of infinite plates in order to accomplish the separation. The operating line in the stripping section is then drawn from the intersection point of the q-line to the point x_{B}.

The number of theoretical plates can be determined by counting the number of times the horizontal steps touches the VLE curve, counting from x_{D} to x_{B}. From this procedure it can be concluded that there is a correlation between the number of theoretical plates and reflux ratio, where the choice of this combination is essential from an economical point of view. This is due to the reflux ratio influencing the OPEX and the number of plates impacts the CAPEX

Mechanical Design

The purpose of the mechanical design is to select either plates or packing as the internals and calculate the height and diameter of the column. The choice of column internals is often based on the column diameter, where packing is preferred for smaller columns where the diameter is below 1 m, while plates are mainly used in larger columns where the diameter is above 1 m. Not only are packed columns more feasible compared to plate columns at small diameters, but the accessibility of plate columns at these diameters are also limited which results in difficulties when installing or maintaining the plates.[Ibrahim, 2014] This concludes that packing will be used if the diameter of the column is less than 1 m and plates are utilised if the diameter is greater than 1 m. Since the height and diameter are determined differently for the plate- and packed column, the mechanical design must be performed by both procedures in order to determine which are best suited, from the resulting diameters.

Plate Column

In order to determine the height of the plate column, the number of actual plates must firstly be defined. The actual number of plates is determined by performing the process design which estimates the number of theoretical plates, from which the number of plates are increased to correct for non-ideal conditions. The height of the column between the top plate and the bottom plate is proportionally increasing as function of the number of actual plates, where the proportionality factor is the plate spacing. For reasons of accessibility the minimum plate spacing is within the range of 0.45 m to 0.60 m, depending on the diameter of the column. Greater plate spacing results in lower column diameter, which will be presented afterwards, however it increases the height of the column. As such an economical trade-off needs to be considered between the column height and diameter.[Ibrahim, 2014] In general the plate spacing is dependent on the diameter of the column, where:

- Plate spacing = 0.45 m for column diameter less than 1.5 m
- Plate spacing = 0.60 m for column diameter in the range of 1.5 m to 6.0 m
- Plate spacing = 0.75 m for column diameter greater than 6.0 m

Due to practical aspects, an additional 1.22 m is added, to the column height, above the top plate in order to keep liquid from entering the condenser. Furthermore, an additional 3.05 m is added to the column height, below the bottom plate, in order to ensure sufficient surge capacity. From this the total column height can be determined.[Seader et al., 2011] A maximum height of 53 m is recommended, due to wind load and foundation considerations [Coker, 2007]. If the estimated height of the distillation column extends 53 m, either the plate spacing must be reduced which would reduce the height, or the single column must be split into multiple smaller distillation columns in series.

Proper dimensioning of the column diameter is crucial, since it influences the plate efficiency, pressure drop throughout the column and the performance in general. In order for the distillation column to operate efficiently, the following conditions must be fulfilled:

- The liquid flows from plate to plate only at the downcomers, which is located at the periphery of the plate.
- The liquid does not weep through the gaps in the plates.
- The liquid is not carried by the vapour to the plate above.
- The vapour only flows through the gaps of the plate.
- The vapour is not carried down by the liquid in the downcomers.

These criteria can be fulfilled by dimensioning the diameter of the column in accordance to the vapour flow rate. Weeping will occur if the vapour flow rate is insufficient. Oppositely, if this flow rate is too great the vapour will carry the liquid to the above plate. The general design procedure is to estimate the maximum allowable vapour velocity, and thereby reduce it by 20 wt% as a safety factor.[Seader et al., 2011] The maximum allowable vapour velocity is defined by the Sounders-Brown equation shown in Eq. 2.24

$$v_{\mathrm{max}} = C \cdot \sqrt{\frac{\rho_{\mathrm{L}} - \rho_{\mathrm{V}}}{\rho_{\mathrm{V}}}} \tag{2.24}$$

where C is the capacity factor, ρ is the density and the subscripts L and V denotes the liquid and vapour streams, respectively. The capacity factor can be determined theoretically, where numerous factors are included such as the droplet diameter and the drag coefficient. However, it is usually obtained from correlations based on empirical data acquired from experiments. Different factors are included depending on the chosen correlation, where a well known and often used capacity correlation is the Fair's capacity (C_{F}) as shown in Figure 2.14 on the next page.[Stichlmair, 2010]

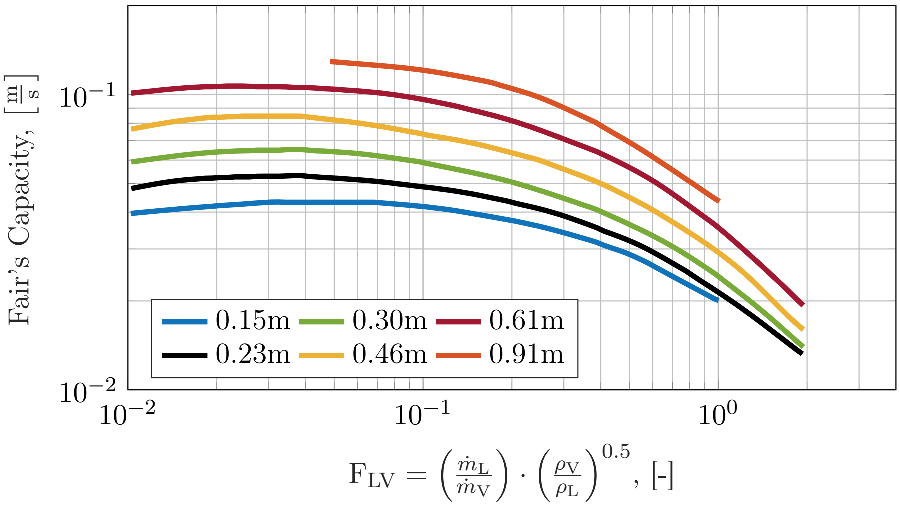

Figure 2.14: Fair's capacity correlation for different plate spacings as function of the liquid-vapour flow factor, $\mathrm{F_{LV}}$. Adapted from Stichlmair [2010].

The value estimated in Figure 2.14 depends on the plate spacing and the liquid-vapour flow factor ($\mathrm{F_{LV}}$), as shown in Eq. 2.25

$$\mathrm{F_{LV}} = \frac{\dot{m}_\mathrm{L}}{\dot{m}_\mathrm{V}} \cdot \sqrt{\frac{\rho_\mathrm{V}}{\rho_\mathrm{L}}} \tag{2.25}$$

where $\dot{m}$ is the mass flow. The value for the capacity factor C in Eq. 2.24 on the preceding page is defined from Fair's capacity, estimated by Figure 2.14, and correction factors as shown in Eq. 2.26

$$C = \mathrm{F_{ST}} \cdot \mathrm{F_F} \cdot \mathrm{F_{HA}} \cdot \mathrm{C_F} \tag{2.26}$$

where $\mathrm{F_{ST}}$ is the surface tension correction factor, $\mathrm{F_F}$ is the foaming correction factor and $\mathrm{F_{HA}}$ is the "Hole-to-active area" ratio correction factor.

Figure 2.14 is based on a subsystem where the surface tension of the liquid is 0.02 N/m. If the surface tension of the actual subsystem differs from this value, the capacity factor must be corrected according to Eq. 2.27

$$\mathrm{F_{ST}} = \left(\frac{\sigma_\mathrm{L}}{0.02}\right)^{0.02} \tag{2.27}$$

where σ is the surface tension of the liquid stream. The presence of foam in distillation columns results in pressure drops and reduced mass transfer. $\mathrm{F_F}$ adjusts for this effect, whereas it is unity for non-foaming subsystems and between 0.5 to 0.75 for foaming subsystems. Chen et al. [2007] investigated the foaming effect of a MeOH-H_2O solution in a distillation column. The study concluded through empirical data, that no foaming took place if the MeOH concentration was 50 wt% or above, however, foaming was observed for MeOH concentration of 30 wt%. This results in the necessity of further investigating the foaming behaviour when the actual composition of the solution is known. The remaining correction factor from Eq. 2.26 is $\mathrm{F_{HA}}$, which is calculated from the ratio of vapour hole area, A_h, to the plate surface area, A_a.

$$\begin{aligned} \mathrm{F_{HA}} &= 1.0 \quad \text{for} \quad A_\mathrm{h}/A_\mathrm{a} \geq 10\,\% \\ \mathrm{F_{HA}} &= 0.9 \quad \text{for} \quad A_\mathrm{h}/A_\mathrm{a} = 8\,\% \\ \mathrm{F_{HA}} &= 0.8 \quad \text{for} \quad A_\mathrm{h}/A_\mathrm{a} = 6\,\% \end{aligned}$$

The ratio of $A_\mathrm{h}/A_\mathrm{a}$ is typically in the range of 5 % to 15 %. A low hole area percentage allows higher efficiency for the plate, however, it comes at the expense of increased pressure drop. As such, the hole area percentage of the plate is chosen depending on the operating conditions of the distillation column, whereas the typical ranges are 5 % to 10 % for pressure levels relatively close to ambient pressure and 10 % to 16 % for vacuum. [SeperationTechnology.com, 2012] [Chuang and Nandakumar, 2000] Since the operational pressure is 110 kPa, as presented in 2.5.1 on page 24, a hole area ratio of 8 % is chosen of which the corresponding value for $\mathrm{F_{HA}}$ becomes 0.9.

With the definition of all the parameters in Eq. 2.24 on page 31 made, the maximum allowable vapour velocity can be calculated. Given the maximum vapour velocity, the corresponding diameter can be determined from the continuity equation as seen in Eq. 2.28

$$D = \left(\frac{4 \cdot \dot{m}_\mathrm{V}}{\mathrm{f} \cdot \pi \cdot v_\mathrm{max} \cdot \left(1 - \frac{A_\mathrm{d}}{A_\mathrm{tot}}\right) \cdot \rho_\mathrm{V}} \right)^{0.5} \tag{2.28}$$

where f is the flooding factor, A_tot is the total column cross-sectional area and A_d is the cross-sectional area of the downcomer. The ratio $A_\mathrm{d}/A_\mathrm{tot}$ in Eq. 2.28 is estimated by the liquid-vapour flow factor, outlined in [Seader et al., 2011], to be:

$$\begin{array}{lll} A_\mathrm{d}/A_\mathrm{tot} = 0.1 & \text{for} & \mathrm{F_{LV}} \leq 0.1 \\ A_\mathrm{d}/A_\mathrm{tot} = 0.1 + \frac{\mathrm{F_{LV}} - 0.1}{9} & \text{for} & 0.1 < \mathrm{F_{LV}} < 1.0 \\ A_\mathrm{d}/A_\mathrm{tot} = 0.2 & \text{for} & \mathrm{F_{LV}} \geq 1.0 \end{array}$$

This concludes the mechanical design procedure for plate columns. The following presents the mechanical design procedure for fractional distillation utilising packed columns.

Packed Column

The packed column has continuous contact with liquid and vapour throughout the column, however, it is analysed in the mechanical design procedure as being a segmented column. The packed portion of the column is divided into segments of equal height. The height of these segments are known as the height equivalent to a theoretical plate (HETP). The height of the column can then be calculated by the number of equilibrium plates and the HETP-value, as shown in Eq. 2.29

$$\mathcal{L} = \mathrm{N_{eq}} \cdot HETP \tag{2.29}$$

where $\mathrm{N_{eq}}$ is the number of theoretical equilibrium plates. The number of theoretical equilibrium plates is determined from the McCabe-Thiele method, as earlier presented. The HETP-value is measured experimentally and it varies with the packing type, size and vapour flow rate. It is however known that most packings of the same size have approximately the same HETP-value, leading to a simplified estimation of the HETP-value as shown in Eq. 2.30

$$HETP = \frac{100}{a_\mathrm{p}} + 0.10 \tag{2.30}$$

where a_p is the surface area per volume of packing. Eq. 2.30 is, however, restricted to low viscous fluids at low to moderate pressure. This results in corrections to the HETP-value if the liquid dynamic viscosity is above 0.04 Pa · s, however, this is not necessary in the presented study since the viscosities of H_2O and MeOH are in the order of $0.001\,\mathrm{Pa \cdot s}$. A typical HETP-value for industrial applications is within 0.3 m to 0.6 m.[Wankat, 2012] An investigation of the market for structured packings will be performed, in order to determine which packing is best suited and estimate a realistic value of a_p.

There are numerous manufacturers of structured packings who all have different products depending on the customer's needs. A well-known manufacturer of packing is the Swiss company 'Sulzer', who likewise have multiple products. These products are designed to operate at specific conditions, for instance in corrosive- or reactive environments, or at vacuum pressure or pressurised conditions. None of these conditions are however present in the presented study, since the feed stream consists of a MeOH-H_2O solution and the distillation column operates at 110 kPa. Hence, the "Mellapak" packing is chosen, which according to Sulzer, is an 'all-rounder' packing, which is typically used in refinery applications, operating from vacuum to moderate pressure [Sulzer, 2021b].

There exists numerous types of the Mellapak packing where an example is the "Mellapak 250.Y" and "Mellapak 250.X" [Sulzer, 2021a]. The conventional notation of the type includes two geometric indicators, the first is a number that specifies the a_p value, which can range from $2\,\mathrm{m^2/m^3}$ to $750\,\mathrm{m^2/m^3}$ [Sulzer, 2021a]. The second is the channel flow angle relative to horizontal, where Y and X denotes values of 45 ° and 60 °, respectively [Lassauce et al., 2014]. The general trade-off in the performance of packing is in the relation between the HETP-value and pressure drop. The HETP-value describes the efficiency of the packing where a high efficiency yields a low HETP-value. It is typically the a_p value shown in Eq. 2.30 on the previous page which is increased if the objective is to enhance the efficiency, however, by increasing a_p the pressure drop rises as well. The pressure drop depends both on the a_p value and the flow conditions, where a general allowable pressure drop in packed columns are $1\,\mathrm{kPa/m}$.[Lassauce et al., 1994] This results in the necessity to acquire experimental results in order to determine the most feasible packing type. However, the Mellapak 250.Y is widely used in industrial applications and Yang et al. [2003] used this packing for a MeOH-H_2O solution. As such the Mellapak 250.Y is utilised even though a more feasible alternative might be available.

Similar to the height of the column, the diameter of this packed bed column must also be determined. This is done as described by Towler and Sinnott [2008]. The vapour mass flow rate per unit column cross-sectional area is determined of which it can be used to calculate the required diameter corresponding to this mass flow. However, in order to determine this mass flow, a correlation factor $\mathrm{F_{pack}}$ is required to be determined as may be seen in Eq. 2.31

$$\dot{m}_\mathrm{V}^\star = \left(\frac{\mathrm{F_{pack}} \cdot \rho_\mathrm{V} \cdot (\rho_\mathrm{L} - \rho_\mathrm{V})}{13.1 \cdot a_\mathrm{p} \cdot \left(\frac{\mu_\mathrm{L}}{\rho_\mathrm{L}} \right)^{0.1}} \right)^{0.5} \tag{2.31}$$

where μ is dynamic viscosity. In order to determine $\mathrm{F_{pack}}$ the liquid-vapour flow factor, $\mathrm{F_{LV}}$, is calculated and used in Figure 2.15 on the next page. Furthermore, the pressure drop must also be determined, where it should be noted that values above 0.8 kPa or below 0.08 kPa, should be avoided to prevent flooding or attain sufficient liquid distribution, respectively.

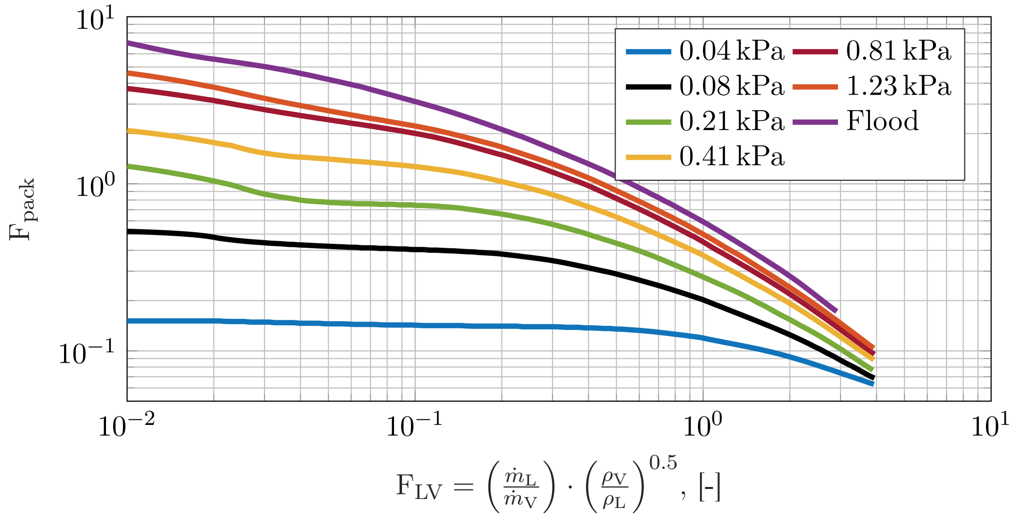

Figure 2.15: Factor, F_{pack}, at various liquid-vapour flow factor values, F_{LV}, and pressure drop curves. Adapted from Towler and Sinnott [2008].

Given F_{pack}, the vapour mass flow rate per unit column cross-sectional area can be calculated from which the required column diameter can be determined as Eq. 2.32.

$$D = \sqrt{\frac{4}{\pi} \cdot \frac{\dot{m}_V}{\dot{m}_V^{\star}}} \tag{2.32}$$

The above section concludes the general procedure in performing the designing of the fractional distillation column. Depending on the input stream to the distillation, which will be determined from the MeOH production outlined in Chapter 4 on page 59, it can be determined from the knowledge presented in the above analysis, which internal of the fractional distillation column should be utilised. The designing of the actual distillation column and its performance will be presented in Chapter 4.

2.6 Methanol to Alternative Products

MeOH may either be used as an end product or as an intermediate in the production of other chemicals, as was outlined in Chapter 1. As an end product the MeOH is primarily used in the transport- and chemical sector where the applications of MeOH are versatile. The MeOH is used in the transport sector either as a direct fuel blending or as a raw material to produce fuel additives such as MTBE. MTBE has a high octane number of which it can replace other currently used additives in gasoline fuels, hence reducing pollution [Bertau et al., 2014]. Back in the 1980s, the M15 (15 vol% MeOH to gasoline) fuel blend was chosen to be the optimal blend concentration, since this is the highest concentration that can be introduced with little modification required in the fuel system of the vehicles [methanol.org, 2014]. Commercial interest of M15 has since increased, especially in China, where the number of provinces that have been commercialising M15 blends are 26 out of 31 provinces [Bertau et al., 2014]. China is the main consumer of MeOH, accounting for around 40 wt% of the global market in 2010, where a third of this MeOH was used in the fuel consumption, representing about 5 wt% of China's fuel pool [methanol.org, 2020].

If MeOH is used as an intermediate it may instead be converted to other chemicals, such as benzene, toluene and xylene (BTX). These three chemicals are all light Aromatic hydrocarbons, which are used extensively in the chemical industry to produce polymers, fibres, pesticides and pharmaceuticals.[Li et al., 2017][Gong et al., 2021]

Currently BTX is mainly produced from carbon sources which are not carbon neutral, such as coal and methane [Ren et al., 2020][Lunsford, 2000]. However, with the overall increased interest in converting the global society to rely on Green products, the need for producing Green BTX presents itself, which must be produced from carbon neutral sources.

Further incentive to produce BTX is that the feed stream may not be restricted to be pure MeOH. Multiple studies have been conducted regarding the conversion of Ethanol to BTX, where the conclusion has been that the influence of H_2O in the reaction had no influence on the conversion rate or the product distribution. Since Ethanol and MeOH are relatively similar this assumption is assumed to also be valid for the MeOH to BTX conversion.[Hannon et al., 2019] Therefore, since the input stream consists of a mixture of H_2O and MeOH, it may become unnecessary to perform the otherwise energy expensive distillation needed if MeOH is the desired end product.

Yet, the production of Green BTX must be profitable to achieve market and consumer interest. Hence, it becomes necessary to conduct a techno-economic analysis between the most profitable end products, being either MeOH or BTX. To do so the production of BTX must, similar to the MeOH, be analysed to obtain information about the conversion rate and energy requirements of such a subsystem. A study done by Na et al. [2018] investigated the BTX synthesis based on MeOH. A schematic of their subsystem may be seen in Figure 2.16.

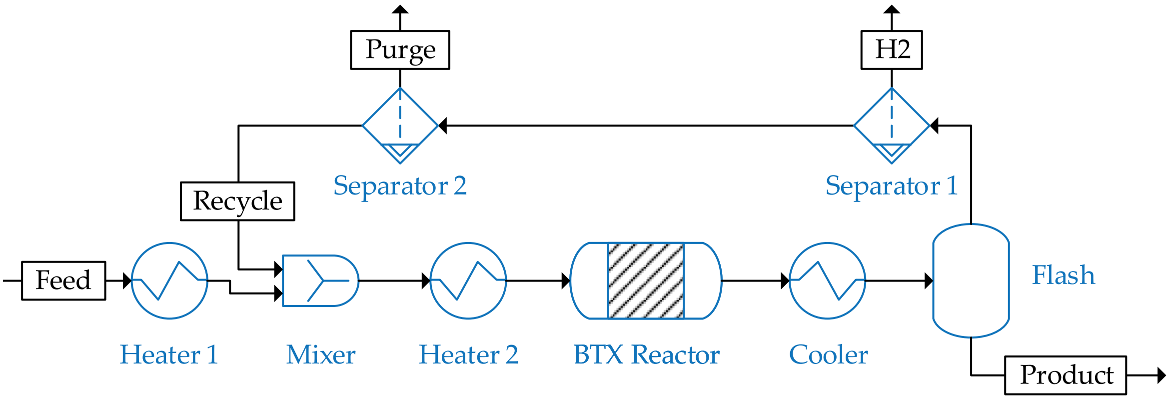

Figure 2.16: Schematic of the BTX synthesis subsystem, based on Na et al. [2018].

Similar to the MeOH synthesis, a feedback loop is incorporated in order to increase the product yield. The subsystem consists further of a flash separator and two separators. The purpose of the flash is to separate the unconverted reactants from the products in order to recycle them. The first separator, separates the excess H_2 from the feedback stream. The latter excess stream, can be assumed to only consist of H_2, from which it could be recycled back to the MeOH synthesis, since H_2 is a valuable reactant. Due to the feedback loop, there is a concern that the undesired products could accumulate in this subsystem. To avoid this problem the second separator is implemented. The last major component in this subsystem is the reactor where different reactors can be utilised. The production of BTX may be achieved using either fluidised-bed and fixed-bed reactors. Problems, such as rapid catalyst deactivation due to high temperatures in the fluidised-bed reactor, and back-mixing of gases and undesired side reactions in the fixed-bed reactor, are observed.[Wang et al., 2014] To overcome these problems much research has gone into the operating conditions and the catalyst used.[Li et al., 2017][Gong et al., 2021]

The catalysts generally used consist of ZSM-5 zeolite, which can be modified with Zinc, Silver or Gallium, thereby promoting the production of BTX.[Gong et al., 2021] During the production of BTX, numerous intermediates and other by-products are produced leading to complex reaction schemes. This has lead to two approaches in the research where the reactions are either described individually with their respective kinetics or by lumping the kinetics of similar components, thereby representing a macroscopic reaction scheme.[Wang et al., 2019][Mihail et al., 1983] By lumping the kinetics, the number of reactions can be reduced from over 50 reactions to mere 10 reactions, thereby greatly simplifying the process.[Mihail et al., 1983]

The reactions chosen to describe the BTX production in the presented study is obtained from a study by Na et al. [2018], who lumped the kinetics to a total of 13 reactions, which includes the production of Light Gases, Olefin, Alkanes, Aromatics and Heavy aromatics. A reaction diagram of these lumped products may be seen in Figure 2.17.

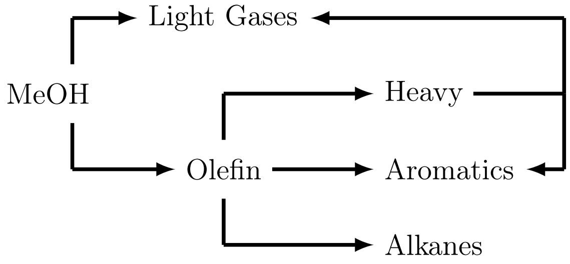

Figure 2.17: Reaction diagram of MeOH to Light Gases, Olefin, Heavy, Aromatics and Alkanes.[Na et al., 2018]

The 13 reactions occurring in the conversion of MeOH are as listed in Table 2.5.

Table 2.5: MeOH conversion to Light Gases, Olefin, Alkanes, Aromatics and Heavy, with corresponding pre-exponential factors and activation energies. Furthermore, the exponents represent the order of reaction for the corresponding species.[Na et al., 2018]

Category	Reaction	$A_C \left[\frac{kmol}{kg \cdot h}\right]$	$E_A \left[\frac{kJ}{kmol}\right]$
Light Gases	$3\,[CH_3OH]^2 \rightarrow CO + CO_2 + CH_4 + 4\,H_2$	5,804.84	52,616.98
Olefin	$3\,[CH_3OH]^2 \rightarrow C_3H_6 + 3\,H_2O$	405.71	22,546.73
Alkanes	$2\,[C_3H_6]^2 + 3\,[H_2]^0 \rightarrow 3\,C_2H_6$	2.34	34,357.66
	$[C_3H_6]^2 + [H_2]^0 \rightarrow C_3H_8$	37.78	
	$4\,[C_3H_6]^2 + 3\,[H_2]^0 \rightarrow 3\,C_4H_{10}$	98.38	
	$5\,[C_3H_6]^2 + 3\,[H_2]^0 \rightarrow 3\,C_5H_{12}$	182.51	
	$2\,[C_3H_6]^2 + [H_2]^0 \rightarrow C_6H_{14}$	92.20	
Aromatics	$2\,[C_3H_6]^2 \rightarrow C_6H_6 + 3\,H_2$	89,598.98	83,317.18
	$7\,[C_3H_6]^2 \rightarrow 3\,C_7H_8 + 9\,H_2$	701,035.63	
	$8\,[C_3H_6]^2 \rightarrow 3\,C_8H_{10} + 9\,H_2$	1,392,565.70	
	$3\,[C_3H_6]^2 \rightarrow C_9H_{12} + 3\,H_2$	644,002.22	
Heavy	$10\,[C_3H_6]^2 \rightarrow 3\,C_{10}H_{14} + 9\,H_2$	249.52	42,759.35
	$[C_{10}H_{14}]^1 + 2\,[H_2]^0 \rightarrow C_8H_{10} + 2\,CH_4$	520.78	93,000.05

As shown in Figure 2.17 on the previous page and further also in Table 2.5 on the preceding page MeOH is converted to Light Gases and an Olefin. The Olefin serves as the reactant for all consecutive Alkanes, Aromatics and Heavy reactions. The Aromatics include benzene, toluene, xylene and 1,2,4-Trimethylbenzene, denoted C_6H_6, C_7H_8, C_8H_{10} and C_9H_{12}, respectively. These Aromatics are the desired products, however, in their reactions H_2 is produced. This increases the amount of H_2, which is a reactant for the production of Alkanes, thereby promoting its production.

The implementation of these reactions will be further discussed in Chapter 4 on page 59, where the combined system modelling of MeOH to BTX is presented.

Throughout this chapter the different processes and components have been analysed and discussed from which the actual implementation can be performed. The subsequent chapter will present the implementation of the dynamic models, whereas Chapter 4 on page 59 will present the implementation of the steady state models.

Chapter 3

Dynamic Modelling

As previously discussed the CO_2 and H_2 are acquired from fluctuating sources. The objective of this chapter is to elaborate on and utilise the knowledge presented in the former Chapter 2, and thereby perform the modelling of the dynamic processes within the system, in order to obtain a steady flow of CO_2 and H_2. These flows will be used as inputs for the upcoming Chapter 4 on page 59 regarding the steady state modelling of the remaining subsystems of the systems. The dynamic modelling consists of four dynamic subsystems, which are the carbon capture, electrolysis and storage of CO_2 and H_2. Both the carbon capture and electrolysis subsystems have fluctuating inputs where the storage tanks are utilised in order to acquire steady flows, as may be seen in Figure 3.1.

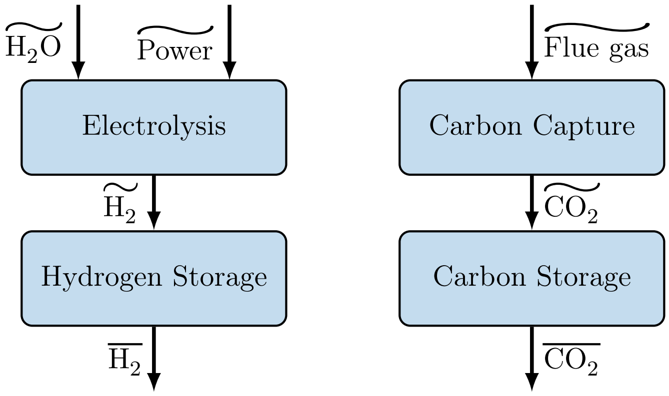

Figure 3.1: Overview of unit operations for H_2 and CO_2 streams.

3.1 Carbon Capture

The carbon capture technology, which was outlined in the former Section 2.1, will be presented in greater detail in the following section. The conceptual carbon capture subsystem may be seen once again in Figure 3.2 utilising the absorption method with MEA as the solvent.

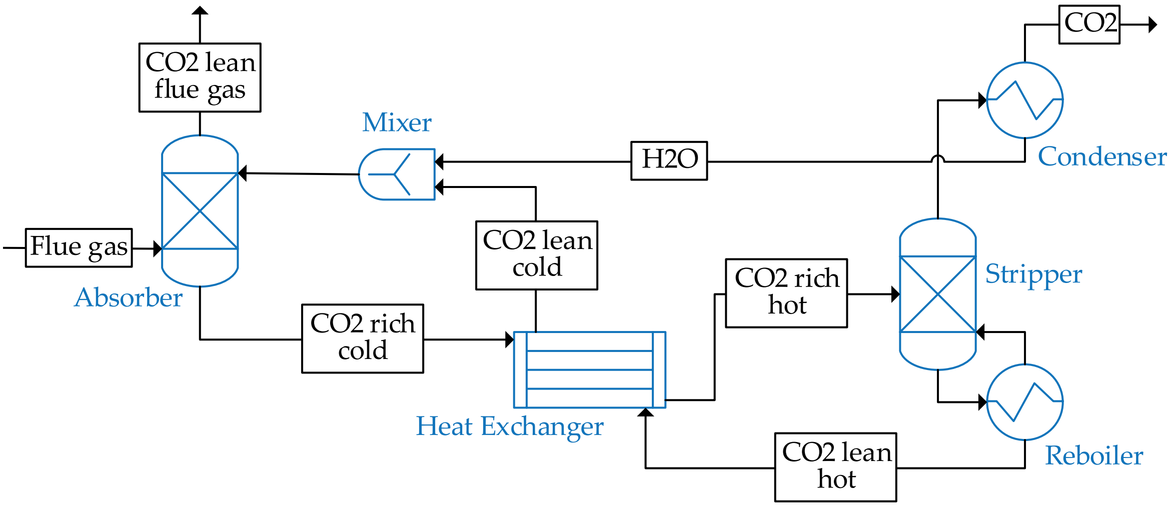

Figure 3.2: Schematic of the carbon capture subsystem, utilising the absorption method with MEA as the solvent.

In order to model such a subsystem several considerations and investigations must be made for the individual components, as will be outlined in the following. The modelling of the carbon capture was carried out in the Aspen Plus software, hence some of the considerations are a necessity caused by the operation of the software. The equation of state specified for the carbon capture model is the Redlich-Kwong coupled with the electrolyte Non-Random Two Liquid (elec-NRTL) model. This method is suitable for systems in which non-idealities occur as described in the Aspen Plus software.

A part of modelling such a system is to also determine the dimensions of the components. These are known to affect, among others, the fraction of CO_2 being absorbed in the capture process. It was shown in Figure 1.4 on page 6 that the CO_2 supply fluctuates. Since RenoNord combusts both waste- and fossil feedstock it is impossible to determine which part of the CO_2 emission can be considered Green. Therefore, the carbon capture process could be modelled as a steady state model where the input flow would equal the mean flow of the CO_2 contributed from the waste feedstock. This can be done since RenoNord also emits CO_2 which is produced from the fossil feedstock. Therefore, when the CO_2 flow contributed from the waste feedstock is lower than its mean, the system will still be able to operate with the same flow rate. I.e, depending on the month some of the captured CO_2 will originate from fossil feedstocks, but the annual consumption would correspond to the actual CO_2 originated from waste feedstock. This is however not desired, since it is expected that in the future the incineration plants will only be supplied from waste feedstocks. Therefore, if the total amount of emitted CO_2 originates from waste feedstocks, the above mentioned method cannot be utilised, and a dynamic system is required.

Due to the fluctuating flow rate of the flue gas the operational conditions as well as the required dimensions are expected to differ. In order to account for this, the dimensions will be determined from the annual mean flow of the CO_2 contributed from the waste feedstock, from which it will be analysed if the desired operation can be maintained by only varying the solvent flow rate and the energy consumption. If this is not the case, alternative methods must be considered.

3.1.1 Absorber

The absorber is the component responsible for the absorption of the CO_2 present in the flue gas. Firstly, the type of Aspen Plus unit component must be chosen. Since the chemistry defined in Section 2.1.3 involves several ions it results in non-ideality of the liquid phase. In Aspen Plus the RadFrac unit component is able to account for these non-idealities, along with interphase transfers, chemical reactions etc.[Madeddu et al., 2019]

In the RadFrac unit component different inputs must be specified. Firstly, the Rate-Based mode is chosen as it is the most common approach for reactive absorption-stripping. This approach utilises the Lewis and Whitman two-film theory which expresses the mass transfer across the interface of two stagnant fluids by considering molecular diffusion.

Then, the number of segments is to be decided. In the RadFrac unit component the modelling of the typically used ideal plug-flow, for this kind of system, is done through the number of segments. The number of segments represent a series of continuous-stirred tank reactors which, when approaching infinity, will resemble plug-flow. Hence, a sufficient number of segments are required to achieve plug-flow. A total of 100 segments were chosen to be sufficient for both the absorber, and the later described stripper, as reported by the study done by Madeddu et al. [2019].

Both the absorber and the stripper are packed columns, chosen over the plate ones because the packing provides a higher contact area and less pressure drop. The chosen packing for both the columns is Sulzer Mellapak 250Y.

The parameters of the absorber must then be specified in regards to its height, diameter and the lean solvent flow rate. This in done through an investigation of the liquid temperature and the flue gas composition through the absorber, when varying the above dimensions. A base size is first established, which is then scaled. The height of this base size is defined to be 100 m as this is considered to be an infinitely long column. Then the flow rate and diameter is varied until a 90 wt% CO_2 absorption rate is achieved from the flue gas into the solvent, which is the targeted rate according to Section 2.1. The flow rate of the flue gas from RenoNord is defined by the CO_2 emissions outlined in Chapter 1 and it was assumed that the only additional species are H_2O and N_2 [Madeddu et al., 2019]. This resulted in a flue gas composition from RenoNord with $CO_2 = 0.21$, $H_2O = 0.04$ and $N_2 = 0.75$, on mass fraction basis, where the annual mean flow rate is approximately 19 kg/s. With the specified CO_2 absorption rate of 90 wt% and the given flue gas composition the resulting base size has a diameter of 5.53 m and solvent flow rate of 60 kg/s.

The base size solvent flow rate (ψ) is then linearly scaled by a factor, while the column diameter and height is iteratively reduced to match the previously defined 90 wt% CO_2 absorption rate. To determine the most suitable dimensions the following Figures 3.3 on the next page and 3.4 on the following page are investigated. Figure 3.3 on the next page depicts the liquid temperature within the absorber column, with an inlet temperature of 313 K for both the flue gas and liquid. The temperature is influenced by the chemical reactions, which for the absorption is exothermic, but also by the vaporisation and condensation of H_2O.

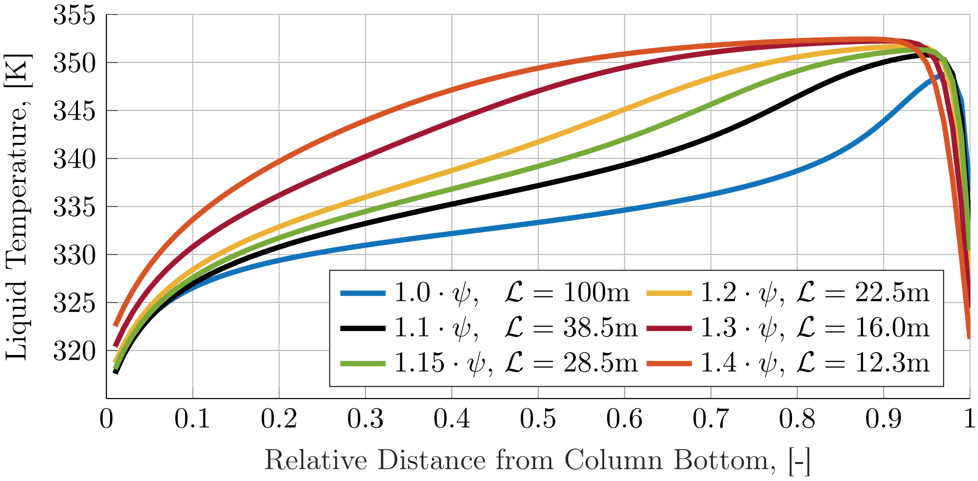

Figure 3.3: Liquid temperature in the absorber column, with varying solvent flow rates and the corresponding column height, at various distances from the column bottom.

As shown in Figure 3.3 a peak occurs at the top of the column, regardless of solvent flow rate and the corresponding column height. This peak is mainly due to the lean solvent entering at the top of the column, i.e. at a relative distance from the bottom equal to 1. An important consideration for the liquid temperature is that the bulge should have a relatively uniform gradient until the peak located at a relative distance of 0.95. A uniform gradient indicates that the absorption reactions occur evenly throughout the reactor. This is observed not to be the case when the scaling factor falls below 1.1 or exceeds 1.2. This indicates isothermal regions within the column which is undesired, as it implies low rates of CO_2 transfer. This can also be seen by analysing the molar fraction of CO_2 in the flue gas. The absorption of CO_2 in the flue gas occurs either relatively rapidly in the top or bottom of the absorber for the low- and high solvent flow rate factor, respectively. However, when the solvent flow rate factor is between 1.1 to 1.2 the absorption of CO_2 occurs relative uniformly throughout the absorber as may be seen in Figure 3.4.

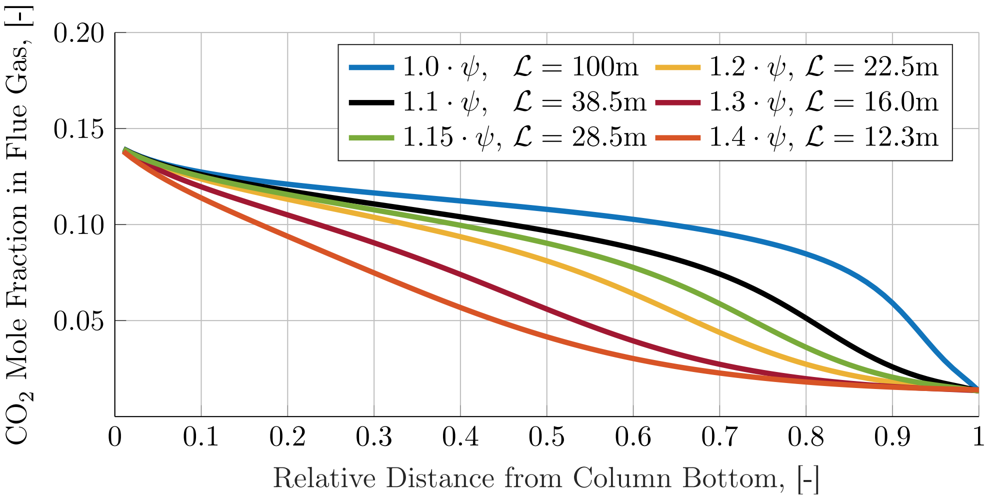

Figure 3.4: CO_2 flue gas composition in the absorber column, with varying solvent flow rates and the corresponding column height, at various distances from the column bottom. The inlet temperature for both the flue gas and solvent is 313 K.

Considering the above figures, it is determined that a lean solvent flow rate equal to 1.15 times the base size is a suitable compromise between column height and solvent flow rate, while simultaneously having only a small isothermal region. The resulting dimensions for the absorber becomes 28.5 m and 3.67 m for the height and diameter, respectively. With a lean solvent flow rate of 69 kg/s, which is used as the input flow for the stripper.

3.1.2 Stripper

The purpose of the stripper is the opposite of the absorber, meaning the previously captured CO_2 has to be extracted from the now rich solvent. In order to strip the rich solvent it is heated by a reboiler, as described previously in Section 2.1.3, where the distillation rate of the stripper is increased until all of the previously absorbed CO_2 is released. The corresponding reboiler duty is 13.87 MW. Unlike the absorber dimensions, the dimensions of the stripper cannot be determined in the same fashion. This is due to the reboiler being the sole influence on the reversal of the absorption reactions that occurred in the absorber, as was reported in Madeddu et al. [2019]. Hence, instead of changing a flow rate, as was done for the absorber, the liquid temperature profile is investigated only through the packing height, i.e. height of the column. Lastly, the diameter is determined through the design specification in Aspen Plus, which defined its value to be 2.07 m.

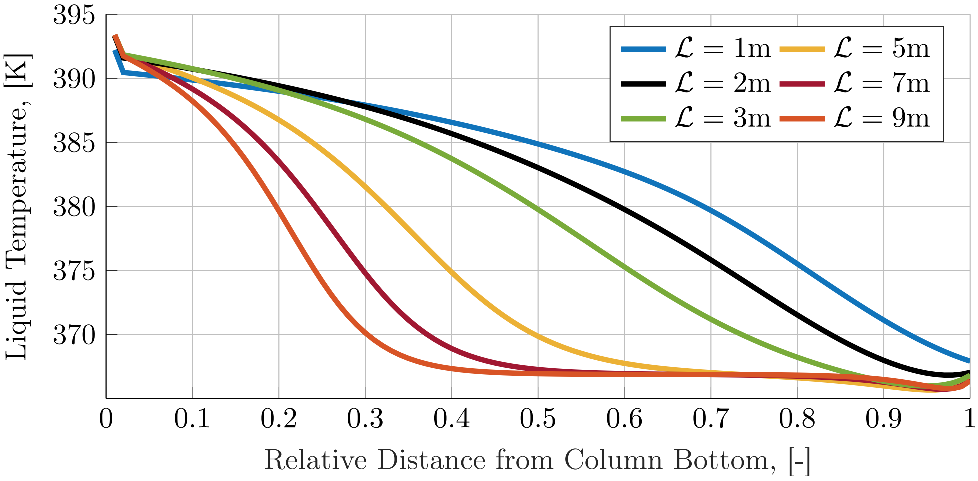

Figure 3.5: Liquid temperature in stripper column, with varying column height, at various distances from the column bottom, with an inlet temperature of 367 K.

As shown in Figure 3.5 when the column height exceeds 3 m an increasingly large isothermal region appears in the column. Hence, it is without advantage to increase the height to a value above 3 m. Also, it is common to not have a column height/diameter ratio equal to or below 1, hence the height of 3 m is used for stripper.[Nittaya et al., 2014]

3.1.3 Additional Components

The conceptual process of the carbon capture subsystem was presented in Figure 3.2 on page 40, however, additional components are needed in order to run the subsystem. A short description of the purpose of these additional components will be given in the following.

After the absorber, a separator is placed with a split fraction of 1 wt%, which is imposed to remove convergence problems associated with the later presented makeup stream.

Following the separator a pump is placed, which is implemented to increase the pressure of the rich solvent to a value of 5 bar. This is done to raise the vapour pressure of CO_2, as was explained in Section 2.1.3. The value is however higher than the required chosen pressure in the Stripper of 1.8 bar. The additional pressure is only required to avoid partial vaporisation in the upcoming Heat exchanger, which could result in corrosive acid breakout.[Madeddu et al., 2019] Then the cold rich solvent enters a counter-current heat exchanger, where it is heated by utilising the lean solvent exiting the Reboiler of the Stripper. The rich solvent is raised to a temperature of 100 °C, as was explained in Section 2.1.3.

The now heated rich solvent is then reduced in pressure through a pressure valve, since the corrosive acid breakout is no longer of concern and the pressure required for the Stripper is only 1.8 bar.

After the earlier presented Stripper, the vapour, in the form of CO_2 and H_2O, enters a condenser unit. The objective of the condenser is to separate the CO_2 from the stream, by converting the H_2O to liquid state. It is essential that the CO_2 stream becomes pure, since any significant content of H_2O has undesired influence on the downstream subsystem of the storage. The performance of the condenser is dependent on the operational condition, where high pressure and low temperature yield the highest degree of separation, while not crossing the freezing point of H_2O. A sensitivity analysis has been conducted, to investigate if sufficient separation can be achieved by the condenser. This sensitivity analysis concluded that a moisture content of 0.1 wt% is acquired at the operational conditions of 5 bar and 5 °C, which is deemed sufficient. In order to achieve this condensation, three components are incorporated, being a compressor, cooler and flash separator. The vapour mixture is firstly compressed to the desired pressure and further cooled. After the cooler, the separation of the CO_2 and H_2O can be achieved from a flash separator.

Lastly, the cooled and depressurised lean solvent exiting the Stripper, enters a mixer together with the condensed H_2O stream and a makeup stream. The makeup stream is required to resupply the subsystem with a small proportion of H_2O vapour which is lost through the drain. The newly combined lean solvent flow is slightly cooled to match the desired inlet stream temperature to the absorber. Following this stream the cycle is complete and the loop may continue its operation as may be seen in Figure 3.6 on the facing page.

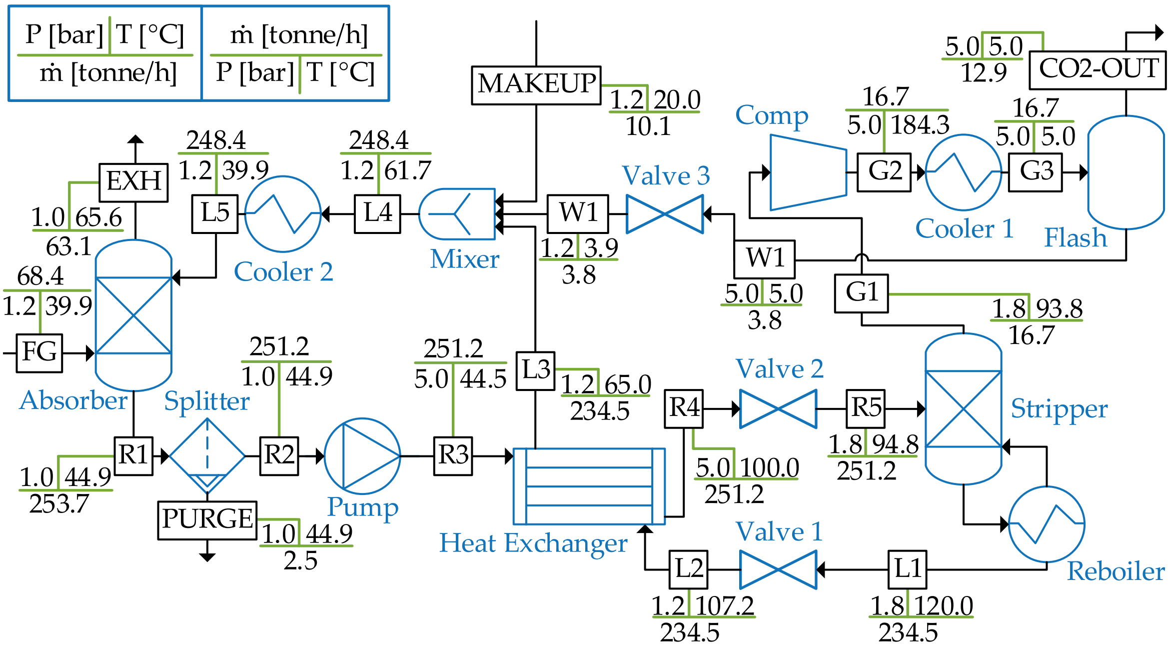

Figure 3.6: The carbon capture subsystem with the belonging stream temperature, pressure and mass flow rate, for the steady state case.

The figure illustrates all the components needed in order to achieve the carbon capture with the belonging stream temperature, pressure and mass flow rate. The stream properties are defined for the steady state case, whereas the mass flow rate would differ when the model is converted into a dynamic model, which will be done in the following subsection. The dimensions of this carbon capture subsystem, designed for the annual mean CO_2 flow from RenoNord, has the dimensions listed in Table 3.1.

Table 3.1: Parameters of the carbon capture subsystem.

	Value	Unit
Absorber Diameter	3.62	[m]
Absorber Length	28.50	[m]
Stripper Diameter	2.07	[m]
Stripper Length	3.00	[m]
Solvent flow rate	65.15	[kg/s]
Reboiler duty	13.89	[MW]

3.1.4 Dynamic Carbon Capture

Throughout this section the carbon capture has been dimensioned from the annual mean flow of CO_2. However, since this flow varies on an annular basis, it was expected that the desired CO_2 capture rate of 90 wt% could be maintained, by adjusting the solvent flow rate and reboiler duty. This has been analysed, where it was determined that the minimum and maximum variation of the mean flow is approximately 17 wt%. It was concluded that scaling the solvent flow rate and reboiler duty linearly, the CO_2 capture rate of 90 wt% could be maintained. This may be seen in Figure 3.7 on the following page.

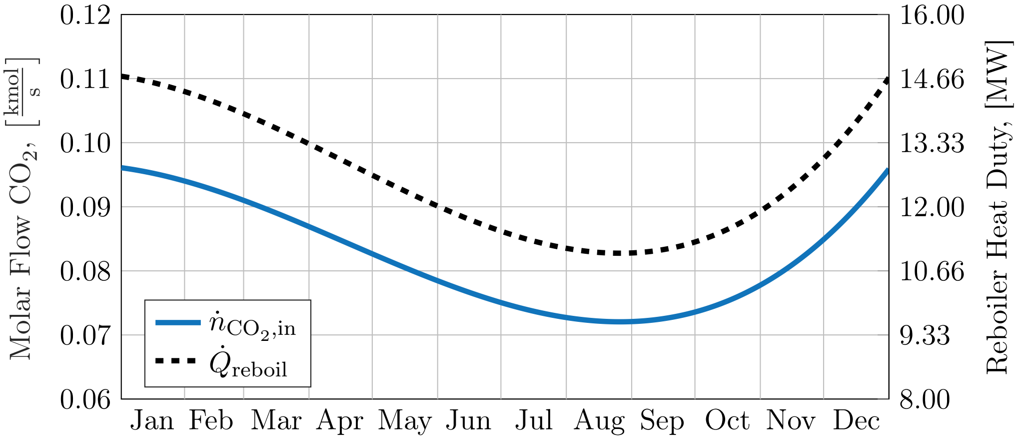

Figure 3.7: Variation in CO_2 molar flow rate and reboiler heat duty throughout a year.

When the subsystem is scaled in accordance to the varying flue gas, then the varying and hence dynamic carbon capture, can be expressed as shown in Figure 3.7. To achieve this in a real application the solvent flow rate and reboiler duty must be constantly monitored to maintain a CO_2 capture rate of 90 wt%, which could be accomplished by a sensor that tracks the amount of flue gas and its CO_2 content to which the two parameters in the subsystem should be varied accordingly.

3.2 Storage of Carbon Dioxide

To account for the fluctuating CO_2 flow, storage of this is required. This will enable a constant CO_2 flow to enter the MeOH synthesis as desired. As was discussed in Section 2.3.2, the storage will be done as compressed gas, from which a compressor is required. An overview of the compression and storage process may be seen in Figure. 3.8.

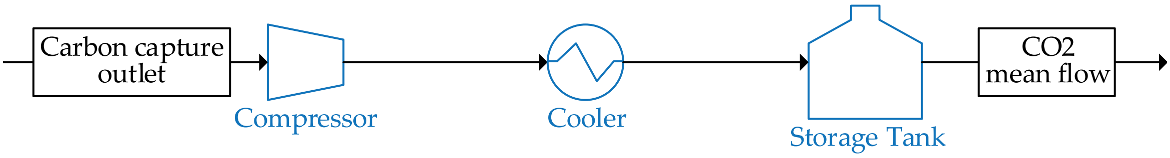

Figure 3.8: Schematic of storage tank with corresponding compressor and cooler.

From Figure 3.8 it may be seen that a cooler is implemented between the compressor and the storage tank. This is done to decrease the temperature of the CO_2, since the compressor is assumed to be adiabatic. The operating conditions of the subsystem varies depending on the physical properties and the desired conditions. The compression is also assumed to operate with a corresponding isentropic efficiency of 0.74, due to this value being the default efficiency [Klein and Nellis, 2017]. The cooler is assumed to have no pressure loss, and ideal cooling to its surroundings.

3.2.1 Storage Tank Analysis

Since the CO_2 flow entering the storage tank has been determined from the carbon capture subsystem, the output of the storage tank can be defined as the mean which may be seen in Figure 3.9 on the facing page.

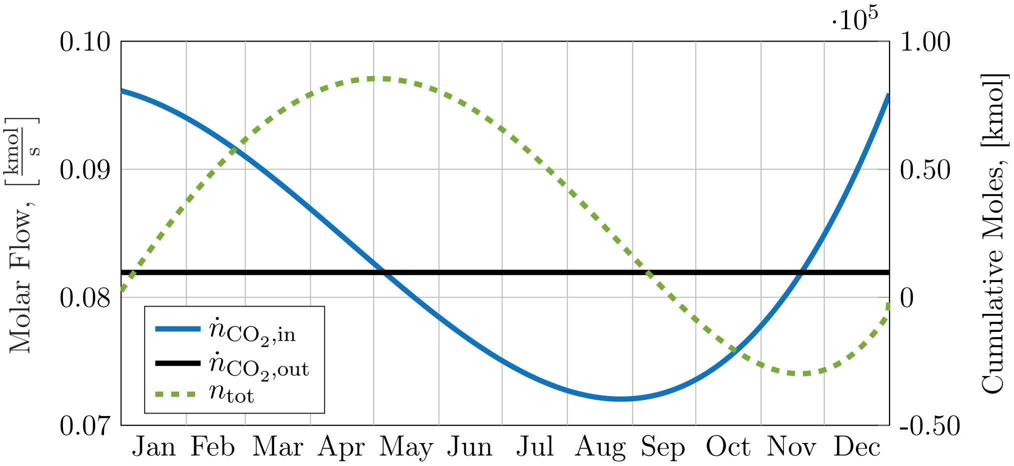

Figure 3.9: Molar flows entering and exiting the CO_2 storage tank along with the cumulative moles.

From Figure 3.9 it can be seen that during the summertime, the entering CO_2 flow is reduced and becomes lower than the mean CO_2 flow exiting. However, in the autumn the trend becomes opposite. This is also illustrated in Figure 3.9 where n_{tot} is the total moles in the storage tank. Throughout the year it may be seen that the total number of moles becomes less than zero. In order to account for this problem, the storage tank has been defined to have an initial amount of CO_2 such that the total number of moles does not become negative or zero. However, the change in the total number of moles in the storage tank directly influences the required power of the compressor as well as the required cooling. The power of the compressor is defined from the energy balance as may be seen in Eq. 3.1

$$\frac{dn_{CO_2}}{dt} \cdot h_{in} + \frac{\dot{W}_{rev}}{\eta} = \frac{dn_{CO_2}}{dt} \cdot h_{out} \tag{3.1}$$

where h_{in} is the specific enthalpy before the compressor, $\dot{W}_{rev}$ is the power of the compressor with the corresponding isentropic efficiency η and h_{out} is the specific enthalpy after the compressor. h_{in} is defined from the inlet temperature and pressure, while h_{out} is defined from the entropy and outlet pressure, due to the assumption of isentropic compression. However, the outlet pressure is fluctuating and depends on the outlet temperature and the specific volume of the storage tank. The latter is defined from the volume of the storage tank and the total number of moles in the storage tank which are defined from a molar balance, which may be seen in Eq. 3.2.

$$\frac{dn_{tot}}{dt} = \frac{dn_{in}}{dt} - \frac{dn_{out}}{dt} + n_{ini} \tag{3.2}$$

Due to the fluctuating inlet flow of CO_2, the outlet pressure will also vary, and therefore so will the power required for the compressor.

From the first law of thermodynamics the cooling can be determined as may be seen in Eq. 3.3

$$\Delta Q = \Delta E - \Delta W \tag{3.3}$$

where E is the total energy. From the above presented equations, the power of the compressor as well as the heat removed in the cooler can be determined. However, these can be minimised which will be done in the following section.

3.2.2 Optimisation of Compressor

As discussed, the required power for the compressor is dependent on the outlet pressure which is defined from the specific volume as may be seen in Eq. 3.4

$$\frac{d\nu_s}{dt} = \frac{V_{tank}}{\frac{dn_{tot}}{dt}} \tag{3.4}$$

where ν_s is the specific volume, V_{tank} is the volume of the tank and n_{tot} is the total moles in the tank. The greater the value of ν_s, the larger the pressure becomes and thereby the required power. Therefore, to reduce the required power the volume of the tank may be increased. The minimum pressure in the tank throughout the year must however be considered when defining its volume. If the volume of the tank is increased too much the pressure will approach a vacuum, if the initial moles in the tank is not adjusted as well. In the upcoming chapter it has been determined from optimisation that the pressure in the MeOH synthesis must be 32 bar. If the minimum pressure in the tank is greater than the 32 bar, the pressure can be used as the driving force of the molar flow, assuming no pressure loss. Therefore, the volume has been constrained by a minimum pressure in the tank of 32 bar. Furthermore, the inlet conditions for the compressor equals the outlet conditions from the carbon capture subsystem, where the outlet temperature and pressure are 5 °C and 5 bar, respectively. However, in Section 2.3 the saturation pressure as function of the temperature for CO_2 was analysed. At 5 °C the corresponding saturation pressure is approximately 40 bar, which depending on the season and volume of the tank, could be exceeded. Therefore, the CO_2 is heated to 25 °C before entering the compressor since this is the inlet temperature for the MeOH synthesis and this corresponds to a saturation pressure of approximately 64 bar, which was not violated. The monthly variation in the required compressor power for various storage volumes may be seen in Figure 3.10.

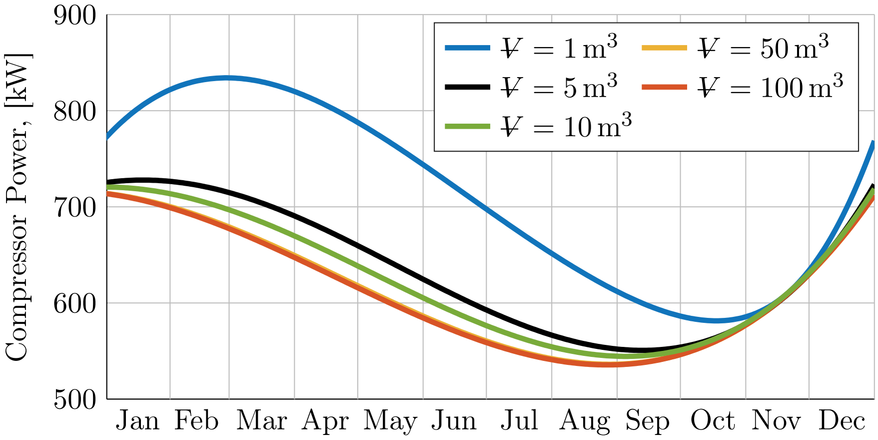

Figure 3.10: Compressor power as function of the months at different tank volumes, with a minimum pressure in the tank at 32 bar.

From Figure 3.10 it may be seen that when the volume increases the required compressor power decreases. This occurs since the power of the compressors are affected by the pressure which varies depending on the volume. Therefore with a larger tank volume, the influence of the inlet- and outlet molar flows, have less of an influence towards the pressure. It can be concluded that the larger the tank volume is, the less power is required from the compressor, however, physical aspects must also be taken into consideration. Underground pressure tanks are known to be build up to 100 m^3 [Nordic, 2021]. The relative difference in compressor power between 50 m^3 and 100 m^3 could be assumed negligible, from which there is no incentive to investigate larger storage tanks, hence the volume of the storage tank is chosen to be 100 m^3.

Another approach to minimise the required power of the compressor is to apply multiple compression stages. This is done since a smaller temperature difference between the inlet and outlet of the compressor reduces the rate of entropy generation, and thereby the required power [Klein and Nellis, 2017]. In order to apply this, the pressure ratio for each compression is assumed to be alike as seen in Eq. 3.5

$$\mathrm{PR}_{\mathrm{stage}} = \mathrm{PR}_{\mathrm{tot}}^{\frac{1}{\mathrm{N}}} \tag{3.5}$$

where $\mathrm{PR}_{\mathrm{stage}}$ is the pressure ratio for each stage dependent on the number of stages N, and $\mathrm{PR}_{\mathrm{tot}}$ is the total pressure ratio defined as in Eq. 3.6

$$\mathrm{PR}_{\mathrm{tot}} = \frac{P_{\mathrm{out}}}{P_{\mathrm{ini}}} \tag{3.6}$$

where P_{out} is the outlet pressure after the last compressor, and P_{ini} is the initial pressure. The inlet pressure for each compression can therefore be determined from Eq. 3.7.

$$P_{\mathrm{in,i}} = P_{\mathrm{ini}} \cdot \mathrm{PR}_{\mathrm{stage}}^{\mathrm{i\text{-}1}} \quad \text{for} \;\; \mathrm{i} = 1..\mathrm{N} \tag{3.7}$$

Furthermore, the outlet pressure for each compression can be determined from Eq. 3.8.

$$P_{\mathrm{out,i}} = P_{\mathrm{ini}} \cdot \mathrm{PR}_{\mathrm{stage}}^{\mathrm{i}} \quad \text{for} \;\; \mathrm{i} = 1..\mathrm{N} \tag{3.8}$$

Lastly the temperature at the inlet of each compressor is constrained to be equal, to replicate an isothermal compression. The effect of multiple compression stages may be seen in Figure 3.11 where N denotes the number of compressors.

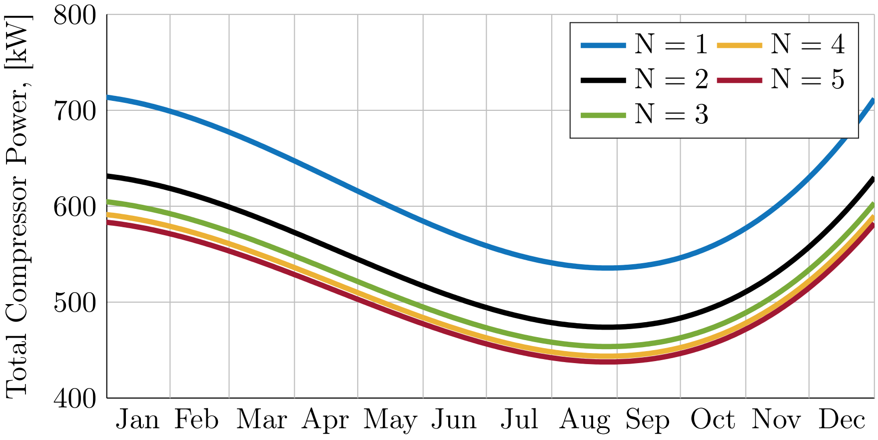

Figure 3.11: Total compressor power for CO$_2$ as function of months with different number of compression stages, for a tank volume of 100 m^3.

From Figure 3.11 it may be seen that the required power decays exponentially with an increased number of compression stages. In order to determine the number of compression stages, the CAPEX of this process should be taken into account. At some point the savings in power is no longer feasible compared to the CAPEX, however, the CAPEX is not known, hence the relative power reduction is required to be analysed. The relative power reduction when increasing the stages by one is approximately 11.5 %, 4.3 %, 2.3 %

and 1.4 %, respectively from one to five. The relative change between four and five stages is assumed infeasible with respect to the savings contrary to the CAPEX, from which 4 stage compression is chosen. The compression process of CO_2 may be seen in Figure 3.12 with the corresponding pressure and temperature based on a yearly mean CO_2 input. The temperature and pressure are shown in order to indicate the range for each compressor and cooler.

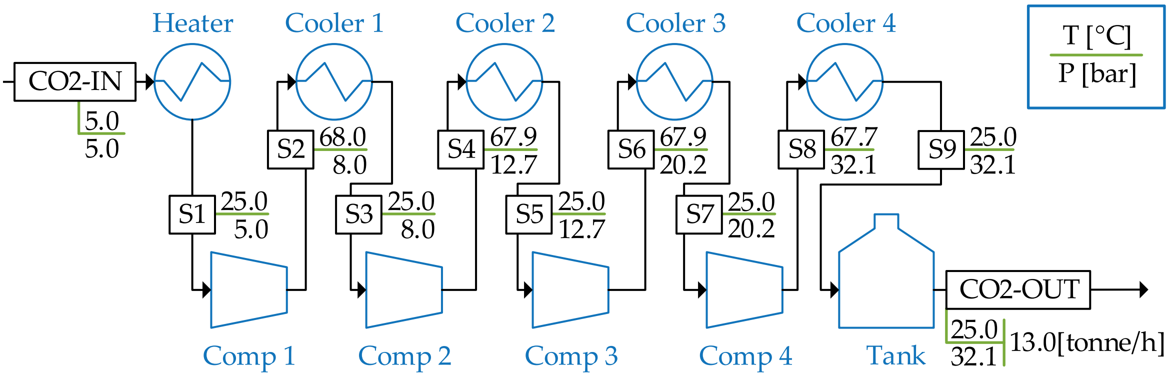

Figure 3.12: Compression and storage of CO_2 with 4 compression stages and coolers. The corresponding temperatures and pressures are based on a yearly mean input.

With the subsystem given in Figure 3.12 the fluctuating CO_2 can be converted into a steady flow entering the MeOH synthesis with the desired pressure and temperature.

3.3 Electrolysis

Similar to the carbon capture, the input for the electrolysis is also fluctuating. The CO_2 is however the limiting reactant in the MeOH synthesis, from which the electrolysis is sized accordingly. The mean flow of H_2 exiting the storage tank is therefore determined from an optimisation of the MeOH synthesis process done in the following chapter 4 on page 59. With the mean flow known, the objective of this modelling is therefore to determine the size of the electrolysis subsystem in order to supply this mean flow. In order for the MeOH to be classified as being Green, all of the required energy of the system must be acquired from renewable sources.

It is of interest to place wind turbines and PV panels on site to supply the system. The electrolysis is known to be one of the processes with the highest energy consumption in such a system [GreenLab, 2021]. Due to the size of the system investigated in the presented study, it is assumed to be unrealistic that onsite wind turbines and PV panels will be able to supply the total energy requirement of the entire system. The electricity generated by these renewable energy sources are known to fluctuate, hence making them suitable suppliers for the electrolysis, due to its storage capabilities. Contrary, the other processes requires a steady energy contribution, which must be contributed from external sources. It is therefore of interest to determine the power consumption of the electrolysis subsystem in order to estimate the required number of wind turbines and PV panels.

As discussed in Section 2.2, the electrolyser is based on a study by Sánchez et al. [2018], with an approximately 10 kW bench scale system. This model has been scaled linearly to meet the required H_2 flow rate for the MeOH synthesis. Results acquired from bench scaled systems are known not always to be representative for large scaled systems, from which the obtained results will be further discussed. The study has been validated in the temperature range of 20 °C to 80 °C where it was previously discussed that the electrolyser should be operated at relatively high temperatures in order to decrease the cooling. The upper limit of what has been validated is therefore chosen, being 80 °C. The mean flow of the H_2 is used to define the size of the system where the current is defined to be 0.42 A, from which the corresponding cell voltage and Faraday's efficiency can be estimated. The area (A) of a cell is defined to be 0.1 m^2, which is equal to the study by Sánchez et al. [2018], from which the corresponding number of cells can be determined. These values may be seen in Table 3.2.

Table 3.2: Independent- and dependent values for the electrolyser.

Parameter	Value	Unit
$\overline{n}_{H_2}$	0.2152	[kmol/s]
I	0.42	[A]
A	0.10	[m^2]
V_{cell}	2.01	[V]
η_F	0.94	[-]
N_{cells}	104,822	[-]
$\dot{W}_{elec}$	88.45	[MW]
$\dot{Q}_{cool}$	22.38	[MW]

As seen from Table 3.2 the corresponding required power is defined, which is used to determine the required number of wind turbines and PV panels. However, before these are determined it is of interest to analyse if the required power is representative for an upscaled plant. The plant located in Skive, which was discussed in Chapter 1, also utilises electrolysis where its corresponding molar flow rate is approximately 7.81 times less, with a corresponding power of 10 MW. If this electrolysis subsystem was to be upscaled, the corresponding required power would be approximately 13 % less than what is defined in Table 3.2. This was expected since the study by Sánchez et al. [2018] is based on a bench scale system. However, the relative difference is assumed to be acceptable from which it is known that the OPEX could be reduced if better information regarding a commercial electrolyser was given.

3.3.1 Wind Turbines and Photovoltaic Panels

With the mean power known for the electrolyser, the required number of wind turbines and PV panels can be estimated. In Section 1.4.2 the average daily wind speed was discussed as well as the power generation for a 4.2 MW turbine. It was determined that the power generation is affected by the wind speed raised to the power of three from which an averaging of the wind speed will be unrepresentative of the actual power production. The average power generation of the 4.2 MW turbine can be determined from the average daily wind speed which equals 0.448 MW, corresponding to approximately 10 % of the rated capacity. Contrary, the relative difference between the generated power and actual rated capacity in Denmark for onshore wind turbines is at least twice as large, which may be seen in Figure 3.13 on the next page. [Denmark, 2021].

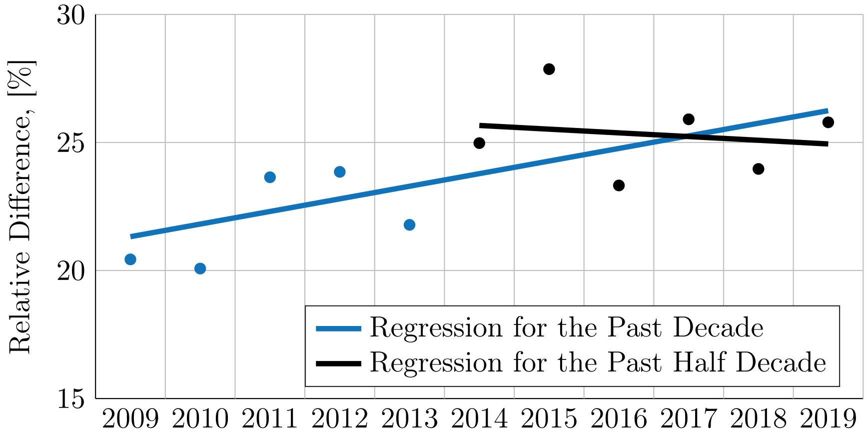

Figure 3.13: Relative difference of generated power and capacity for onshore wind turbines in Denmark throughout the last decade.

From Figure 3.13 it may be seen that the generated power compared to the capacity has increased throughout the last decade. If the past half decade is analysed the ratio is approximately constant at 25 %, from which the model output is corrected to this value, instead of 10 %, as may be seen in Figure 3.14.

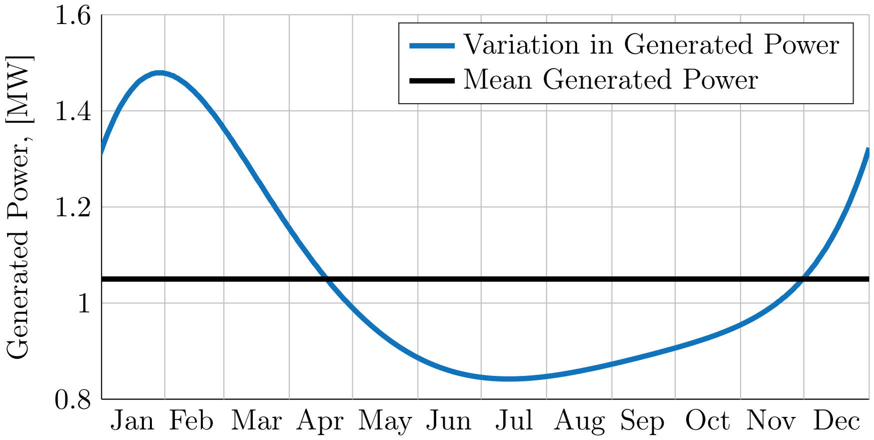

Figure 3.14: Generated power of a 4.2 MW wind turbine as function of months.

From Figure 3.14 it may now be seen that the annual average generated power is scaled. However, PV panels are also desired to be utilised to supply the electrolysis. In Section 1.4.3 the solar irradiance throughout the year was defined as well as the correlation between the generated power and the solar irradiance. The generated power is proportional to the solar irradiance, the area- and efficiency of the cell. The efficiency of the cell is known to differ dependent on the specific type of PV panels. However, due the technological development the different efficiencies have become relatively alike and also with a greater value. Third generation PV panels show promising efficiencies of up to 38 %, however, these are yet to be commercialised.[Sharma et al., 2021] The efficiencies of commercialised PV panels are approximately 20 % to 22 % [CleanEnergyReviews, 2021]. Assuming an efficiency of 22 % the generated power per unit area may be seen in Figure 3.15 on the next page.

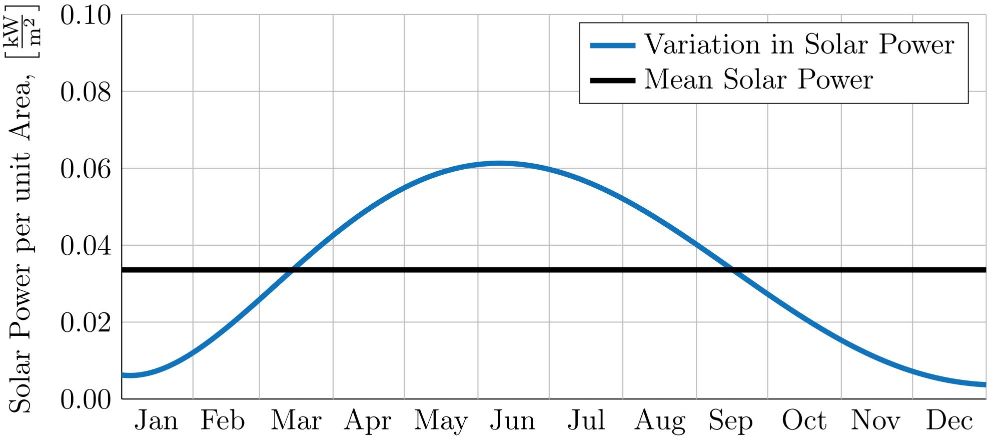

Figure 3.15: Mean- and variation of generated power per unit area for the PV panels.

With the power generation known, for both a 4.2 MW wind turbine and PV panels per m^2 over a year, the available power to be generated can be estimated based on the quantities of each. It is of interest to have the wind turbines and PV panels on site, however, in order to determine if it is possible, the surrounding grounds must be analysed. There are different aspects which requires to be accounted for when installing both wind turbines and PV panels. Some of these are with respect to the optimal operating conditions while others are socioeconomic aspects. Figure 3.16 highlights the surrounding grounds, where the red ground represents RenoNord, the blue- and green grounds are municipal properties and the yellow grounds are private properties.

Figure 3.16: Surrounding grounds of RenoNord, where the red ground represents RenoNord, the blue- and green grounds are municipal properties and the yellow grounds are private properties [Geostyrelsen, 2021].

The blue area consist of three grounds with a total area of 83,784 m^2 where the green area consist of eight grounds with a total area of 180,749 m^2. The Green industrial park located in Skive, which was mentioned in Chapter 1, make up an area of 69,000 m^2 which consist of the MeOH plant, a waste handling facility, a biogas plant, Quantafuel's plant, an electrolysis plant and excess space. The blue area is therefore reserved for the construction of the different subsystems, which leaves the green area as the only nearby available area for the wind turbines and PV panels. However, wind turbines must be placed with a certain distance between each other and the ground area is relatively small, from which it could be assumed that against payment, the wind turbines could be placed on the surrounding private grounds. The green area is therefore only used for the PV panels. In order to place the wind turbines on the surrounding private grounds, several laws must be taken into account which may be seen in the following:

- The municipal plan in Aalborg restricts the noise from the wind turbines to be a maximum of 37 dB at the nearby housing [Kommune, 2021a], which requires a distance of approximately 500 m [Europe, 2020].
- The distance between the wind turbine and the nearby housing must be no less than four times the total height of the wind turbine.
- The distance between the wind turbine and public roads or railroads must be 250 m or 1.7 times of the total height.
- The distance between the wind turbine and a high voltage power line must be at least the distance of the total height of the wind turbine.[Kommune, 2021b]

The surrounding grounds with the noise- and high voltage power line constrains implemented may be seen in Figure 3.17.

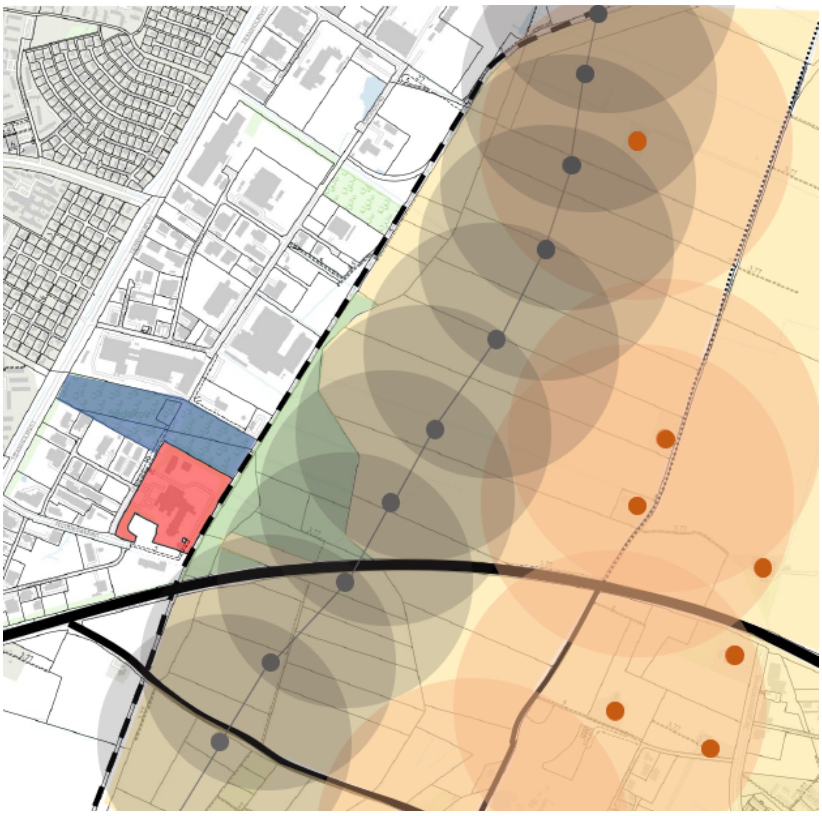

Figure 3.17: Surrounding grounds to RenoNord, where a high voltage power line as well as the surrounding houses are illustrated.

The red ground represents RenoNord, the blue- and green grounds are municipal properties and the yellow grounds are private properties. The orange dots are nearby houses where the faded orange circles represent the corresponding 500 m radius. The grey dots are high voltage towers and the grey lines between are the high voltage power lines, the faded grey circles represent the corresponding 200 m radius [Vestas, 2020]. Due to the nearby houses and the high voltage power line, it is not possible to place any wind turbines on site. However, further east of RenoNord it should be possible to place wind turbines since the geographical population decreases. It was determined that a wind turbine with a capacity of 4.2 MW has a annual average generated power of approximately 1 MW, from which it would require approximately 84 wind turbines since the PV panels has a generated power of approximately 5.3 MW to supply just the electrolyser. This would be an unrealistic one-time investment to make, however, it is shortly analysed what a realistic number of wind turbines would be. The remaining power will therefore be supplied by the grid, which must also be produced from renewable energy sources to maintain the classification of Green products.

The industrial park located in Skive has 13 wind turbines on site where the molar flow of the H_2, produced by the electrolyser, is approximately eight times less, indicating that an investment of more than 13 wind turbines would be realistic for the present system. However, the geographical population surrounding Aalborg municipal is relatively high from which a relatively big wind turbine park could become difficult to establish. Without conducting a further analysis, 20 wind turbines are assumed to be a suitable number, due to the complications which occur from the geographical population and the corresponding socioeconomic dilemmas. The total installed wind capacity is therefore 84 MW where the total actual power is approximately 21.01 MW. The total installed PV capacity is 9.54 MW where the total actual power output is approximately 5.32 MW.

3.3.2 Storage of Hydrogen

The entire ground surrounding RenoNord, marked in green, is used to install PV panels, and further 20 4.2 MW wind turbines are installed as well. This leads to an approximate annual mean power of 62.13 MW being required from the grid. The annual average distribution of the supplied power is therefore 6.0 %, 23.8 % and 70.2 % for the PV panels, wind turbines and the grid, respectively. The corresponding H_2 molar flow, produced depending on these energy sources, may be seen in Figure 3.18.

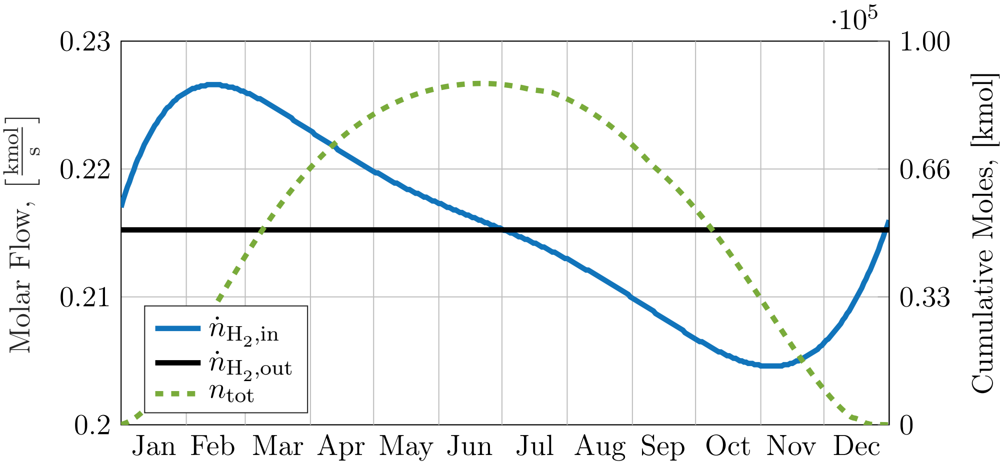

Figure 3.18: Molar flow entering and exiting the H_2 storage tank along with the cumulative moles.

From Figure 3.18 the molar flow of H_2 exiting the storage tank may be seen as well as the accumulative number of H_2 moles within. Similar to the previously described storage of CO_2, an increased volume of the H_2 storage tank can also reduce the required power from the compressor. A volume has been fixed at 100 m^3 identical to the CO_2 storage tank. The influence of multiple compression stages may be seen in Figure 3.19, where the corresponding total compressor power is illustrated. While the CO_2 flow exiting the carbon capture was heated before entering the first compressor, the H_2 flow exiting the electrolysis is not. The operating conditions for the electrolyser is as earlier mentioned 80 °C and 7 bar, which would also be the exiting conditions for the H_2 flow, if separation was not needed. The H_2 stream exiting the electrolyser also contains H_2O, which needs to be separated. This is done in a flash separator, however, in order to achieve an almost ideal separation, the temperature is lowered to 25 °C whereas the pressure is maintained at 7 bar. These two latter conditions become the inlet conditions for first compressor.

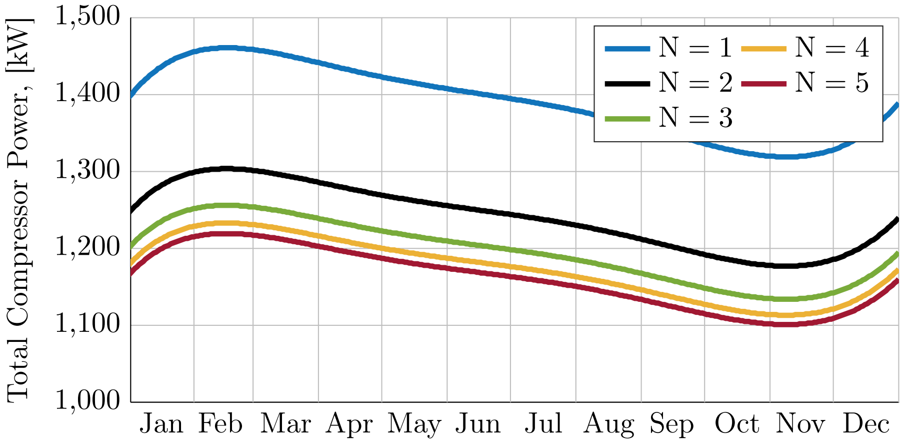

Figure 3.19: Total compressor power for H_2 as function of months with different number of compression stages, at a tank volume of 100 m^3.

Similar to the total compressor power for the CO_2 flow, the total compressor power for the H_2 flow decays exponentially as the compressor stages increase. In order to determine the number of compression stages, the CAPEX of this process should be taken into account, which was also done for the CO_2 storage. The relative power reduction when increasing the stages by one is approximately 10.8 %, 3.7 %, 1.8 % and 1.1 %, respectively from one stage to five. The relative change between four and five is assumed infeasible with respect to the energy savings contrary to the CAPEX, from which four stage compression is chosen. The total compressor power for the H_2 is larger than the power required for the CO_2 compression, which is among others due to the difference in flow rate. The compression process of H_2 may be seen in Figure 3.20 on the next page with the corresponding pressure and temperature based on a yearly mean H_2 input. The temperature and pressure are shown in order to approximate the range for each compressor and cooler.

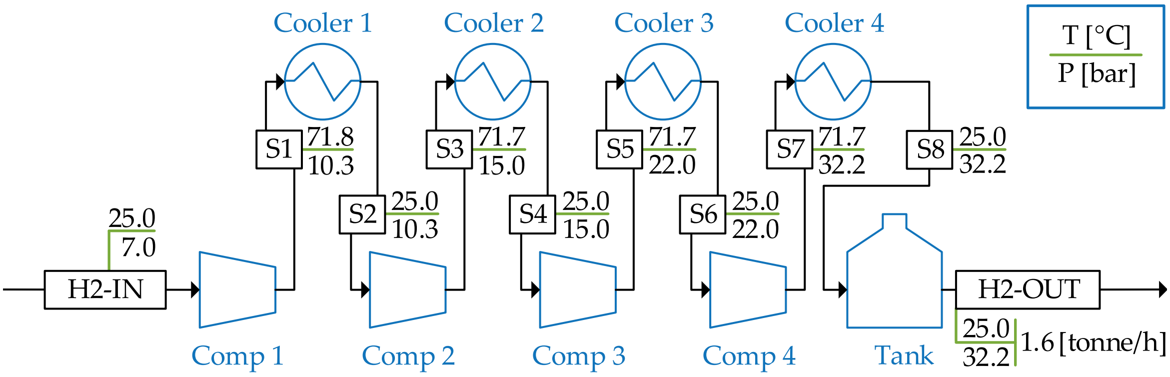

Figure 3.20: Compression and storage of H_2 with 4 compression stages and coolers. The corresponding temperatures and pressures are based on a yearly mean input.

Throughout this chapter the dynamic aspects regarding the carbon capture and electrolysis have been defined, from which storage tanks are utilised to convert the fluctuating flows of CO_2 *and* H_2 *into constant flows. The outputs from the storage tanks will be used as input for the MeOH synthesis in the following Chapter 4 on page 59.*

[This page is intentionally left blank]

Chapter 4

Steady State Modelling

From the previous chapter, the fluctuating flows of CO_2 and H_2 have, by means of storage, been converted into steady state flows which are desired for the following processes, which is the MeOH synthesis and the subsequent subsystems. The steady state inputs are desired to avoid partial loading which entails a reduced efficiency.

4.1 Methanol Synthesis

The objective of the MeOH synthesis is to determine the liquid flow exiting the flash separation, where the inputs for this subsystem are CO_2 and H_2. In order to acquire valid results, a representative equation of state must be chosen. Due to the relatively high pressures used in the MeOH synthesis, which will be the outcome of this model, the Redlich-Kwong-Soave equation of state with a modified Huron-Vidal mixing rule (RKSMHV) is chosen. The Peng-Robinson equation of state with a modified Huron-Vidal mixing rule could also have been utilised, however, the study done by [Ghanbari et al., 2017] investigated the difference between both equations of states, yet, without the modified mixing rule. They concluded the use of the Redlich-Kwong-Soave equation of state should be chosen if modification to the equation of state is done, which is the case for the presented study.

The molar flow of CO_2 is the limiting reactant and is determined from the carbon capture whereas the molar flow of H_2 is adjusted to optimise the MeOH yield. From the molar flow of H_2, the corresponding electrolysis subsystem and size of the H_2 storage was defined. A schematic of the MeOH synthesis can be seen in Figure 4.1 on the next page. As was discussed in section 2.4 the subsystem consists of a reactor where pure CO_2 and H_2 enters along with the gases from the feedback-loop. The gases exiting the reactor enters a flash separator in order to separate the products from unconverted reactants. Additionally, a separator is implemented to avoid accumulation of unwanted products.

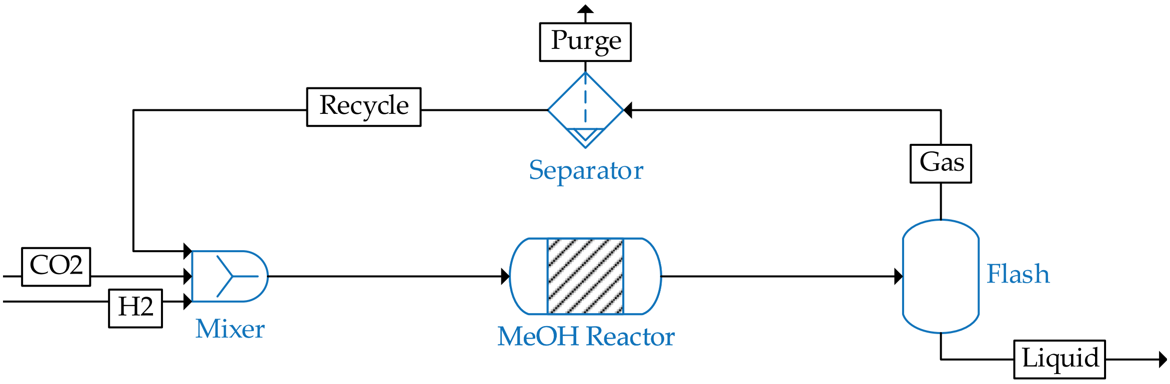

Figure 4.1: Schematic of the MeOH synthesis subsystem.

It may be seen that the subsystem does not contain any components which adjusts the pressure or temperature. These operation conditions will however be determined trough an optimisation.

4.1.1 Optimisation of Methanol Production

Optimisation is a tool which estimates an optimum depending on the variables and constraints. The variables, which affect the optimum MeOH molar flow exiting the flash separator, are the ratio of H_2 to CO_2, the size of the reactor, temperatures and pressures. The OPEX could also have been included, to account for the change in cost compared to the change in the molar flow of MeOH. This cost would include the costs associated with utility and the production of H_2. This will however not be included in order to simplify the optimisation. In addition, this optimisation does not include any influence of CAPEX. Even with relatively few variables, the complexity of the optimisation is relatively large. To ease the convergence, good initial values are needed.

The size of the reactor are based on the supplied molar flow of CO_2 and a study done by Bussche and Froment [1996]. Given their dimensions and CO_2 molar flow, scaling can be performed. Since their reactor length and diameter are known, a ratio between them can be defined as $L/D = 9.49$, from which the corresponding reactor volume can be determined. The CO_2 molar flow of the presented study is much greater than in Bussche and Froment [1996], being approximately 4.3e+6 times larger, where the reactor volume is scaled by the same quantity. From the L/D ratio and CO_2 molar flow, the initial length and diameter can be determined as may be seen in Table 4.1 on the facing page. In order to further reduce the complexity of the optimisation, boundaries are applied which may also be seen in Table 4.1 on the next page.

In order to determine the H_2 molar flow, a starting point is to analyse the reactions given in Section 2.4. It may be seen that the hydrogenation of one mole CO_2 requires three moles H_2 to form one mole MeOH. However, this ratio is constrained to the input of this subsystem, but since a feedback-loop is incorporated this will affect the supplied H_2 molar flow. Essentially, the kinetics indirectly determine the optimum supplied H_2 molar flow, however, as an initial value the molar flow is defined to be three times larger than the CO_2 molar flow, corresponding to the stoichiometric balance, as may be seen in Table 4.1 on the facing page with the associated boundaries.

From Section 2.4 it is known that both the reactor and flash separator are temperature and pressure dependent. From the study done by Bussche and Froment [1996], it is known that the kinetics have been validated in the temperature range of 180 °C to 280 °C, which defines the boundaries whereas the initial value is defined as the median. With respect to the pressure, only the upper boundary has been defined from the study, which is 51 bar. The lower boundary is defined to be 10 bar, and the initial value is defined to be the median, which may be seen in Table 4.1. From Section 2.4 it was determined that the operation of the flash separator is determined from the chemical potentials. Since the objective is to optimise the MeOH flow exiting the MeOH synthesis, it is desired to attain a high pressure in the flash separator since this increases the evaporation temperature. Additionally, the temperature is desired to be maintained relatively low. The boundaries for the temperature of the flash separator are defined to be 30 °C to 90 °C and the initial value is defined by the median as may be seen in Table 4.1.

Table 4.1: Initial values and associated boundary values.

	Initial value	Lower value	Upper value	Unit
CO_2 molar flow	0.0816	-	-	kmol/s
H_2 molar flow	0.2448	0.1	0.6	kmol/s
Length	24.3	3.0	30.0	m
Diameter	1.3	1.0	3.0	m
Reactor inlet temperature	230.0	180.0	280.0	°C
Reactor inlet pressure	25.5	10.0	51.0	bar
Flash separator temperature	60.0	30.0	90.0	°C
Flash separator pressure	25.5	10.0	51.0	bar

With the initial values and boundaries defined the optimisation can be performed. The optimisation is based on the Sequential Quadratic Programming (SQP) algorithm. With the objective function being to optimise the liquid MeOH molar flow, the resulting operational conditions may be seen in Figure 4.2.

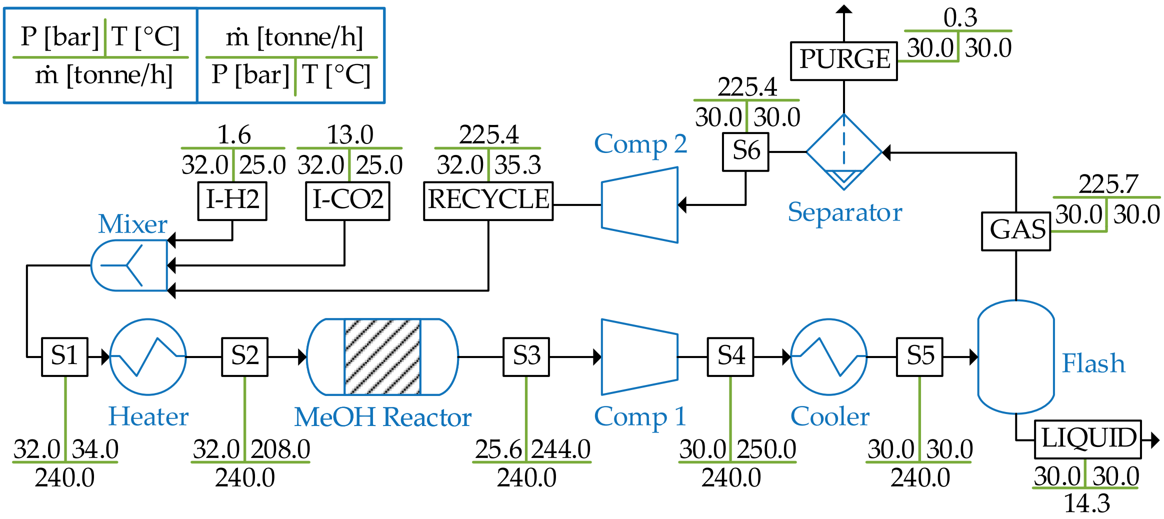

Figure 4.2: Process diagram of the MeOH synthesis subsystem with the corresponding temperatures, pressures and mass flow rate.

In Figure 4.2, additional components have been implemented compared to the schematic shown in Figure 4.1 on the preceding page, in order to reach the optimised temperatures and pressures in the subsystem. These components includes a heater, two compressors and a cooler. The Heater heats the reactants to a temperature of 208.0 °C prior to the Reactor. The Reactor is defined as being adiabatic from which it can be seen that the temperature has increased to 244.0 °C. Additionally the pressure drops throughout the reactor from 32.0 bar to 25.6 bar. Since the optimised operational conditions for the Flash separator is 30 bar and 30 °C, both compression and cooling of this stream is required. The pressure is increased in the first compressor and the temperature is decreased in the Cooler. Since the output of the Reactor needs to be cooled and the input heated, a heat exchanger could be implemented to reduce the OPEX. This will be further analysed in the following Chapter 5 on page 89. The optimum pressure of the reactor is 32.0 bar, while the pressure of the recirculated gases are 30 bar. As such a second compressor is implemented to increase the pressure of the gases by 2 bar.

The resulting molar flow of H_2 from the optimisation yields a reduction compared to its initial value. The initial value corresponded to a molar flow three times larger compared to CO_2, however, the final value corresponds to approximately 2.6. The optimum molar flow of H_2 becomes 0.2152 kmol/s which is used to define the size of the electrolyser. Lastly the dimensions of the reactor have been determined by the optimisation to be 2.1 m and 6.46 m for its diameter and length, respectively. The associated conversion rates may be seen in Figure 4.3 as function of the reactor length. Furthermore, the corresponding gradients are also illustrated.

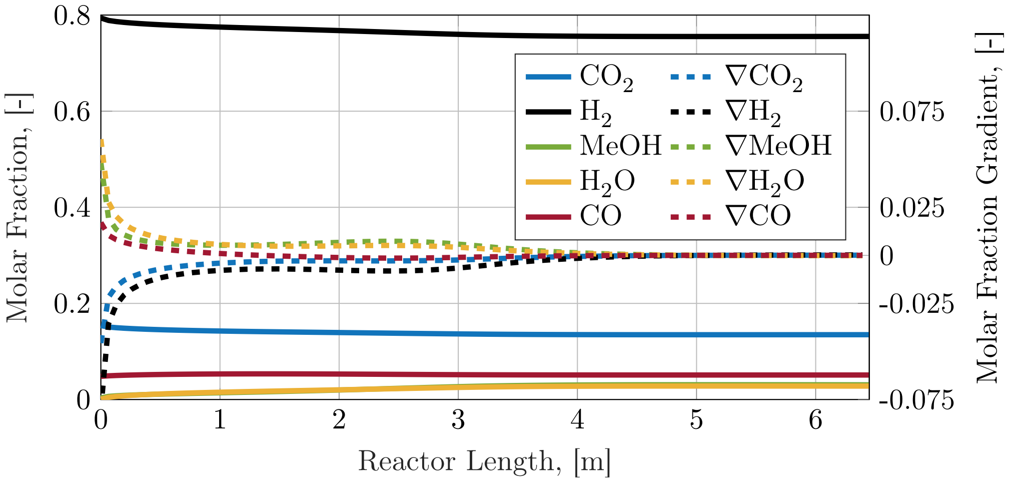

Figure 4.3: The MeOH synthesis conversion rates and conversion gradients, with a diameter of 2.1 m.

From the molar fractions it may be seen that the H_2 is the dominating species, which was to be expected due to its flow being approximately 2.6 larger than the CO_2. Also, the molar composition of MeOH, H_2O and CO increases as expected while H_2 and CO_2 decreases, which may be seen from the gradients. From the gradients it may also be seen that the largest conversion rates occur within the first meter of the reactor, whereas they all approach zero somewhere between 4 m to 5 m downstream. The reason why the reactor length has been optimised to be above 6 m and not somewhere in between 4 m to 5 m, is due to lack of variables in the optimisation algorithm. If the CAPEX of the reactor was to be included in this optimisation, it is expected that the optimum length would be closer to the point where the gradients approach zero. The difference in MeOH production depending on the reactor length being approximately 4.5 m or 6.46 m is assumed to be insignificant, compared to the costs of extending the reactor. If the reactor length is reduced to 4 m the reduction of the MeOH molar flow exiting the flash separator is approximately 0.02 mol%, from which this length is chosen to reduce the CAPEX. Furthermore, the pressure loss is also reduced by approximately 2.9 bar which lowers the costs of the compressor. The resulting values of the optimisation algorithm are shown in Table 4.2.

Table 4.2: Final values for the MeOH synthesis optimisation.

	Initial value	Optimised value	Unit
CO_2 molar flow	0.0816	0.0816	kmol/s
H_2 molar flow	0.2448	0.2152	kmol/s
Length	24.3	4.0	m
Diameter	1.3	2.1	m
Reactor inlet temperature	230.0	208.0	°C
Reactor inlet pressure	25.5	32.0	bar
Flash separator temperature	60.0	30.0	°C
Flash separator pressure	25.5	30.0	bar

Applying the resulting values of the optimisation, the corresponding liquid composition of the mixture exiting the flash separator may be seen in Table 4.3.

Table 4.3: Mass fraction and mass flow of the liquid output from the flash separator.

Species	Mass fraction [%]	Mass flow [kg/s]
MeOH	57.29	2.27
H_2O	32.42	1.28
H_2	0.04	1.57e-3
CO_2	10.11	0.40
CO	0.20	5.32e-3

It may be seen from Table 4.3 that some of the gases remain dissolved in the liquid in the output of the flash separator, which might be undesired in the downstream unit operations. The gas and H_2O content must be separated if the end product is commercial Green MeOH, which has a purity requirement of 99.85 wt%. This may however not be necessary if the objective is to produce BTX, since H_2O, H_2, CO_2 and CO are all byproducts in the BTX synthesis, as earlier presented in Section 2.6. This results in two different downstream subsystems which will be presented and modelled in the following sections.

4.2 Separation of Methanol

In the first subsystem the subsequent key component to the reactor is the distillation column which separates the MeOH-H_2O solution, when the desired end product is Green MeOH. The relative volatility is the driving factor in the distillation technique, whereas the gases presented in Table 4.3 will end up in the distillate stream. This is undesired since the MeOH is the lighter species in the binary MeOH-H_2O solution, hence the majority of the MeOH ends up in the distillate stream. This leads to a choice between either degassing the mixture prior to the liquid-liquid distillation column or from the distillate stream containing the MeOH and gases. However, in order to perform the procedure for distilling the binary MeOH-H_2O solution, as presented in Section 2.5.3, the degassing process must take place prior to the distillation column.

A suitable equation of state must be chosen in order to produce valid results. The non-random two-liquid (NRTL) equation of state is chosen for this analysis and the remaining processes presented in this section. This is due to the relatively low pressures used throughout this section, making it the suitable approach according to the Aspen Plus software.

4.2.1 Degassing of Liquid Phase

The gases are dissolved in the liquid, however, they can be released by changing the temperature and pressure. The pressure influences the maximum number of moles of gas that can be dissolved in the mixture, which is defined by Henry's law presented in Eq. 4.1

$$H_C = \frac{p_g}{x} \tag{4.1}$$

where H_C is the Henry's constant and p_g is the partial pressure of the specific gas. Henry's law states that the maximum number of moles of gas dissolved in the mixture is proportional to the partial pressure. Additionally, the Henry's constant is temperature dependent and the Henry's constants for CO, CO_2 and H_2 all increase as temperature increases. Hence, the expected outcome is that the performance of the degassing process is enhanced at decreased pressure and elevated temperature. An investigation has been conducted to determine if the degassing process is sufficient by simply applying these operational conditions, which is carried out by feeding the stream into a flash separator. The pressure of the liquid exiting the MeOH synthesis is 30 bar whereas the desired pressure region for the degassing process is relatively low. The operational conditions of the consecutive liquid-liquid distillation column with respect to the pressure is 1.1 bar. The pressure of the degassing process is therefore varied from 5 bar to 1 bar. The temperature of the liquid exiting the MeOH synthesis is 30 °C whereas the feed stream for the distillation process is desired to retain its liquid state, where an estimated boiling point for the mixture is 70 °C at standard pressure. The temperature of the degassing process is therefore varied from 30 °C to 60 °C. The results of this analysis may be seen in Figure 4.4.

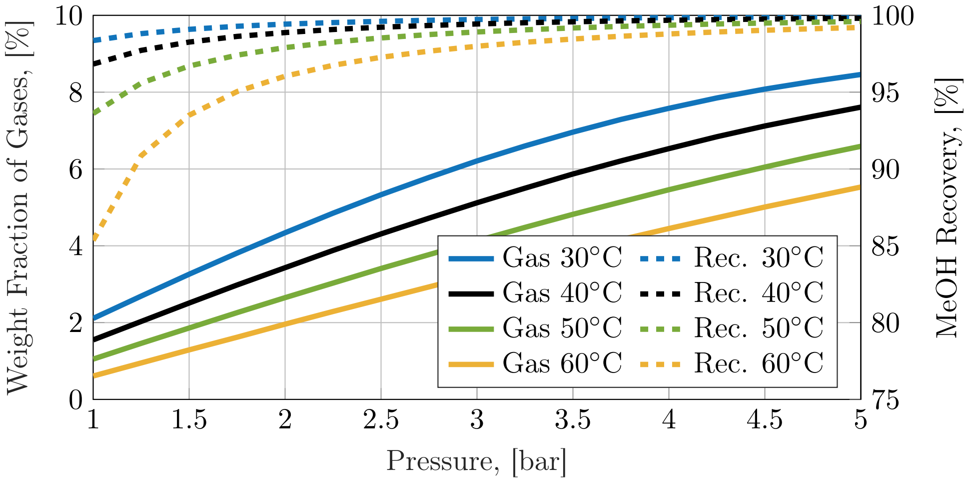

Figure 4.4: The mass fraction of the dissolved gases are denoted Gas and the MeOH recovery is denote Rec., at different temperatures as function of pressure.

From figure 4.4 it becomes evident that manipulating the operational conditions of the flash separator decreases the amount of dissolved gases, however, this comes at the expense of MeOH recovery. At the operational conditions of 1 bar and 60 °C the content of dissolved gases is approximately 0.61 wt%. The separation remains insufficient, due to the impurity tolerance of the pure MeOH being 0.15 wt%. From the relation that this process comes at the expense of MeOH recovery, it is obvious that a more complex separation method is required. Such a method could be the fractional distillation technique.

The distillation is performed in the Aspen Plus software of which three unit components are available, named DSTWU, Distl and RadFrac. Both the DSTWU and Distl units are known as simple unit components, since they require relatively few inputs from the user. The DSTWU unit component is typically used in designing of the distillation column. It estimates either the minimum reflux ratio or the number of plates, by defining one of these. This unit component additionally calculates the optimum feed plate location, as well as condenser- and reboiler duty. The Distl unit component estimates condenser- and reboiler duties, which requires the number of plates, reflux ratio and overhead product rate to be defined. Both of these units are however not suited, due to the non-ideal characteristics of the mixture [Miroshnichenko and Vrabec, 2015] [Corsaro et al., 2018].

The RadFrac unit component is, compared to the other units, a more rigorous model, which requires additional input specifications [Aspen Technology, 2000]. In addition to the number of plates and reflux ratio, the RadFrac unit component also requires specifications for bottoms rate, feed plate location, plate spacing and column diameter. The number of plates, reflux ratio and feed plate location all influence the performance of the distillation column. The number of plates is associated with the CAPEX of the column whereas the reflux ratio influences the OPEX. This results in the necessity of an optimum study to find the most feasible combination, as will be presented in Section 4.2.2 on page 69.

The determination of optimum feed plate location is also essential in the designing of distillation columns, due to its influence on the performance of the column, where a non-ideal location results in increased boiling and condensing duties [Taqvi et al., 2016]. In contrary to the design process for a binary solution, presented in Section 2.5.3, this mixture consists of multiple species of which the McCabe-Thiele method is not applicable. Column designing for a multi-species mixture is a known issue, where a study done by Labarta [2001] have developed more sophisticated models to overcome this challenge. An alternative to performing these models is to make an optimisation study in Aspen Plus. Taqvi et al. [2016] conducted an optimisation of the reboiler duty, where multiple parameters such as feed plate location and number of plates were included. They implemented this into Aspen Plus with predefined specifications such as reflux ratio and purity requirement. The distillation column presented in this section is coupled to a subsystem where the bottom product is transported to an additional distillation column. This results in an increased complexity if the previously mentioned algorithm is applied.

Due to these complications a simplification has been applied of which only the boil-up ratio is varied and as such a sensitivity analysis has been performed. The boil-up ratio is equivalent to the reflux ratio, but it concerns the bottom product instead of the distillate stream. The boil-up ratio is investigated since the MeOH will accumulate in the bottom stream. If the number of plates are specified to be three, the feed location is not required to be analysed, since plate No. one and three represent the condenser and reboiler, respectively. The feed stream is defined according to Table 4.3 on page 63, where the temperature is equal to the output of the MeOH synthesis, being 30 °C. The distillation column is known to operate within the boiling points of the involved species. This results in a preliminary investigation regarding the influence of the temperature of the feed stream to the performance of the column. This investigation showed that the temperature had no significant influence, hence heating or cooling prior to the distillation column will not be done, neither for the degassing- nor the following liquid-liquid distillation. The pressure is defined as 1.1 bar, which is the common operation pressure when distilling a MeOH-H_2O solution, as presented in Section 2.5.1. Additionally, the rate of the bottom product is specified to be 3.55 kg/s corresponding to the sum of the MeOH- and H_2O flow from Table 4.3 on page 63. By fixating the bottom rate, the condenser- and reboiler duties will be determined by Aspen Plus according to the varied boil-up ratio.

The determination of the mechanical design is, similar to the process design, complicated for a multi-species mixture. The determination of mixture properties such as: density, viscosity and surface tension is complicated when the mass fraction of each species is unknown throughout the column. This leads to the necessity of designing the distillation column by utilising the Aspen Plus software. Aspen Plus has an implemented function which constructs a hydraulic plot. The hydraulic plot concerns the factors presented in the mechanical design in Section 2.5.3, where the factors differ if the internals of the distillation column are plates or packing. A suitable diameter is chosen from the hydraulic plot in order to satisfy efficient operation of the distillation column. The hydraulic plot changes depending on the vapour- and liquid flow rates throughout the distillation column of which the determination of the column diameter becomes an iterative process depending on the individual boil-up ratio value. In order to properly explain the procedure of determining the diameter from the hydraulic plot, the following hydraulic plots are generated from the optimal boil-up ratio determined by the currently investigated sensitivity analysis.

For plate columns, the diameter is determined from the maximum vapour mass flow, also known as flooding. However, a safety factor is applied, generally specified to 80 %, from which the minimum allowable diameter is defined.

The hydraulic plot for the plate column is shown in Figure 4.5.

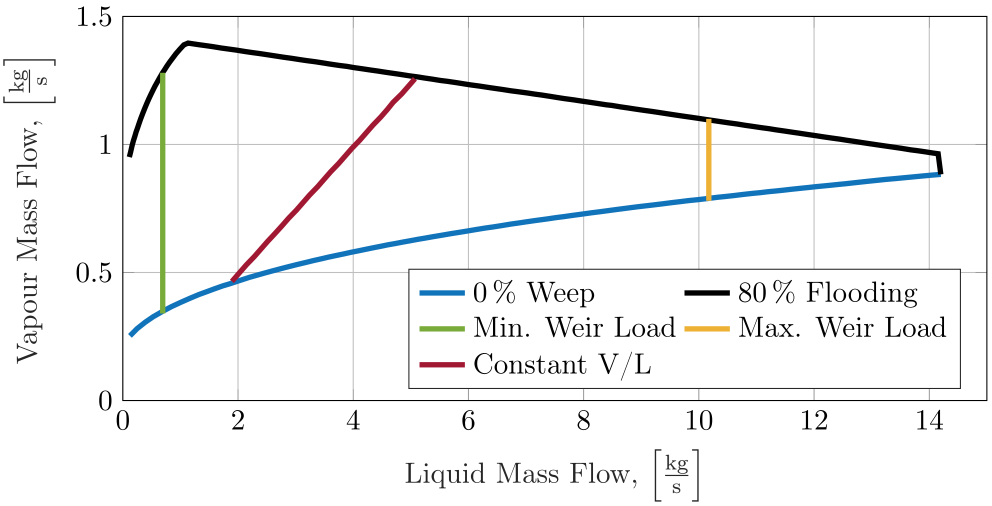

Figure 4.5: Hydraulic plot for plate column.

In addition to the allowable vapour mass flow, the factors: 0 % weep, constant V/L, minimum- and maximum weir load are all included in Figure 4.5. Weeping occurs when the vapour mass flow is insufficient at keeping the liquid from weeping through the holes in the plate which is undesired. The minimum- and maximum weir load refer to the liquid level on the plate, due to frictional forces and it defines the operating range of the liquid mass flow. If the liquid mass flow rate is insufficient, the liquid will not flow throughout the column properly and if the liquid mass flow exceeds the maximum, the vapour will not be able to sufficiently travel through the liquid. As such the actual liquid- and vapour mass flow rate must be within these boundaries. If these criteria are fulfilled the diameter does not influence the performance of the distillation column. This is shown by the Constant V/L line in Figure 4.5 on the facing page, which represents the liquid- and vapour velocity. The operating point will as such be somewhere on the Constant V/L line, where the CAPEX will be reduced, when the operating point approaches the minimum allowable diameter. From the hydraulic plot shown in Figure 4.5 on the preceding page, the minimum allowable diameter is indirectly determined to be 0.92 m.

As previously discussed, both the diameter for the plate- and packed column must be determined. With respect to the packed column the primary factor in the hydraulic plot is the pressure drop, as shown in Figure 4.6.

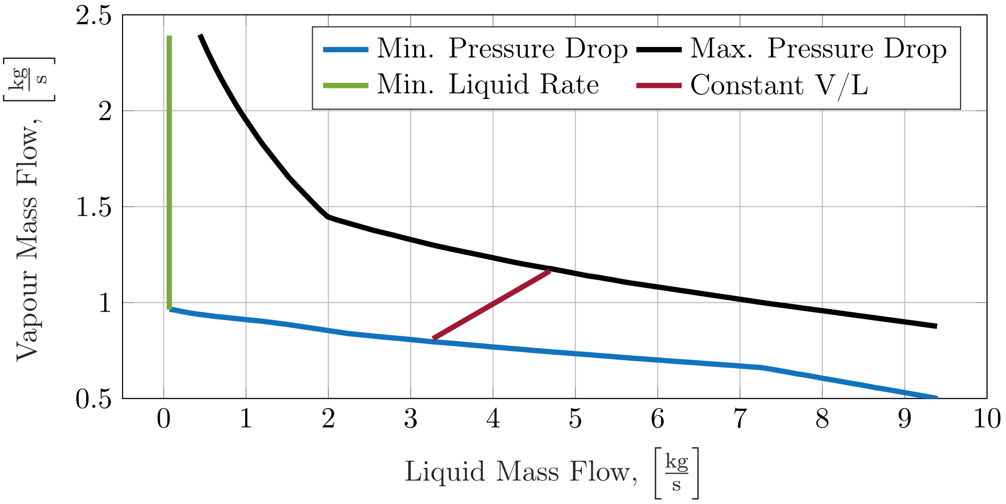

Figure 4.6: Hydraulic plot for packed column.

As earlier presented in Section 2.5.3, the allowable pressure drop range is within 0.08 kPa/m to 0.8 kPa/m, corresponding to Min. pressure drop and Max. pressure drop in Figure 4.6, respectively. Additionally, the liquid mass flow rate must be larger than the minimum value, also shown in Figure 4.6. The minimum allowable diameter is estimated from the Constant V/L line when it intersects with the maximum allowable pressure drop, which indirectly yields a diameter of 0.81 m.

As previously discussed in Section 2.5.3, the diameter must be greater than 1 m for the plate column to be considered. However, the plate column diameter was determined to be 0.92 m, hence the packed column will be used, with a diameter of 0.81 m. In order to conduct the sensitivity analysis, regarding the boil-up ratio, the column diameter had to be determined. Given the above mentioned diameter, the analysis can be conducted, where the results may be seen in Table 4.4 on the next page.

Table 4.4: Sensitivity results for distillation yield.

Boil-up ratio [-]	Gaseous content in bottom [wt%]	Recovered MeOH [wt%]
0.10	1.07e-1	99.84
...	...	...
0.31	1.02e-2	99.98
0.32	9.79e-3	99.99
0.33	9.43e-3	99.99

From Table 4.4 it becomes evident that a packed column with 3 segments of packing is capable of sufficiently degassing the mixture, with respect to the previously defined purity requirement. With an impurity tolerance of 0.15 wt% an acceptable gaseous content of 0.01 wt% has been chosen. This corresponds to a boil-up ratio of 0.32 for the distillation column in question, where the duties of the condenser and reboiler are 0.990 MW and 1.578 MW, respectively. Figure 4.7 shows the operational conditions of the involved streams for this distillation column.

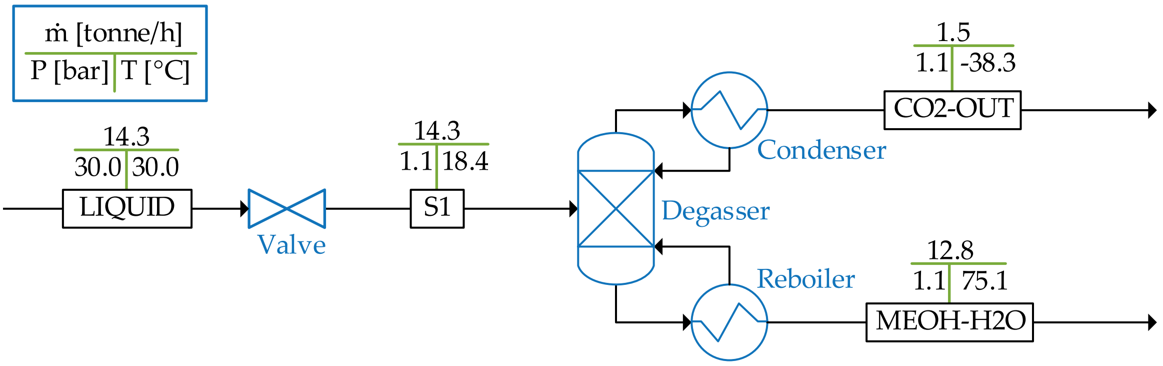

Figure 4.7: Packed distillation column for the degassing subsystem with corresponding streams temperature and pressure.

The distillate stream consists of approximately 98 wt % CO_2 which is known to be the limiting reactant for the MeOH synthesis. Furthermore, the mass flow of this stream is approximately equal to 12 wt% of the CO_2 feed stream, used in the previously presented MeOH synthesis, from which there is a potential for recirculating this gas stream in order to enhance the MeOH yield. Even though this stream cannot be considered as pure CO_2, the other species within this stream are H_2 and CO which can both contribute to an enhanced MeOH production due to hydrogenation of CO. In order to implement this feedback stream, re-scaling of the entire system will however be a necessity, which will be discussed in the upcoming Chapter 5 on page 89.

The bottom product of this degassing distillation column, will then be fed into the liquid-liquid distillation column, where the composition is as presented in Table 4.5 on the next page.

Table 4.5: Mass flows and composition of bottom stream.

Species	Mass fraction [%]	Mass flow [kg/s]
MeOH	63.85	2.27
H_2O	36.14	1.28
H_2	1.57e-11	5.59e-13
CO_2	9.43e-3	3.35e-4
CO	1.11e-7	3.97e-9

The gaseous content of the bottom stream is approximately 0.01 wt% of which the gases are considered negligible in the remainder of this system.

4.2.2 Distillation of Liquid-Liquid

The remaining process is the distillation of MeOH from the binary MeOH-H_2O stream presented in Table 4.5. The process- and mechanical design of this column will be presented firstly, and subsequently its performance will be evaluated.

Process Design

While fulfilling the purity requirement of commercial MeOH, different combinations of reflux ratios and number of plates are possible. This is due to their intercorrelation, as earlier presented in Section 2.5.3. The reflux ratio impacts the OPEX, while the number of plates influences the CAPEX. The optimum combination results in the lowest total costs of the distillation column as shown in Figure 4.8.

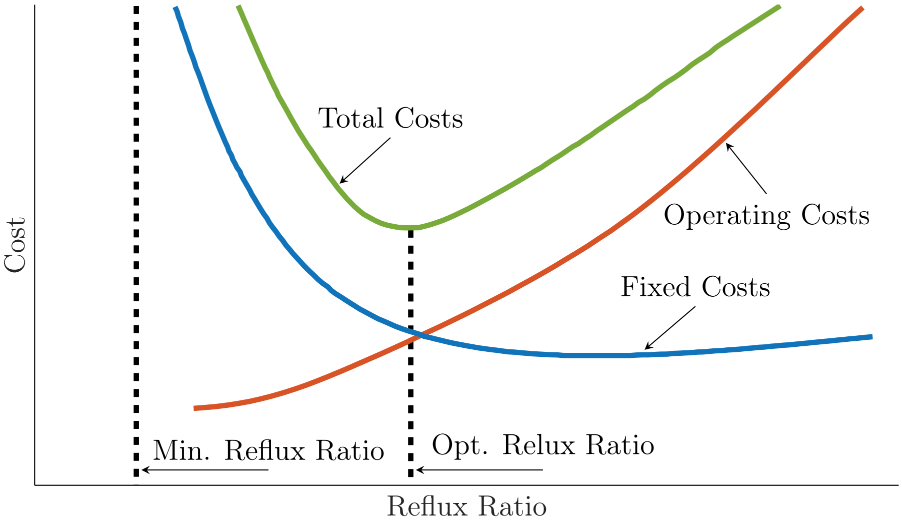

Figure 4.8: Costs of distillation column versus reflux ratio. Adapted from [Gaurav et al., 2016].

Typically, the optimum reflux ratio is in the range of 1.2 to 1.5 times the minimum reflux ratio [Coker, 2007]. A value of 1.5 has been chosen, from which the reflux ratio can be estimated. The minimum reflux ratio is determined from the McCabe-Thiele diagram, by evaluating the operational line in the rectifying section. The slope of this operational line is defined by the reflux ratio, where the minimum reflux ratio is when this line intersects the vapour equilibrium curve, as presented in Section 2.5.3. The units in the McCabe-Thiele diagram are molar based of which the MeOH purity requirement of 99.85 wt%

must be converted to molar fraction, which yields 0.9973. By specifying the molar fraction of MeOH in the bottom stream to be 1 mol%, the resulting minimum reflux becomes 0.72. This constraint has been defined in order to ensure a relatively high recovery rate of the MeOH. The McCabe-Thiele diagram shown in Figure 4.9 is defined by the corrected molar reflux ratio being 1.08 which is used to determine the number of theoretical plates and optimum feed plate location.

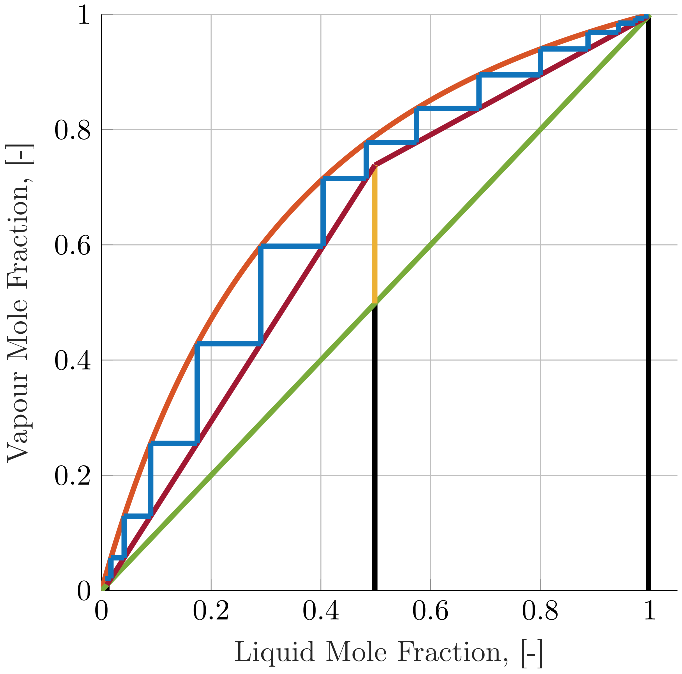

Figure 4.9: McCabe-Thiele diagram of this distillation column.

From Figure 4.9, the resulting number of theoretical plates and feed plate location is 15 and 8, respectively. This concludes the process design from which the mechanical design can be performed.

Mechanical Design

The mechanical design will be performed based on the procedure presented in Section 2.5.3. The first objective is to determine which column is best suited, either the plate- or packed column, where the choice is based on the diameter of the distillation column. The calculations for estimating the diameter of the distillation column is done in Appendix B. However, the composition of the reflux is unknown, as such a sensitivity analysis is performed in order to estimate the influence of the composition to the resulting diameter. The calculated diameter of the plate column and the packed column as function of composition of the reflux is shown in Table 4.6 on the facing page.

Table 4.6: Column diameter as function of composition.

MeOH composition of reflux [wt%]	Plate column [m]	Packed column [m]
0	1.30	1.45
10	1.51	1.48
20	1.54	1.51
30	1.57	1.53
40	1.60	1.55
50	1.42	1.58
60	1.45	1.60
70	1.50	1.63
80	1.55	1.66
90	1.60	1.70
100	1.67	1.74

From Table 4.6 it is evident that the column diameter is within the range of 1.30 m to 1.74 m, where it also is shown that the diameter of the column increases as function of the MeOH composition of the reflux. In general the resulting diameter for the packed column is larger than for plate column, except in the MeOH composition range of 10 wt % to 40 wt %, due to the influence of foaming occurring in a plate column. The foaming was previously assumed to be present within this composition range. Since the calculated column diameter is larger than 1 m, it is concluded that the plate column is best suited for distilling the MeOH-H_2O solution. It is expected that the reflux will consist of insignificant amounts of H_2O due to the purity requirement of MeOH being 99.85 wt % of which the diameter of 1.67 m is chosen.

The height of the plate column is determined by Eq. 4.2

$$\mathcal{L} = \text{plate spacing} \cdot \mathrm{N} + 1.22 + 3.05 \tag{4.2}$$

where N is the number of plates and the constants are due to practical aspects as presented in Section 2.5.3. By defining the number of plates to be 15 and a plate spacing of 0.60 m, the height of the plate column becomes 13.27 m. This concludes the both the process- and mechanical design of the column of which it will be implemented in Aspen Plus to determine its performance.

Model

The distillation column is modelled according to the presented design specifications. Additionally, the distillate rate is specified of which Aspen Plus determines the corresponding condenser- and reboiler duty. The distillate rate is specified according to Table 4.5 on page 69, where the distillate rate is set to equal the mass flow of MeOH. The results of this distillation column is shown in Table 4.7.

$MeOH_D$	$MeOH_B$	H_2O_D	H_2O_B	$MeOH_D$	$MeOH_B$	Recovery
$\left[\frac{kg}{s}\right]$				[wt%]		
2.24	0.03	0.03	1.26	98.76	2.18	98.77

Table 4.7: Mass flow and composition outputs from the distillation column. The distillate is denoted D, whereas the bottom is denoted B. The mass fraction of the input is 63.86 wt % and 36.14 wt % of MeOH and H_2O, respectively.

From Table 4.7 on the previous page it becomes evident that the current design is insufficient at separating the MeOH, as a purity of only 98.78 wt % can be achieved. This was expected since the process design defined by the McCabe-Thiele method would be inadequate, due to the violation of two assumptions of which the McCabe-Thiele method is based upon. The two violated assumptions are that the heat of vaporisation of the two species must be equal and that the plates are ideal. The application of these assumptions are represented by the horizontal and subsequent vertical lines in the McCabe-Thiele diagram. If the two species have identical heat of vaporisation, then the energy released when a mole of H_2O condenses equals the required energy for one mole of MeOH to evaporate. The assumption regarding ideal plates make it such that a vapour-liquid equilibrium is achieved at each plate. [Ravi, 2007] The difference in the heat of vaporisation of the two species is approximately 15 %[Egineeringtoolbox.com, 2010][Egineeringtoolbox.com, 2018]. Non-ideal plates are a common issue in distillation column design, where numerous correlations exist to define an estimated efficiency [Neutrium.net, 2018] [Duss and Taylor, 2018]. This results in the necessity of re-designing the distillation column.

The two major parameters in the process design of the distillation column is the reflux ratio and the number of plates, as earlier presented. The reflux ratio is fixed due to the earlier presented relation between the simplified optimum reflux ratio and the minimum reflux ratio. As such, a sensitivity analysis will be conducted where the number of plates are varied from the theoretical value of 15 plates to 81 plates, the latter corresponding to the maximum height of 53 m according to earlier presented practical aspects in Section 2.5.3. However, the feed plate location is unknown and must be estimated since it also has a significant influence on the performance of the distillation column, as earlier presented. This results in the necessity of defining the feed plate location as function of the number of plates. This was done by Taqvi et al. [2016] where a fixed ratio of 2/3 times the number of plates defined the feed plate location. This ratio was determined from an optimisation in Aspen Plus where the minimum reboiler duty was determined at the feed plate location equivalent to 2/3 times the number of plates. The feed plate location is dependent on numerous factors such as number of plates, molar fractions of distillate, feed and bottom product, which may be determined from the McCabe-Thiele method. This yielded a feed plate location at the eighth plate, where the total number is 15, as shown in Figure 4.9 on page 70. The feed plate location ratio of 8/15 is kept constant in this analysis where the resulting MeOH purity and MeOH recovery is shown in Figure 4.10.

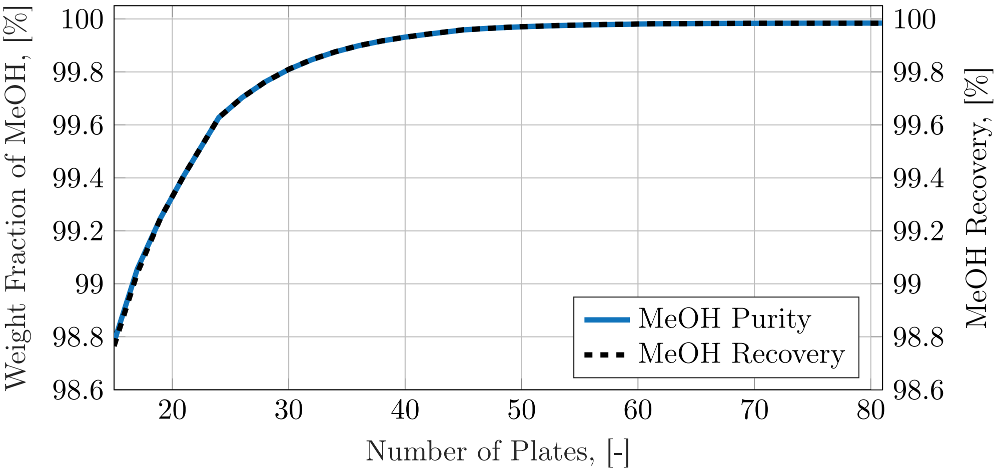

Figure 4.10: MeOH purity and MeOH recovery as function of number of plates.

From Figure 4.10 on the facing page it becomes evident that the increased number of plates results in a sufficient separation. The MeOH purity requirement is fulfilled when the distillation column contains 34 plates, where the corresponding feed plate location is 18. This results in a MeOH recovery of 99.86 wt % corresponding to producing 2.27 kg/s. The corresponding duties of the condenser and reboiler are 5.19 MW and 5.35 MW. The belonging stream temperatures, pressures, and mass flow rates for the column may be seen in Figure 4.11.

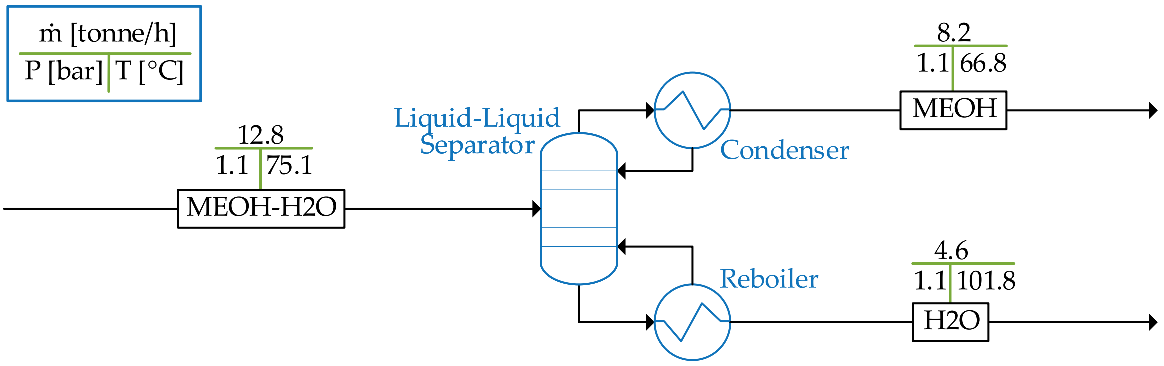

Figure 4.11: Plate distillation column for the liquid-liquid subsystem with corresponding streams temperature and pressure.

4.3 BTX Synthesis

In System 2 it is of interest to investigate the conversion of MeOH to other chemicals, which might be more profitable, such as BTX, as was presented in Section 2.6. The product distribution stated in Na et al. [2018] is defined from the outlet of a flash separator and not the reactor. However, Na et al. [2018] only defines the operational conditions for the reactor and not the flash separator. As such, the use of the kinetics stated in Na et al. [2018] becomes limited. In order to account for this, a model similar to theirs is designed in order to obtain equal results. If this model replicates similar results for the product distribution, the model is deemed viable for incorporation into System 2. Na et al. [2018] defines the equation of state to be the Universal Quasichemical (UNIQUAC), which is suitable for systems with strongly non-ideal liquid mixtures and liquid-liquid equilibrium, from which the following model is based upon. The system defined by Na et al. [2018], with the limited stream information, may be seen in Figure 4.12 on the following page.

An overview of the different components and streams required for this process is shown in Figure 4.12 on the next page.

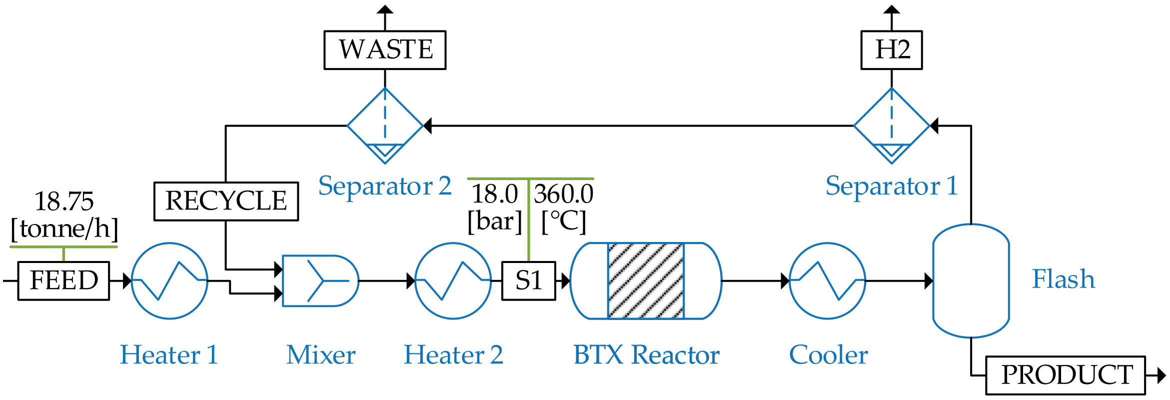

Figure 4.12: Process diagram of the MeOH to BTX subsystem, defined by Na et al. [2018] with the limited stream information[Na et al., 2018].

The feed supplied to the reactor is a mixture of a pure MeOH and a recycle stream, where the MeOH stream has a flow rate of 18,750 kg/h. Two heaters are implemented prior to the reactor: the first is only being used to heat the pure MeOH feed, while the second heats up the mixture. The mixture stream is heated in coherence to Na et al. [2018], where a temperature of 360 °C is chosen as a compromise between BTX production and catalyst degradation. If the temperature in the reactor increases too much it may result in coke formation and hereby catalyst deactivation, hence the input temperature should not be increased without this consideration. The pressure for the subsystem is kept at a value of 18 bar as assigned by Na et al. [2018].

The reactor itself is adiabatic, with a length of 5 m and diameter of 3.1 m, catalyst loading of 24.95 tonne and catalyst density of 2 g/cm^3. The catalyst used is ZSM-5. The reactions occurring in the reactor, which was outlined in Table 2.5 on page 37, are overall exothermic, resulting in the stream exiting the reactor being warmer than its feed stream. In order to extract the BTX in the flash separator it is crucial that it is at liquid state, from which it must be cooled, or the flash separator must operate at a elevated pressure level. However, since other products than BTX is produced, the separation of these will also be affected by the operational conditions of the flash separator. Na et al. [2018] states that the BTX conversion produces a relatively large amount of excess H_2 which is then separated after the flash separator. Due to its significant flow rate, it could be feasible to recycle it to the MeOH synthesis and thereby reduce the required amount of electrolysis, which will be discussed in Chapter 5 on page 89. The separation fraction for H_2 in the separator is specified to 98 wt%. Equal to the MeOH synthesis, a separator is incorporated in the feedback loop in order to purge some of the impurities which could otherwise accumulate. The recycle ratio is determined to be 8.2 as defined by Na et al. [2018], which is the ratio between the recycled flow and the feed, as shown in Eq. 4.3.

$$\text{Recycle ratio} = \frac{\dot{n}_{\text{recycle}}}{\dot{n}_{\text{feed}}} \tag{4.3}$$

The recycled gas is used to effectively control the temperature rise caused by the exothermic reactions in the reactor.

When directly implementing the above described subsystem into Aspen Plus, along with the reactions presented in Section 2.6, the product stream did not provide similar results to those presented by Na et al. [2018]. This is attributed to the general information, provided in the study and the few other publications on the subject, not being detailed. Because of this it became necessary to consider the subsystem as a grey box model, meaning some specifications were not supplied by the study used to create the model, thereby making it a necessity to fit the model to provide equal results.

This was achieved by investigating the activity coefficients of the reactions as well as the temperature and pressure of the flash separator. The activity coefficients are essentially scalar multipliers on the reaction rates. Hence, the actual reaction rate of the different reactions is a product of the reaction activity and the intrinsic reaction rate, the latter being the only parameter provided by Na et al. [2018], which was presented in Table 2.5 on page 37.

In order to determine the activity coefficients, temperature and pressure of the flash separator, such the desired conversion rates stated in Na et al. [2018] can be obtained, an optimisation algorithm is defined to approach these rates. If sufficient data had been given the problem could be solved algebraic, however, this is not possible due to the lack of information. Through a preliminary investigation it was determined that the optimisation had difficulties converging, due to the number of variables and constraints. The reaction scheme is defined from 13 reactions, where an equal number of activity coefficients are defined as variables. Additionally, 2 variables are introduced being the temperature and pressure of the flash separator, from which the total number of variables becomes 15. Essentially, 7 constraints could be defined, being the molar fraction of the five lumped products after the flash separator, the annual flow rate of Aromatics and the outlet temperature of the reactor. However, if all 7 constraints were applied the optimisation algorithm became too restricted from which the temperature of the reactor was not included, but evaluated in the post-processing. The molar fractions of the lumped products after the flash separator are given by Na et al. [2018], however, the molar fractions of each species are not given, which could have eased the optimisation. The annual production of Aromatics is also defined by Na et al. [2018], which is used as a constraint. Since the given information from the study is limited, the results obtained from the optimisation algorithm were expected to differ from the stated values given by Na et al. [2018]. The acquired results attained by the optimisation algorithm as well as the results given by Na et al. [2018], and the corresponding relative- and absolute difference, may be seen in Table 4.8.

Table 4.8: Relative- and absolute differences between the results by Na et al. [2018] and the acquired results attained in the presented study, with a reflux ratio at 8.2 and the inlet temperature of the reactor at 360 °C, where the annual production is defined by 8,000 hours.

Category	Unit	Presented study	Na et al. [2018]	Rel. Diff.	Abs. Diff.
Alkanes	[wt%]	18.07	18.30	1.28	0.23
Aromatic	[wt%]	22.16	23.10	4.08	0.94
Heavy	[wt%]	0.94	1.00	5.97	0.06
Light Gases	[wt%]	1.36	1.30	-4.59	-0.06
Others	[wt%]	57.48	56.30	-2.10	-1.18
Reactor outlet Temp.	[°C]	432.00	428.00	-0.93	4.00
Aromatic production	[tonne/year]	31,738.60	31,751.50	0.04	14.19

The corresponding activity coefficients from the optimisation may be seen in Table 4.9 on the next page. The first activity coefficient (R1) corresponds to the first reaction given in Table 2.5 on page 37, R2 equals the second reaction, etc.

Table 4.9: Activity coefficients for the presented study.

Activity	Value [-]	Activity	Value [-]	Activity	Value [-]
R1	2.0000	R6	1.0199	R11	0.5699
R2	2.8699	R7	1.0199	R12	0.1447
R3	1.0199	R8	0.5699	R13	0.4699
R4	1.0199	R9	0.5699	-	-
R5	1.0199	R10	0.5699	-	-

Furthermore, the operational temperature and pressure for the flash separator is 32 °C and 4.2 bar, respectively. As may be seen from Table 4.9, the activity coefficients for all Aromatics, being R3 to R7, are identical and likewise are the activity coefficients for all the Alkanes, being R8 to R11. The first activity coefficient, R1, is the only integer, which is due to manual fittings performed in the post-processing. The biggest concern of the optimisation algorithm regards whether the Aromatics were representative or not, since these are the desired products. However, the relative difference in the Aromatic production can be assumed negligible due to its value of 0.04 %. Similar to the annual production, the relative differences for the rest of the variables are also assumed to be representative due to the lack of information provided by Na et al. [2018].

In order to further analyse if the fitting is representative, the tendencies of the conversion rates are analysed. Due to the lack of information, the actual values are not evaluated since no reference values are given. However, Na et al. [2018] states that the conversion of MeOH is almost complete at the end of the reactor, from which conversion rate of the MeOH may be seen in Figure 4.13.

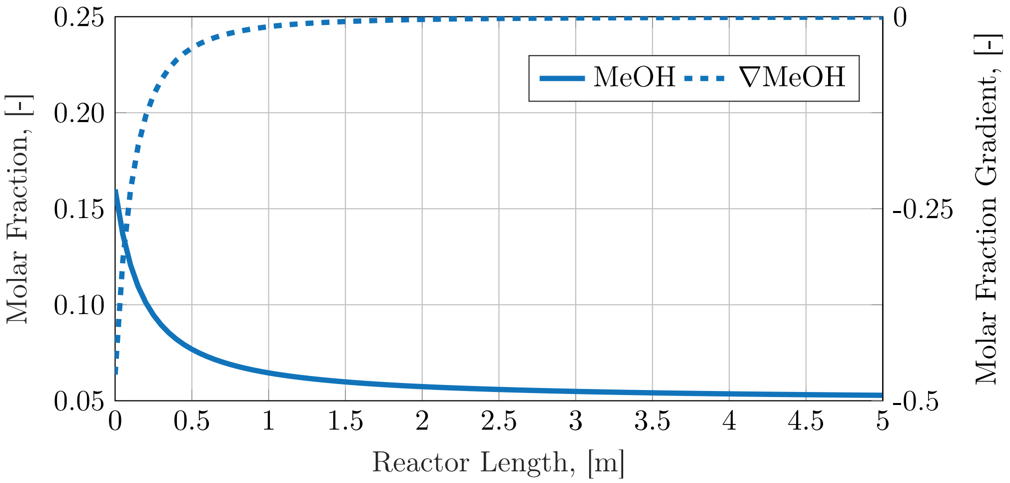

Figure 4.13: MeOH conversion as function of the reactor length and conversion gradient.

From Figure 4.13 it may be seen that the molar composition of MeOH approaches zero towards the end of the reactor. Even though nothing is stated regarding the conversion rates of the remaining products, they have still been analysed in order to determine if the tendencies look representative, which may be seen in Appendix C. Given all the conversion rates, the fitted model has been deemed representative for the results provided by Na et al. [2018], from which the fitted model can be used to estimate the production of Aromatics given the output of the MeOH synthesis previously presented in Table 4.3 on page 63.

4.3.1 Feed Composition

The fitted model is implemented into the subsystem of the presented study, of which the feed is based on the output of the MeOH synthesis subsystem. The model is originally based on an input stream of pure MeOH, whereas the input in this subsystem consists of: MeOH, H_2O, CO, CO_2 and H_2. As earlier presented in Chapter 2.6 there should be no influence of H_2O on the conversion of MeOH to Aromatics, however, the H_2O could still benefit the overall subsystem. In the study done by Na et al. [2018], they utilise a feedback loop in order to control the temperature of the reactor due to the overall reactions being exothermic. However, since the input for this subsystem also contains H_2O, which does not react, it is expected to absorb some of the released heat due to its relatively high heat capacity. The feedback ratio is as previously stated 8.2, meaning the recycled stream is 8.2 larger than the input of pure MeOH. If this ratio would be reduced due to the additional content of H_2O it could essentially reduce the size of the subsystem.

Secondly, the input stream also consists of CO and CO_2 which could affect the reactions. However, the kinetics defined by Na et al. [2018] do not include any reactions in which these gases are reactants, even though they constitute a relatively large molar fraction throughout the reactor. This leads to the hypothesis that the reactions would have been included in the kinetic data, if they were occurring. Lastly, H_2 is also present in the feed stream which is used as a reactant in the reactions regarding Alkanes, and it becomes a by-product for the Aromatics reactions. However, as previously discussed, there is a relatively large amount of excess H_2 in the subsystem, from which the additional content of H_2 might not affect the reactions.

Even though a change in the composition of the feed does not affect the kinetics, it should be investigated whether some of the species in the feed must be removed prior to the reactor for other reasons. It is assumed that the H_2O should not to be removed before the reactor, since it as mentioned can be used to cool the reactor and thereby reduce the recycle ratio. Contrary, CO, CO_2 and H_2 may affect the product flow rate composition negatively. This may occur since they are more volatile compared to the Alkanes, as such these could be recycled instead of the Alkanes. If the amount of recycled Alkanes is reduced due to this, the total flow rate of Alkanes could be reduced. In order to analyse if this hypothesis is valid, two simulations will be conducted, one with- and one without CO, CO_2 and H_2 in the feed stream.

Prior to this implementation of the different feed streams, two adjustments have been made to the model. Firstly, the recycle ratio has been adjusted for each feed stream, in order to maintain the previously defined outlet temperature of 432 °C. Secondly, the volume of the reactor is scaled to match the flow rate defined by the MeOH synthesis. In order to apply scaling, the ratio between the diameter and length of the reactor is kept constant. This has been done in order to maintain a space velocity relatively close to the initial value given from the previous model done with only MeOH as the feed. When scaling the reactor, the total catalyst mass must be taken into account, since the conversion rate unit is defined as $\mathrm{kmol}/(\mathrm{kg}\cdot\mathrm{h})$ where the mass represents the total mass of the catalyst. If the reactor volume is reduced, the total mass of the catalyst must also be reduced by the same factor.

Given these considerations three simulations have been conducted in order to investigate the composition of the lumped products in the product stream, as well as their individual mass flow rates. The first simulation, denoted S1 in Table 4.10 on the next page, is the reference results defined by a feed stream only consisting of MeOH, and an input feed flow rate of 18,750 kg/h, which is the rate given in Na et al. [2018]. The second simulation, denoted S2 in Table 4.10, is defined with a feed- flow rate and composition equal to the exiting flow of the MeOH synthesis, where MeOH, H_2, H_2O, CO_2 and CO are present. The third simulation, denoted S3 in Table 4.10, is defined with a feed- flow rate and composition equal to the exiting flow after the degassing process has been applied, from which only MeOH and H_2O are present as presented in Table 4.5 on page 69.

The mass flow rates of each simulation, denoted S1m, S2m and S3m, respectively, are also listed. The mass flow rates of the Alkanes, Aromatics and Heavy for S2m and S3m have been scaled relative to their individual difference to the amount of MeOH entering in the feed stream, which is denoted S2m* and S3m*. This has been done in order to make them comparable to the reference mass flow rate, S1m. The amount of MeOH in the feed stream for S2 and S3 are approximately 2.3 times less than the reference mass flow rate in S1. Lastly, the ratio between scaled mass flow rates of S2m* and S3m* relative to S1 have been analysed in order to investigate the influence of the gases in the feed stream.

Table 4.10: Mass fractions and mass flows for the three simulations. The scaled mass flow rates of S2 and S3 with respect to S1 is also shown, as well as the ratio between the scaled mass flow rates and S1.

	Unit	Alkanes	Aromatic	Heavy	Light Gases	Others	Sum
S1	[wt%]	18.06	22.16	0.94	1.36	57.48	100.00
S2	[wt%]	9.40	13.45	0.57	4.65	71.93	100.00
S3	[wt%]	11.49	13.86	0.59	1.20	72.86	100.00
S1m	[kg/h]	3232.20	3965.07	168.24	243.11	10284.98	17893.59
S2m	[kg/h]	1189.72	1703.82	72.19	588.86	9108.60	12663.19
S3m	[kg/h]	1429.58	1724.17	73.20	149.58	9066.36	12442.89
S2m*	[kg/h]	2729.69	3909.24	165.63	-	-	-
S3m*	[kg/h]	3294.61	3973.52	168.70	-	-	-
S2m*/S1m	[-]	0.844	0.986	0.984	-	-	-
S3m*/S1m	[-]	1.019	1.002	1.003	-	-	-

From the first three rows of Table 4.10, the composition of the lumped products may be seen. As expected the results from the second simulation show that the lumped Alkanes, Aromatics and Heavy have decreased, due to the presence of H_2, H_2O, CO_2 and CO in the feed stream, from which both the composition of the Light Gases and Others have increased. From the third simulation the composition of Others has also increased due it containing more H_2O. The contribution of the Light Gases are however, as expected, lowered compared to the second simulation since H_2, CO_2 and CO are no longer present in the feed stream.

As mentioned the mass flow rates of S2m and S3m have been scaled to make them more comparable to the reference mass flow rate of S1m. The last two rows in Table 4.10 shows the relative difference in the mass flow rates from the scaled mass flow rates. This is done in order to investigate the influence of H_2, CO_2 and CO in the feed stream.

As seen from the second last row, where the gases are present in the feed stream, the composition of Alkanes are approximately 15 wt% less than the reference mass flow rate. However, if the gases are removed prior to the process, the Alkanes, Aromatics and Heavy products are all within a 2 wt% margin from the reference mass flow rates as may be seen in the last row. Therefore, the previously presented degassing distillation utilised in the purification of MeOH in System 1 is also included in System 2 in order to increase the flow rate of the Alkanes. This yields a diameter and length of the reactor to be 2.7 m and 4.4 m, respectively. Furthermore, the total catalyst weight has been reduced to 16.96 tonne. Given this analysis the corresponding conversion rates for the Aromatics, Alkanes, Light Gases, Heavy and Others, are visualised in the following four figures, respectively.

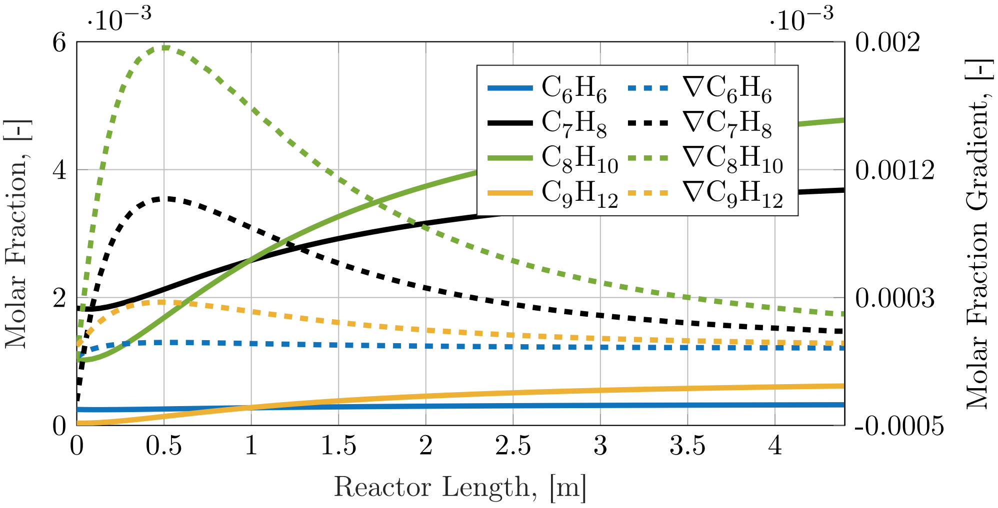

Figure 4.14: Aromatics conversion as function of the reactor length and conversion gradient.

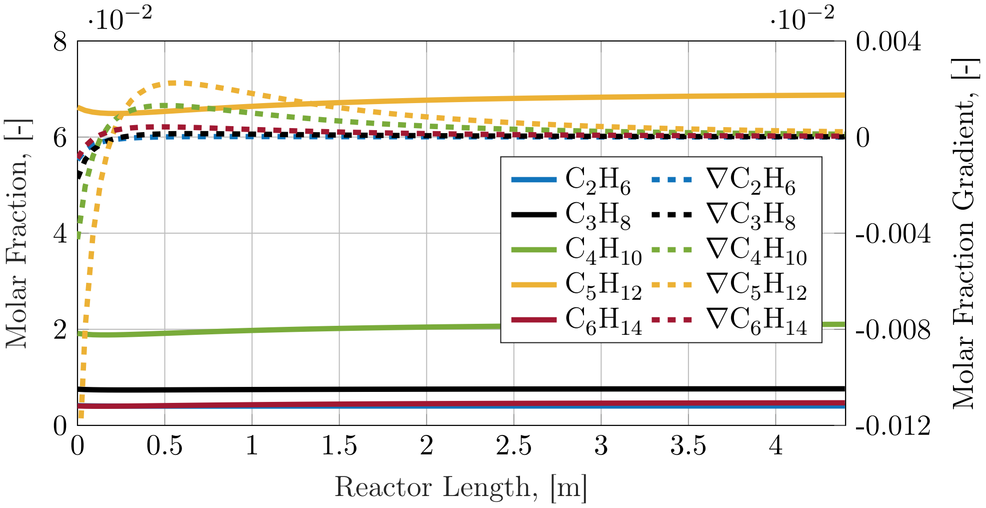

Figure 4.15: Alkanes conversion as function of the reactor length and conversion gradient.

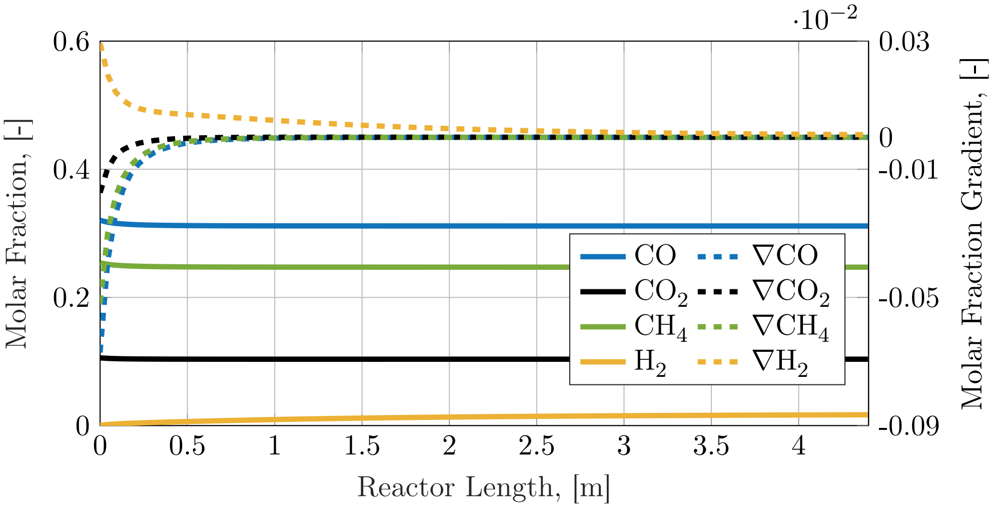

Figure 4.16: Light Gases conversion as function of the reactor length and conversion gradient.

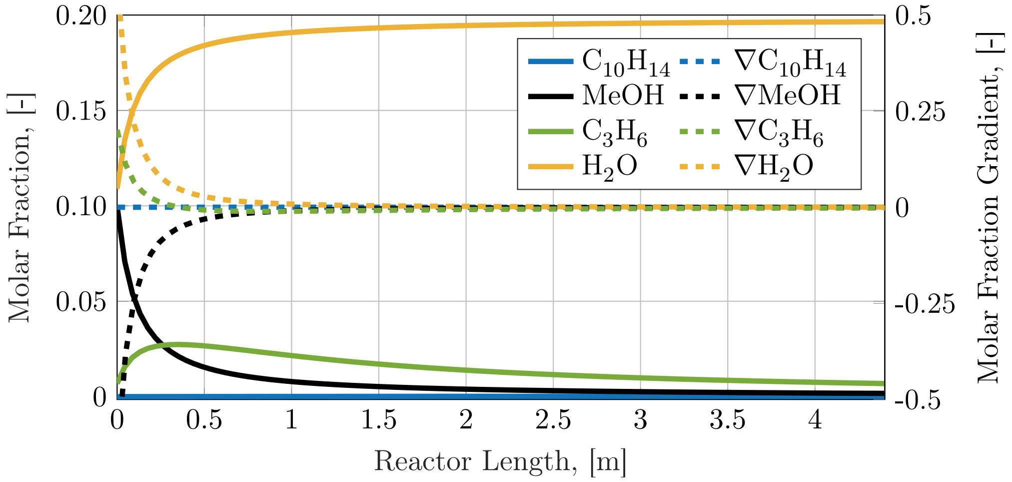

Figure 4.17: Heavy and Others conversion as function of the reactor length and conversion gradient.

The tendencies of the four figures above may be compared to those defined from the study done by Na et al. [2018] which are given in Appendix C. The tendencies can be assumed to be equal, however, the actual values differ due to the contribution of H_2O in the feed stream. The induvidual streams belonging temperature, pressure and mass flow rate may be seen in Figure 4.18.

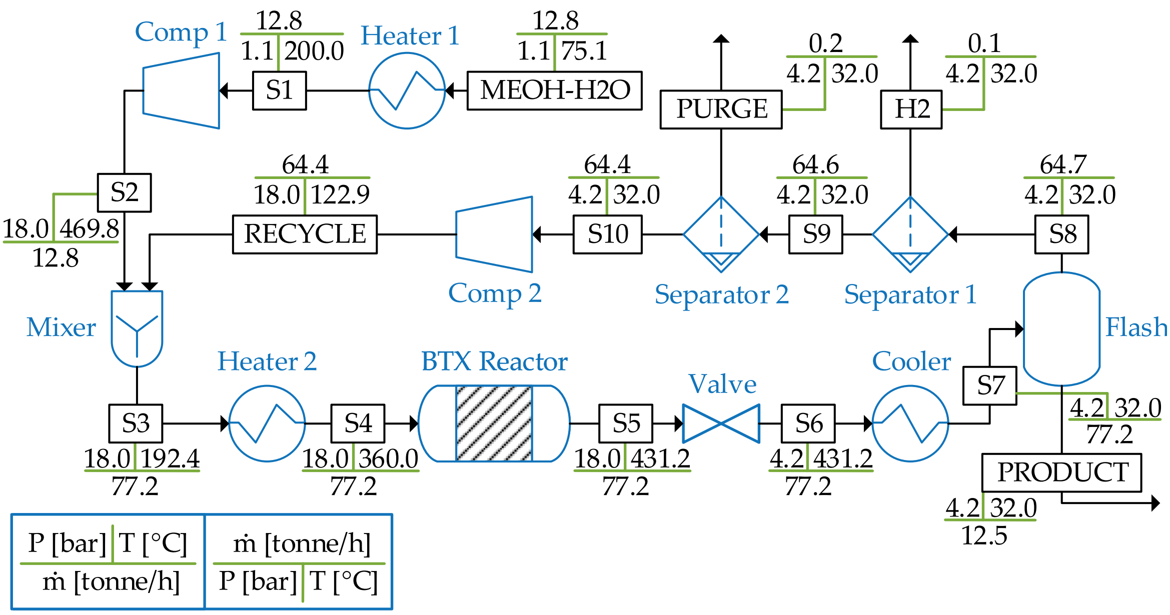

Figure 4.18: BTX synthesis subsystem, with belonging temperatures, pressures and mass flow rates.

The output stream composition of the Flash separator yields a mixture consisting of 17 different species. An analysis is required in order to determine which products must be separated to make the subsystem as feasible as possible. This will be presented in the following as well as the processes associated with the separations.

4.3.2 Distillation of BTX

The kinetics of the BTX process is based on a study by Na et al. [2018] where the species are lumped into Alkanes, Aromatics, Heavy, Light Gases and Others, from which the amount of each species is unknown and hence cannot be verified. Furthermore, the use of MeOH to produce BTX is not well described in the literature, of which no other comparisons could be made to verify the product distribution. As a result, it cannot be determined if the production of the individual species in the presented study is representative. Hence, a concern is raised in regards to the sale of the various products, as their prices vary up to a factor of 500, as shown in Table 4.11 on the facing page. Regardless, since the content of each lumped product were verified to those presented by Na et al. [2018] and the individual content within each lumped product cannot be further investigated, the production of the individual species is accepted.

Before the BTX, or any other valuable produced products, can be sold, they should be separated. However, it is of interest to investigate which species in the product stream are worth purifying. This is determined based on weight fraction of the individual species within this stream and their respective market prices. These are presented in Table 4.11 on the next page.

Table 4.11: The annual mass flow rate of the output stream S3 is 109,000 tonne/year, and the products are ordered in regards to their boiling points. The prices for C_6H_{14}, C_9H_{12} and $C_{10}H_{14}$ are scaled to match their expected bulk prices, since quantities at a maximum of only 0.5 kg were available. As an estimation, the asking prices of C_6H_{14} and C_9H_{12} have been reduced by 70 %, while $C_{10}H_{14}$ has been reduced by 90 %. The annular price is given in million USD.
The sources for prices are given by:
[1] [Mathis, 2020][OfficeOfEnergyEfficiency&RenewableEnergy, 2010][NREL, 2011]. [2] - .
[3] [Dinkin, 2016][GlobalPetrolPrices, 2021].
[4] [FederalReserveBankOfDallas, 2020][U.S.-E.I.A., 2019]. [5] - .
[6] [Echemi, 2021a][IHS, 2014]. [7] [Ycharts, 2021][U.S.EnergyInformationAdministration, 2020].
[8] [Nasdaq, 2021][U.S.EnergyInformationAdministration, 2020]. [9] [GlobalSources, 2021a][Alibabba, 2021a].
[10] [FischerScientific, 2021][GlobalSources, 2021b].
[11] [Echemi, 2021e][Methanex, 2021][MMSA-MethanolInstitute, 2021][Gelsenchem, 2021].
[12] [Echemi, 2021b][S&Pglobal, 2021]. [13] - .
[14] [Echemi, 2021c][SunSirs, 2021a]. [15] [Echemi, 2021d][SunSirs, 2021b].
[16] [Alibabba, 2021b][ChemicalBook, 2021]. [17] [AlfaAesar, 2021][eMolecules, 2021].

Lump	Species	Boiling Point [°C]	[wt%]	USD/tonne	MUSD/year	Source
Light gas	H_2	-252.76	0.00	3,395	-	[1]
Light gas	CO	-191.45	0.15	-	-	[2]
Light gas	CH_4	-161.49	0.16	1,388	0.244	[3]
Alkane	C_2H_6	-88.60	0.03	51	0.002	[4]
Light gas	CO_2	-78.45	0.89	-	-	[5]
Other	C_3H_6	-47.70	0.19	1,125	0.239	[6]
Alkane	C_3H_8	-42.04	0.28	353	0.106	[7]
Alkane	C_4H_{10}	-0.50	3.01	394	1.291	[8]
Alkane	C_5H_{12}	36.07	6.77	2,000	14.764	[9]
Alkane	C_6H_{14}	60.26	1.40	3,176	4.860	[10]
Other	CH_3OH	64.70	0.83	386	0.348	[11]
Aromatic	C_6H_6	80.09	0.13	988	0.143	[12]
Other	H_2O	100.00	71.84	-	-	[13]
Aromatic	C_7H_8	110.63	3.71	848	3.433	[14]
Aromatic	C_8H_{10}	139.12	8.52	865	8.034	[15]
Aromatic	C_9H_{12}	169.38	1.49	3,078	4.992	[16]
Heavy	$C_{10}H_{14}$	196.84	0.59	34,571	22.169	[17]
Total	-	-	-	-	60.626	-

In general, the separation in BTX producing systems are performed through distillation, however, as the boiling points of the different species presented in Table 4.11 are relatively similar this method does not suffice.[Sweeney and Bryan, 2000] E.g. the difference of boiling points for C_6H_{14} and CH_3OH is only 4.44 °C of which the separation of these species by distillation will be too costly.

Instead, methods such as liquid-liquid extraction and extractive distillation can be used, the difference being that liquid-liquid extraction utilises solubility only, while extractive distillation utilises both solubility and boiling point differences.[Hernandez, 2013] Both techniques involve the use of a solvent to perform the extraction of the BTX from the multi-species product stream. However, due to the complexity of designing even simple distillation for binary mixtures, as shown for the MeOH-H_2O distillation in Section 4.2 on page 63, the modelling of distilling the product stream from the BTX synthesis is considered out of scope of the presented study. Instead, the required number of components and utility will be approximated based on literature concerning a similar subsystem.

It should however be noted that the resulting utility may be inaccurate compared to an actual subsystem. However, from the separation of Green MeOH, presented in Section 4.2, the combined utility was 13.1 MW, which included both the degasser and distillation column. Comparatively, e.g. the electrolyser has a power utility usage of 88.5 MW and further cooling utility of 22.4 MW, from which it may be assumed that the variation of the estimated utility for the BTX separation process does not affect the total utility relatively much. This hypothesis will be further investigated from a sensitivity analysis, which will be conducted in Chapter 6 on page 103.

Chen et al. [2015] produced Aromatics from ethane of which the product stream of the study consisted of 10 species: H_2, CH_4, C_2H_4, C_2H_6, C_3H_6, C_3H_8, C_6H_6, C_7H_8, C_8H_{10} and C_9H_{12} which is somewhat comparable to those given in Table 4.11 on the previous page. Chen et al. [2015] performed the separation in four main components: a multistage compressor, a flash separator and two distillation columns, which is illustrated in Figure 4.19.

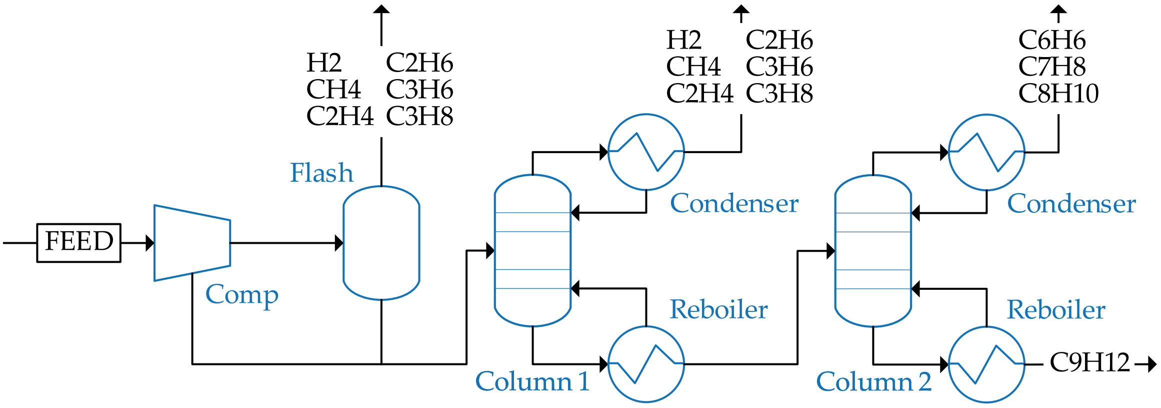

Figure 4.19: Separation procedure used by Chen et al. [2015].

The combined multistage compressor and flash separator, separates a lumped gaseous product, due to them being reactants in the production of Aromatics. The species within the lumped gaseous product, which is the least volatile, is the C_3H_8. Contrary, in the lumped BTX product, C_6H_6 is the species which is the most volatile. Therefore, in order to separate the lumped gaseous product from the rest, these two species are of interest. The boiling point difference between them is 122.04 °C at ambient pressure, from which the simplest separation method can be utilised, a flash separator. It is combined with a multistage compressor which enhances the separation.

Approximately 97.36 wt % of the combined mass flow of the lumped gases are separated by the previously mentioned components, from which further separation of the gases are required. The liquid stream enters a distillation column where the remaining gases are separated. Finally, the now gas-free liquid stream enters a distillation column where C_6H_6, C_7H_8 and C_8H_{10} are separated as a lumped product from C_9H_{12}. It can therefore be concluded that they do not utilise any of the previously described extraction methods, making ordinary distillation an option.

If the procedure from Chen et al. [2015] is performed for the product stream of the presented study, the outcome of the separation will be as shown by the divisions in Table 4.12 on the next page.

Table 4.12: Separation specified by Chen et al. [2015] applied to its product composition and the composition of the presented study.

Species	Boiling Point [°C]	Chen et al. [2015]	Presented study	Product lump
H_2	-252.76	✓	✓	Gaseous
CO	-191.45	-	✓	
CH_4	-161.49	✓	✓	
C_2H_4	-130.70	✓	-	
C_2H_6	-88.60	✓	✓	
CO_2	-78.45	-	✓	
C_3H_6	-47.70	✓	✓	
C_3H_8	-42.04	✓	✓	
C_4H_{10}	-0.50	-	✓	Liquid
C_5H_{12}	36.07	-	✓	
C_6H_{14}	60.26	-	✓	
CH_3OH	64.70	-	✓	
C_6H_6	80.09	✓	✓	
H_2O	100.00	-	✓	
C_7H_8	110.63	✓	✓	
C_8H_{10}	139.12	✓	✓	
C_9H_{12}	169.38	✓	✓	Remaining
$C_{10}H_{14}$	196.84	-	✓	

However, from Table 4.12 it may be seen that this separation results in three lumped products, being Gaseous, Liquid and Remaining, where additional species now exist. As previously stated the species must be separated in order to be sold, from which considerations must be made regarding which products are worth separating.

In Chen et al. [2015] the gaseous products were lumped since, they are reactants in the BTX production, whereas the main reactants for the MeOH synthesis are H_2 and CO_2, while H_2, CH_3OH and C_3H_6 are the main reactants in the BTX synthesis. Given CO_2 and C_3H_6 are present in the lumped Gaseous stream for the presented study, there is a potential of recirculating them to the latter mentioned processes. However, this results in the necessity of separating them from the lumped Gaseous stream, where the remaining can be discarded. Another approach is to separate each species in the lumped Gaseous stream, after which they can be sold. However, the motivation of both approaches would be based on an economical perspective, in order to determine the feasibility of each. The mass flow of CO_2 in this stream is 0.85 wt % of the CO_2 input to the MeOH synthesis. Similarly, the influence of recirculating the C_3H_6 is determined to be insignificant, since it is approximately five times smaller than the mass fraction of CO_2. Likewise, the turnover of selling all the species in the lumped Gaseous stream, if all the species were to be separated, is approximately 0.591 MUSD, according to Table 4.11 on page 83. This is however less than 1 % compared to the total turnover if all the species in the product stream are sold. As such it may be concluded that it is not worth to separate the each species in the lumped Gaseous stream, where it will instead be discarded. Due to the majority of the stream being CO_2 it is assumed it can be released into the atmosphere, and as such there is no further expense associated with this stream. Given that no separation of the species which are within the Gaseous lumped product is needed for the presented study, it is assumed that the separation can be achieved from a multistage compressor and a flash separator as stated by Chen et al. [2015].

The rest of this product stream consists of the lumped Liquid- and Remaining stream presented in Table 4.12 on the preceding page. The rest of the separations will be performed by distillation, from which the boiling point becomes the decisive variable.

The Liquid lumped product consists of three Alkanes, three Aromatics, H_2O and MeOH. It would be of interest to separate each species within the Liquid lumped product, however, this will not be done. The study of Chen et al. [2015] assumes BTX can be sold as one lumped product, from which it is also assumed that the three Alkanes can be sold as one. However, the least volatile species of the three Alkanes is C_6H_{14} which has a boiling point approximately 4 °C lower than MeOH. This could result in the distillation of Alkanes being infeasible, as earlier presented, whereas an alternative method could be the extraction- or extractive distillation processes. In order to avoid the alternative methods, a simplification has instead been made, which is that this stream, consisting of MeOH and Alkanes, can be sold as one product. As such the distillation method is utilised where the distilled product consists of MeOH and the previously mentioned Alkanes.

The remaining species in the lumped Liquid stream is BTX and H_2O. Since Chen et al. [2015] states that it is possible to sell BTX as a lumped product, it is also the approach of the presented study. However, as may be seen in Table 4.12 on the previous page the boiling point of H_2O is in between the boiling point of C_6H_6 and C_7H_8. This leads to two approaches, either being to separate C_6H_6 and then H_2O by distillation, from which C_6H_6 can be sold separately and further C_7H_8 and C_8H_{10} as a lumped product. Otherwise the H_2O can be separated from this mixture by the extraction- or extractive distillation method from which the three Aromatics can be sold as a lumped product. However, the income of C_6H_6 is only associated with a turnover of 0.143 MUSD/year, which is approximately 0.21 % compared to the total revenue if all the species are sold individually as shown in Table 4.11 on page 83. Since the turnover with respect to C_6H_6 is deemed insignificant another approach can be made, which is to distil the C_6H_6 along with the H_2O and afterwards sell C_7H_8 and C_8H_{10} as a lumped product.

The content of H_2O in the distillate stream will become 99.82 wt %. Due to this relatively high purity, it might be a possibility to discard the stream into a water reservoir and hereby not result in an additional expense. However, C_6H_6 is known to be a toxic chemical, as such it must be further investigated if the content of C_6H_6 is sufficiently low to be discarded, or if a purification process is required [for Disease Control and Prevention, 2021]. The amount of C_6H_6 permitted in waste water, which is to be discarded into a water reservoir, is not publicly available, but an estimate can be made based on the restrictions for drinking water. This assumption is based on the expectation that the tolerance of chemicals in drinking water is similar to those in waste water. The maximum allowable content of C_6H_6, and other Aromatics, within drinking water in Denmark is 0.001 mg/kg [Scientific, 2003]. Since the current concentration of C_6H_6 within the stream is 1,800 mg/kg it becomes a necessity to purify this stream. Numerous methods exists for treating H_2O containing C_6H_6 such as solvent stripping and biological treatment, yet, these processes are considered out of scope for modelling in the presented study [ATSDR, 2007]. It will instead be further discussed and accounted for in Chapter 6 on page 103.

With the Liquid lumped product being separated, only C_9H_{12} and $C_{10}H_{14}$ remain, which can be separated by a distillation column due to the difference in their boiling points being 27.46 °C. The separation process of the products produced by the BTX synthesis, is as such achieved from six key components: one multistage compressor, one flash separator and four distillation columns, as shown in Figure 4.20 on the facing page.

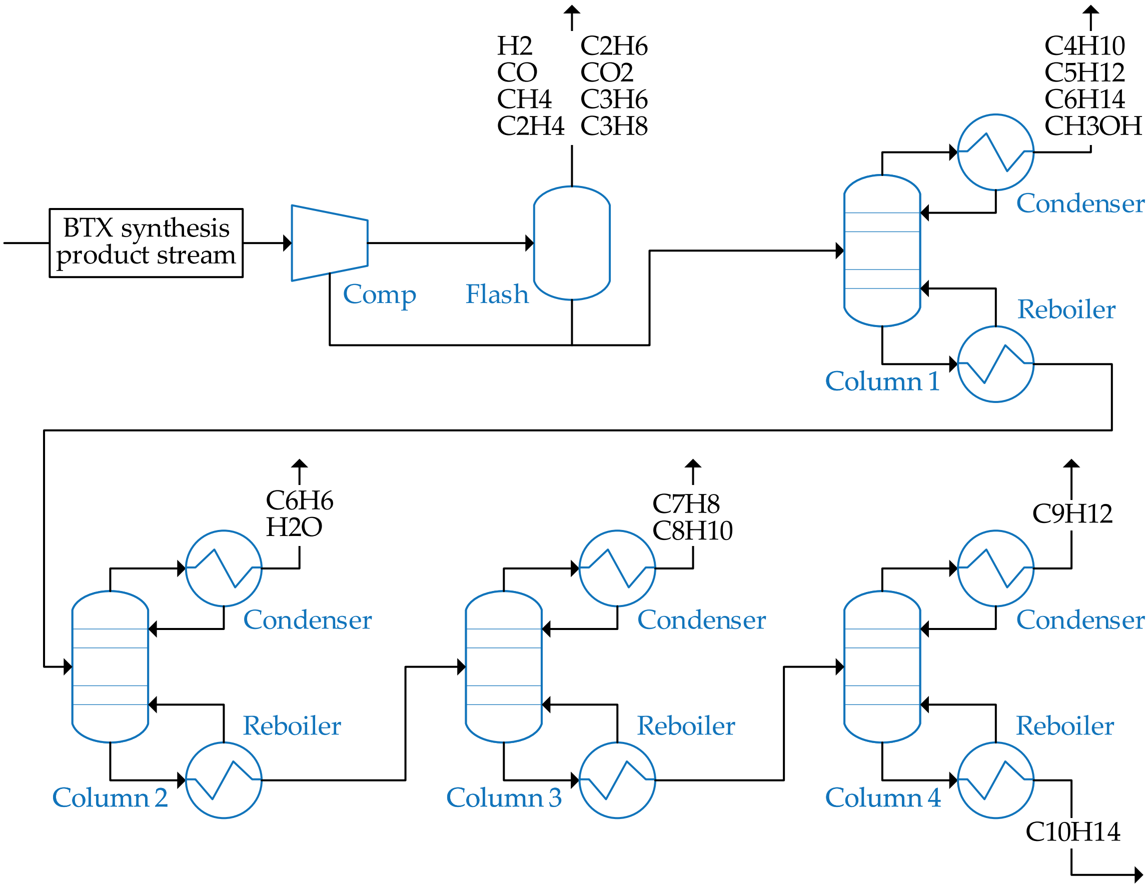

Figure 4.20: Separation subsystem for the product stream from the BTX synthesis subsystem.

The estimation of the utility requirement for the different components is based on the utility listed in Chen et al. [2015], where the difference in mass flow between their study and the presented study will be used as a scaling factor. The compression is done in four stages where the stream is cooled in between the stages. The total electricity and heat duty listed in Chen et al. [2015] for the multistage compressor is 215.13 MW, however the mass flow of the stream is approximately 20.76 times larger than the mass flow shown in Table 4.10 on page 79. By scaling the utility, the estimated utility for the multistage compressor utilised in the presented study becomes 10.36 MW. The second component is the flash separator, however, this is treated as a passive component of which there is no utility requirement.

The remaining components are the distillation columns, which are all equipped with a condenser and a reboiler. In order to estimate the utility of the four distillation columns, the two distillation columns in Chen et al. [2015] have been analysed.

The first distillation column in Chen et al. [2015] separated the remaining gases, which were not separated by the combined compressor and flash separator. The difference in boiling point, between the least volatile species in the Gaseous lumped product, C_3H_8, and the most volatile liquid in the remaining stream, C_6H_6, is approximately 120 °C. The second distillation column in Chen et al. [2015] separates BTX from C_9H_{12}. The difference in boiling point, between the least volatile species in the Liquid lumped product, C_8H_{10}, and the remaining species, C_9H_{12}, is approximately 30.26 °C.

The difference in boiling points between the least volatile distillate compared to the most volatile bottom product for the four distillations columns for the presented study are in the range of 10.6 °C to 30.26 °C. As such the following estimations of utility for the four distillation columns, will be based on the utility for the second distillation column listed by Chen et al. [2015]. The total utility of the condenser and reboiler for this distillation column is 16.96 MW with an input mass flow of 57,076 kg/hr.

The first distillation column in the presented study will separate the Alkanes and CH_3OH as a lumped product, where the mass flow of the feed stream is approximately 4.67 times less than the feed stream of the reference distillation column, of which the scaled utility becomes 3.64 MW. This procedure is repeated for the remaining three distillation columns where their utility becomes 3.19 MW, 0.53 MW and 0.08 MW, respectively. The total utility of the four distillation columns hence becomes 7.44 MW. However, as previously discussed, these values may not be representative which will be further analysed in the sensitivity analysis in Chapter 6 on page 103.

Throughout this chapter the steady state subsystems have been defined from which either MeOH or BTX may be produced. Additionally, combining the dynamic subsystems presented in Chapter 3 with these steady state subsystems, System 1 and System 2 may be defined. With System 1 and 2 defined, heat- and mass integration within both systems may be incorporated as will be done in the following Chapter 5 on the next page.

Chapter 5

Heat- and Mass Integration

Throughout Chapter 3 and 4 the different subsystems have been modelled independently of each other, with the exception that the output stream from one subsystem was defined as the inlet for the subsequent subsystem. However, by coupling the subsystems, optimisation can be performed in order to reduce the OPEX, which can be done with respect to the mass- and energy balances. Some of the individual subsystems produce species which can be used as inputs in other processes. Furthermore, the temperature varies throughout the two systems from $-38\,^\circ\mathrm{C}$ to $431\,^\circ\mathrm{C}$, hence heat exchangers can be implemented to exchange energy between the streams in the system, and thereby decrease the required utility. These modifications will reduce the OPEX, however, it should also be mentioned that these modifications will increase the CAPEX, due to the introduction of additional components. Furthermore, these additional components will also increase the complexity of the overall system, meaning more maintenance are required which affects the OPEX. This aspect will be used to determine where it should be feasible to implement feedback loops as well as heat exchangers.

The above mentioned analysis will only be done for the two steady state subsystems, which is the MeOH synthesis to purified MeOH and the MeOH synthesis to BTX, while the dynamic subsystems of electrolysis, carbon capture and gas storage are omitted as explained below.

The carbon capture has three mass stream outlets, being the CO_2 stream, a drain and the remaining flue gas. However, none of the two latter mass streams can be utilised elsewhere in the overall system, hence mass integration for the carbon capture will not be done. Heat integration is however also of interest, where a heat exchanger is already implemented. This is incorporated in order to preheat the CO_2 rich solvent before the stripper, and cool the CO_2 lean solvent before the absorber. A cooler is also implemented before entering the absorber. However, no additional cold streams are available to remove this excess energy, neither by the carbon capture subsystem, nor from the steady state subsystems with the heat integration presented later in this chapter. Further mass- or heat integration for the carbon capture will therefore not be done. Similar to the carbon capture, the electrolyser and the storage subsystems for CO_2 and H_2 also require cooling, however, as discussed no excess cooling streams are available making external utility a necessity. From the upcoming analysis it is determined that relatively large quantities of H_2O exits the steady state subsystems which could be recycled to the electrolyser. However, since these are not modelled in the same software, this feedback is not recycled, but it will be further discussed when determining the OPEX for the electrolyser in Chapter 6 on page 103.

The following analysis will therefore only be conducted for the two steady state subsystems, one where Green MeOH is the desired end product, and the other where BTX is the desired end product.

5.1 System 1: Methanol as End Product

The integration of heat exchangers are based on its influence on the economic balance between CAPEX and OPEX. In order to perform the heat exchanger integration the energy content within each individual stream are analysed, determined by the mass flow and the specific heat capacity. Figure 5.1 on the next page illustrates the entire steady state subsystem of System 1, with the stream names and their belonging heat capacity and temperature.

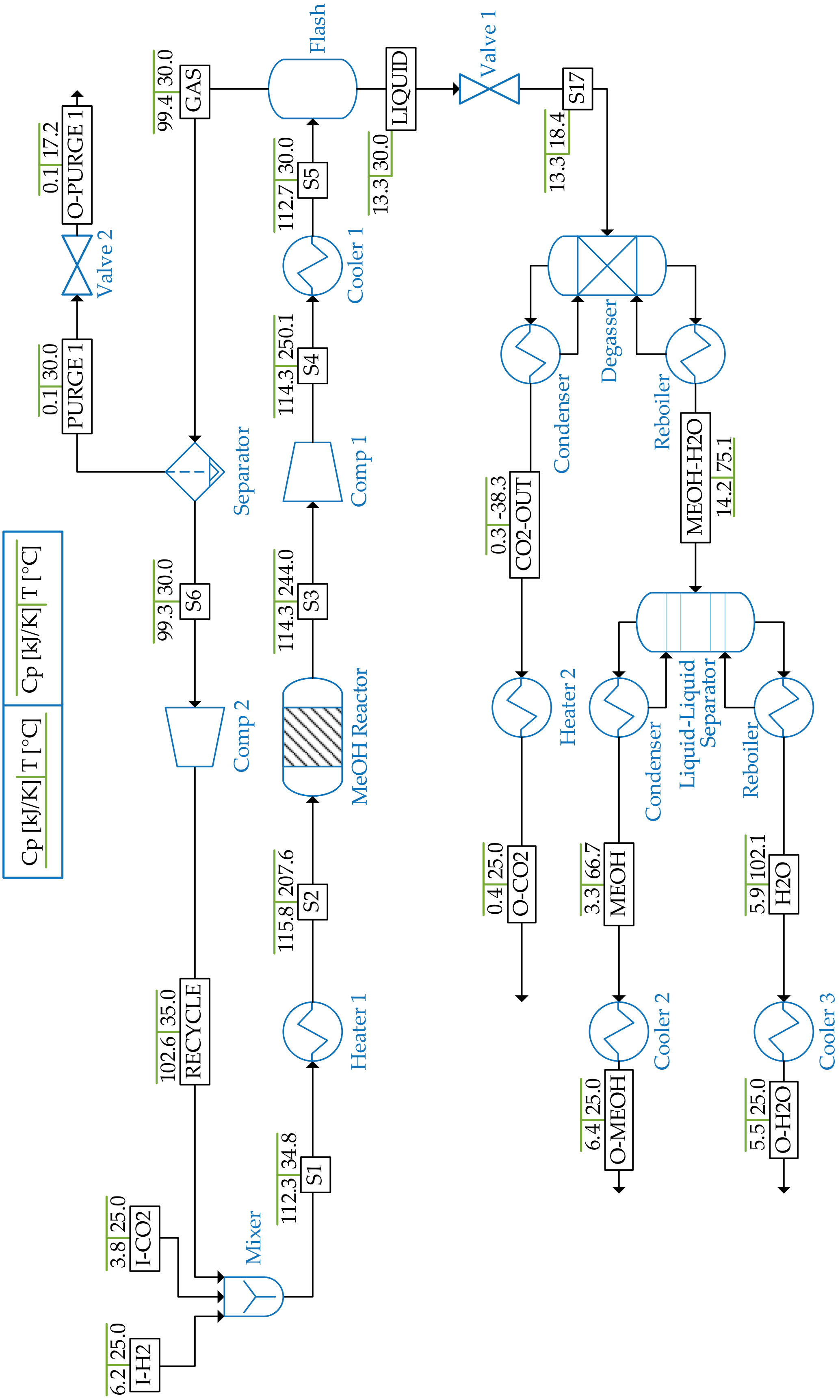

Figure 5.1: Steady state subsystem of System 1 with belonging stream names and their heat capacity and temperature.

From Figure 5.1 on the preceding page it can at first be concluded that the heat capacity for the majority of the streams within the feedback loop of the MeOH synthesis, are more than 10 times greater than the streams outside the feedback loop. This was expected due to the relatively large difference in the mass flow from the input of CO_2 and H_2 compared to the recycled stream, which corresponds to relatively large utility requirements for Heater 1 and Cooler 1. From streams S1, S2, S4 and S5 it can be concluded that the feed which enters this subsystem must be heated from 35 °C to 208 °C and cooled from 250 °C to 30 °C, which has been done by Heater 1 and Cooler 1, respectively. Instead a heat exchanger can be utilised, where a countercurrent heat exchanger is used in order to obtain a greater heat transfer compared to a cocurrent heat exchanger. This type of heat exchanger will be used for any additional heat exchangers which are to be implemented, all with a pinch temperature of 10 °C since this value is commonly used [Klein and Nellis, 2017]. The objective of implementing heat exchangers is to reduce the utility and if possible, the number of heaters and coolers. In order to determine whether Heater 1 or Cooler 1 can be removed, the theoretical amount of heat transfer between the two streams must be determined from an energy balance as in Eq. 5.1. This energy balance determines the theoretical equilibrium temperature for two streams which can be used in order to implement a heat exchanger

$$\dot{m}_1 \cdot c_{\mathrm{p},1} \cdot (T_1 - T_{\mathrm{eq}}) = \dot{m}_2 \cdot c_{\mathrm{p},2} \cdot (T_{\mathrm{eq}} - T_2) \tag{5.1}$$

where $c_{\mathrm{p,n}}$ is the individual specific heat capacity and T_{eq} is the equilibrium temperature. Since the temperature of S1 and S5 are similar, neither Heater 1 nor the Cooler 1 can be removed, however, their utilities can be decreased if a heat exchanger is implemented.

In order to further utilise the energy within the stream S5, a second heat exchanger can be implemented. The recycled stream RECYCLE has a temperature of 35 °C from which further heat transfer should be possible. When implementing heat exchangers the quality of the energy for the different streams must be taken into account where the temperature is the decisive variable. The stream S4 should therefore firstly supply heat to S1 and thereafter RECYCLE in order to reduce the utility of Heater 1 and Cooler 1.

If the purifying process of the produced MeOH is analysed it may be seen that the final temperatures of streams CO2-OUT, MEOH and H2O are −38 °C, 67 °C and 102 °C, respectively. Since these are the end products, they should be heated or cooled to ambient temperatures. Stream CO2-OUT is the only stream which needs heating whereas MEOH and H2O require cooling. From Figure 5.1 on the preceding page it may be seen that the heat capacity of CO2-OUT is relatively low compared to the other two streams. Due to its relatively low heat capacity only one of the other two streams can be cooled. H2O consists of approximately 100 wt% H_2O which could potentially be recycled to the electrolyser. However, a purifier might be a necessity in order to achieve the purity requirement in the electrolyser. Since the electrolyser operates at 80 °C it could be feasible to maintain the energy within the H_2O such that less heat is required for the electrolyser, assuming the purifier can operate at elevated temperatures. Regardless of this assumption, the MeOH must be cooled, from which stream MEOH is chosen to be cooled by stream CO2-OUT. Since the assumption regarding the recycling of the H_2O stream H2O cannot be verified at this point, the stream is cooled to 25 °C similar to MEOH. As mention there is a relatively large difference between stream CO2-OUT and MEOH with respect to their individual heat capacity, and furthermore the MeOH exiting the liquid-liquid separator is at vapour state and its temperature is 67 °C. Given these conditions and the predefined pinch temperature of 10 °C, the temperature of CO2-OUT should be able to reach a value of 57 °C. This is however not desired since this stream should be recycled into the MeOH synthesis from which an elevated temperature above 25 °C would affect the two mentioned heat exchangers, from which 25 °C is chosen.

The CO_2 stream O-CO2 could, as mentioned, be incorporated into a feedback loop since this stream consists of approximately 100 wt% CO_2 and with a mass flow of 12.3 wt% compared to the inlet mass flow of I-CO2. Since relatively much energy has been put into the carbon capture subsystem to separate the pure CO_2 from the flue gas, and given the mass flow of this stream, it should be recycled. This would increase both the income of the system and its CAPEX since the entire system would have to be upscaled. This results in the necessity of repeating the optimisation algorithm for the MeOH synthesis which would affect the required supply of H_2 and thereby the electrolyser and storage. Furthermore, the degasser and liquid-liquid separator would also have to be upscaled. With respect to the system, where BTX is the desired end product, the optimisation and fitting of the BTX production would also have to be redone. Due to limitations this will not be done.

The heat exchanger network, for the system where Green MeOH is the end product, may be seen in Figure 5.2 on the next page.

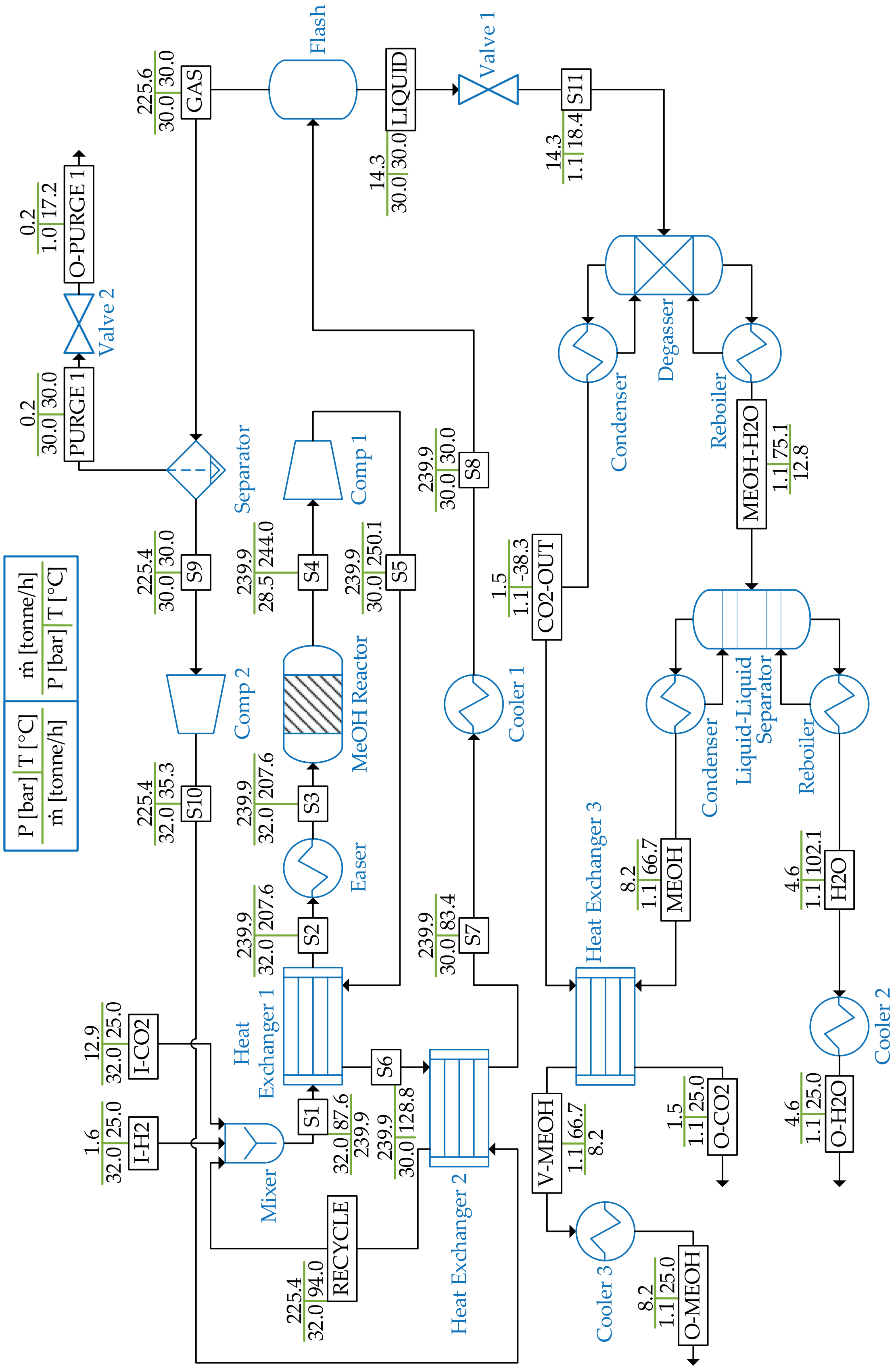

Figure 5.2: Heat exchanger network incorporated in the steady state subsystem of System 1, where Green MeOH is the desired end product.

As presented, three heat exchangers are incorporated in the system, as illustrated in Figure 5.2 on the facing page. It is also shown that the stream exiting the reactor is able to supply enough heat to the inlet stream of the reactor such that it may reach its desired temperature of 208 °C without any additional heating from a heater. It may however also be noticed that a heater, named Easer, remains implemented before the reactor, though, it may also be seen that there is no temperature difference through it. This heater should not be installed in real applications as it is only used to ease the model convergence of this subsystem.

Cooler 1, before the flash separator, is however still required as may be seen in Figure 5.2 on the preceding page. Yet, its utility has been decreased since it is only required to cool the exit stream of the reactor from 83 °C to 30 °C instead of 250 °C to 30 °C.

The third heat exchanger is, as discussed, implemented between the outlet stream of CO2-OUT and MEOH in order to heat the CO_2 to 25 °C. Regardless, if this stream is recirculated in a feedback loop to the MeOH synthesis or discarded into the atmosphere, the latter being the current approach, it is assumed that it must be heated. It may be seen that the temperature of the MeOH does not decrease throughout this heat exchanger, which is due to its latent heat of condensation. Prior to the heat exchanger the MeOH is at vapour state, but afterwards a fraction of the vapour is condensed. Further cooling of the MeOH stream as well as the H_2O stream is still required.

Given the integration of the heat exchanger network, a comparison of the subsystem with and without heat exchangers can be done. For this comparison it is of interest to analyse the total utility cost of the heaters, coolers and heat exchangers. This may be seen in Table 5.1, where the total number of heaters, coolers and heat exchangers are also listed.

Table 5.1: Utility cost and number of components for System 1 with- and without a heat exchanger network (HEN) incorporated. The savings between System 1 with and without a HEN is also shown.

	Without HEN	With HEN
No. Heaters	2	0
No. Coolers	3	3
No. Heat Exchangers	0	3
Utility cost [USD/year]	11,495,748	341,640
Savings	97.0%	

From Table 5.1 it may be seen that the total utility cost is reduced by 97.0 %, due to the integration of the heat exchangers. In order to achieve this reduction of the utility cost, the two heaters are replaced by three heat exchangers. This affects the CAPEX, however, due to the significant saving in utility cost this is deemed profitable.

With this system, where MeOH is the end product, now also optimised in regards to utility, its OPEX and CAPEX can be determined. This is explored in the following Chapter 6 on page 103.

5.2 System 2: BTX as End Product

In this system, where the BTX synthesis is incorporated as an extension to System 1 without the liquid-liquid separator, the heat exchanger network until and including the MeOH synthesis subsystem is kept equal. However, in order to produce the BTX a second reactor is implemented, from which relatively large temperature differences occur once again, similar to the MeOH synthesis. This may be seen in Figure 5.3 on the next page where the entire steady state subsystem of System 2, with the stream names and their belonging heat capacity and temperature are illustrated.

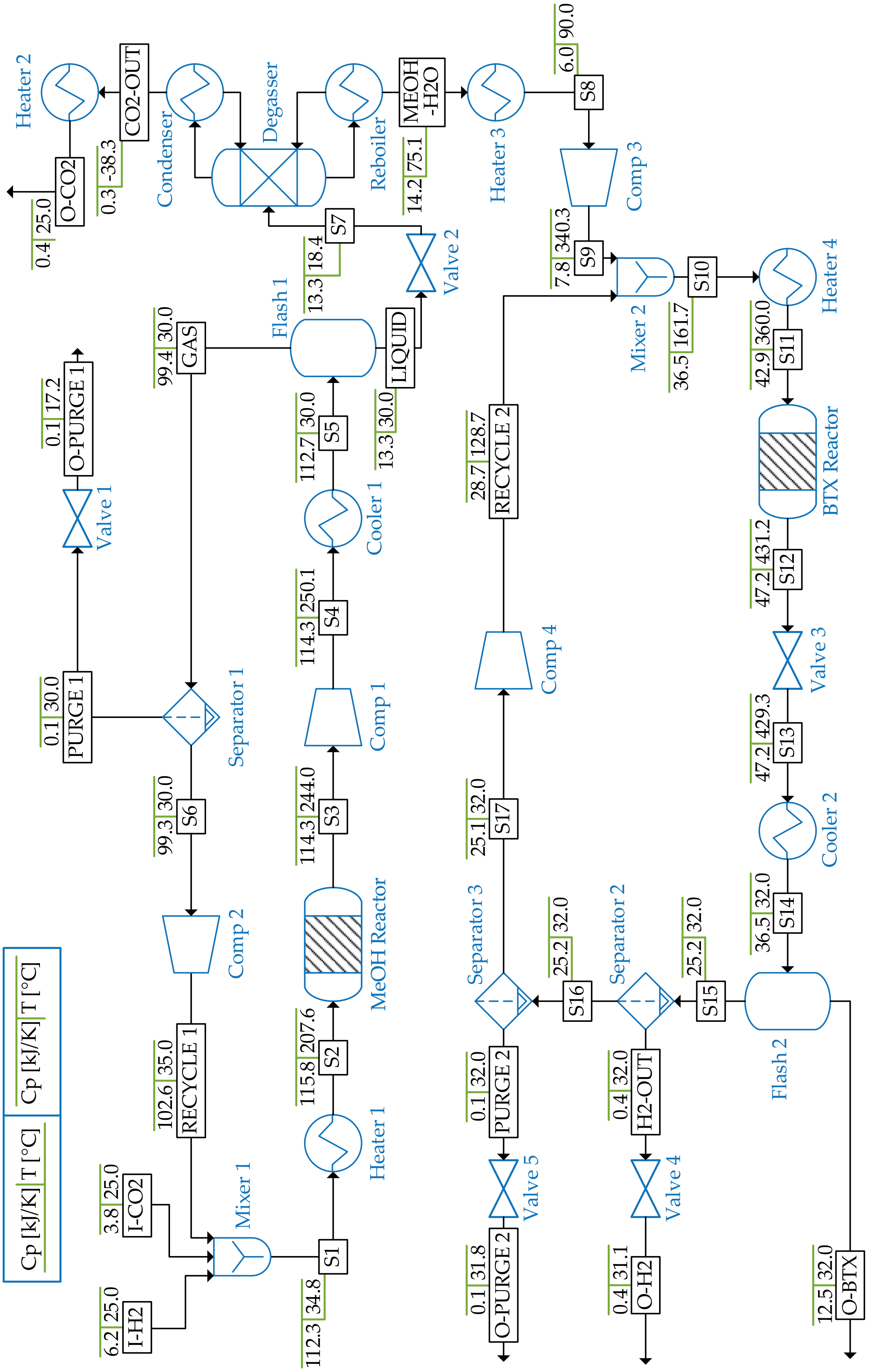

Figure 5.3: Steady state subsystem of System 2 with belonging stream names and their heat capacity and temperature.

Due to the relatively big temperature differences between the inlet and exit of the BTX reactor, a heat exchanger network can be implemented similar to the one for the MeOH synthesis. From the streams S10, S11, S13 and S14 it can be concluded that the feed which enters the BTX reactor must be heated from 162 °C to 360 °C and cooled from 429 °C to 32 °C, which currently has been achieved by a heater and a cooler.

Similar to the MeOH synthesis, a heat exchanger is firstly implemented between the stream exiting the reactor and the inlet stream due to the elevated temperatures. Contrary to the MeOH synthesis, an additional heat exchanger is not implemented to the feedback loop stream. Instead the liquid stream MEOH-H2O exiting the degasser is utilised. Several aspects affect the placement of the second heat exchanger, due to the different pressures throughout the BTX production. The pressure of the liquid stream exiting the degasser MEOH-H2O is 1.1 bar, whereas the pressure for the stream entering the BTX reactor must be 18 bar. After the BTX reactor the pressure must be reduced to 4.2 bar for the flash separator, Flash 2. Since compression of a stream also increases its temperature this must be accounted for when placing the second heat exchanger. The feedback stream RECYCLE2 currently enters Mixer 2 with a pressure of 4.2 bar, which must be pressurised to 18 bar prior to this mixer. The pressure of the streams entering and exiting Mixer 2, should be equal in order to avoid back flow. The fluid mixture in stream RECYCLE2 is at vapour state from which a compressor can be implemented. Contrary, the fluid mixture MEOH-H2O which exits the degasser is at liquid state, which should be vaporised before compression. The second heat exchanger can therefore be implemented to this stream in order to vaporise the liquid before the compression. However, since the temperature increases when compressing a gas, this must be accounted for when designing the heat exchanger network. If the heat transfer for the second heat exchanger is too great the additional temperature increment from the compression will result in a temperature too high before the reactor from which cooling would then be required. Furthermore, when compressing a vapour its saturation temperature is affected, which could make the vapour condense within the compressor, if the initial temperature is not high enough. Both of these considerations must therefore be accounted for when designing the heat exchanger network.

Similar to System 1, the CO_2 stream O-CO2 must also be heated from −38 °C to 25 °C since it should be recycled back to the MeOH synthesis as previously discussed. This is achieved from the BTX product stream O-BTX.

As presented in Section 4.3, H_2 is separated from the feedback loop in the BTX production which is then incorporated in a separate feedback loop to the MeOH synthesis. This is done through Separator 2, from which the stream O-H2 is recycled. The molar flow of this stream is approximately 6 mol% of the initial H_2 flow in stream I-H2. This would reduce the CAPEX and OPEX with respect to the electrolyser and the storage subsystem. The implementation of the heat exchanger network as well as the additional feedback stream may be seen in Figure 5.4 on the facing page.

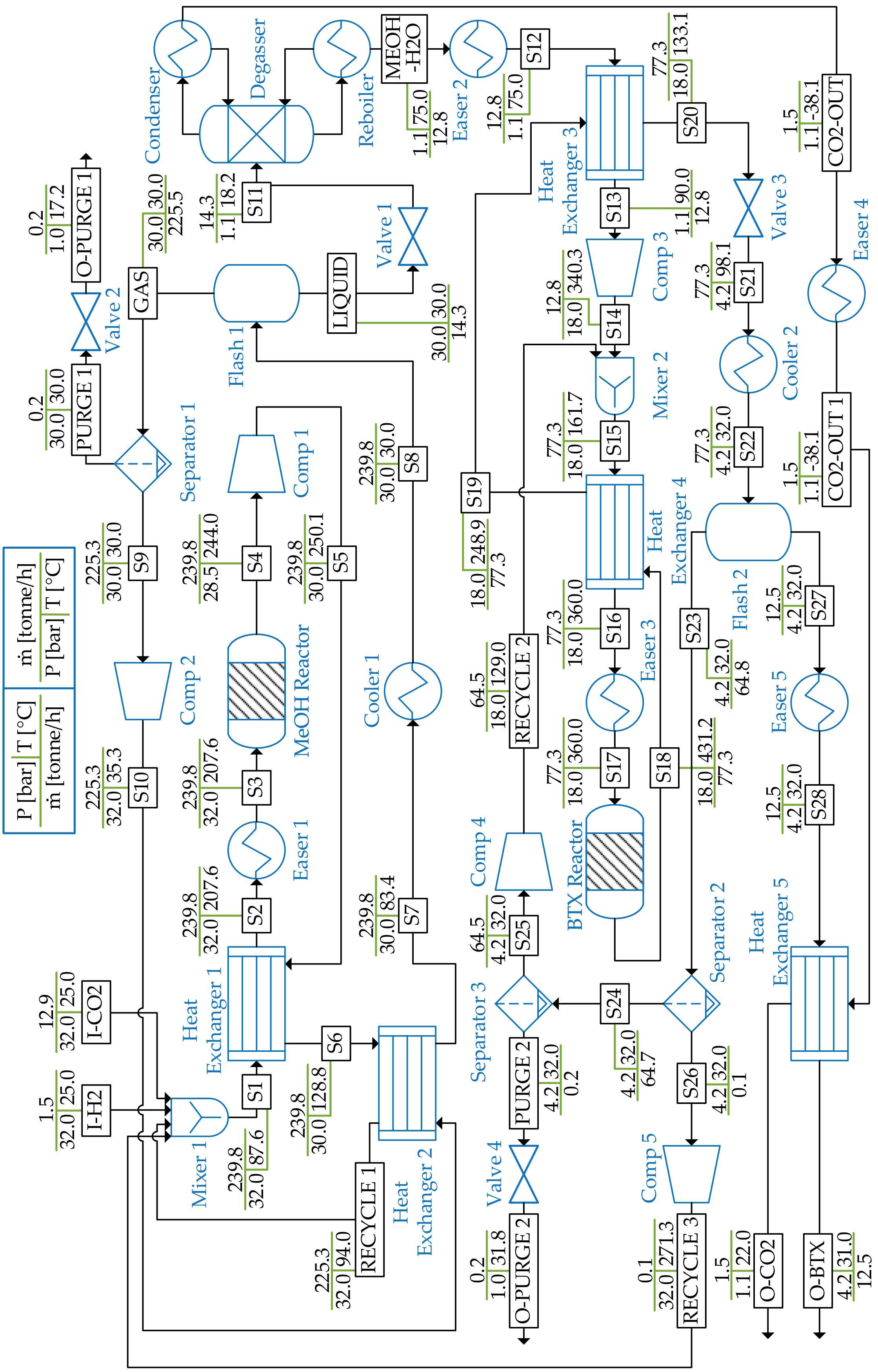

Figure 5.4: Heat exchanger network as well as the feedback streams incorporated in the steady state subsystem of System 2, where BTX is the desired end product.

From Figure 5.4 on the previous page it may be seen that the heat exchanger network with respect to the MeOH synthesis is equal to system 1, as mentioned. Three additional heat exchangers, Heat Exchanger 3, Heat Exchanger 4 and Heat Exchanger 5, are implemented in the MeOH to BTX process. Heat Exchanger 4 is incorporated between the outlet and inlet of the BTX reactor, whereas Heat Exchanger 3 is incorporated before the compression of the liquid output from the degasser. Given these two heat exchangers and further the compressors Comp 3 and Comp 4, the heater before the BTX reactor can be removed. However, similar to the MeOH production a heater, denoted Easer, is still implemented before the BTX reactor, whose function remains to ease the model convergence. In total, five heaters, which have no contribution to the system except easing the model convergence, are implemented in Figure 5.4 on the preceding page named Easer 1 to Easer 5. Cooler 2 located before the flash separator Flash 2 remains, but its utility has been decreased since it is only required to cool the exit stream of the BTX reactor from 98.1 °C to 32 °C instead of 429 °C to 32 °C.

The last heat exchanger, Heat Exchanger 5, is used to heat the CO_2 stream $\boxed{\text{O-CO2}}$. However, due the temperature of the BTX product stream $\boxed{\text{S28}}$ being 32 °C and the pinch temperature defined as 10 °C, the outlet temperature of $\boxed{\text{O-CO2}}$ is limited to 21 °C. This limit is imposed since the product stream $\boxed{\text{O-BTX}}$ exits at a temperature of 31 °C. It was desired to heat the $\boxed{\text{O-CO2}}$ stream to 25 °C. As it should be heated regardless if it is used in a feedback loop to the MeOH synthesis or discarded into the atmosphere, the latter being the current approach. It is however determined that an additional heater is not necessary due to its heat capacity being insignificantly small compared to the recycled MeOH stream $\boxed{\text{RECYCLE1}}$. The BTX product stream $\boxed{\text{O-BTX}}$ exits at a temperature of 31 °C which is accepted since further separation of the individual species is required anyway. Lastly, it may also be seen from Figure 5.4 on the previous page that the separated H_2 is recycled back to the MeOH synthesis.

Given the integration of the heat exchanger network, a comparison of the system with and without heat exchangers can be done. For this comparison it is of interest to analyse the total utility costs for the heaters, coolers and heat exchangers. This may be seen in Table 5.2, where the total number of heaters, coolers and heat exchangers are also listed.

Table 5.2: Utility cost and number of components for System 2 with and without a heat exchanger network (HEN) incorporated. The savings between System 2 with and without a HEN is also shown.

	Without HEN	With HEN
No. Heaters	4	0
No. Coolers	2	2
No. Heat Exchangers	0	5
Utility cost [USD/year]	18,228,859	484,603
Savings	97.3%	

From Table 5.2 it may be seen the total utility cost is reduced by 97.3 %, due to the integration of the heat exchangers. In order to achieve this reduction of the utility cost, the four heaters are replaced by five heat exchangers. This affects the CAPEX, however, due to the significant saving in utility cost this is deemed profitable.

With this system, where BTX is the end product, now also optimised in regards to utility, it may be determined what the costs of construction and operation are. This is explored in the following Chapter 6 on page 103.

Throughout this chapter heat- and mass integration for the steady state subsystems of System 1 and 2 have been conducted. This yielded a reduction in the utility of the heaters and coolers of 97.0 % *and* 97.3 % *for System 1 and 2, respectively. Additionally, mass integration was performed for System 2, where the* H_2*, produced in the BTX synthesis, was recirculated to the MeOH synthesis. With System 1 and 2 defined, the CAPEX and OPEX for both can be estimated, which will be done in the following Chapter 6 on page 103.*

[This page is intentionally left blank]

Chapter 6

Economic Assessment of the Systems

This chapter seeks to investigate the economic aspects of the two systems described in the previous chapters. The economic aspects will concern the equipment cost, cost of operation, income from sale of products and loan repayment. The costs of some of these parameters are deemed difficult to estimate, of which a cost range will be listed. A baseline value will therefore be defined from which a sensitivity analysis for each system will further investigate the influence of these varying parameters. The goal of this economic analysis is therefore to assess the feasibility of the two systems and thereby indicate if they produce a profit or deficit. The rate of exchange has been fixed at 0.16 DKK/USD in accordance to the rate on the 1st of May, 2021.

6.1 Economics of Subsystems

The initial equipment investment and cost of operation are often classified as capital expenditures (CAPEX) and operational expenditures (OPEX), respectively. CAPEX consists of all facets in regards to initial purchase of any equipment, installation of the equipment, acquisition of land and further development of used technologies. OPEX concerns day to day expenditures such as maintenance of equipment, and in the case of the presented study the consumption of utility and other feed materials for the system. Hence, in summation, CAPEX is any one-time expenses which will last for many years to come, while OPEX is continuously paid expenses on a daily to annual basis.

In order to estimate the feasibility of the two different systems, it is therefore necessary to investigate both the CAPEX and OPEX in conjunction to determine the potential profit of the systems. To do so the CAPEX and OPEX of the individual subsystems must be determined, which will be presented in Section 6.3 on page 110 and 6.4 on page 112.

It should be noted that any CAPEX and OPEX not listed in the sections below, are values determined by the Aspen Plus Process Economic Analyzer (APEA). The price estimated by APEA includes the equipment and installation costs. Equipment cost concerns the bare cost of the components that make up the system. Installation cost concerns any material used to construct the system and other expenditures. Together they make up the expected total cost of constructing the given system, which is hence the CAPEX. Regarding OPEX, APEA estimates the demand for electricity, cooling and heating for the different components in the subsystem.

Before considering the given CAPEX- and OPEX values, it should be noted from which year the respective values originate. In APEA, the CAPEX and OPEX are both determined using a price basis from the year of 2015, as may be reviewed in the APEA help menu. Similarly, for any subsystem not determined in APEA, the price is dependent on the specific year that the sources acquired their prices from. As a result, it would be a complicated process if these values were to be converted to values of the year 2021. Although a rough estimate could be achieved by considering both the inflation rate and a price index for every component of every subsystem, it was chosen not to account for either. Therefore, the various values displayed in the following tables, are based on the values acquired directly from their source of origin.

6.1.1 Carbon Capture

The CAPEX and OPEX of the carbon capture subsystem is determined by APEA. However, the cost of the solvent used, MEA, is based on the current market price. The price presented by Echemi [2021f] is from 2021, while the price in Intratec [2007] is from 2007. Since the lowest price presented by Intratec [2007] matches the price by Echemi [2021f], this price is assumed to be representative of the current market value being 1,400 USD/tonne. In ASPEN Plus, only the flow rate of the MEA can be defined, and since no pipe sizes are specified, the total amount of MEA in the subsystem cannot be specified. It can however be approximated from the volume of the absorber and stripper, since they are assumed to contribute most of the total volume for the subsystem. Their combined volume is 310 m^3, where the absorber constitutes 300 m^3 of this volume. The volume occupied by the solvent in the absorber is presumed to be 10 vol%, and the concentration of MEA in the solvent is 30 wt%, from which the resulting volume of MEA is approximately 9 m^3. Which, when its density is accounted for, equals about 10 tonne thereby costing a total of 14,000 USD.

With respect to the degradation of the solvent, this has been investigated by Davis and Rochelle [2009]. They present a MEA degradation rate of about 13.5 wt% on an annual basis under conditions similar to those observed in the carbon capture subsystem. Hence, 13.5 wt% of the MEA must be replaced annually, resulting in an additional OPEX.

The CAPEX and OPEX of the carbon capture subsystem are listed in the Tables in Section 6.3 and 6.4.

6.1.2 Hydrogen and Carbon Dioxide Storage

The CAPEX of the two storage tanks, where the first stores CO_2 and the second stores H_2, are assumed equal due to their pressure and volume being identical at 32 bar and 100 m^3. An investment cost is estimated by C. van Leeuwen [2018], resulting in 45.6 USD/m^3. Furthermore, they estimate an operation and maintenance (O&M) cost, which due to the relatively low pressure in the storage tank, is taken as 0.5 % of the initial CAPEX.

The storage units also require compression before their respective stream may enter the MeOH reactor, hence a multistage compressor is required as presented in Chapter 3, which is determined through APEA.

The CAPEX and OPEX of the H_2 and CO_2 storage subsystems are listed in the Tables in Section 6.3 and 6.4.

6.1.3 Electrolysis

The CAPEX of the electrolyser is based on Brynolf et al. [2018], where a price interval is given for the expected alkaline electrolyser cost in 2030, where an interval of 480 USD/kW to 1,080 USD/kW is given, with the baseline specified to equal the median being 780 USD/kW. Hence, the CAPEX of the electrolyser is determined according to its power input.

The OPEX for the electrolyser includes its O&M, power consumption, stack replacement and its H_2O supply. The O&M is defined by Brynolf et al. [2018] to equal about 3.5 % of the baseline CAPEX. Additionally, the stacks are specified to have a lifetime of approximately 10.85 years, after which a stack replacement is required. The cost of this replacement is specified to equal 50 % of the baseline CAPEX cost, hence this annual OPEX can be expressed as 4.6 % of the baseline CAPEX of the electrolyser.[Brynolf et al., 2018]

Regarding the H_2O supply to the electrolyser, it must be taken into account that it operates on purified H_2O. To achieve purified H_2O, a demineraliser subsystem is required. Firstly, the tap water is acquired from the local water supply, which has an asking price of 2.2 USD/m^3 [AalborgForsyning, 2021b]. However, in order to reduce this expense, the excess H_2O produced in both systems could be recirculated. The demineralisation of H_2O is achieved using a subsystem similar to the one constructed by Commission [2000]. The input H_2O investigated by Commission [2000] contains more than three times the maximum allowable amount of Na^+ and Cl^- ions in Danish tap water, hence if only these ions were to be removed the subsystem of the presented study would be overdimensioned. Although the recirculated H_2O in the present study contains other species than the impurities present in Commission [2000], which is MeOH for System 1 and C_6H_6 in System 2, the overdimensioning is assumed to equalise this. Hence, the CAPEX and OPEX of the H_2O demineraliser is determined by scaling their system to match the given flow rate in the presented study, the costs of which are listed in the Tables in Section 6.3 and 6.4.

6.1.4 Wind- and Solar Power

Wind- and solar power is desired, not only to produce free power in the long term, but also to compensate for the relatively large power consumption of the systems, which is mainly attributed to the electrolyser. The total installed wind- and solar capacity are, as mentioned in 3.3.1, 84 MW and 9.54 MW, respectively. The CAPEX and OPEX of both technologies are based on Agency [2019], where their CAPEX are listed as 1,325 USD/kW and 750 USD/kW, while their OPEX are 30 USD/kW and 9.5 USD/kW, for wind- and solar power, respectively.

6.1.5 Methanol Synthesis

The CAPEX and OPEX of the MeOH synthesis subsystem is determined by APEA. However, the cost of the catalyst, Cu/ZnO/Al2O3, used in the reactor must be estimated by alternative means. The price is approximated based on the information provided by CatCost [2020], where the catalyst price can be estimated based on its metallic composition. This resulted in a price of about 17,500 USD/tonne.

Regarding the degradation of the catalyst, this is investigated by Alarifi [2016]. They present a catalyst degradation rate resulting in a lifetime of four years, meaning all of the catalyst must be fully replaced at this frequency, resulting in an additional OPEX.

The CAPEX and OPEX of the MeOH synthesis subsystem are listed in the Tables in Section 6.3 and 6.4.

6.1.6 BTX Synthesis

Similar to the MeOH synthesis, the CAPEX and OPEX of the BTX synthesis subsystem is also determined by APEA. However, the cost of the catalyst, ZSM-5, used in the reactor is based on Hannon et al. [2020] and Alibaba [2021], where an interval of approximately

5,000 USD/tonne to 30,000 USD/tonne is reported. Due to the difficulty of estimating which price is representative, the median price is taken.

The degradation of this catalyst is investigated by Hannon et al. [2020]. They present the catalyst degradation rate which results in a lifetime of nine months, meaning all of the catalyst must be fully replaced at this frequency, resulting in an additional OPEX.

The CAPEX and OPEX of the BTX synthesis subsystem are listed in the Tables in Section 6.3 and 6.4.

6.1.7 Separation of System 2 Products

The modelling associated with the separating of the products produced by System 2 was concluded to be out of scope for the presented study. Instead, the number of components and their required utility were estimated based on literature concerning a similar subsystem. This resulted in a separation subsystem with a multistage compressor, a flash vessel and four distillation columns. The utility of each component was estimated based on the required utility listed in this literature and scaled by the difference in mass flow to the presented study. This procedure is repeated when estimating the equipment costs of each of the latter mentioned components. It is likely that the equipment costs cannot be scaled linearly, however, since the modelling has not been performed for the components it has been assumed.

According to Chen et al. [2015] the cost of the multistage compressor and flash vessel are approximately 32,137,300 USD and 496,300 USD, respectively. The distillation column, which is to be scaled, is coupled to a condenser and reboiler where the cost of the entire unit is 1,688,200 USD.

The multistage vessel have both the highest utility requirement according to Section 4.3.2, further it is also the component with the highest cost. This indicates that it may be beneficial to investigate if other components could replace the multistage compressor. However, the subsystem defined by Chen et al. [2015] is similar to the subsystem of the presented study, as such the components remains the same.

If the cost is scaled linearly the cost of the multistage compressor and flash vessel becomes 1,548,000 USD and 23,900 USD, respectively. The cost of each of the four distillation columns becomes 358,000 USD, 313,800 USD, 52,100 USD and 7,900 USD.

6.2 Economics of Additional Parameters

The previous section concerned the economics of each subsystem, whereas this section includes the economics of additional parameters which affect both systems.

6.2.1 Electricity Price

The costs associated with electricity is of significant importance due to the relatively large consumption of power for both systems, which is mainly attributed to the electrolyser. Hence, it is assumed that the determination of the economics of the systems are sensitive to a variation in electricity prices. The price of the electricity is specified according to Energistyrelsen [2021b], Energistyrelsen [2021c] and eurostat [2021], corresponding to 0.043 USD/kWh, 0.05 USD/kWh and 0.073 USD/kWh, respectively. It should be noted that these prices are only achievable since both systems exceed an annual power consumption of 150 GWh.

6.2.2 Initial CAPEX Loan

Due to the relatively large CAPEX of the two systems, presented in Table 6.1 and 6.2, it is deemed a necessity to borrow the capital from financial institutions, such as a bank. However, it is difficult to gather decent estimates for such loans without making an enquiry to the banks. Due to these difficulties, the interest rate and payback period will be varied between 1 % to 5 % and 10 years to 30 years, respectively, in the sensitivity analysis in Section 6.6 on page 115.

6.2.3 Oxygen Production and Price

O_2 is a byproduct produced in the electrolyser, which has not earlier been evaluated in the presented study. However, the produced O_2 mass flow from the electrolyser is 3.44 kg/s in System 1 and 3.25 kg/s in System 2 of which the production volume is considered significant. The difference in O_2 production is due to the recirculation of excess H_2 produced from the BTX synthesis, as such the production volume of the electrolyser in System 2 is reduced.

The possible usage of O_2 in RenoNord's incineration plant was evaluated in Section 2.1, which concluded that it would increase the concentration of CO_2 in the flue gas since the flue gas would contain less N_2. This would result in a reduction of the dimensions of the absorber in the Carbon Capture subsystem, since it was dimensioned in regards to the mass flow of flue gas. Additionally, it was mentioned that utilising O_2 in the incineration plant may increase the adiabatic flame temperature within the combustor, hence increase the power output of the incineration plant. The O_2 can therefore be used on site by the incineration plant of RenoNord, or it could be sold.

A company which is known to have a high consumption of O_2 is Rockwool, which is located in Hobro approximately 36 km from the incineration plant of RenoNord. Currently, the O_2 is supplied to their factory by trucks, from which it could be lucrative to install a pipeline between the proposed plant of the presented study and Rockwool. From a similar study it was concluded that Rockwool would support such a deal.[EnergiNet, 2018]

It is difficult to estimate the possible revenue associated with the sale of O_2 to Rockwool, since the asking price would have to be negotiated. It is of interest for Rockwool to purchase the O_2 cheap compared to other suppliers, meanwhile it is of interest for the presented study to sell the O_2 without further processing. This could be possible if a pipeline was to be connected between RenoNord and Rockwool, where the distance of 36 km is deemed to not pose any problems. The assumption is made according to pipelines that transport natural gas, which are known to exceed more than 1,000 km [Husseini, 2018]. Since the O_2 will be delivered to Rockwool by pipelines, the asking price will be based on the costs associated with onsite production costs. A study done by Dorris et al. [2016] estimates the asking price to be within 26 USD/tonne to 40 USD/tonne [Dorris et al., 2016]. It should however be noted that this price range is based on literature from 2005 and 2007 of which this asking price range might not be representative. It is expected that the asking price will be lowered as the technology develops. Yet, FRED [2021] states the opposite, where the asking price of O_2 has only increased since 2003. As a result, it becomes uncertain if the current asking price associated with onsite production of O_2 should be above or below the range of 26 USD/tonne to 40 USD/tonne. This will be accounted for in the sensitivity analysis by varying the asking price of O_2 from 20 USD/tonne to 60 USD/tonne, with the baseline being 40 USD/tonne.

6.2.4 Green Chemicals

The asking prices for the MeOH and the products produced from the BTX synthesis, previously listed in Table 4.11 on page 83, were all asking prices for what is considered Black chemicals. This classification is equal to the one initially presented for, for example H_2, which can be classified as either Black, Grey or Green, depending on its production method.

The classification 'Green product' is a relatively modern term, from which prices for the products under consideration are difficult to estimate. It is expected that Green products are more expensive than Black products, due to additional production expenditures. Although Green products are more expensive to produce, it provides companies with the option of branding their products as being Green, making them able to charge a premium price for their products.[Klenert et al., 2018] The ability to sell Green products at premium prices are stated by EnergiNet [2019] and DrivKraftDanmark [2021], where bio-diesel is shown to have a value of 1.6 to 2.0 times the value of Black diesel. Similarly, Mikulski [2018] states a Green MeOH price which is approximately two times the price of Black MeOH.

The support towards the use of Green products is hence assumed to also be applicable to the products of consideration in the presented study. Hence, the influence of being able to sell these products at premium prices will be investigated during the sensitivity analysis in Section 6.6.

6.2.5 Heating and Cooling

Independently of which system is of consideration, external cooling and heating is required. Chapter 5 concluded that the utility costs associated with heaters and coolers could be reduced by heat integration. This reduced the utility costs of these components by 97 % and 97.3 % for System 1 and System 2, respectively. However, additional components require heating such as the reboilers that are coupled to the distillation columns, which become an expense determined by APEA. This is represented in Table 6.3 and 6.4 where the heating is provided by steam.

APEA also determines the costs associated with cooling, yet this is not used. The cooling could instead become an income rather than an expense, if the excess heat is sold as district heating. The plant of the presented study will be located next to the incineration plant RenoNord which is already coupled to the district heating network, of which it is expected that the installation costs associated with coupling this plant to the network, will be insignificant. Depending on the season of the year, the temperature of the water returning from the consumers vary. However, independently of the season the temperature should drop approximately 30 °C to 35 °C from the initial temperature at the consumers.[Forsyning, 2020] Assuming an inlet temperature of 40 °C and an outlet temperature of 75 °C the integration of the district heat network into both systems can be analysed.

In System 1, the distilled H_2O exits the distillation column at a temperature of 102 °C which could be used for district heating, since it must be cooled. However, it is expected that this revenue is insignificant due to its relatively low mass flow compared to other streams in this system. As such district heating will not be integrated for System 1.

In System 2, the output of the BTX reactor is cooled to 137 °C by two heat exchangers after which it is cooled by a cooler to 32 °C. The mass flow rate for this stream compared to the formerly mentioned stream in System 1 is approximately 22 times larger. Given the elevated temperature and mass flow a part of the heat, removed by the cooler, could instead be utilised in the district heating network. The heat transfer for this heat exchanger is determined from the inlet and outlet temperature for the district heating stream, yielding a total of approximately 327,000 GJ on an annual basis. The price at which the energy can be sold is 4.15 USD/GJ, corresponding to a total income of approximately 1,300,000 USD [PwC.dk, 2020].

Additional cooling is required for different components throughout the systems, where district cooling could be an option. A district cooling network is currently being established which transfers energy to the quarry located near Rørdal. This network will be available for industrial partners in the eastern part of Aalborg, which also includes RenoNord, and it is already connected to Aalborg University Hospital.[AalborgForsyning, 2021a] According to AalborgForsyning [2021a], the pipelines are placed relatively close to RenoNord and as such it is expected to be possible to connect to these pipelines, hence the instillation costs would be minor. Utilising the district cooling would be an expense, however, it is expected that this expense will be insignificant compared to the overall OPEX of the plant, as such its influence is excluded in the remainder of the presented study. The assumption regarding cooling from district cooling will be further discussed in Chapter 7 on page 121.

6.3 CAPEX of the Systems

The CAPEX assessment of the different subsystems used in the two systems, illustrated in Figure 5.2 and 5.4 in the former Chapter 5, is determined using APEA and the results are listed in Table 6.1 and 6.2. Furthermore, the CAPEX of the wind and solar power, H_2O demineraliser, electrolyser, storage units, and BTX separation unit is determined using the information presented in the above Section 6.1.

Table 6.1: CAPEX of System 1, where distilled MeOH is sold as the final product. The cost of the subsystems and the total CAPEX is given in USD.

Subsystem	Component	Equipment cost [USD]	Installation cost [USD]
Carbon Capture	Absorber	1,996,200	2,464,600
	Comp	15,000	100,000
	Cooler 1	2,000	20,000
	Cooler 2	57,100	158,500
	Flash	1,800	10,200
	Heat Exchanger	1,562,200	2,575,000
	Pump	16,400	73,300
	Stripper	190,200	516,000
	MEA solvent	14,000	-
Total	-	**3,854,900**	**5,917,600**
Wind power	-	111,300,000	-
Solar power	-	7,158,000	-
H_2O demineraliser	-	1,179,400	-
Electrolyser	-	68,987,900	-
H_2 storage	-	12,898,800	-
CO_2 Storage	-	7,213,300	-
Total	-	**208,737,400**	-
Figure 5.2	Comp 1	61,100	223,700
	Comp 2	853,000	1,067,800
	Cooler 1	152,200	293,400
	Cooler 2	127,600	255,600
	Cooler 3	16,600	76,700
	Degasser	78,800	487,500
	Flash	10,000	20,000
	Heat Exchanger 1	123,300	255,900
	Heat Exchanger 2	65,500	187,100
	Heat Exchanger 3	7,800	46,200
	L-L-Separator	328,500	839,700
	MeOH Reactor	85,400	232,800
	MeOH catalyst	291,900	-
Total	-	**2,201,700**	**3,986,400**
CAPEX	-	**224,698,000**	

Table 6.2: CAPEX of System 2, where MeOH is converted to BTX and other chemicals which are sold as the final products. The cost of the subsystems and the total CAPEX is given in USD.

Subsystem	Component	Equipment cost	Installation cost
Carbon Capture	Absorber	1,996,200	2,464,600
	Comp	15,000	100,000
	Cooler 1	2,000	20,000
	Cooler 2	57,100	158,500
	Flash	1,800	10,200
	Heat Exchanger	1,562,200	2,575,000
	Pump	16,400	73,300
	Stripper	190,200	516,000
	MEA solvent	14,000	-
Total	-	**3,854,900**	**5,917,600**
Wind power	-	111,300,000	-
Solar power	-	7,158,000	-
H_2O demineraliser	-	1,112,500	-
Electrolyser	-	65,076,200	-
H_2 storage	-	12,827,500	-
CO_2 Storage	-	7,213,300	-
BTX separation	-	2,303,700	-
Total	-	**206,991,200**	-
Figure 5.4	BTX Reactor	181,800	511,400
	Comp 1	61,100	223,700
	Comp 2	853,000	1,067,800
	Comp 3	2,342,700	2,544,800
	Comp 4	1,640,600	1,872,400
	Comp 5	1,400,600	1,518,700
	Cooler 1	152,100	293,300
	Cooler 2	68,300	178,400
	Degasser	78,600	487,300
	Flash 1	10,000	20,000
	Flash 2	34,400	133,900
	Heat Exchanger 1	126,600	259,400
	Heat Exchanger 2	65,500	187,100
	Heat Exchanger 3	24,700	105,800
	Heat Exchanger 4	40,300	241,100
	Heat Exchanger 5	8,300	44,900
	MEOH Reactor	85,400	232,800
	Separator 2	28,000	144,400
	MeOH catalyst	291,900	-
	BTX catalyst	296,800	-
Total	-	**7,780,600**	**9,999,500**
CAPEX	-	**234,543,800**	

6.4 OPEX of the Systems

The OPEX assessment of the different subsystems used in the two systems, illustrated in Figure 5.2 and 5.4 in Chapter 5, is determined using APEA and the results are listed in Table 6.3 and 6.4. Furthermore, the OPEX of the wind and solar power, H_2O supply, H_2O demineraliser, electricity, electrolyser, storage units, catalysts, and BTX separation is determined using the information presented in the above Sections 6.1 and 6.2.

Table 6.3: OPEX of System 1, where distilled MeOH is sold as the final product. The annual cost of the subsystems and the total OPEX is given in USD.

Subsystem	OPEX Type	Unit	Quantity	Unit cost	Annual cost [USD]
Carbon Capture	Electricity	kW	89.6	0.05 USD/kWh	39,300
	Cooling water	MW	5.0	≈ 0	0
	Low P. steam	tonne	211,800	17.95 USD/tonne	3,801,800
	MEA solvent	tonne	1.4	1,400 USD/tonne	1,900
Wind power	O&M	MW	84.0	30 USD/kW	2,520,000
Solar power	O&M	MW	9.5	9.5 USD/kW	90,700
Tap water	Consumable	m^3	81,730	2.20 USD/m^3	179,400
H_2O demin.	O&M	m^3	1.22e+5	0.54 USD/m^3	66,000
Electrolyser	Electricity	MW	88.6	0.05 USD/kWh	38,739,300
	Cooling	MW	22.4	≈ 0	0
	O&M	-	-	3.5% CAPEX	2,414,600
	Stack rep.	-	-	4.61% CAPEX	3,179,200
CO_2 Storage	Electricity	kW	505.0	0.05 USD/kWh	221,200
	Cooling	kW	373.7	≈ 0	0
	O&M	-	-	0.5% CAPEX	≈ 0
H_2 Storage	Electricity	kW	1173.7	0.05 USD/kWh	514,100
	Cooling	kW	1029.3	≈ 0	0
	O&M	-	-	0.5% CAPEX	≈ 0
Figure 5.2	Electricity	kW	520.7	0.05 USD/kWh	228,100
	Cooling water	MW	16.068	≈ 0	0
	Refrigerant	tonne	52,800	≈ 0	0
	Low P. steam	tonne	105,400	17.95 USD/tonne	1,890,900
	High P. steam	tonne	800	25.82 USD/tonne	21,100
	MeOH catalyst	tonne	4.2	17,500 USD/tonne	73,000
OPEX					**53,980,400**

Table 6.4: OPEX of System 2, where MeOH is converted to BTX and other chemicals which are sold as the final products. The annual cost of the subsystems and the total OPEX is given in USD.

Subsystem	OPEX Type	Unit	Quantity	Unit cost	Annual cost [USD]
Carbon Capture	Electricity	kW	89.6	0.05 USD/kWh	39,300
	Cooling water	MW	5.0	≈ 0	0
	Low P. steam	tonne	211,800	17.95 USD/tonne	3,801,800
	MEA solvent	tonne	1.6	1,400 USD/tonne	1,900
Wind power	O&M	MW	84.0	30 USD/kW	2,520,000
Solar power	O&M	MW	9.5	9.5 USD/kW	90,700
Tap water	Consumable	m^3	36,638	2.20 USD/m^3	80,400
H_2O demin.	O&M	m^3	1.15e+5	0.54 USD/m^3	62,200
Electrolyser	Electricity	MW	83.4	0.05 USD/kWh	36,542,800
	Cooling	MW	21.1	≈ 0	0
	O&M	-	-	3.5% CAPEX	2,277,700
	Stack rep.	-	-	4.61% CAPEX	2,998,900
CO_2 Storage	Electricity	kW	505.0	0.05 USD/kWh	221,200
	Cooling	kW	373.7	≈ 0	0
	O&M	-	-	0.5% CAPEX	≈ 0
H_2 Storage	Electricity	kW	1,107.2	0.05 USD/kWh	484,900
	Cooling	kW	1,029.3	≈ 0	0
	O&M	-	-	0.5% CAPEX	≈ 0
Figure 5.4	Electricity	kW	4,614	0.05 USD/kWh	2,021,000
	Cooling water	MW	19.0	≈ 0	0
	Refrigerant	tonne	52,800	≈ 0	0
	Low P. steam	tonne	27,500	17.95 USD/tonne	494,000
	MeOH catalyst	tonne	4.2	17,500 USD/tonne	73,000
	BTX catalyst	tonne	22.6	17,500 USD/tonne	395,700
BTX Sep. Column	Electricity	MW	7.4	0.05 USD/kWh	3,258,700
BTX Sep. Compressor	Electricity	MW	10.4	0.05 USD/kWh	4,537,700
OPEX					**59,904,800**

6.5 Economic Assessment

The costs associated with the above CAPEX and OPEX Tables of 6.1 to 6.4 are compiled into pie-charts, shown in Figure 6.1, to signify the distribution of the various subsystems. The category Others in the pie-charts with respect to the CAPEX, consists of the H_2O demineraliser and storage units. With respect to OPEX it consists of H_2O supply, H_2O demineraliser and storage units.

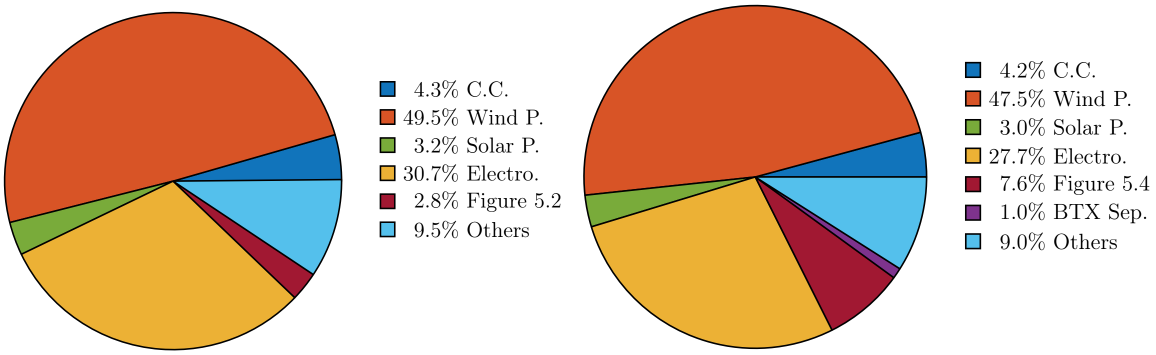

(a) CAPEX of System 1. **(b)** CAPEX of System 2.

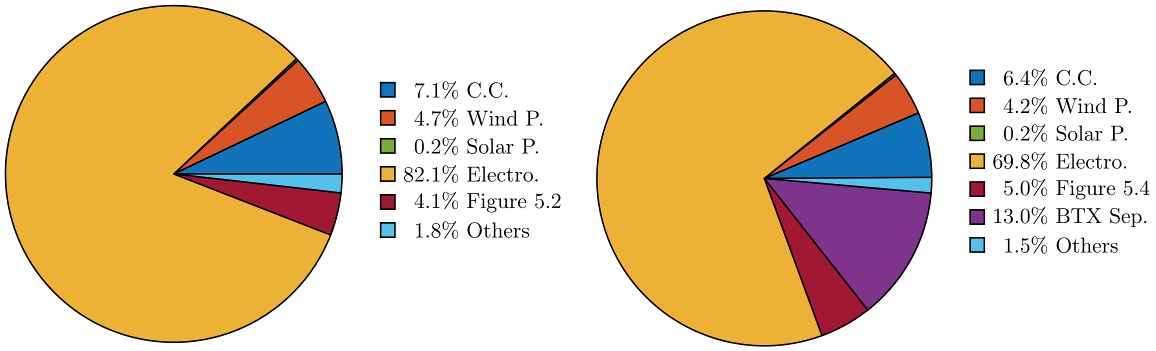

(c) OPEX of System 1. **(d)** OPEX of System 2.

Figure 6.1: Distribution of CAPEX and OPEX from Table 6.1 to 6.4. The pie-charts include the following: carbon capture (C.C.), wind power (Wind P.), solar power (Solar P.), electrolyser (Electro.), the subsystems shown in Figure 5.2 and 5.4, and BTX separation (BTX Sep.) for System 2.

According to Table 6.1 and 6.2 the CAPEX is increased by approximately 10 MUSD from System 1 to System 2. The majority of this increment is due to the steady state subsystem of System 2 being more expensive than for System 1. In addition, the separation of the products produced by the BTX synthesis result in an additional expense. This is illustrated in Figure 6.1(a) and 6.1(b). Additionally, the electrolyser is reduced for System 2 compared to System 1 resulting in lowering the fractional CAPEX of this unit.

With respect to the OPEX, System 2 is approximately 6 MUSD/year more expensive than System 1, where the differences of the two systems are indirectly shown in Figure 6.1 (c) and (d). System 2 introduces the separation of BTX which increases the OPEX. Additionally, the steady state subsystem in System 2 further increases the OPEX. However, as seen from Table 6.4 on the previous page the contribution of the electrolyser, with respect to the OPEX, is reduced for System 2. This occurs since H_2 is recirculated from the BTX synthesis to the MeOH synthesis, of which the utility requirement of the electrolyser is reduced.

6.6 Sensitivity Analysis

Given the CAPEX and the OPEX, a sensitivity analysis can be conducted for each system. As discussed, some of the parameters with respect to both the CAPEX and OPEX are relatively unreliable, meaning their values may not be representative. Even though this is the case for multiple parameters, only a few are of interest due to their expected significant influence towards the profit. Within the first eight rows in Table 6.5 on the following page are the parameters which are of interest for both systems, whereas the last row is only investigated when considering System 2. In total, seven parameters are of interest for both systems: the electricity price, CAPEX and OPEX of the electrolyser, the interest rate and payback period for the loan, the asking price of the O_2 and lastly the asking prices for the products.

The price of the electricity, as well as the interest rate and payback period, are parameters which are affected by the size of the system. Independent of which end product is desired, the total electricity demand is of a magnitude which corresponds to the cheapest available prices, since both exceeds 150 GWh/year. However, these values differ, and furthermore they have a significant influence on the profit. A baseline value of 0.05 USD/kWh was chosen, where the minimum and maximum value were defined to be 0.043 USD/kWh to 0.073 USD/kWh due to the variation in the literature. The interest rate and payback period are dependent on multiple aspects, however both of these values are expected to have a relatively large impact towards the profit. An interest rate of 3 % and a payback period of 20 years were chosen to define as the baseline values. Due to their influence, these have been cross varied as may be seen in Table 6.5 on the next page, such that the interest rate and payback period has been investigate for 1-, 3- and 5 % for 10-, 20- and 30 years.

As discussed, the electrolyser has the greatest power consumption within the systems independent of which end product is desired. In Section 3.3 it was stated that the model of the electrolyser was based on empirical data obtained from a bench scaled setup. It was further also concluded that if a commercial electrolyser was to be scaled, the power consumption could be reduced by 13 %. Therefore, as the baseline value for the electrolyser is defined from the bench scaled model, the influence of a power consumption being 90 % and 80 % of the baseline power consumption is investigated. Similar to the power consumption for the electrolyser, its CAPEX is also known to vary due to technological development. The baseline value for the CAPEX has been defined to be 780 USD/kW where the influence of a lower value at 480 USD/kW and an increased value at 1,080 USD/kW are further analysed. The primary product from the electrolyser is the H_2, however O_2 is also produced, which could be sold. As previously discussed the price of the O_2 can vary from which it is included in the sensitivity analysis. The baseline value is defined by an asking price of 40 USD/tonne from which it has been varied by ±50 %.

The last parameter which is expected to influence both systems is the asking price for the end products. Initially the asking prices of the products were defined to equal those produced from non-renewable sources. However, it is expected that the asking prices should be greater when the products are produced from renewable sources. All of the product prices have therefore been upscaled by a factor of 1.5 and 2.0 in the sensitivity analysis.

For System 2, an additional parameter is of interest, which is the separation of the products produced from the BTX synthesis. As stated in Section 2.6 the product stream, when producing BTX, consists of 17 different species from which the complexity of modelling this separation was deemed out of scope for the presented study. Instead it was based on literature with a similar product stream, however, due to the inequality of product species, the CAPEX and OPEX for this process is expected to differ. The major difference between the product streams is the absence of H_2O in the literature. This occurs due to their reactant being ethane instead of MeOH. Since the separation of H_2O is relatively energy demanding, the baseline values for the CAPEX and OPEX are only upscaled, by a factor of 1.5 and 2.0.

All the values used in the sensitivity analysis may be seen in Table 6.5.

Table 6.5: Parameters which will be analysed in the sensitivity analysis.

Parameter	Unit	Baseline Value	Variation 1	Variation 2
Electricity Price	[USD/kWh]	0.05	0.0426	0.0726
Electrolyser OPEX	[%]	100	90	80
Electrolyser CAPEX	[USD/kW]	780	480	1080
Interest Rate - 10 years	[%]	3	1	5
Interest Rate - 20 years	[%]	3	1	5
Interest Rate - 30 years	[%]	3	1	5
O_2 Price	[USD/tonne]	40	20	60
Green Price factor	[-]	1.0	1.5	2.0
Worst/Best Case	[-]	-	Worst	Best
BTX separation factor	[-]	1.0	1.5	2.0

From Table 6.5 the discussed variations may be seen, as well as their initial values. However, an additional factor is also investigated denoted Worst/Best Case. This is included in order to investigate the minimum and maximum obtainable profit. The Best case is defined with the lowest prices for the electricity as well as the CAPEX and OPEX of the electrolyser. Furthermore, it is also defined with the lowest BTX separation factor and with the highest asking price for the products. The interest rate is reduced to 1 % whereas the payback period is kept at 20 years. Contrary, the Worst case is defined opposite to the Best case.

With the baseline values defined for both systems, the sensitivity analysis can be conducted.

6.6.1 Sensitivity Analysis for System 1

Given the baseline values, the CAPEX and profit can be estimated for System 1 as may be seen in Table 6.6 on the facing page. The annual profit during the loan is determined using Eq. 6.1, which predicts the necessary yearly payment needed to pay back the loan with a fixed interest rate

$$\kappa = \beta \cdot (1+\gamma)^{\lambda} - \frac{\tau}{\gamma} \cdot ((1+\gamma)^{\lambda} - 1) \tag{6.1}$$

where κ is the balance after λ number of periods, β is the initial loan, τ is the yearly payment, and γ is the interest rate per period. κ is set equal to zero to determine the yearly payment required to payback the loan, and the equation is isolated with respect to τ.

Table 6.6: CAPEX for baseline System 1 where MeOH is the desired end product, as well as the total loan expenditure. The profit during the payback of the loan and the profit after the loan is also shown.

	Price [USD]
CAPEX	224,698,000
Total Loan Expenditure	302,064,500
Annual Profit During Loan	-25,576,100
Annual Profit After Loan	-10,472,900

From Table 6.6, the CAPEX and the total loan expenditure may be seen, which corresponds to a cost for the loan of approximately 77,366,500 USD. It may further be seen that both during and after the payback of the loan, System 1 produces a deficit. However, as formerly discussed, different parameters have a relatively significant influence on the possible profit from which a sensitivity analysis is required. The sensitivity analysis for System 1 may be seen in Figure 6.2.

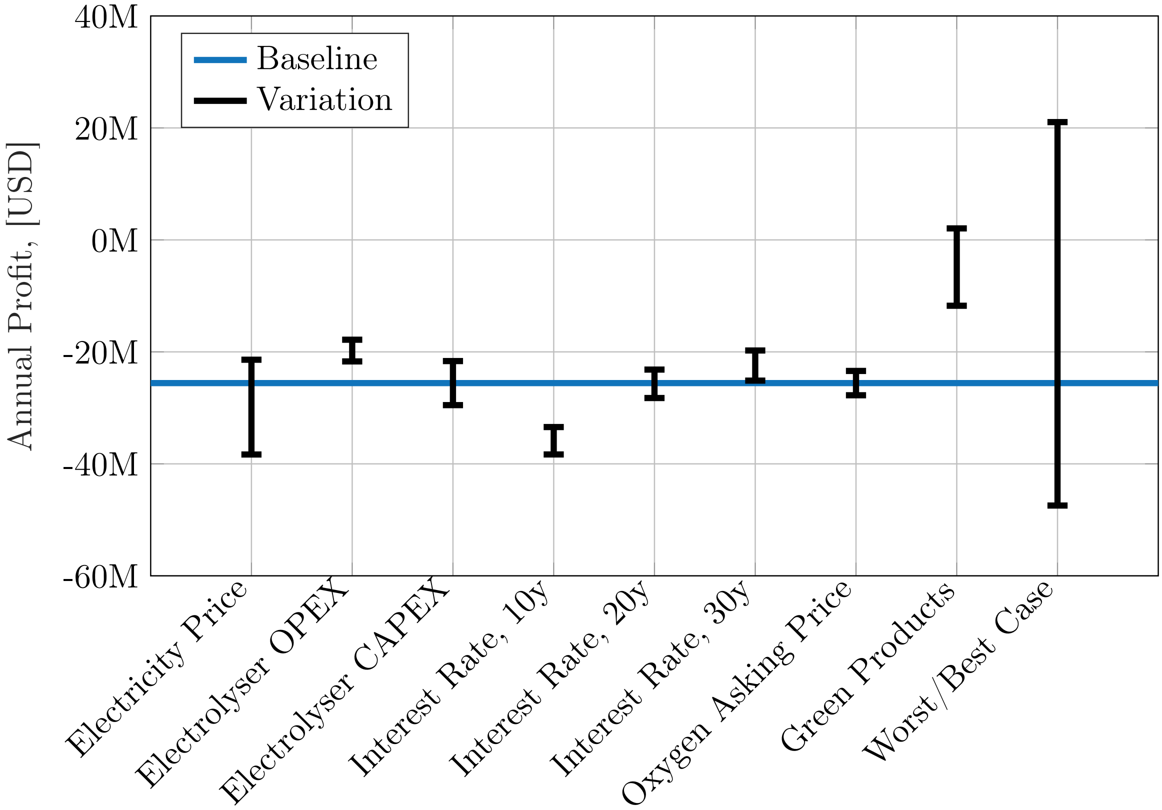

Figure 6.2: Sensitivity analysis for System 1, varied according to Table 6.5 on the preceding page.

As was shown in Table 6.6 it may also be seen in Figure 6.2 that the baseline value for System 1 results in a deficit. This was expected since the asking price for the Green MeOH is defined to equal the price of MeOH produced by non-renewable sources. However, in order to be classified as Green MeOH, electrolysis is required for the supply of H_2. This has a relatively large impact on the baseline value for the MeOH which may be seen from the first three variations in Figure 6.2. Here it is shown that a reduction in the electricity price can reduce the deficit by approximately 15 %. Furthermore, the variations of the OPEX for the electrolyser, corresponds to reductions of the deficit by approximately 15 %

and 30 %. Lastly, with respect to electrolyser, the CAPEX has also been varied which corresponds to a change in the baseline value by ±12 %. It can therefore be concluded that as an isolated component the electrolyser has a relatively significant influence towards the possible profit, from which more precise values with respect to the electrolyser is required in order to determine the possible profit.

From the consecutive three variations, the influence of the interest rate linked with the payback period may be seen. As expected it can be concluded that with a higher interest rate, the deficit increases. Likewise, the shorter the payback period, the greater the deficit becomes. The latter occurs since the price for the loan decreases as the payback period is shortened, however, the loan has to be payed back faster which affects the possible profit during the payback period. Also, the relative change between 10- and 20 years is greater than for 20- and 30 years, which is due to the influence of the interest rate. It can therefore be concluded that the interest rate has a relatively significant influence towards the possible profit.

Additionally, the asking price of O_2 was varied. It may be seen that this variation has the smallest influence towards the baseline value. It was varied by ±50 % from the baseline value corresponding to a change in the deficit by approximately ±9 %. It can hereby be concluded that the asking price for the O_2 is the least significant value of those which were varied.

From Figure 6.2 on the previous page it may be seen that the variation of the asking price for the end products has the greatest influence on the baseline value as an isolated parameter. Yet, by up-scaling the asking price of the Green MeOH by a factor of 1.5 System 1 will remain unprofitable, whereas a factor of 2.0 corresponds to a profit of approximately 2,056,300 USD. This trend was expected since the production of MeOH from non-renewable sources are well developed, resulting in relatively cheap prices. However, by producing Green MeOH the processes are more energy demanding as was concluded due to the electrolyser. It can therefore be concluded that it is necessary to increase the asking price for the Green MeOH in order to produce a profit. This influence may further also be seen in the last variation which is the Worst- and Best case. From this analysis it can be concluded that the Worst case results in a deficit of 47,445,500 USD, whereas the Best case results in a profit of approximately 21,041,000 USD.

From the sensitivity analysis regarding System 1, it can be concluded that the baseline value produces a deficit. It can further be concluded that the model is mostly sensitive with respect to the asking price for the Green MeOH. Therefore, in order to estimate if System 1 can become profitable, a precise value for the asking price of the produced Green MeOH is required.

6.6.2 Sensitivity Analysis for System 2

Given the baseline values, the CAPEX and profit can be estimated for System 2 where BTX is the desired end product as may be seen in Table 6.7 on the facing page. The annual profit during the loan is determined using Eq. 6.1 on page 116, which predicts the necessary yearly payment needed to pay back the loan with a fixed interest rate.

Table 6.7: CAPEX for baseline System 2, where BTX is the desired end product, as well as the total loan expenditure. The profit during the payback of the loan and further also the profit after the loan is also shown.

	Price [USD]
CAPEX	234,543,800
Total Loan Expenditure	315,300,400
Annual Profit During Loan	1,212,300
Annual Profit After Loan	16,977,300

From Table 6.7 the CAPEX and the total loan expenditure may be seen, which corresponds to a cost for the loan of approximately 80,756,600 USD. Contrary to System 1, System 2 produces a profit both during and after the payback period of the loan. Also, similar to System 1, different parameters have a relatively significant influence towards the possible profit from which a sensitivity analysis is required. The sensitivity analysis for System 2 may be seen in Figure 6.3.

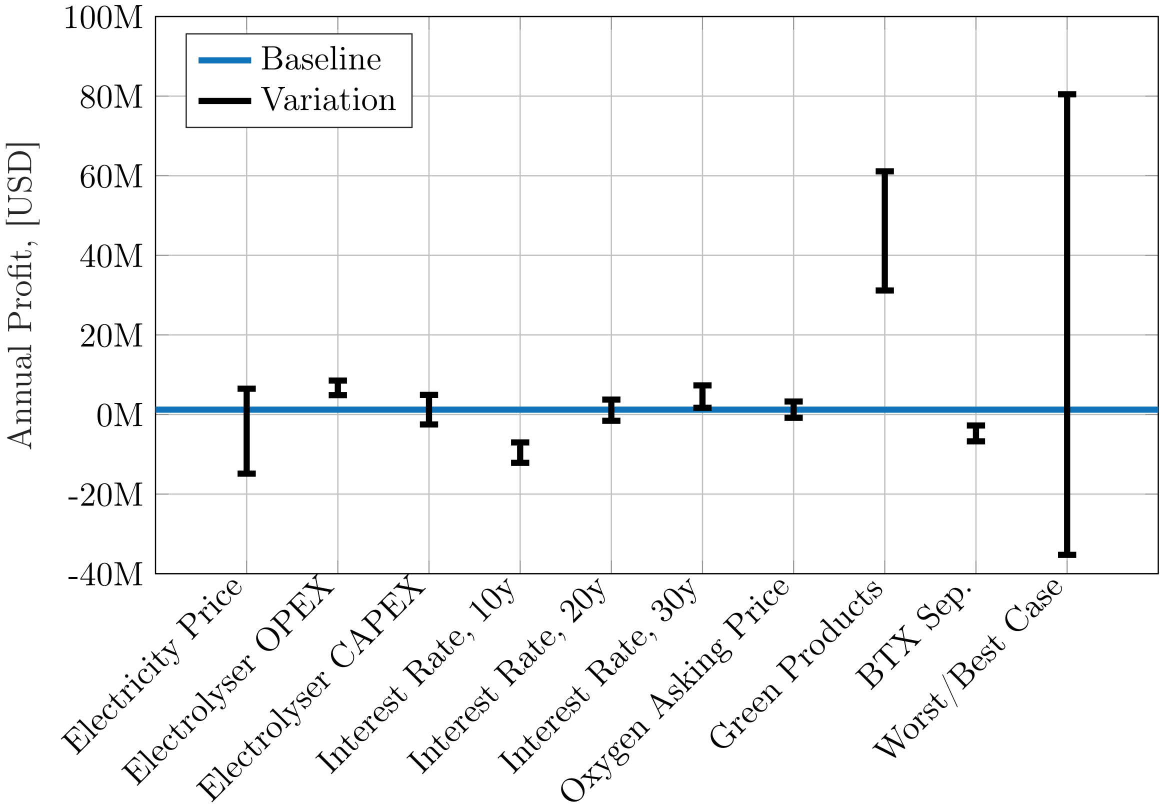

Figure 6.3: Sensitivity analysis for System 2, varied according to Table 6.5 on page 116.

As was shown in Table 6.7 it may also be seen in Figure 6.3 that the baseline value for System 2 results in a profit. From System 2, H_2 was separated and recycled back to the MeOH synthesis from which the electrolyser was reduced in size. This reduction affects the absolute influence of the electrolyser towards the baseline value. The sensitivity analysis of System 1 showed that regardless of the variation in the electricity price and the CAPEX or OPEX of the electrolyser, a profit would not be produced. However, these variations affect System 2, such that it may produce a deficit, instead of the profit defined from the baseline value. Given the baseline value for System 2 being relatively close to 0 MUSD, a variation of the electricity price changes whether System 2 produces a profit or deficit. This trend is also equal for the variation of the CAPEX for the electrolyser. However, as expected the reduction of the OPEX for the electrolyser only increases the profit. It can therefore be concluded that System 2 is relatively sensitive to the electrolyser, when determining whether it produces a profit or deficit.

The variation of the interest rate and payback period also affects whether System 2 produces a profit or deficit. Regardless of the interest rate, when the payback period is 10 years, System 2 produces a deficit. However, depending on the interest rate with a payback period of 20 years, System 2 either produces a profit or a deficit. Though, with a payback period of 30 years System 2 produces a profit regardless of the interest rate. It can therefore be concluded that the interest rate and payback period is crucial when estimating whether System 2 will produce a profit or deficit.

The variation of the O_2 asking price affects the baseline value by approximately $\pm 80\,\%$, however, regardless of which value is chosen, the output remains a profit. It can be concluded that the possible profit is relatively sensitive to the asking price of the O_2. It can however be seen from the figure that the parameter which has the greatest influence towards the possible profit, is the asking price for the products. By increasing the asking price for the products by a factor of 1.5 and 2.0, the profit increases by a factor of 13 and 25, respectively. This may further also be seen from the Best case scenario which increases the profit by a factor of 32, yielding a profit of approximately 80,469,000 USD. The Worst case corresponds however to a deficit of approximately $-35{,}267{,}100$ USD. One of the parameters which contributes to this relatively large deficit is the separation of the product stream from the BTX subsystem. The conversion of MeOH to BTX results in a product distribution of 17 species. In order to separate these and thereby sell them, a number of simplifications were made. To account for this simplification, the CAPEX and OPEX for the BTX separation have been increased by a factor of 1.5 and 2 which both result in a deficit.

From the sensitivity analysis of System 2, it can be concluded that the baseline value produces a profit. However, this profit is relatively sensitive with respect to the mentioned parameters, from which it could produce a deficit instead of profit. Similar to System 1, System 2 is also most sensitive with respect to the asking price of the Green products. However, similar to System 1, precise values for the asking prices are required in order to estimate the potential of the System 2.

From both sensitivity analyses it may be concluded that two parameters have the greatest influence towards the baseline value, being the electricity price and the asking prices for the products. In general, System 1 is less sensitive to all the parameters compared to System 2, with respect to a change in whether it produce a deficit or profit. This occurs since System 1 produces a relatively large deficit, compared to System 2 which produces a small profit. Since System 2 only produces a small profit it is more sensitive to all the parameters with respect to whether or not it produces a deficit or profit.

Since the electricity price and the asking prices for the products have such significant influence, it can be concluded that these values should be further investigated in order to estimate a more representative feasibility for both systems. Nonetheless, System 2, where BTX is the desired end product, displays the greatest possible profit, from which it may be concluded that System 2 should be chosen rather than System 1. It should however be noticed that the possible profit from System 2 is based on a product distribution which has not been validated. Therefore, in order to definitively conclude which system is the most profitable, this product distribution must be validated.

Chapter 7

Discussion

In this chapter the most considerable assumptions will be discussed. The first concerns the cooling and the second concerns the product distribution of System 2. A significant amount of cooling is required throughout the two systems, where an initial assumption was applied that it could mainly be supplied by district cooling. With respect to the product distribution for System 2, this assumption was made due to literature listing the species as lumped products. However, this clearly influenced the feasibility of System 2 as presented in 6.

7.1 Cooling

Cooling is required throughout the systems which was either supplied by the district heating network or district cooling. If district heating is utilised the cooling could become a revenue, whereas the district cooling could be supplied from the quarry located in Rørdal. Regarding district heating, only one stream was chosen, in System 2, to transfer energy, due to the constraint that the integration of district heating must result in an income. However, the Danish government has designed the law regarding district heating such that it is not profitable for companies to rely on this income to be significant in their total profit. This has been done in order to force companies to become more energy efficient [Energistyrelsen, 2021a]. Therefore, since the additional income is used as the constraint, it results in only one stream being utilised, from which the remaining cooling must be supplied from district cooling. The required district cooling of System 1 was determined to be 44.86 MW and 46.46 MW for System 2, according to Table 6.3 and 6.4 on page 113. It has been assumed that the district cooling is supplied from the quarry located in Rørdal. A district cooling network from the formerly mentioned quarry, is already connected to "Aalborg University Hospital" where the pipelines are located near RenoNord. As such it is expected that the installation costs would be insignificant if either system of this presented study was to be connected. Even though this cooling system should be fairly easy to access, the capacity must be considered. The currently established district cooling network has a capacity of 7.3 MW which is able to be upgraded to a capacity of 11.0 MW [Pedersen, 2021]. This suffices the cooling requirement of "Aalborg University Hospital" of which it is expected that an excess cooling of at least 3.7 MW would be available from the quarry located in Rørdal. Yet, this does not suffice the cooling requirement of the systems of the presented study, hence an alternative solution must be made. As such the cooling of "Nordjylland Power Station" will be investigated in order to assess if the cooling of the systems of the presented study could utilise the same cooling procedure.

This power station is a coal fired combined heat- and power plant located just north of Aalborg, by the coast of the Limfjord. The cooling of the power plant is supplied by water from the fjord, after which the heated water is discharged back into the fjord. It was assessed in 1993, prior to the establishment of the plant, that it would not significantly impact the fjord if this method was utilised [Amt, 1993]. The temperature difference between the inlet and outlet of the cooling water is 12 °C and its maximum volume flow is estimated to be $27\,\mathrm{m^3/s}$ [Naturstyrelsen, 2011][Kommune, 2011]. Applying the same temperature difference, the corresponding volume flow of cooling water in the presented study can be compared to the quantity used by this power station, to estimate if it would be realistic to utilise the fjord to cool the systems. Assuming the H_2O to be at standard conditions for the calculations, the corresponding volume flows of System 1 and System 2 become $0.89\,\mathrm{m^3/s}$ and $0.93\,\mathrm{m^3/s}$, respectively. However, even if this implementation is deemed achievable, it would require further agreement with Aalborg municipality and the Danish government due to the possible environmental impact. Utilising this method, the assumption regarding negligible OPEX associated with cooling is accepted. Yet, this implementation might increase the CAPEX significantly which should also be included.

7.2 Product Distribution of System 2

In Table 4.11 on page 83 the prices for the different species produced in the BTX synthesis were shown where it was found that they varied from 51 USD/tonne to 34,571 USD/tonne. Since the distribution of the species has not been validated, the income for the products formed in the BTX synthesis may not be representative, due to this relatively large price variation. The study of which the reaction scheme is based on, only defines the lumped product distribution of the Light Gases, Alkanes, Aromatics, Others and Heavy. Since the individual molar fraction of the species within these lumped products cannot be validated and their individual prices vary significantly, the profit for these products may not be representative. This could influence the economics such that System 1 may be more lucrative than System 2. Therefore, in order to validate the possible income of selling the products it is required that experiments are conducted in order to determine the product distribution of each species.

Chapter 8

Conclusion

The objective of the presented study was to conduct a techno-economic analysis, in order to determine if the production of Green methanol would be more profitable compared to converting it to Green BTX. In order to make this assessment, modelling of the entire system was required, from the initial constituents being the CO_2 captured in the flue gas of RenoNord and the H_2 dissociated from H_2O electrolysis. Two models were designed, one for each system, depending on the desired end product. Both models were designed equally up to the point where the produced methanol should either be distilled or converted into BTX.

Both the carbon capture and electrolyser were made as dynamic models, due to the fluctuation of the CO_2 flow caused by variations in heat and electricity produced by RenoNord. Furthermore, the electricity supplied to the electrolyser varied, due to it partly being supplied from renewable sources. The renewable energy was partly produced by 20 4.2 MW wind turbines and PV panels with a capacity of 9.5 MW, while the remainder was supplied by the grid. The modelling of the carbon capture subsystem was based on literature. The electrolyser was based on a bench scaled system, where it was determined that the energy contribution could be reduced by 13 % if it was scaled according to the performance of a commercialised electrolyser. It was of interest to operate the methanol synthesis at steady state in order to avoid partial loading which could reduce its efficiency. In order to achieve this, storage of both CO_2 and H_2 was incorporated to convert the fluctuating inputs into steady state outputs. The methanol synthesis was also based on a literature, from which an optimisation algorithm was implemented, in order to achieve the highest yield of methanol. The end product for the first system was Green methanol from which two different distillations were implemented to achieve high purity Green methanol. The purpose of the first distillation, was to remove the gases which were dissolved in the liquid. Secondly, a liquid-liquid distillation was implemented in order to separate the remaining mixture, consisting of water and methanol.

System 2 was implemented as a continuation of System 1 after its first distillation, where only the liquids remained from the methanol synthesis. The BTX synthesis was also based on literature. The conversion of methanol into BTX is unexplored from which limited data were available. The study, from which the BTX conversion was based upon, only defined the lumped product distributions and not the individual species. As such it became difficult to verify the resulting product distribution. In order replicate the results listed in the study, an optimisation algorithm was implemented which resulted in acceptable differences, from which the product distribution was defined. Following the BTX synthesis, separation of these products was required. The methanol to BTX conversion resulted in 17 species from which modelling this separation would be complex. Instead the separation of these species would be based on literature. A relatively similar study was found, which defined a separation subsystem for the products acquired from the conversion of Ethane to BTX. The major difference, between the presented study and this literature, was the water that occurred when converting methanol to BTX compared to Ethane to BTX. However, from the study a separation subsystem was defined such that the most profitable species could be separated.

With both systems defined, heat integration was applied for both systems in order to reduce their utilities. This resulted in a utility cost reduction for heaters, coolers and heat exchangers at 97.0 % and 97.3 % for System 1 and System 2, respectively. Before concluding which system would be the most profitable, a sensitivity analysis was conducted for each system in order to investigate the influence of different parameters, which were expected to significantly influence the profit. From these sensitivity analyses it was determined that System 1, where methanol was the desired end product, produced a deficit, contrary to System 2 where BTX was the desired end product. System 1 produced an annual deficit of 25,576,100 USD but showed the potential profit of 21,041,000 USD when considering the Best case. System 2 produced an annual profit of 1,212,300 USD but showed a potential profit of 80,469,000 USD when considering the Best case scenario. Initially, the asking prices were based on products which were produced from non-renewable sources. However, the products of the presented study were produced from renewable sources from which they could be classified as Green products, of which it was expected that these products had a greater asking price. As such the asking prices of the products were varied in the sensitivity analysis, which concluded that these had the greatest influence on their profitability.

Initially, it could be concluded that System 2 was the most profitable system, however, one simplification must be taken into account, which was with respect to the separation of the products produced in the BTX subsystem. The Alkanes: C_4H_{10}, C_5H_{12} and C_6H_{14} were separated as one lumped product along with the excess methanol, and sold as one, which was known to not be representative. BTX consist of benzene, toluene and xylene where the two latter species were separated together and sold as one. The benzene was separated along with the excess water and further discarded due to its relatively low annual amount. Both C_9H_{12} and $C_{10}H_{14}$ were separated and sold individually.

The presented study can hence conclude that two robust models have been designed which can be used to determine which end product is most profitable. Yet, it is necessary to acquire precise prices for the end products to determine the profitability of the two systems, as well as the product distribution of the BTX production.

Bibliography

AalborgForsyning. Fjernkøling, 2021a. URL `https://aalborgforsyning.dk/erhverv/Koling`.

AalborgForsyning. Erhvervskunder (ekskl. moms, inkl. statslig afgift) ved aalborg vand a/s, 2021b. URL `https://aalborgforsyning.dk/media/m0sjx52j/vand-erhverv-februar-2021.pdf`.

D. Aaron and C. Tsouris. Separation of co2 from flue gas: A review. *Separation Science and Technology*, 40(1-3):321–348, 2005. doi:https://doi.org/10.1081/SS-200042244.

C. Acar and I. Dincer. Comparative assessment of hydrogen production methods from renewable and non-renewable sources. *International Journal of Hydrogen Energy*, 39(1): 1–12, 2014. doi:https://doi.org/10.1016/j.ijhydene.2013.10.060.

I. R. E. Agency. Renewable power generation costs in 2019, 2019. URL `https://www.irena.org/-/media/Files/IRENA/Agency/Publication/2020/Jun/IRENA_Power_Generation_Costs_2019.pdf`.

A. Alarifi. Modeling, analysis and optimization of the gas-phase methanol synthesis process, 2016. URL `https://uwspace.uwaterloo.ca/bitstream/handle/10012/10156/Alarifi_Abdulaziz.pdf;jsessionid=C880FAA24C9CA88BB72A2E805937E763?sequence=1`.

AlfaAesar. L04493 1,2,4,5-tetramethylbenzene, 97+%, 2021. URL `https://www.alfa.com/en/catalog/L04493/`.

Alibaba. zeolite zsm 5 catalyst, 2021. URL `https://www.alibaba.com/showroom/zeolite-zsm-5-catalyst.html`.

Alibabba. Alibabba, 2021a. URL `duct-detail/Pentane-Pentane-China-Supplier-Pentane-ISO_1600144634772.html?spm=a2700.7724857.normal_offer.d_title.5bdd56e5yyBfp3&s=p`.

Alibabba. Iso sgs 99% pseudocumene psc, 2021b. URL `https://www.alibaba.com/product-detail/ISO-SGS-99-Pseudocumene-PSC-1_1600200294473.html?spm=a2700.7724857.normal_offer.d_title.5887735bqC7CBS`.

Americanchemistry. Olefins uses and benefits, 2020. URL `https://www.americanchemistry.com/olefinspanel/Uses-and-Benefits.html`.

N. Amt. Regionplan nordjyland tillæg nr.26. Technical report, Miljøministeriet Naturstyrelsen, 1993. URL `https://naturstyrelsen.dk/media/nst/Attachments/RPT026.pdf`.

I. Aspen Technology. Aspen plus user guide, 2000. URL `https://web.ist.utl.pt/ist11038/acad/Aspen/AspUserGuide10.pdf`.

ATSDR. Toxicological profile for benzene, 2007. URL `https://wwwn.cdc.gov/TSP/ToxProfiles/ToxProfiles.aspx?id=40&tid=14`.

A. Benato, A. Macor, and A. Rossetti. Biogas engine emissions: Standards and on-site measurements. *Energy Procedia*, 126( ):398–405, 2017. doi:https://doi.org/10.1016/j.egypro.2017.08.278.

M. Bertau, H. Offermanns, L. Plass, F. Schmidt, and H.-J. Wernicke. *Methanol: The Basic Chemical and Energy Feedstock of the Future*, volume Springer, edition, 2014. ISBN 978-3-642-39708-0.

S. Brynolf, M. Taljegard, M. Grahn, and J. Hansson. Electrofuels for the transport sector: A review of production costs. *Renewable and Sustainable Energy Reviews*, 81(2):1887–1905, 2018. doi:https://doi.org/10.1016/j.rser.2017.05.288.

M. Bui, C. Adjiman, A. Bardow, E. Anthony, A. Boston, S. Brown, P. Fennell, S. Fuss, A. Galindo, and L. Hackett. Carbon capture and storage (ccs): the way forward. *Energy & Environmental Science*, (5): , 2018. doi:https://doi.org/10.1039/c7ee02342a.

K. M. V. Bussche and G. F. Froment. A steady-state kinetic model for methanol synthesis and the water gas shift reaction on a commercial cu/zno/al2o3 catalyst. *Journal of catalysis*, 161(0156):1–10, 1996. doi:-.

A. Z. C. van Leeuwen. Innovative large-scale energy storage technologies and power-to-gas concepts after optimisation, 2018. URL `https://www.storeandgo.info/fileadmin/downloads/deliverables_2019/20190801-STOREandGO-D8.3-RUG-Report_on_the_costs_involved_with_PtG_technologies_and_their_potentials_across_the_EU.pdf`.

CatCost. Catcost spreadsheet (version 1.0.4), 2020. URL `https://catcost.chemcatbio.org/documentation?fbclid=IwAR1OA4XxgSOMVaTiCi5u8_750p8rHcvkAOlroKvrYTkxm292J6gQeletYCQ`.

ChemicalBook. Cas database list, 2021. URL `https://www.chemicalbook.com/Price/1-2-4-Trimethylbenzene.htm`.

A. Chen, F. Crowley, J. Lym, and P. Sanchez. Production of btx from ethane, 2015. URL `https://repository.upenn.edu/cbe_sdr/73/`.

G. Chen, T. Cai, K. Chaung, and A. Afacan. Foaming effect on random packing performance. *Chemical Engineering Research and Design*, 85(2):278–282, 2007. doi:https://doi.org/10.1205/cherd06095.

K. T. Chuang and K. Nandakumar. Tray column: Design, 2000. URL `https://hobbybrennen.ch/download/file.php?id=1818`.

CleanEnergyReviews. Most efficient solar panels, 2021. URL `https://www.cleanenergyreviews.info/blog/most-efficient-solar-panels`.

A. Coker. *Ludwig's Applied Process Design for Chemical and Petrochemical Plants*, volume 1. Gulf Professional Publishing, 4 edition, 2007. ISBN 978-0-7506-7766-0.

E. Commission. Demineralised water production from river water using membrane separation technology, 2000. URL `https://webgate.ec.europa.eu/life/publicWebsite/project/details/1306`.

C. Corsaro, F. Mallamace, S. Vasi, S. Chen, H. E. Stanley, and D. Mallamace. Contrasting microscopic interactions determine the properties of water/methanol solutions. *Frontiers of Physics*, 13( ): , 2018. doi:10.1007/s11467-017-0685-7.

C. Cui, X. Li, H. Sui, and J. Sun. Optimization of coal-based methanol distillation scheme using process superstructure method to maximize energy efficiency. *Energy*, 119( ):110–120, 2017a. doi:https://doi.org/10.1016/j.energy.2016.12.065.

C. Cui, J. Sun, and X. Li. A hybrid design combining double-effect thermal integration and heat pump to the methanol distillation process for improving energy efficiency. *Chemical Engineering and Processing: Process Intensification*, 119( ):81–92, 2017b. doi:https://doi.org/10.1016/j.cep.2017.06.003.

C. Cui, S. Liu, and J. Sun. Optimal selection of operating pressure for distillation columns. *Chemical Engineering Research and Design*, 137( ):291–307, 2018. doi:https://doi.org/10.1016/j.cherd.2018.07.0281.

F. Dalena, A. Senatore, A. Marino, A. Gordano, M. Basile, and A. Basile. *Methanol*, volume Elsevier, edition, 2017. ISBN 978-0-444-63903-5.

F. Dalena, A. Senatore, M. Basile, S. Knani, A. Basile, and A. Lulianelli. Advances in methanol production and utilization, with particular emphasis toward hydrogen generation via membrane reactor technology. *Multidisciplinary Digital Publishing Institute*, 8 (98): , 2018. doi:https://doi.org/10.3390/membranes8040098.

Danish Meteorological Institute. *Vejrarkiv*. `https://www.dmi.dk/vejrarkiv/`, 2020. Seen: 10/02-2021.

Dansk Fjernvarme. *Solvarme*. `http://www.solvarmedata.dk/`, 2020. Seen: 10/02-2021.

J. Davis and G. Rochelle. Thermal degradation of monoethanolamine at stripper conditions. *Energy Procedia*, 1(1):327–333, 2009. doi:https://doi.org/10.1016/j.egypro.2009.01.045.

W. Denmark. Antal vindmøller og kapacitet, 2021. URL `https://winddenmark.dk/tal-fakta/fakta-om-vind-danmark/antal-vindmoeller-kapacitet`.

S. Dinkin. Increasing the profit ratio, 2016. URL `https://www.thespacereview.com/article/2893/1#:~:text=Liquid%20methane%20costs%20about%20%241.35,which%20fuel%20will%20be%20cheaper`.

C. Dorris, E. Lu, S. Park, and F. Toro. High-purity oxygen production using mixed ionic-electronic conduction sorbents, 2016. URL `https://repository.upenn.edu/cgi/viewcontent.cgi?article=1080&context=cbe_sdr`.

DR.DK. *Danske CO2-giganter øger udslip, men slipper for at betale klima-afgifter*. `https://www.dr.dk/nyheder/penge/danske-co2-giganter-oeger-udslip-men-slipper-betale-klima-afgifter`, 2020. Seen: 11/02-2021.

DrivKraftDanmark. Biobrændstoffer, 2021. URL https://www.drivkraftdanmark.dk/priser/biobraendstoffer/.

D. J. Durbin and C. Malardier-Jugroot. Review of hydrogen storage techniques for on board vehicle applications. *International Journal of Hydrogen Energy*, 38(34):14595–14617, 2013. doi:https://doi.org/10.1016/j.ijhydene.2013.07.058.

M. Duss and R. Taylor. Predict distillation tray efficiency, 2018. URL https://www.aiche.org/resources/publications/cep/2018/july/predict-distillation-tray-efficiency.

Echemi. Propylene china domestic price, 2021a. URL https://www.echemi.com/productsInformation/pid_Seven1855-propylene.html.

Echemi. Benzene china domestic price, 2021b. URL https://www.echemi.com/productsInformation/pid_Seven2868-benzene.html.

Echemi. Toluene china domestic price, 2021c. URL https://www.echemi.com/productsInformation/temppid160704000607-toluene.html.

Echemi. Xylene china domestic price, 2021d. URL https://www.echemi.com/productsInformation/pd1707041010-xylene.html.

Echemi. Methanol reagent china domestic price, 2021e. URL https://www.echemi.com/productsInformation/pd20150901274-methanol-reagent.html.

Echemi. Ethanolamine china domestic price, 2021f. URL https://www.echemi.com/productsInformation/pid_Seven5556-ethanolamine.html.

Egineeringtoolbox.com. Water - heat of vaporization, 2010. URL https://www.engineeringtoolbox.com/water-properties-d_1573.html.

Egineeringtoolbox.com. Methanol - thermophysical properties, 2018. URL https://www.engineeringtoolbox.com/methanol-methyl-alcohol-properties-CH3OH-d_2031.html.

eMolecules. -, 2021. URL https://orderbb.emolecules.com/search/#?query=95-93-2&system-type=BB&p=1.

EnergiNet. Energiværker: Put vind i brændstoftanken, 2018. URL https://energinet.dk/Om-os/Historier-fra-Synergi/Energivaerker-put-vind-i-braendstoftanken.

EnergiNet. Ptx in denmark before 2030, 2019. URL https://energinet.dk/-/media/8BF0CD597E1A457C8E9711B50EC2782A.PDF.

EnergiStyrelsen. Årlig energistatistik, 2020. URL https://ens.dk/service/statistik-data-noegletal-og-kort/maanedlig-og-aarlig-energistatistik.

Energistyrelsen. Det betaler sig at udnytte overskudsvarme internt, 2021a. URL https://sparenergi.dk/offentlig/produktion/overskudsvarme/om-overskudsvarme.

Energistyrelsen. Elprisstatistik andet halvår 2020, 2021b. URL https://ens.dk/sites/ens.dk/files/Statistik/elprisnotat_2_halvaar_2020.pdf.

Energistyrelsen. Oversigts- og sammenligningsværktøj, 2021c. URL `https://ens.dk/service/statistik-data-noegletal-og-kort/priser-paa-el-og-gas`.

M. Errico, C. Madeddu, D. Pinna, and R. Baratti. Model calibration for the carbon dioxide-amine absorption system. *Applied Energy*, 183( ):958–968, 2016. doi:https://doi.org/10.1016/j.apenergy.2016.09.036.

W. Europe. Environment & planing, 2020. URL `https://windeurope.org/policy/topics/environment-planning/`.

eurostat. Energy for transport: 8% from renewable sources, 2020. URL `https://ec.europa.eu/eurostat/web/products-eurostat-news/-/ddn-20200123-2`.

eurostat. Electricity prices for non-household consumers, 2021. URL `https://appsso.eurostat.ec.europa.eu/nui/show.do?dataset=nrg_pc_205&lang=en`.

FederalReserveBankOfDallas. Energy indicators, 2020. URL `https://www.dallasfed.org/research/energy/indicators/2020/en2002.aspx`.

FischerScientific. Isohexane, contains <5% n-hexane, certified ar for analysis, 2021. URL `https://www.fishersci.nl/shop/products/isohexane-5-n-hexane-certified-ar-analysis-4/p-7073060`.

H. S. Fogler. *Elements of Chemical Reaction Engineering*. Pearson Education, 5 edition, 2016. ISBN 9780133887518.

C. for Disease Control and Prevention. Facts about btx, 2021. URL `https://emergency.cdc.gov/agent/benzene/basics/facts.asp`.

D. Forsyning. Afkøling, 2020. URL `https://dinforsyning.dk/da-dk/varme/afk%C3%B8ling`.

FRED. Producer price index by industry: Industrial gas manufacturing: Oxygen, 2021. URL `https://fred.stlouisfed.org/series/PCU325120325120A`.

S. Freguia. Modeling of co2 removal from flue gases with monoethanolamine, 2002. URL `https://www.researchgate.net/publication/237052975_Modeling_of_CO2_Removal_from_Flue_Gas_with_Monoethanolamine`.

A. García, J. Loría, A. Marín, and Y. López. Short-cut methods for multicomponent batch distillation, 2017. URL `https://www.intechopen.com/books/distillation-innovative-applications-and-modeling/short-cut-methods-for-multicomponent-batch-distillation`.

M. Gardiner. Doe hydrogen and fuel cells program record, 2009. URL `https://www.hydrogen.energy.gov/pdfs/9013_energy_requirements_for_hydrogen_gas_compression.pdf`.

A. Gaurav, F. Ng, and G. Rempel. A new green process for biodiesel production from waste oils via catalytic distillation using a solid acid catalyst – modeling, economic and environmental analysis. *Green Energy & Environment*, 1(1):62–74, 2016. doi:https://doi.org/10.1016/j.gee.2016.05.003.

Gelsenchem. Historical methanol pricing, 2021. URL `https://www.gelsenchem.de/en/historical-methanol-pricing/`.

Geostyrelsen. Matrikelkort, 2021. URL `https://kort.matrikel.dk/spatialmap?fbclid=IwAR2m1CwI_uHuatT2D3sevMRicr9ZjqB3BjHWTLwuF3EIxYDDv7fmfjCKKjQ`.

M. Ghanbari, M. Ahmadi, and A. Lashanizadegan. A comparison between peng-robinson and soave-redlich-kwong cubic equations of state from modification perspective. *Cryogenics*, 84(1):13–19, 2017. doi:https://doi.org/10.1016/j.cryogenics.2017.04.001.

GlobalPetrolPrices. Methane prices, 2021. URL `https://www.globalpetrolprices.com/methane_prices/#:~:text=Methane%20prices%2C%2026%2DApr%2D,0.79%20U.S.%20Dollar%20per%20liter`.

GlobalSources. Qingdao eastchem inc., normal pentane price, 2021a. URL `https://www.globalsources.com/si/AS/Qingdao-Eastchem/6008835305510/pdtl/Normal-Pentane-Price-109-66-0/1139998874.htm`.

GlobalSources. Liangxin petrochemical technology development co. ltd, 2021b. URL `https://www.globalsources.com/si/AS/Liangxin-Petrochemical/6008843210595/pdtl/isohexane/1045127099.htm?AGGType=pure`.

Q. Gong, T. Fang, Y. Xie, R. Zhang, M. Liu, F. Barzagli, J. Li, Z. Hu, and Z. Zhu. High-efficiency conversion of methanol to btx aromatics over a zn-modified nanosheet-hzsm-5 zeolite. *Industrial & Engineering CHemistry Research*, 64(4):1633–1641, 2021. doi:https://doi.org/10.1021/acs.iecr.0c06342.

Green Hydrogen Systems. *First eMethanol plant in Denmark produces liquid electricity*. `https://greenhydrogen.dk/1235-2/`, 2020. Seen: 10/02-2021.

GreenLab. *GreenLab to be catalyst for global P2X market*. `https://www.greenlab.dk/knowledge/greenlab-to-be-catalyst-for-global-energy-market-within-p2x/`, 2019. Seen: 10/02-2021.

GreenLab. *How CO2 is turned into green fuel*. `https://www.greenlab.dk/knowledge/reintegrate-makes-green-methanol/`, 2020. Seen: 10/02-2021.

GreenLab. Greenlab - mainpage, 2021. URL `https://www.greenlab.dk/`.

GreenLab Skive Biogas Aps. *Anlægget*. `https://greenlabskivebiogas.dk/anlaegget/`, 2021. Seen: 10/02-2021.

I. Halvorsen. *Minimum Energy Requirements in Complex Distillation Arrangements*, volume Norwegian University of Science and Technology, edition, 2001. ISBN 82-471-5304-1.

J. Hannon, L. Lynd, O. Andrade, P. Benavides, G. Beckham, M. Biddy, N. Brown, M. Chagas, B. Davison, T. Foust, T. Junqueira, M. Laser, Z. Li, T. Richard, L. Tao, G. Tuskan, M. Wang, J. Woods, and C. Wyman. Technoeconomic and life-cycle analysis of single-step catalytic conversion of wet ethanol into fungible fuel blendstocks. *Proceedings of the National Academy of Sciences*, 117(23):–, 2019. doi:http://dx.doi.org/10.1073/pnas.1821684116.

J. R. Hannon, L. R. Lynd, O. Andrade, P. T. Benavides, G. T. Beckham, M. J. Biddy, N. Brown, M. F. Chagas, B. H. Davison, T. Foust, T. L. Junqueira, M. S. Laser, Z. Li, T. R. L. Tao, G. A. Tuskan, M. Wang, W. Woods, and C. E. Wyman. Technoeconomic and life-cycle analysis of single-step catalytic conversion of wet ethanol into fungible fuel blendstocks. *PNAS*, 117(23):12576–12583, 2020. doi:https://doi.org/10.1073/pnas.1821684116.

J. P. G. Hernandez. Extractive distillation with ionic liquids as solvents : selection and conceptual process design, 2013. URL `https://doi.org/10.6100/IR751728`.

C. Hobson and C. Márquez. Renewable methanol report. Technical report, Methanol Institute, 2018. URL `https://www.methanol.org/wp-content/uploads/2019/01/MethanolReport.pdf`.

S. E. Hosseini and M. A. Wahid. Hydrogen production from renewable and sustainable energy resources: Promising green energy carrier for clean development. *Renewable and Sustainable Energy Reviews*, 57:850–866, 2016. doi:https://doi.org/10.1016/j.rser.2015.12.112.

T. Husseini. Transporting oil and gas: the world's longest pipelines, 2018. URL `https://www.offshore-technology.com/features/worlds-longest-pipelines/`.

H. Ibrahim. Design of fractionation columns, 2014. URL `https://www.intechopen.com/books/matlab-applications-for-the-practical-engineer/design-of-fractionation-columns`.

ICIS. Methyl tertiary butyl ether (mtbe) uses and market data, 2010. URL `https://www.icis.com/explore/resources/news/2007/11/05/9076054/methyl-tertiary-butyl-ether-mtbe-uses-and-market-data/`.

IHS. Global propylene market, 2014. URL `http://cdn.ihs.com/www/pdf/asia-chem-conf/Carr.pdf`.

Intratec. Monoethanolamine price chart sample, 2007. URL `https://www.intratec.us/chemical-markets/monoethanolamine-price`.

S. Jackson and E. Brodal. A comparison of the energy consumption for co2 compression process alternatives. *IOP Conference Series: Earth and Environmental Science*, 167( ): , 2018. doi:https://doi.org/10.1088/1755-1315/167/1/012031.

J. K. Kaldellis, M. Kapsali, and K. A. Kavadias. Temperature and wind speed impact on the efficiency of pv installations. experience obtained from outdoor measurements in greece. *Renewable Energy*, 66( ):612–624, 2014. doi:https://doi.org/10.1016/j.renene.2013.12.041.

S. Klein and G. Nellis. *Thermodynamics*, volume Cambridge University Press, 3 edition, 2017. ISBN 978-0-521-19570-6.

D. Klenert, L. Mattauch, E. Combet, O. Edenhofer, C. Hepburn, R. Rafaty, and N. Stern. Making carbon pricing work for citizens. *nature climate change*, 8:669–677, 2018. doi:https://doi.org/10.1038/s41558-018-0201-2.

A. Kommune. Lokalplan 5-9-101. Technical report, Aalborg Kommune, 2011. URL `http://apps.aalborgkommune.dk/images/teknisk/PLANBYG/lokplan/05/5-9-101.pdf`.

A. Kommune. Kommuneplan, 2021a. URL `http://www.aalborgkommuneplan.dk/retningslinier/14_teknisk_forsyning/142/1426.aspx`.

A. Kommune. Kommuneplan, 2021b. URL `http://www.aalborgkommuneplan.dk/retningslinier/14_teknisk_forsyning/142/1422.aspx`.

J. Labarta. Resume of the extension of the ponchon and savarit method for designing ternary rectification columns, 2001. URL `https://www.researchgate.net/publication/279480162_Resume_of_the_extension_of_the_Ponchon_and_Savarit_method_for_designing_ternary_rectification_columns`.

A. Lassauce, P. Alix, L. Raynal, A. Royon-Lebeaud, and Y. Haroun. Performance characteristics of various types of mellapak packings (productivity, pressure differential, and deficiency). *Chemical and Petroleum Engineering*, 30(-):118–125, 1994. doi:https://doi.org/10.1007/BF01147885.

A. Lassauce, P. Alix, L. Raynal, A. Royon-Lebeaud, and Y. Haroun. Pressure drop, capacity and mass transfer area requirements for post-combustion carbon capture by solvents. *Oil & Gas Science and Technology - Revue d'IFP Energies nouvelles*, 69(6):1021–1034, 2014. doi:https://doi.org/10.2516/ogst/2013154.

A. Laude, O. Ricci, G. Bureau, J. Royer-Adnot, and A. Fabbri. Co2 capture and storage from a bioethanol plant: Carbon and energy footprint and economic assessment. *International Journal of Greenhouse Gas Control*, 5(5):1220–1231, 2011. doi:https://doi.org/10.1016/j.ijggc.2011.06.004.

D. Y. C. Leung, G. Caramanna, and M. M. Maroto-Valer. An overview of current status of carbon dioxide capture and storage technologies. *Renewable and Sustainable Energy Reviews*, 39( ):426–443, 2014. doi:https://doi.org/10.1016/j.rser.2014.07.093.

Z. Li, A. W. Lepore, M. F. Salazar, G. S. Foo, B. H. Davison, Z. Wu, and C. K. Narula. Selective conversion of bio-derived ethanol to renewable btx over ga-zsm-5. *Royal Society of Chemistry*, 19( ):4189–4458, 2017. doi:https://doi.org/10.1039/c7gc01188a.

LindeGas. Propylene, 2020. URL `https://www.linde-gas.com/en/products_and_supply/gases_fuel/propylene.html`.

Linkedin. I/s reno-nord, 2021. URL `https://www.linkedin.com/company/i-s-reno-nord`.

W. Liu, H. Zuo, J. Wang, Q. Xue, B. Ren, and F. Yang. The production and application of hydrogen in steel industry. *International Journal of Hydrogen Energy*, ( ): , 2021. doi:https://doi.org/10.1016/j.ijhydene.2020.12.123.

J. Lunsford. Catalytic conversion of methane to more useful chemicals and fuels: a challenge for the 21st century. *Catalysts Today*, 63(2-4):165–174, 2000. doi:https://doi.org/10.1016/S0920-5861(00)00456-9.

W. Luyben. Distillation column pressure selection. *Separation and Purification Technology*, 168( ):62–67, 2016. doi:https://doi.org/10.1016/j.seppur.2016.05.015.

C. Madeddu, M. Errico, and R. B. G. Barker. *CO2 Capture by Reactive Absorption-Stripping Modeling, Analysis and Design*, volume 1. Springer, 1 edition, 2019. ISBN 978-3-030-04578-4.

S. S. Makridis. Chapter 1 - hydrogen storage and compression, 2016. URL `https://arxiv.org/pdf/1702.06015`.

A. Mamudu, E. Okonkwo, S. Okocha, E. Okoro, F. Elehinafe, and K. Igwilo. The design of an integrated crude oil distillation column with submerged combustion technology. *The Open Chemical Engineering Journal*, 13:7–22, 2019. doi:http://dx.doi.org/10.2174/1874123101912010007.

W. Mathis. Toomuch green hydrogen in europe could add cost for decades, 2020. URL `https://www.bloomberg.com/news/articles/2020-09-04/too-much-green-hydrogen-in-europe-could-inflate-cost-for-decades`.

W. McCabe, J. Smith, and P. Harriott. *Unit Operations of Chemical Engineering*, volume McGraw-Hill Book Co., 5 edition, 1993. ISBN 0-07-112738-0.

Methanex. Methanex posts regional contract methanol prices for north america, europe and asia., 2021. URL `https://www.methanex.com/our-business/pricing`.

methanol.org. M15 methanol gasoline blends, 2014. URL `http://methanolfuels.org/wp-content/uploads/2013/10/M15-Methanol-Gasoline-Blends-Fact-Sheet.pdf`.

methanol.org. China: The leader in methanol transportation, 2020. URL `https://www.methanol.org/wp-content/uploads/2020/04/China-Methanol-Fact-Sheet-1.pdf`.

R. Mihail, S. Straja, G. Maria, G. Musca, and G. POP. A kinetic model for methanol conversion to hydrocarbons. *Chemical Engineering Science*, 38(9):1581–1591, 1983. doi:https://doi.org/10.1016/0009-2509(83)80094-3.

M. Mikulski. Public final report-methanol as an alternative fuel for vessels, 2018. URL `http://dx.doi.org/10.13140/RG.2.2.29463.11686`.

S. Miroshnichenko and J. Vrabec. Excess properties of non-ideal binary mixtures containing water, methanol and ethanol by molecular simulation. *Journal of Molecular Liquids*, 212( ):90–95, 2015. doi:https://doi.org/10.1016/j.molliq.2015.08.058.

MMSA-MethanolInstitute. Methanol price and supply/demand, 2021. URL `https://www.methanol.org/methanol-price-supply-demand/`.

L. Na, C. Like, Y. Tianhui, L. Minzhe, and L. Dianhua. Simulation of the methanol to aromatics process with annual output of 70000tons. *Natural Gas Chemical Industry*, 43(6): 90–95, 2018. doi:-.

Nasdaq. Mont belvieu normal butane, 2021. URL `https://www.nasdaq.com/market-activity/commodities/ad0:nmx`.

M. Naturstyrelsen. Vandplan 2009 – 2015. limfjorden. Technical report, Naturstyrelsen, 2011. URL `https://mst.dk/media/129570/12-limfjorden-_med_forside.pdf`.

Neutrium.net. Mccabe-thiele plot, 2017. URL `https://neutrium.net/unit-operations/distillation/mccabe-thiele-plot/`.

Neutrium.net. Distillation tray efficiency, 2018. URL `https://neutrium.net/equipment/distillation-tray-efficiency/`.

H. C. Nikolajsen. Miljøredegørelsen 2019. Technical report, Aalborg Portland A/S, 2019. URL `https://www.aalborgportland.dk/baeredygtighed/miljoeredegoerelsen/`.

T. Nittaya, P. L. Douglas, E. Croiset, and L. A. Ricardez-Sandoval. Dynamic modeling and evaluation of an industrial-scale co2 capture plant using monoethanolamine absorption processes. *Industrial & Engineering Chemistry Research*, 53(28):11411–11426, 2014. doi:https://doi.org/10.1021/ie500190p.

C. Nordic. Jordtanke, 2021. URL `https://www.cghnordic.com/products/jordtanke/`.

NREL. Hydrogen production cost analysis, 2011. URL `https://www.nrel.gov/hydrogen/production-cost-analysis.html`.

OfficeOfEnergyEfficiency&RenewableEnergy. Doe technical targets for hydrogen production from electrolysis, 2010. URL `https://www.energy.gov/eere/fuelcells/doe-technical-targets-hydrogen-production-electrolysis`.

J. A. Okolie, B. R. Patra, A. Mukherjee, S. Nanda, A. K. Dalai, and J. A. Kozinski. Futuristic applications of hydrogen in energy, biorefining, aerospace, pharmaceuticals and metallurgy. *International Journal of Hydrogen Energy*, ( ):, 2021. doi:https://doi.org/10.1016/j.ijhydene.2021.01.014.

M. Pedersen. Aalborg forsyning runder milepæl: Kæmpe 'sugerør' sænkes ned i kridtsø, 2021. URL `https://www.energy-supply.dk/article/view/786636/aalborg_forsyning_runder_milepael_kaempe_sugeror_saenkes_ned_i_kridtso?rel=related`.

M. Pilling. Foaming in fractionation columns, 2015. URL `https://www.digitalrefining.com/article/1001169/foaming-in-fractionation-columns#.YIJwCZAzZhE`.

M. Pilling and B. Holden. Choosing trays and packings for distillation, 2009. URL `http://www.razifar.com/cariboost_files/Choosing_20Trays_20and_20packings_20for_20distillation.pdf`.

PwC.dk. Oversigter over godtgørelse og satser m.m., 2020. URL `https://www.pwc.dk/da/afgiftsvejledningen/godtgorelse-satser.html#content-free-1-990a-par_tabsnewhome6`.

M. Rashied, M. K. A. Mesfer, H. Naseem, and M. Danish. Hydrogen production by water electrolysis: A review of alkaline water electrolysis, pem water electrolysis and high temperature water electrolysis. *International Journal of Engineering and Advanced Technology (IJEAT)*, 4(3):80–93, 2015. doi:.

T. A. H. Ratlamwala, M. A. Gadalla, and I. Dincer. Performance assessment of an integrated pv/t and triple effect cooling system for hydrogen and cooling production. *International Journal of Hydrogen Energy*, 36(17):11282–11291, 2011. doi:https://doi.org/10.1016/j.ijhydene.2010.11.121.

R. Ravi. A rigorous analysis of mccabe-thiele assumptions and their consequences: Critical role of parallel enthalpy lines. *Chemical Engineering Communications*, 193(1):55–68, 2007. doi:https://doi-org.zorac.aub.aau.dk/10.1080/009864490923493.

X. Ren, S. Zhao, J.Cao, X. Zhao, X. Feng, Y. L. i, J. Zhang, Z. Wang, and H. Bai. Effect of coal ranks on light aromatics production during reforming of pyrolysis volatiles over hzsm-5 under ar and h2-assisted atmospheres. *Journal of Analytical and Applied Pyrolysis*, 152( ):104958, 2020. doi:https://doi.org/10.1016/j.jaap.2020.104958.

RenoNord. *MILJØREDEGØRELSE 2019*. `https://renonord.dk/media/aarsrapporter/renonord_miljoeredegoerelse_2019.pdf`, 2019. Seen: 12/02-2021.

RoyalGlobalEnergy. Methanol, 2020. URL `https://royalglobalenergy.com/service/methanol/`.

S. Dyck-Madsen. *Stor klimagevinst ved opsamling af CO2 fra affaldsforbrænding*. `https://concito.dk/concito-bloggen/stor-klimagevinst-ved-opsamling-co2-fra-affaldsforbraending`, 2020. Seen: 11/02-2021.

E. Scientific. Kvalitetskrav til drikkevand, 2003. URL `https://www.granly-vand.dk/info/guide-drikkevand_lav.pdf`.

J. Seader, E. Henley, and D. Roper. *Separation Process Principles - Chemical and Biochemical Operations*, volume -. John Wiley & Sons, Inc, 3 edition, 2011. ISBN 978-0-470-48183-7.

SeperationTechnology.com. Distillation column tray selection & sizing – 1, 2012. URL `http://seperationtechnology.com/distillation-column-tray-selection-1/`.

D. Sharma, R. Mehra, and B. Raj. Comparative analysis of photovoltaic technologies for high efficiency solar cell design. *Superlattices and Microstructures*, 153:106861, 2021. doi:https://doi.org/10.1016/j.spmi.2021.106861.

L. Sorsamäki and M. Nappa. Design and selection of separation processes. Technical report, Technical Research Centre of Finland, 2015. URL `https://www.vttresearch.com/sites/default/files/julkaisut/muut/2015/VTT-R-06143-15.pdf`.

S&Pglobal. Platts global benzene price index, 2021. URL `https://www.spglobal.com/platts/en/our-methodology/price-assessments/petrochemicals/pgpi-benzene`.

State of Green. *During COP25, Denmark passes Climate Act with a 70 per cent reduction target*. `https://stateofgreen.com/en/partners/state-of-green/news/during-cop25-denmark-passes-climate-act-with-a-70-per-cent-reduction-target/`, 2019. Seen: 11/02-2021.

J. Stichlmair. Distillation, 2. equipment. *ULLMANN'S Encyclopedia of Industrial Chemistry*, 11, 2010. doi:https://doi.org/10.1002/14356007.o08_o01.

Sulzer. Structured packings for distillation, absorption and reactive distillation, 2021a. URL `https://www.sulzer.com/-/media/files/products/separation-technology/liquid_liquid_extraction/brochures/structured_packings.ashx`.

Sulzer. Structured packings energy-efficient, innovative and profitable, 2021b. URL `https://www.sulzer.com/-/media/files/products/separation-technology/distillation-and-absorption/brochures/structured_packings.ashx?la=en`.

SunSirs. China toluene spot price, 2021a. URL `http://www.sunsirs.com/uk/prodetail-177.html`.

SunSirs. Chemical spot price:xylene, 2021b. URL `http://www.sunsirs.com/commodity-price/petail-Xylene-1222.html`.

W. A. Sweeney and P. F. Bryan. Kirk-othmer encyclopedia of chemical technology, btx processing. *ECT*, 4(3):264–277, 2000. doi:https://doi-org.zorac.aub.aau.dk/10.1002/0471238961.02202419230505.a01.

M. Sánchez, E. Amores, L. Rodrígues, and C. Clemente-Jul. Semi-empirical model and experimental validation for the performance evaluation of a 15 kw alkaline water electrolyzer. *International Journal of Hydrogen Energy*, 43(45):20332–20345, 2018. doi:https://doi.org/10.1016/j.ijhydene.2018.09.029.

S. M. Sørensen. sus@renonord.dk, renonord, co2 emission, 2020.

S. Taqvi, L. Tufa, and S. Muhadozir. Optimization and dynamics of distillation column using aspen plus. *Procedia Engineering*, 148( ):978–984, 2016. doi:https://doi.org/10.1016/j.proeng.2016.06.484.

G. Towler and R. Sinnott. *Chemical Engineering Design: Principles, practice and economics of plants and process design.*, volume -. Elsevier, 1 edition, 2008. ISBN 978-0-7506-8423-1.

F. Ullmann, Y. Y. W. GERHARTZ, F. Campbell, R. Pfefferkorn, and J. Rounsaville. *ULLMANN'S Encyclopedia of Industrial Chemistry*, volume Wiley-VCH, 7 edition, 2011. ISBN 9783527306732.

U.S.-E.I.A. Natural gas weekly update, 2019. URL `https://www.eia.gov/naturalgas/weekly/archivenew_ngwu/2019/02_14/`.

U.S.EnergyInformationAdministration. Prices for hydrocarbon gas liquids, 2020. URL `https://www.eia.gov/energyexplained/hydrocarbon-gas-liquids/prices-for-hydrocarbon-gas-liquids.php`.

A. Veawab, A. Aroonwilas, and P. Tontiwachwuthikul. Co2 absorption performance of aqueous alkanolamines in packed columns. *ACS Division of Fuel Chemistry, Preprints*, 47:49–50, 2002. URL `https://www.researchgate.net/publication/283837909_CO2_absorption_performance_of_aqueous_alkanolamines_in_packed_columns`.

Vestas. 4 mw platform, 2020. URL `https://www.vestas.com/en/products/4-mw-platform/v150-4_2_mw#!`

A. Viswanath, T. Ghosh, D. Prasad, N. Dutt, and K. Rani. *Viscosity of Liquids Theory, Estimation, Experiment, and Data.*, volume -. Springer, 1 edition, 2007. ISBN 978-1-4020-5482-2.

T. Wang, X. Tang, X. Huang, W. Qian, Y. Cui, X. Hui, W. Yang, and F. WEI. Conversion of methanol to aromatics in fluidized bed reactor. *Catalysts Today*, 233( ):8–13, 2014. doi:https://doi.org/10.1016/j.cattod.2014.02.007.

T. Wang, X. Tang, X. Huang, W. Qian, Y. Cui, X. Hui, W. Yang, and F. WEI. Deactivation kinetics of individual c6–c9 aromatics' generation from methanol over zn and p comodified hzsm-5. *Royal Society of Chemistry*, 9( ):22327, 2019. doi:https://doi.org/10.1039/c9ra02587a.

P. Wankat. *Separation Process Engineering: Includes Mass Transfer Analysis*, volume -. Prentice Hall, 3 edition, 2012. ISBN 978-0-13-138227-5.

T. Wilberforce, A. G. Olabi, E. T. Sayed, K. Elsaid, and M. A. Abdelkareem. Progess in carbon capture technologies. *Science of the Total Environment*, 761( ): , 2021. doi:https://doi.org/10.1016/j.scitotenv.2020.143203.

Wind Turbine Models. *Vestas V126-3.45*. `https://en.wind-turbine-models.com/turbines/1249-vestas-v126-3.45`, 2020. Seen: 10/02-2021.

K. Winther. Methanol as motor fuel. Technical report, Dansk Technological Institute, 2019. URL `http://danskbiomethanol.dk/Papers/Report%20DK.pdf`.

N. Yang, K. Chuang, A. Afacan, M. Resetarits, and M. Binkley. Improving the efficiency and capacity of methanol-water distillation trays. *Industrial & Engineering Chemistry Research*, 42(25):6601–6606, 2003. doi:https://doi.org/10.1021/ie030407n.

Ycharts. Mont belvieu propane spot price, 2021. URL `https://ycharts.com/indicators/mont_belvieu_propane_spot_price`.

J. Zhang, L. Zhang, H. Liu, A. Sun, R. Liu, and R. Liu. *Electrochemical Technologies for Energy Storage and Conversion*, volume Weinheim, Germany : Wiley-VCH, edition, 2011. ISBN 3-527-32869-6.

Appendix A

Acquired Results from the Sensitivity Analysis of Flash Distillation

T	MeOH_D	MeOH_B	$\text{H}_2\text{O}_\text{D}$	$\text{H}_2\text{O}_\text{B}$	MeOH_D	MeOH_B	Recovery
[°C]	$\left[\frac{\text{kg}}{\text{s}}\right]$				[wt%]		
72	0.00	0.65	0.00	0.35	0.00	65.00	0.00
73	0.07	0.58	0.01	0.34	86.64	63.17	10.38
74	0.20	0.45	0.04	0.31	85.04	58.81	30.88
75	0.30	0.35	0.06	0.29	83.39	54.54	46.50
76	0.38	0.27	0.09	0.26	81.71	50.41	58.61
77	0.44	0.21	0.11	0.24	79.97	46.43	68.12
78	0.49	0.16	0.14	0.21	78.17	42.64	75.68
79	0.53	0.12	0.17	0.18	76.31	39.06	81.76
80	0.56	0.09	0.19	0.16	74.36	35.68	86.71
81	0.59	0.06	0.23	0.12	72.34	32.50	90.79
82	0.61	0.04	0.26	0.09	70.21	29.53	94.18
83	0.63	0.02	0.30	0.05	67.98	26.76	97.02
84	0.65	0.00	0.35	0.00	65.00	0.00	100.00

Table A.1: Mass flow outputs from the flash distillation at different temperatures. The distillate is denoted D, whereas the bottom is denoted B. The weight fractions of the input is 65 wt% MeOH and 35 wt% H_2O.

T	$MeOH_D$	$MeOH_B$	H_2O_D	H_2O_B	$MeOH_D$	$MeOH_B$	Recovery
[°C]	$\left[\frac{kg}{s}\right]$				[wt%]		
73	0.00	0.60	0.00	0.40	0.00	60.00	0.00
74	0.04	0.56	0.01	0.39	85.04	58.81	6.43
75	0.16	0.44	0.03	0.37	83.39	54.54	26.29
76	0.25	0.35	0.06	0.34	81.71	50.41	41.74
77	0.32	0.28	0.08	0.32	79.97	46.43	53.92
78	0.38	0.22	0.11	0.29	78.17	42.64	63.65
79	0.43	0.17	0.13	0.27	76.31	39.06	71.51
80	0.47	0.13	0.16	0.24	74.36	35.68	77.92
81	0.50	0.10	0.19	0.21	72.34	32.50	83.22
82	0.53	0.07	0.22	0.18	70.21	29.53	87.64
83	0.55	0.05	0.26	0.14	67.98	26.76	91.36
84	0.57	0.03	0.30	0.10	65.64	24.17	94.52
85	0.58	0.02	0.34	0.06	63.16	21.76	97.23
86	0.60	0.00	0.40	0.00	60.00	0.00	100.00

Table A.2: Mass flow outputs from the flash distillation at different temperatures. The distillate is denoted D, whereas the bottom is denoted B. The weight fractions of the input is 60 wt% MeOH and 40 wt% H_2O.

Appendix B

Distillation Column Diameter

This appendix will present the procedure of calculating the diameter of the distillation column which distillates the MeOH-H_2O solution. The feed stream is shown in Table B.1.

Table B.1: Feed stream components.

Species	Weight fraction [%]	Mass flow [kg/s]
MeOH	63.94	2.27
H_2O	36.16	1.28

The following two specifications are applied for the mechanical designing of the column diameter. The MeOH purity of the distillate stream must be 99.85 wt % or 99.73 mol% and the molar reflux ratio is fixed to 1.08, which was gained from the process design.

The operational conditions throughout the distillation column is defined based on the boiling point of the MeOH and H_2O, as such it is assumed that the temperature at the top plate is the same as the saturation temperature of MeOH. The distillation column operates at 1.1 bar of which the saturation temperature of MeOH becomes 67.12 °C. Multiple component properties are required in the following calculations. These are shown in Table B.2.

Table B.2: Properties at top plate conditions, $T = 67.12\,^{\circ}\mathrm{C}$ and $P = 1.01\,\mathrm{bar}$.

Species	State	Property	Symbol	Value	Unit
MeOH	N/A	Molecular Weight	MW_{MeOH}	32	[kg/kmol]
H_2O	N/A	Molecular Weight	$MW_{\mathrm{H_2O}}$	18	[kg/kmol]
MeOH	Gas	Density	$\rho_{\mathrm{MeOH,g}}$	2.26	[kg/m^3]
MeOH	Liquid	Density	$\rho_{\mathrm{MeOH,l}}$	745.7	[kg/m^3]
H_2O	Gas	Density	$\rho_{\mathrm{H_2O,g}}$	0.70	[kg/m^3]
H_2O	Liquid	Density	$\rho_{\mathrm{H_2O,l}}$	979.40	[kg/m^3]
MeOH	Liquid	Surface tension	$\sigma_{\mathrm{MeOH,l}}$	1.87e-2	[N/m]
H_2O	Liquid	Surface tension	$\sigma_{\mathrm{MeOH,l}}$	6.50e-2	[N/m]
MeOH	Liquid	Viscosity	$\mu_{\mathrm{H_2O,l}}$	3.25e-4	[kg/(m · s)]
H_2O	Liquid	Viscosity	$\mu_{\mathrm{MeOH,l}}$	4.20e-4	[kg/(m · s)]

Firstly, the mass flow of the streams must be defined, however, the acquired reflux ratio from the McCabe-Thiele diagram in Section 4.2 is based on mole fraction, as such the mole flows of the streams are required to be defined. The mole flow of the distillate stream is determined by Eq. B.1

$$\dot{n}_{\mathrm{D}} = \frac{\dot{m}_{\mathrm{MeOH,feed}}}{MW_{\mathrm{MeOH}} \cdot 0.9973} = 0.07\,\mathrm{kmol/s} \tag{B.1}$$

where $\dot{n}$ is molar flow, the subscript D denotes the distillate stream, $\dot{m}$ is mass flow, MW is the molecular weight and 0.9973 is the molar fraction purity requirement. The mole flow of the vapour stream is determined based on the distillate stream and the reflux ratio as shown in Eq. B.2

$$\dot{n}_\mathrm{V} = \dot{n}_\mathrm{D} \cdot (1 + \mathrm{R}) = 0.15\,\mathrm{kmol/s} \tag{B.2}$$

where R is the reflux ratio and the subscript V denotes the vapour stream. The mole flow of the liquid stream is determined by subtracting the distillate stream from the vapour stream as shown in Eq. B.3

$$\dot{n}_\mathrm{L} = \dot{n}_\mathrm{V} - \dot{n}_\mathrm{D} = 0.08\,\mathrm{kmol/s} \tag{B.3}$$

where L denotes the liquid stream. The mass flow rate of the distillate stream is then determined by the composition of each component and their molecular weight as shown in Eq. B.4

$$\dot{m}_\mathrm{D} = \dot{n}_\mathrm{D} \cdot \mathrm{x}_\mathrm{MeOH,D} \cdot MW_\mathrm{MeOH} + \dot{n}_\mathrm{D} \cdot \mathrm{x}_\mathrm{H_2O,D} \cdot MW_\mathrm{H_2O} = 2.63\,\mathrm{kg/s} \tag{B.4}$$

where x is the molar fraction within the liquid. This procedure repeats for the liquid stream, however, the composition of this stream is unknown of which a sensitivity analysis is conducted in order to determine the influence of the composition on the resulting diameter. As such the MeOH composition of the liquid stream is varied between 0 wt % to 100 wt %. The following presents the calculations, when the liquid consists of 50 wt % of MeOH in the liquid stream. At first the equivalent molar fraction of MeOH is based on the weight fraction by Eq. B.5

$$\mathrm{x}_\mathrm{MeOH,L} = \frac{\mathrm{wt}_\mathrm{MeOH,l}/MW_\mathrm{MeOH}}{\mathrm{wt}_\mathrm{MeOH,l}/MW_\mathrm{MeOH} + \mathrm{wt}_\mathrm{H_2O,l}/MW_\mathrm{H_2O}} = 0.36 \tag{B.5}$$

where wt is the weight fraction and l denotes that the property is based on the specie being on liquid state. The molar fraction of H_2O is then determined by subtracting the molar fraction of MeOH, calculated in Eq. B.5, from unity. Then, the liquid mass flow is determined by Eq. B.6.

$$\dot{m}_\mathrm{L} = \dot{n}_\mathrm{L} \cdot \mathrm{x}_\mathrm{MeOH,L} \cdot MW_\mathrm{MeOH} + \dot{n}_\mathrm{L} \cdot \mathrm{x}_\mathrm{H_2O,L} \cdot MW_\mathrm{H_2O} = 1.76\,\mathrm{kg/s} \tag{B.6}$$

Finally, the vapour mass flow is calculated by adding the distillate- and liquid mass flow as shown in Eq. B.7.

$$\dot{m}_\mathrm{v} = \dot{m}_\mathrm{D} + \dot{m}_\mathrm{L} = 4.03\,\mathrm{kg/s} \tag{B.7}$$

The weight fraction of the MeOH in the vapour stream is determined by Eq. B.8.

$$\mathrm{wt}_\mathrm{MeOH,V} = \frac{\dot{m}_\mathrm{D} \cdot \mathrm{wt}_\mathrm{MeOH,D} + \dot{m}_\mathrm{L} \cdot \mathrm{wt}_\mathrm{MeOH,L}}{\dot{m}_\mathrm{V}} = 0.78 \tag{B.8}$$

The weight fraction of the H_2O in the vapour stream is then defined by subtracting the result of Eq. B.8 from unity. The density of both the liquid- and vapour stream is then determined by Eq. B.9 and B.10

$$\rho_\mathrm{L} = \rho_\mathrm{MeOH,l} \cdot \mathrm{wt}_\mathrm{MeOH,L} + \rho_\mathrm{H_2O,l} \cdot \mathrm{wt}_\mathrm{H_2O,L} = 862.55\,\mathrm{kg/m^3} \tag{B.9}$$

$$\rho_\mathrm{V} = \rho_\mathrm{MeOH,g} \cdot \mathrm{wt}_\mathrm{MeOH,V} + \rho_\mathrm{H_2O,g} \cdot \mathrm{wt}_\mathrm{H_2O,V} = 1.18\,\mathrm{kg/m^3} \tag{B.10}$$

where ρ is the density of the specie and g denotes that the property is based on the specie being on gaseous state. The estimation of column diameter for both plate column and packed column are determined by the maximum vapour velocity, however, the calculation of the maximum vapour velocity is different for the two cases. As such the column diameter is firstly determined by the procedure of the plate column, where the packed column is investigated afterwards.

The maximum vapour velocity for the plate column is calculated by Eq. B.11.

$$v_{\mathrm{max}} = C \cdot \sqrt{\frac{\rho_{\mathrm{L}} - \rho_{\mathrm{V}}}{\rho_{\mathrm{V}}}} \tag{B.11}$$

The capacity factor C is estimated by Eq. B.12.

$$C = \mathrm{F}_{\mathrm{ST}} \cdot \mathrm{F}_{\mathrm{F}} \cdot \mathrm{F}_{\mathrm{HA}} \cdot C_{\mathrm{F}} \tag{B.12}$$

where F_{ST} is the surface tension factor, F_{F} is the foaming factor, F_{HA} is the hole-to-active area factor and C_{F} is the Fair's capacity. The Fair's capacity is estimated by the Fair's correlation as shown in Figure B.1, where the value is determined by the liquid-vapour flow factor shown in Eq. B.13 and the plate spacing.

$$\mathrm{F}_{\mathrm{LV}} = \frac{\dot{m}_{\mathrm{L}}}{\dot{m}_{\mathrm{V}}} \cdot \sqrt{\frac{\rho_{\mathrm{V}}}{\rho_{\mathrm{L}}}} = 0.0162 \tag{B.13}$$

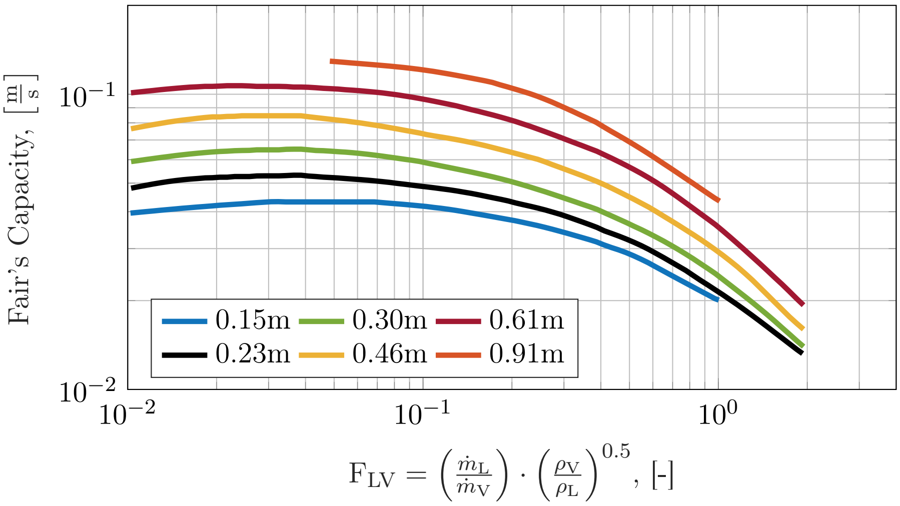

Figure B.1: Fair's capacity correlation for different plate spacing as function of the liquid-vapour flow factor, F_{LV}. Adapted from Stichlmair [2010].

A plate spacing of 0.46 m is chosen, in accordance with Section 2.5.3, from which the Fair's capacity becomes 0.08 m/s. The surface tension of the liquid stream is calculated by Eq. B.14, from which the surface tension factor (F_{ST}) can be determined by Eq. B.15.

$$\sigma_{\mathrm{L}} = \mathrm{x}_{\mathrm{MeOH}} \cdot \sigma_{\mathrm{MeOH}} + \mathrm{x}_{\mathrm{H_2O}} \cdot \sigma_{\mathrm{H_2O}} = 0.04\,\mathrm{N/m} \tag{B.14}$$

$$\mathrm{F}_{\mathrm{ST}} = \left(\frac{\sigma_{\mathrm{L}}}{0.02}\right)^{0.02} = 1.16\,\mathrm{N/m} \tag{B.15}$$

The foaming factor (F_{F}) is going to vary depending on the liquid composition. It is known from Section 2.5.3 that foam is not present if the MeOH concentration is either above 50 wt% or if the liquid is purely H_2O [Pilling, 2015]. However, within the range of

$0\,\% < \mathrm{wt}_{\mathrm{MeOH}} < 50\,\%$ it is unsure if foaming occurs and how significant it is. If foaming is present in the liquid, the foaming factor is between 0.5 to 0.75 depending on the amount of foam. As such it is a complicated endeavour to properly determine this factor without experimental data. As an estimate the foaming factor is set to 0.5 within the former mentioned range of the MeOH composition of $0\,\% < \mathrm{wt}_{\mathrm{MeOH}} < 50\,\%$. The remaining unknown in Eq. B.12 on the preceding page is (F_{HA}), which was defined to be 0.9 according to Section 2.5.3. Since all the unknowns in Eq. B.11 on the facing page are determined, the diameter of the distillation column can be determined, as shown in Eq. B.16.

$$D = \left(\frac{4 \cdot \dot{m}_{\mathrm{V}}}{\mathrm{f} \cdot \pi \cdot v_{\mathrm{max}} \cdot \left(1 - \frac{A_{\mathrm{d}}}{A_{\mathrm{tot}}}\right) \cdot \rho_{\mathrm{V}}} \right)^{0.5} \tag{B.16}$$

The remaining unknown in Eq. B.16 is the flooding factor f and the ratio $A_{\mathrm{d}}/A_{\mathrm{tot}}$. The flooding factor is set to 0.8 in accordance to Section 2.5.3 and $A_{\mathrm{d}}/A_{\mathrm{tot}}$ is determined by the following

$$\begin{array}{lll} A_{\mathrm{d}}/A_{\mathrm{tot}} = 0.1 & \text{for} & \mathrm{F}_{\mathrm{LV}} \leq 0.1 \\ A_{\mathrm{d}}/A_{\mathrm{tot}} = 0.1 + \frac{\mathrm{F}_{\mathrm{LV}} - 0.1}{9} & \text{for} & 0.1 < \mathrm{F}_{\mathrm{LV}} < 1.0 \\ A_{\mathrm{d}}/A_{\mathrm{tot}} = 0.2 & \text{for} & \mathrm{F}_{\mathrm{LV}} \geq 1.0 \end{array}$$

Since Eq. B.13 on the preceding page yielded approximately 0.02 the corresponding $A_{\mathrm{d}}/A_{\mathrm{tot}}$ becomes 0.1. Applying this values to Eq. B.16 the diameter becomes 1.60 m. This diameter was determined from a plate spacing of 0.46 m, which is suitable when the diameter of the distillation column is less than 1.50 m. Instead the plate spacing should be 0.60 m which is suited when the column diameter ranges from 1.50 m to 6.00 m. By applying the new value for plate spacing, the diameter of the plate column becomes 1.42 m. Similar to the tray column, the packed column will be based on a correlation.

The determination of maximum vapour velocity for packed column is estimated by Eq. B.17.

$$\dot{m}^{\star}_{\mathrm{max}} = \left(\frac{\mathrm{F}_{\mathrm{pack}} \cdot \rho_{\mathrm{V}} \cdot (\rho_{\mathrm{L}} - \rho_{\mathrm{V}})}{13.1 \cdot a_{\mathrm{p}} \cdot \left(\frac{\mu_{\mathrm{L}}}{\rho_{\mathrm{L}}}\right)^{0.1}} \right)^{0.5} \tag{B.17}$$

The unknowns in Eq. B.17 are the correlation factor ($\mathrm{F}_{\mathrm{pack}}$), the surface area per volume of packing (a_{p}) and the dynamic viscosity of the liquid (μ_{L}). The correlation factor is estimated by Figure B.2 on the next page to be 3.35 when a pressure drop of 0.8 kPa is applied and $\mathrm{F}_{\mathrm{LV}} = 0.0162$.

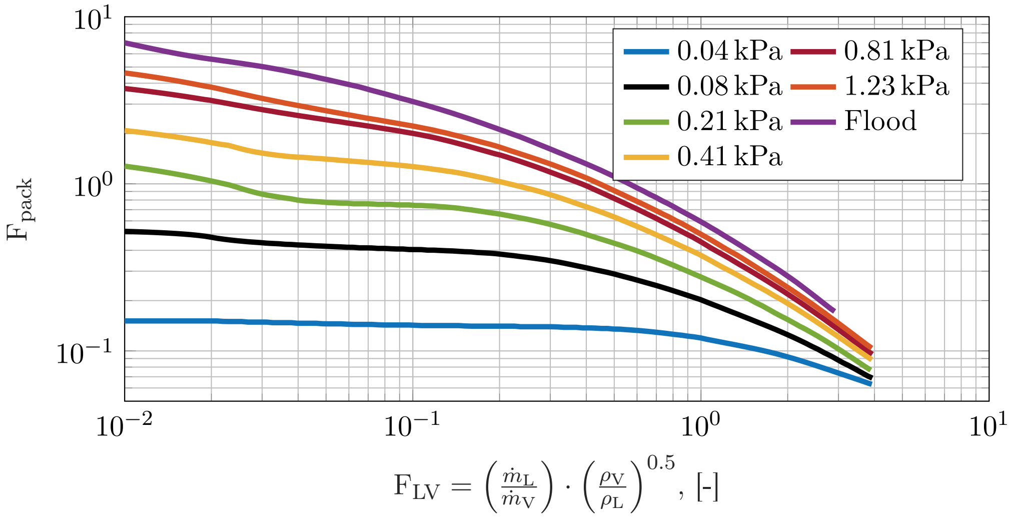

Figure B.2: Factor, $\mathrm{F_{pack}}$, at various flow parameter values F_{LV} and pressure drop curves. Adapted from Towler and Sinnott [2008]

The surface area per volume of packing (a_p) is determined by the chosen packing. According to Section 2.5.3 the packing is chosen to be Mellapak 250.Y, where the number denotes the (a_p) value. The dynamic viscosity of a mixture is known to be difficult to predict of which it is often based on experimental data at the operating conditions and composition Viswanath et al. [2007]. It is however often difficult to acquire correct experimental data from literature, since the operational conditions often differ from the actual system to the systems found in the literature, which is also the case for this study. In order to overcome this challenge, the dynamic viscosity of the binary MeOH-H_2O solution is based on literature data, where the data will be extrapolated to best possibly fit the operating temperature of approximately 67.12 °C. This is shown in Figure B.3 where the dynamic viscosity at temperatures of 25 °C, 30 °C, 35 °C, 40 °C and 50 °C versus the molar composition is acquired from literature. From this data the dynamic viscosity at 67.12 °C is estimated based on trend lines.

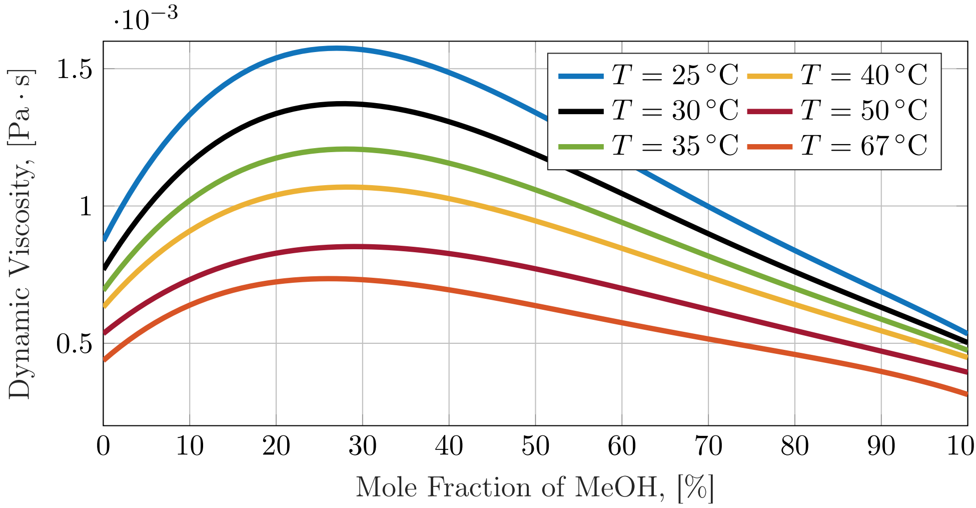

Figure B.3: Dynamic Viscosity versus MeOH molar fraction at different temperatures.

From Figure B.3, the dynamic viscosity is read to be 0.00637 Pa · s. The maximum vapour velocity, shown in Eq. B.17 on the preceding page is then calculated to be 2.06 kg/s. The diameter of the packed distillation column is determined by Eq. B.18.

$$D = \sqrt{\frac{4}{\pi} \cdot \frac{\dot{m}_V}{\dot{m}^{\star}_{\max}}} = 1.58\,\mathrm{m} \tag{B.18}$$

Appendix C

BTX Conversion Rates

Given the information by Na et al. [2018], an optimisation algorithm has been developed, in order to obtain similar results. From the optimisation algorithm the activity coefficients are determined as may be seen in Table C.1. The first activity coefficient (R1) corresponds to the first reaction given in Table 2.5 on page 37, R2 equal the second reaction, etc.

Table C.1: Activity coefficients for the presented study.

Activity	Value [-]	Activity	Value [-]	Activity	Value [-]
R1	2.0000	R6	1.0199	R11	0.5699
R2	2.8699	R7	1.0199	R12	0.1447
R3	1.0199	R8	0.5699	R13	0.4699
R4	1.0199	R9	0.5699	-	-
R5	1.0199	R10	0.5699	-	-

Furthermore, the temperature and pressure of the flash separator in the system have also been fitted in order to obtain similar conversion rates as Na et al. [2018]. This yielded a temperature and pressure of 32 °C and 4.2 bar, respectively.

The following four figures illustrate the conversion rates and gradients for the five lumped products, with an inlet flow composition equal to the one presented by Na et al. [2018]. Figure C.1, C.2, C.3 and C.4 represent the Aromatics, Alkanes, Light Gases and a combination of the Heavy component and Others, respectively.

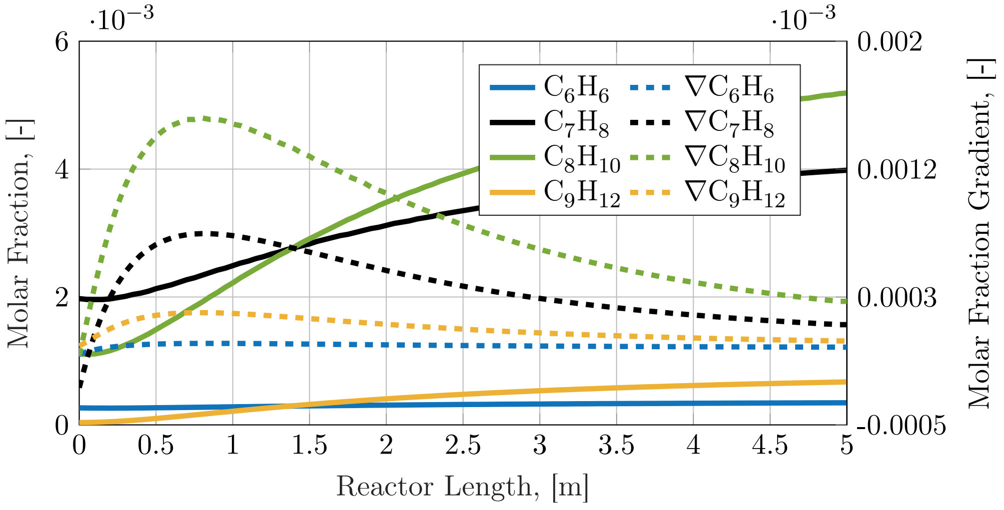

Figure C.1: Aromatics conversion as function of the reactor length and conversion gradient.

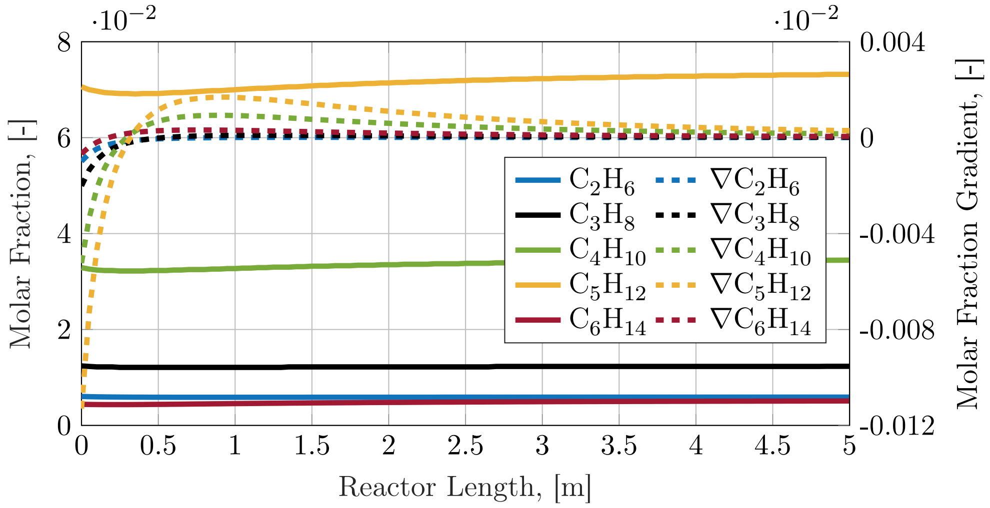

Figure C.2: Alkanes conversion as function of the reactor length and conversion gradient.

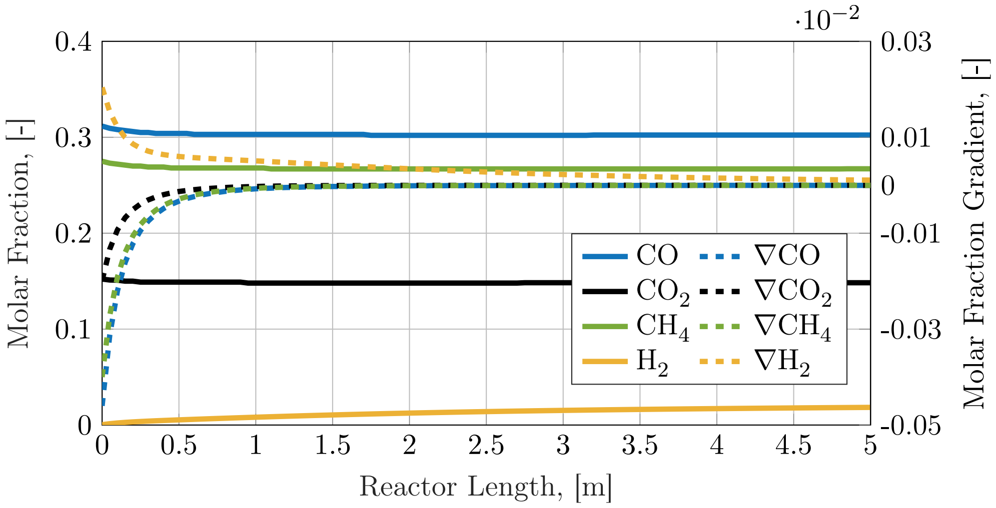

Figure C.3: Light Gases conversion as function of the reactor length and conversion gradient.

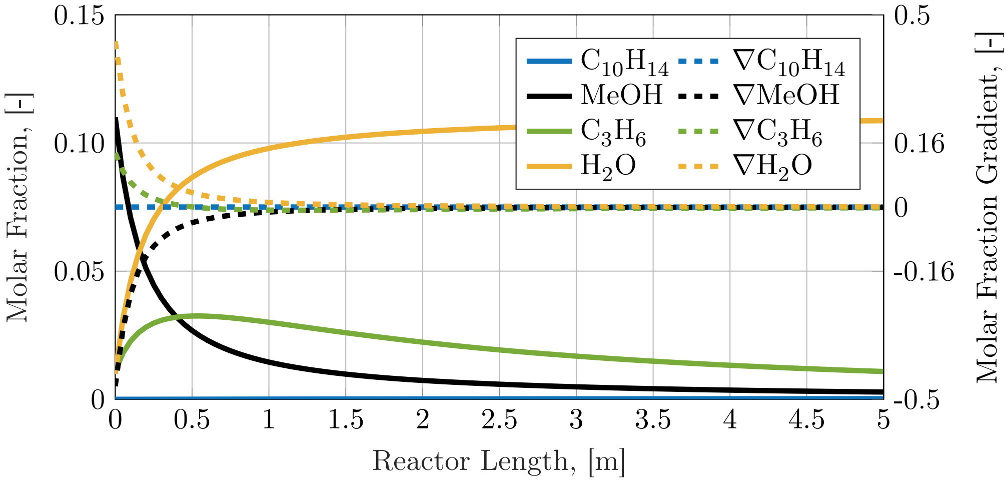

Figure C.4: Heavy and Others conversion as function of the reactor length and conversion gradient.